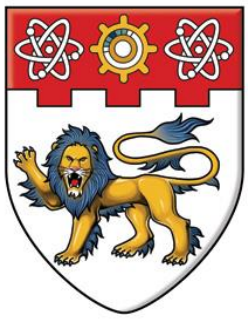

NANYANG TECHNOLOGICAL UNIVERSITY

STRUCTURAL & FUNCTIONAL CHARACTERIZATION OF THE DENGUE VIRUS NON-STRUCTURAL PROTEIN 5 (NS5)

SOH TINGJIN SHERRYL

SCHOOL OF BIOLOGICAL SCIENCES

2017

STRUCTURAL & FUNCTIONAL CHARACTERIZATION OF THE DENGUE VIRUS NON-STRUCTURAL PROTEIN 5 (NS5)

SOH TINGJIN SHERRYL

School of Biological Sciences

A thesis submitted to the Nanyang Technological University in partial fulfilment of the requirement for the degree of Doctor of Philosophy

2017

Acknowledgements

First and foremost, I would like to express my deepest gratitude to both my supervisors, Associate Professor Julien Lescar in NTU and Dr Lim Siew Pheng in Novartis Institute for Tropical Diseases (NITD), for their continuous guidance, encouragement and intense patience throughout my graduate education. Their expertise, meticulous attention and support had been greatly beneficial to me and to the success of my project.

I am grateful to my colleagues in NITD, especially Ms Seh Cheah Chen and Dr Shan Chao who generously shared their knowledge and provided me with ample support and assistance. I would also like to thank my colleagues in NTU, especially Dr El Sahili Abbas and Ms Grace Chan Kar Yarn, who had rendered me with extensive help and advices for my crystallography experiments in NTU.

My heartfelt gratitude also extends to my collaborators, Assistant Professor Luo Dahai, Dr Zhao Yongqian and Dr Subhash G. Vasudevan, for useful and critical discussions which led to the success of three publications.

It was a privilege to work alongside with many brilliant and enthusiastic scientists and I truly enjoyed my stay in NITD and NTU for the past four years. It had been a fulfilling and enriching experience for me.

Lastly, I thank Singapore Economic Development Board (EDB) for funding my research studies.

TABLE OF CONTENTS

List of Figures

List of Tables

List of Appendices

Abbreviations

3’UTR	3’ untranslated region
5’UTR	5’ untranslated region
6’-FAM	6’-carboxyfluorescein
ADE	Antibody-dependent enhancement
BHK	Baby hamster kidney
Bp	Base pair
BSA	Bovine serum albumin
BVDV	Bovine viral diarrhea virus
C	Capsid
CCPM	Corrected counts per minute
cDNA	Complementary deoxyribonucleic acid
CHAPS	3-[(3-Cholamidopropyl)dimethylammonio]-1-propanesulfonate
cHP	Capsid region hairpin
CIP	Calf intestinal alkaline phosphatase
CS	Conserved sequences
DAPI	4′,6-diamidino-2-phenylindole
DAR	Downstream AUG region
DC	Dendritic cells
DC-SIGN	Dendritic cell-specific intercellular adhesion molecule-3-grabbing non-integrin
DENV	Dengue virus
DHF	Dengue hemorrhagic fever
DMEM	Dulbecco’s modified Eagle’s medium
*dn*I	*de novo* initiation
dNTP	deoxynucleoside triphosphate / deoxyribose NTP
ds	double-stranded
dsRNA	Double-stranded ribonucleic acid (RNA)
DSS	Dengue shock syndrome
EC	Elongation complex

EDTA	Ethylenediaminetetraacetic acid
EF-1α	Elongation factor-1α
EMCV	Encephalomyocarditis virus
EMSA	Electrophoretic mobility shift assay
ER	Endoplasmic reticulum
EV71	Enterovirus 71
FAPA	Fluorescence-based alkaline phosphatase-coupled polymerase assays
FBS	Fetal bovine serum
FL	Full-length
FMDV	Foot-and-mouth disease virus
FP	Fluorescent/Fluorescence polarization
GTase	Guanyltransferase
HCV	Hepatitis C Virus
HDVr	Hepatitis delta virus ribozyme
HIV-1	Human immunodeficiency virus-type 1
Hpt	Hour post-transfection
IFA	Immunofluorescence assay
IFN	Interferon
IPTG	Isopropyl-β-D-thiogalactopyranoside
IRES	Internal ribosome entry site
IVT	*in vitro* transcription
JAK-STAT	Janus kinase/signal transducers and activators of transcription
JEV	Japanese encephalitis virus
Kan^{30}	30 μg/ml kanamycin
Kb	kilobase
β-ME	β-mercaptoethanol
MTase	Methyltransferase
NES	Nuclear export signal
NLS	Nuclear localization signal

Ni-NTA	Nickel-nitrilotriacetic acid
NIs	Nucleoside/nucleotide analog inhibitors
NNIs	Non-nucleoside inhibitors
NP	Nucleoprotein
NS3	Non-structural protein 3
NS5	Non-structural protein 5
nt	nucleotide
NTPase	Nucleotide triphosphatase
NTP	Nucleoside triphosphate
ORF	Open reading frame
P/S	Penicillin/streptomycin
PABP	Poly(A)-binding protein
prM	pre-membrane
PTB	Polypyrimidine tract binding protein
PV	Poliovirus
qRT-PCR	Quantitative real-time polymerase chain reaction
RC	Replication complex
RdRp	RNA-dependent RNA polymerase
RF	Replicative form
RFU	Relative fluorescence unit
RI	Replicative intermediate
R_{luc}	*Renilla* luciferase
RLU	Relative light units
rNTP	ribose NTP
RPMI	Roswell Park Memorial Institute
RT	Reverse transcriptase
RT	Room temperature
RTP	Ribavirin 5’-triphosphate
RTPase	RNA triphosphatase

SAM	S-adenosyl-L-methionine
SAR	Structure-activity relationship
SDM	Site-directed mutagenesis
SDS-PAGE	Sodium dodecyl sulphate-polyacrylamide gel electrophoresis
SFV	Semliki Forest virus
SLA	Stem loop A (large stem-loop)
SLB	Stem loop B (short stem-loop)
SPA	Scintillation proximity assay
SPR	Surface Plasmon Resonance
ss	Single-stranded
ssRNA	Single-stranded ribonucleic acid (RNA)
STAT2	Signal transducer and activator of transcription 2
TBEV	Tick-borne encephalitis virus
TGN	Trans-golgi network
TIA-1	T-cell intracellular antigen-1
TIAR	TIA-1-related protein
TR	Terminal region
UAR	Upstream AUG region
UTR	Untranslated region
UV	Ultraviolet
VCD	Virologically confirmed dengue
VPg	viral protein genome-linked
VR	Variable region
VSV	Vesicular stomatitis virus
WNV	West Nile virus
WT	Wild-type
YB-1	Y Box binding protein-1
YFV	Yellow Fever virus
ZIKV	Zika virus

Abstract

Dengue virus (DENV) is the most important arthropod-borne pathogens capable of causing human mortality and morbidity. Currently, there are no antiviral drugs available for treatment of dengue infections. Although a tetravalent DENV vaccine has recently been licensed for use, it has limited efficacy. For DENV, NS5 is the best characterized and most conserved multi-functional protein comprising an N-terminal methyltransferase (MTase) and a C-terminal RNA-dependent RNA polymerase (RdRp). Both play essential roles in viral replication in the host cell. The crystal structure of the DENV full-length NS5 revealed a well-ordered linker region and an inter-domain interface mostly formed by polar residues. Using a combination of biochemical and reverse genetic approaches, the biological relevance of the flexible linker between MTase and RdRp in the DENV-3 NS5 FL and their intra-molecular interactions was investigated. Several conserved interface residues were shown to be important for viral replication, through influencing either MTase or RdRp activities. Other NS5 alanine mutants displayed comparable enzymatic activities as wild-type, but were either less competent or lethal for virus production, suggesting that they play vital but non-enzymatic roles in viral replication and infectivity. Alanine mutations of the linker region showed that the third and fourth residues of the short 3_{10}-helix regulate polymerase *de novo* initiation activity for viral replication in cells. In addition, linker swapping experiment demonstrated that the unique amino acid composition of the linker controls NS5 conformation flexibility for cross-talk between the two domains and for interaction with viral and host proteins in a serotype/virus-specific manner.

By solving crystal structures of ternary complexes between DENV-3 NS5 protein, an authentic cap-0-viral RNA substrate, S-adenosyl-L-homocysteine (SAH) and/or RdRp allosteric inhibitors, we functionally probed these inhibitor and substrate binding sites in the RdRp and MTase with biochemical, biophysical and reverse genetic tools. Based on the catalytically-competent NS5-SAH-cap-0-viral RNA methylation complex, mutagenesis studies targeting the

highly conserved capped-RNA binding groove in the MTase domain was performed. The importance of the polar interaction between NS5 residue E111 and G_2 base of RNA for viral replication as well as the positional requirement G_2 for virus growth were identified. Moreover, residues lining the RNA binding groove exhibited differential reduction in 2'-*O* methylation activity, indicating that these residues are critical for capped-RNA binding and 2'-*O* methyl transfer reaction.

Using compound and fragment-based screening coupled with structure-guided design, we identified two classes of allosteric inhibitors that bound either to the F1 motif, or to the thumb subdomain and priming loop (termed "N-pocket") of the DENV RdRp. Antiviral activities of F1 motif and N-pocket inhibitors were primarily due to an impact on polymerase *de novo* initiation activity rather than elongation during RNA synthesis. Additionally, kinetic characterization showed that the N-pocket inhibitors exhibited mixed inhibition profiles when compete against the RNA or GTP substrate. Resistant mutants raised from these inhibitors were also mapped to the N-pocket of RdRp, confirming that they bind specifically to this pocket to block viral replication. The proposed mode of action for N-pocket compounds is to prevent NS5 RdRp *de novo* initiation and block conformation changes during transition from initiation to elongation.

In order to examine how the viral RNA is recognized and replicated as well as to facilitate drug discovery and design targeting the RdRp, we attempted to obtain crystal structure of NS5 RdRp bound to RNA. A novel fluorescence polarization (FP)-based assay was developed to profile various distinct RNA constructs for their suitability in co-crystallization. Several RNA substrates demonstrated good binding affinity to NS5 protein and were capable of forming functional elongation complexes. Crystallization trials using commercial screening kits were set up, but no crystal structure with bound RNA was obtained. Future work will aim at

optimizing the conditions during assembly and reaction in order to attain more soluble and stable elongation complexes for crystallization.

Overall, these findings provide valuable information on the functions and dynamics of NS5 as well as its molecular interactions with substrates and inhibitors, and have significant implications for the development of antiviral drugs targeting flaviviruses.

1 INTRODUCTION

1.1 Background & Classification of *Flaviviruses*

The *Flaviviridae* is a large family of human and animal pathogens capable of causing severe mortality and morbidity. Members of this family are positive-stranded enveloped RNA viruses which exhibit similarities in virion structure, genome organization and replication strategy, but differ in biological properties and do not harbor serological cross-reactivity. These viruses are classified into three genera – *Pestivirus*, *Hepacivirus* and *Flavivirus*, based on the evolutionary homology of their RNA-dependent RNA polymerases (RdRps). *Flaviviruses* are responsible of causing serious endemic and epidemic disease each year (Figure 1.1) and contains many significant arthropod-borne pathogens, which includes Dengue virus (DENV), Japanese encephalitis virus (JEV), West Nile virus (WNV), Zika virus (ZIKV), Yellow Fever virus (YFV), and Tick-borne encephalitis virus (TBEV) that can cause a broad spectrum of human diseases (1).

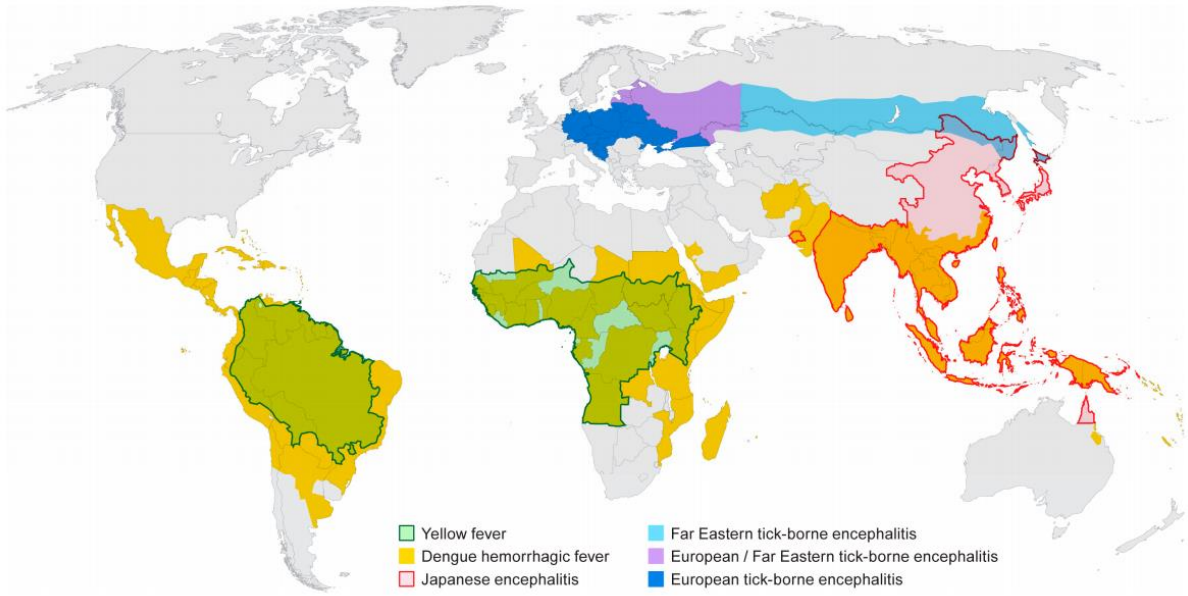

Figure 1.1 The global distribution of flaviviruses. Adapted from (2).

1.2 Epidemiology of Dengue virus

Dengue virus is a major emerging global concern and circulates in nature vectored by *Aedes aegypti* and *Aedes albopictus* mosquitoes. A recent study estimated that there are 390 million

people infected with DENV each year, of which 96 million exhibit disease symptoms (3). There is no definite treatment for dengue and difficulties in controlling the population of mosquito vectors coupled with societal factors have promoted the spread and incidence of DENV in many parts of the world, including the Asia, Africa, and Americas wherever the mosquito vector is present. There are four antigenically unique serotypes of DENV (DENV-1, 2, 3, 4) with significant diversity among them. Infection with any of the four genetically distinct serotypes of DENV can be asymptomatic or can lead to a wide range of clinical manifestations, ranging from acute self-limiting febrile illness to potentially fatal dengue shock syndrome (DSS) and dengue hemorrhagic fever (DHF). The development of lifelong immunity after infection with one of the serotypes is serotype-specific, but secondary infection with another serotype often elicits the progression to more severe diseases through an underlying mechanism called antibody-dependent enhancement (ADE) (4).

Currently, a recombinant yellow-fever-17D-dengue virus, live, attenuated, tetravalent dengue vaccine (CYD-TDV, Sanofi Pasteur, Lyon, France), Dengvaxia, is available as the first vaccine licensed for dengue prevention in the world (5-9). It has undergone 25 clinical studies in many countries around the world with over 40,000 participants in the clinical study program and is now approved for use in several countries including Singapore, Indonesia, Philippines and Thailand. This vaccine requires a three-dose administration over a year and exhibited good safety and immunogenicity profiles against all four DENV serotypes as well as was efficacious against symptomatic, virologically confirmed dengue (VCD). In general, the vaccine is effective in reducing dengue and severe dengue illness by 60 per cent and 84 per cent respectively. However, it demonstrated varied efficacy against different DENV strains and works better for people aged 12 to 45 years. In Singapore where DENV-1 and DENV-2 are the predominant strains, the vaccine is less effective and deemed less clinically and cost-effective to be used for the prevention of dengue. Importantly, it is 81 per cent effective in those with

history of dengue infection compared to 38 per cent in those with no immunity. In addition, younger children who had never been infected by dengue before showed a higher risk of hospitalization and risk of severe dengue if they contracted the virus after getting vaccinated. Thus, given the several drawbacks of the existing vaccine, the availability of vaccines with improved pan-serotype efficacy and safety across a wider range of age groups as well as effective antiviral drugs would prove valuable for the prevention and treatment of dengue infections.

1.3 The life cycle of Dengue virus

Dengue virus can exploit multiple receptors for various cell types and in different host species for entry into the cells. Intradermal mononuclear phagocytes such as monocytes, macrophages and dendritic cells (DC) are usually the primary targets early in infection (10-12). During infection, DENV particle attaches to the surface of a host cell via interactions between the cell surface receptors and viral glycoproteins. C-type lectin dendritic cell-specific intercellular adhesion molecule-3-grabbing non-integrin (DC-SIGN) attachment receptor is involved when DC is infected with DENV. Highly sulfated glycosaminoglycans such as heparin sulfate, which are expressed in many cells types, are also identified to facilitate DENV attachment (13-15). In addition, other proteins on mammalian cells including CD14 and GRP78 (BiP) are also known to function as DENV receptors (16, 17). Furthermore, virus particle opsonized with antibodies, usually in people with history of infection with one DENV serotype, exhibited enhanced binding and increased infectivity in cells expressing immunoglobulin Fc receptors, which may lead to the pathogenesis of DF and DHF (18).

DENV are internalized through distinct entry pathways consisting clathrin-mediated endocytosis or non-classical clathrin-independent endocytosis relying on the host cell type and virus strain or serotype, and are trafficked to an endocytic compartment where the acidic environment induces fusion between the host cell and virus membranes to release nucleocapsid

into the cytoplasm (19, 20). The nucleocapsid is uncoated to dissociate the capsid (C) protein and viral RNA, followed by the replication of genome. The positive-sense viral RNA undergoes translation to produce a large polyprotein which is co- and post-translationally processed by both viral and cellular proteases. The newly synthesized RNA and capsid protein bud into the endoplasmic reticulum (ER) lumen for virus assembly to create immature, non-infectious particles. These virions are transported through the trans-golgi network (TGN) where cleavage of the pre-membrane (prM) proteins by host protease furin occurs to generate mature, infectious viruses which are released from the host cell by exocytosis. A schematic diagram on the life cycle of DENV is shown in Figure 1.2.

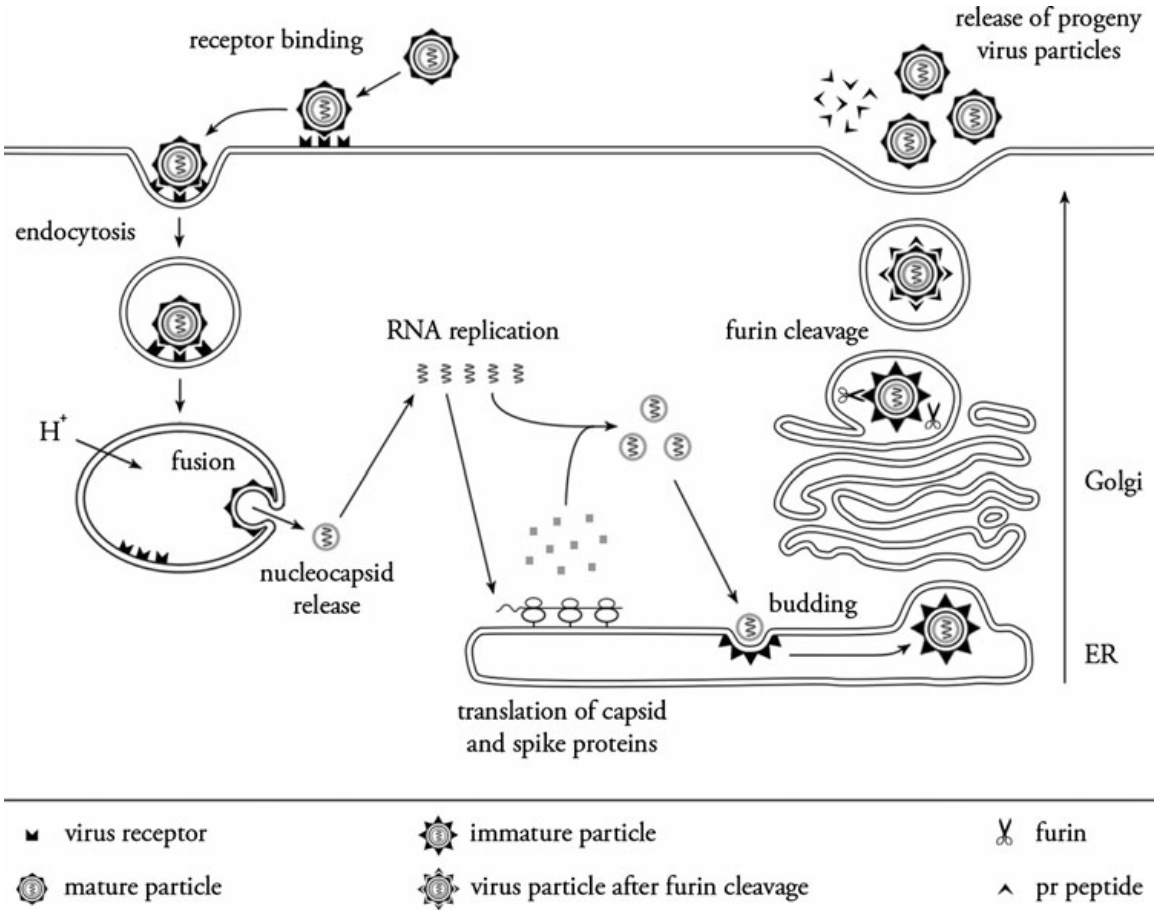

Figure 1.2 The life cycle of Dengue virus. Adapted from (21).

1.4 Dengue virus RNA genome

The DENV genome is a single, positive-strand RNA with a length of about 11 kilobases (kb), consisting of a 5' untranslated region (UTR) with a type 1 cap structure (^{N7Me}G5'-ppp-5'A$_{2'OMe}$)

at its 5' end (22), and a 3'UTR that is not poly-adenylated (Figure 1.3A). The 5'UTR is not well conserved among various flaviviruses, albeit they have common secondary structures that play a role in genome translation (23, 24). This region is about 100 nucleotides long and contains two RNA domains which function specifically during RNA synthesis (Figure 1.3B). The first domain is a large stem-loop (SLA) structure made up of approximately 70 nucleotides which serves as a promoter for viral polymerase recognition during RNA replication (25, 26). The second domain is a short stem-loop (SLB) containing sequences for long range RNA-RNA interaction and replication (27). Between the SLA and SLB structures is an oligo(U) track which serves as a spacer to enhance RNA production (28). Located downstream of the AUG initiation codon inside the capsid coding region is a stable hairpin (cHP) essential for the replication of viral RNA (29). The 3'UTR of approximately 450 nucleotides long also forms distinct structures which have critical roles in RNA synthesis and consists of three domains (I, II and III) (Figure 1.3C). The first domain, situated right next to the stop codon, is highly variable and displays varied size between different DENV serotypes (30, 31). The second domain consists of a characteristic dumbbell structure with conserved sequences (CS), CS2 and RCS2, present in all arthropod-borne flaviviruses (32-35). The RNA elements within the first two domains are not necessarily required for viral replication however they act as enhancers for viral processes (36-39). The third domain is conserved within the 3'UTR and bears a CS1 element prior to the terminal stem-loop structure (3'SL). The 93 nucleotide long 3'SL harbors a short stem loop (sHP) and a large stem loop in which both structures are important for viral RNA replication (40-43).

Genome cyclization is a well-preserved feature of flavivirus genomes and occurs by complementary interactions between the ends of the RNA, namely 5'-3' upstream AUG regions (UAR) and 5'-3'CS (Figure 1.4) (44, 45). The 5'UAR sequence is situated ahead of the AUG start codon in the 5'UTR while the 3'UAR is found within the 3'SL. The 5'CS

sequence is at the start of the capsid coding region whereas the 3'CS is situated before the 3'SL region. Another element, downstream AUG region (DAR), also revealed its importance for 5'-3' genome interaction (44, 46). The 5'DAR follows after the AUG codon whilst the 3'DAR is part of the small hairpin of the 3'SL. Earlier studies have shown the importance of genome cyclization during replication (47, 48). Long-range RNA-RNA interactions are required for the viral polymerase to bind at the SLA structure at the 5' terminus and to relocate to the 3' initiation site for RNA production (25). Mutations of the complementary regions substantially impacted RNA synthesis without affecting translation, and compensatory mutations restoring 5'-3' nucleotide pairing rescued virus replication (27, 48, 49), indicating that complementary RNA interactions are vital for viral replication.

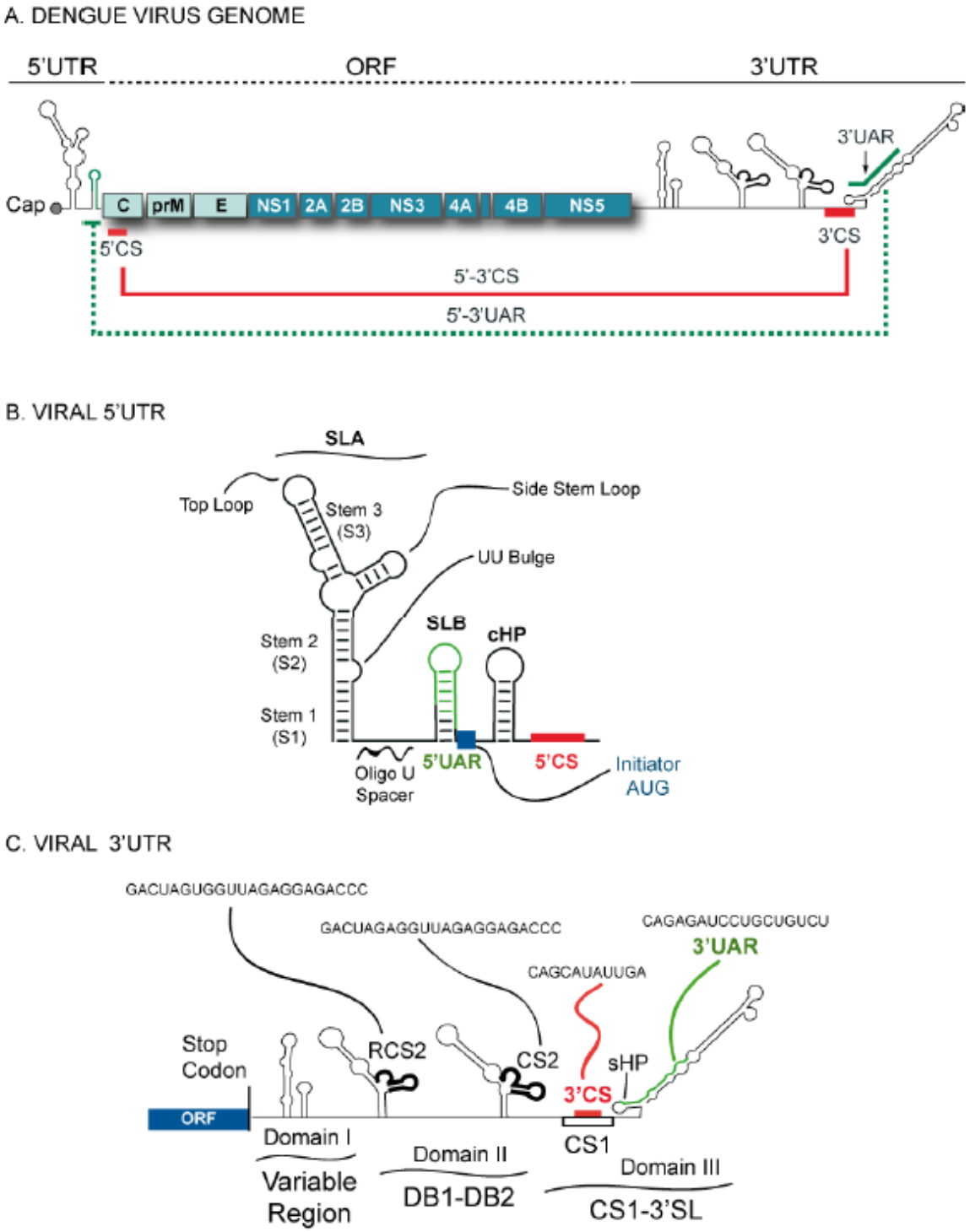

Figure 1.3 Schematic representation of the DENV genome. (A) The DENV genome consists of 5' and 3' UTR regions as well as an open reading frame (ORF) encoding structural (C-prM-E) and non-structural proteins (NS1-NS2AB-NS3-NS4AB-NS5). RNA cyclization occurs by complementary base pairing of 5'-3'UAR (green dotted line) and 5'-3'CS (red solid line). (B) Predicted secondary structure of 5'UTR. (C) Predicted secondary structure of 3'UTR. Adapted from (50).

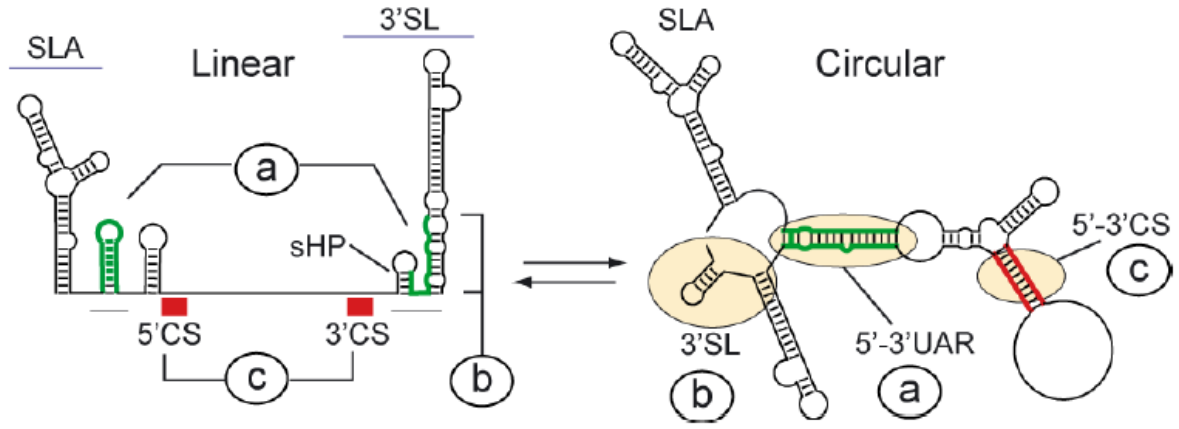

Figure 1.4 Schematic representation of predicted changes between linear and circular conformations of the DENV genome. The complementary sequences (a) 5'-3'UAR (green) and (c) 5'-3'CS (red) interact in the circular form to generate double-stranded regions. Adapted from (50).

1.5 Translation and proteolytic processing

DENV RNA genome displays three main roles in the host cytoplasm: (i) acts directly as mRNA for the production of viral polyprotein (translation), (ii) serves as a template to synthesize minus sense RNA intermediate followed by plus sense progeny RNA (replication), and (iii) gets incorporated into new viral particles (encapsidation). Genome translation is coupled to replication since the synthesis of viral proteins is required for viral genome replication and formation of new virus particles. Thus, the efficiency of translation could be a dominant factor of virus infectivity (51).

Similar to most viruses, DENV depends on the host cell machinery for translation and has developed novel mechanisms to facilitate translational competence. Translation of DENV genome occurs via cap-dependent initiation whereby its 5' m7GpppN cap structure is recognized and bound to the eukaryotic initiation factor (eIF4E), that is part of the cap-binding complex eIF4F consisting of a helicase eIF4A, eIF4E, and an adaptor protein eIF4G (52). This complex then recruits the 43S ribosomal preinitiation complex to form the 48S complex which starts scanning the 5'UTR until it locates a start codon (AUG). To ensure proper start site selection for protein synthesis, the RNA hairpin structure in the capsid gene (cHP) of DENV causes the ribosomal complex to pause momentarily over the authentic AUG as it begins to

unwind the secondary structure of cHP (53). Although DENV RNA lacks a poly(A) tail, it was shown that the poly(A)-binding protein (PABP) could be bound to the 3'UTR region, possibly circularizing the viral genome for efficient translation (54). The ribosomal 40S and 60S subunits then subsequently bind to this complex and form the fully assembled 80S ribosome for translation elongation.

Previous study has demonstrated that inhibiting the cap-dependent mechanism, for instance by suppressing the expression of eIF4E, still allowed DENV replication and translation, suggesting that the virus employed another mechanism for protein synthesis. Several eukaryotic cells and animal viruses such as Poliovirus, a member of the family of *Picornaviridae*, were able to utilize a cap-independent machinery of translation using internal ribosome entry site (IRES) located at the 5'UTR of their genomes (55-57). However, the 5'UTR of DENV does not contain an IRES for ribosome recruitment. Instead, DENV could employ a non-canonical translation initiation mechanism that requires interactions between 5' and 3'UTRs (52, 58). It was proposed that the 3'UTR could recruit the translation initiation elements to the 5' terminus, enabling the recruitment of eIF4G and eIF4A factors in the absence of eIF4E. It was noted that some plant viruses also participated in cap-independent mechanism of translation by 5'-3' RNA interactions and delivery of eIF4F to the 5'UTR by the 3'UTR through long-range base pairing (59-62).

Translation of the single open reading frame (ORF) of DENV genome produces a large polyprotein that is co- and post-translationally processed by host signal peptidase and viral serine-protease to give three structural and seven non-structural proteins (Figure 1.3A). The structural proteins form the viral particle: the capsid [C] protein associates with the viral genome to generate the nucleocapsid whilst the pre-membrane [prM] and envelope [E] proteins insert into the lipid bilayer membrane surrounding the nucleocapsid (63). The non-structural

proteins (NS1, NS2A/B, NS3, NS4A/B and NS5) are important for the replication of RNA, assembly of virus particles, as well as escaping the host immune response (64-66).

1.6 Genome replication

1.6.1 General introduction to polymerases

Replication of genome is carried out by a specific protein called polymerase. This enzyme catalyzes the formation of long chains of DNA or RNA nucleic acids from a template strand by linking deoxyribonucleotides or ribonucleotides respectively. The active site of polymerase harbors binding sites for template, primer and incoming nucleoside triphosphate (NTP) and contains critical amino acids that interact and stabilize the substrates for nucleotidyl transfer reaction. Two divalent metal ions, either Mg^{2+} or Mn^{2+}, are also coordinated by conserved Asp residues in the active site for the catalytic activity of polymerase. One metal ion binds to and lowers the p*K*a of 3'-hydroxyl of the growing daughter strand to facilitate nucleophilic attack on the α-phosphate of incoming NTP (67). The other metal ion interacts with negatively charged oxygens of the phosphates of incoming NTP to position the nucleotide and stabilize the pyrophosphate product generated during phosphodiester bond formation with the nucleophile. Once the cognate nucleoside monophosphate is incorporated into the daughter strand via Watson-Crick base-pairing with the complementary template base, translocation of the primer terminus by one base occurs and the process is repeated again until the template is completely copied or a termination signal is met.

There are four different types of polymerases for transcription and replication depending on the nature of the genome and the need to synthesize mRNA, namely DNA-dependent DNA polymerases (DdDp), DNA-dependent RNA polymerases (DdRp), RNA-dependent DNA polymerases (reverse transcriptase; RdDp) and RNA-dependent RNA polymerases (RdRp) (68). All these four types of polymerases are found in viruses whilst the host cell does not

require RNA-dependent DNA polymerases and RNA-dependent RNA polymerases since its genetic material is DNA.

1.6.2 Viral polymerases

The cellular location of genome replication dictates whether viruses encode their own polymerases or utilize the host polymerases for transcription and replication. Moreover, the genome type (DNA or RNA, double-stranded (ds) or single-stranded (ss), or plus- or minus-sense) and the specific needs of viruses (transcription and/or replication) decide whether viruses convert their genomes into mRNA for translation or synthesize additional copies of genome for encapsidation (Figure 1.5).

DNA viruses, including adenovirus, herpesvirus, bacteriophage T7 and papillomavirus, have either dsDNA (linear or circular) or ssDNA and carry out replication and transcription using DNA-dependent DNA polymerases and DNA-dependent RNA polymerases respectively. Eukaryotic DNA viruses such as papillomavirus and polyomavirus employ host polymerases in the nucleus to transcribe mRNA and replicate their small genomes (69). In contrast, cytoplasmic DNA viruses reside in the cytoplasm most of the time and thus encode their own DNA-dependent DNA and RNA polymerases. These viral DNA-dependent polymerases share similarities to host DNA and RNA polymerases and some of the DNA polymerases like the dsDNA bacteriophage φ29 DdDp even possess proofreading activity. Notably, all DNA-dependent DNA polymerases synthesize genome in a primer-dependent manner, whereas DNA-dependent RNA polymerases bind at a specific promoter region and initiate RNA production in a *de novo* (primer-independent) manner. Following initial RNA synthesis, short oligonucleotides (<10 nucleotides) are aborted and only longer transcripts (~10 nucleotides) undergo processive elongation.

RNA viruses harbor either dsRNA or ssRNA (plus- or minus-sense) genomes and perform replication and transcription using RNA-dependent RNA polymerases. Plus-sense ssRNA

viruses such as poliovirus and flavivirus synthesize their genomic RNA in a membrane-bound replication complex and their genome serves directly as an mRNA for viral protein production during infection. RNA replication occurs by first transcribing the plus-strand RNA into a complementary minus-strand RNA to form a dsRNA intermediate, followed by generation of multiple copies of plus-strand progeny from the new-synthesized minus strand (70). Minus-sense ssRNA viruses such as influenza, hantavirus and Ebola virus contain either segmented or nonsegmented genomes. Their genome has to be transcribed into a plus-strand RNA before it can be used for translation by host enzymes. In addition, the plus-sense RNA is capped and has additional short non-templated nucleotides at its 5'-terminus, possibly acquired from cellular mRNA through a "cap-snatching" mechanism (71-73). During transcription, the viral polymerase docks onto the host mRNA cap and cleaves the 5' end using an endonuclease activity to generate primers for viral RNA transcription. Viruses containing dsRNA genomes include reovirus, rotavirus and birnavirus, and their genomes are always segmented. Since dsRNA cannot be used as mRNA for protein translation, these viruses encode their own RNA-dependent RNA polymerases to make mRNA and replicate their genomes.

There are also viruses which replicate using reverse transcription, i.e. synthesizing DNA from RNA template, and their genomes can be either DNA or RNA. Retroviruses encode its own RNA-dependent DNA polymerase (reverse transcriptase, RT) to convert its ssRNA genome into a dsDNA form through an DNA intermediate, and the dsDNA can be integrated into the host's DNA for subsequent mRNA transcription and translation by cellular machinery. On the other hand, hepatitis B virus harbours a dsDNA genome that is transcribed to mRNA by host polymerase. The progeny RNA is replicated into dsDNA through an RNA intermediate using virally encoded RT.

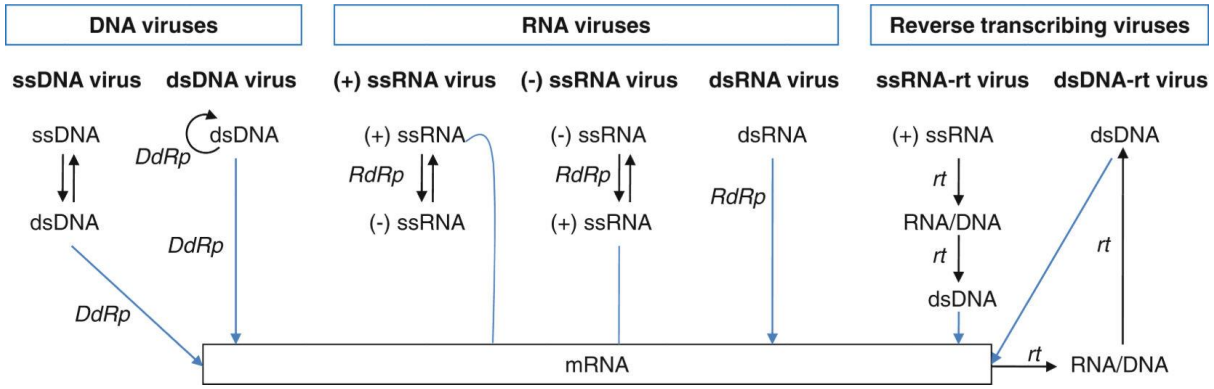

Figure 1.5 Baltimore virus classification scheme. Viral polymerases are classified based on genome type and mechanism of mRNA production (74). Adapted from (68).

All polymerases assume a "cupped" right hand conformation, comprising fingers, palm and thumb domains. The palm domain is highly conserved among various polymerases and contains motifs A and C harboring the catalytic Asp residues important for coordinating two divalent metal ions in the active site. These two conserved sequence motifs are shared among all the four types of polymerases. The interface of fingers and thumb domains forms a template-binding tunnel that reaches the catalytic palm domain. Depending on the requirements to accommodate single-stranded or double-stranded DNA or RNA template as well as the method of initiation (*de novo* or primer-dependent), both domains have varying size and secondary structure in order to form distinct template-binding channels. For instance, DNA or RNA polymerases selectively use amino acids with larger or smaller side chain to bind the 2'-H or 2'-OH moiety of deoxyribose NTPs (dNTPs) or ribose NTPs (rNTPs), correspondingly.

Some viral polymerases have additional domain at their N-termini that may have other essential enzymatic functions during genome transcription and replication. For example, flavivirus RdRp is linked to a methyltransferase domain that is involved in 5'-RNA cap methylation (75). Retrovirus RT has an N-terminal ribonuclease H domain to hydrolyze the RNA strand in RNA-DNA hybrid during replication (76, 77). dsDNA bacteriophage φ29 DdDp has an additional exonuclease domain to proofread, ensuring incorporation of correct nucleotides during DNA

synthesis (78). However, the function of the small domain at the N-terminus of pestivirus NS5B polymerase remains unclear (79).

Viral polymerases can replicate their genomes in the 5' → 3' direction with the use of different mechanisms based on their adaption to the host cell. The first step of the polymerase reaction is initiation in which nucleotidyl transfer takes place at the 3'-end of the template strand. This step can be primer-dependent and viral polymerases could adopt four different strategies – oligonucleotide primer, cap-snatching, protein-priming and copy-back mechanism, to ensure efficient initiation of nucleic acid synthesis (80). All DNA-dependent DNA polymerases, reverse transcriptase and some RNA-dependent RNA polymerases use a short primer to provide 3'-hydroxyl for addition of incoming nucleotide. Several RNA-dependent RNA polymerases from negative-stranded RNA viruses could also make positive-stranded mRNA with cellular-capped oligonucleotides through a "cap-snatching" mechanism as mentioned earlier. Furthermore, some viruses such as ssRNA picornavirus, dsDNA adenovirus and dsDNA RT hepatitis B virus encode a terminal protein that is covalently linked to the 5'-terminus of the genome to provide a hydroxyl group from a Tyr or Ser amino acid to form a phosphodiester bond with the first nucleotide, and the protein-linked primer is then further elongated the entire length of the genome (81, 82). Previous study has shown that recombinant flavivirus RdRp could adopt a "copy-back" mechanism where the 3'-terminus of the RNA template folds back upon itself and acts as a primer, synthesizing a product that has double the size of the template (83). Aside from primer-dependent mechanism, polymerases can initiate nucleic acid production in a *de novo* manner within the need of a primer, and this is more likely to be the mechanism for flavivirus RNA replication during infection. *De novo* initiation requires an initiation NTP which is properly positioned at the 3'-end of the genome to provide a 3'-OH for the incoming NTP, similar to the 3'-OH of a primer terminus in a primer-dependent reaction. As stated earlier, DNA-dependent RNA polymerases can also initiate *de novo* RNA

production via abortive initiation and only longer oligonucleotides (~9-10 nucleotides long) undergo elongation to generate the entire RNA transcript. Following initiation, the next step of the polymerase reaction is processive elongation. Once the polymerase forms a stable association with template and primer, the enzyme consecutively incorporates nucleotides without dissociation. The last phase of the polymerase reaction is termination. It is still elusive on how viral polymerases terminate replication at the 5'-end of the template, and is relatively challenging for viruses with linear genomes. The genome could get progressively shorter over time if the end of the genome is not copied during successive rounds of replication. To overcome this problem, some bacteriophages release their linear genome into the cell for conversion to circular form or integration into the host chromosome, and cellular polymerases could elongate the 3'-hydroxyl group of the nicked dsDNA along the unnicked template strand in a rolling circle method (84). The only exception is DNA-dependent RNA polymerases such as dsRNA bacteriophage T7 DdRp that synthesize RNA transcript until a terminal signal is encountered, and the polymerase-RNA complex dissociates from the dsRNA template.

1.6.3 RNA-dependent RNA polymerases (RdRps)

The first solved crystal structure of an RNA-dependent RNA polymerase (RdRp) was from poliovirus (85) and it adopts the same 'right hand' architecture with palm, fingers and thumb domains as compared to other polymerase structures (86, 87). A unique feature of the RdRp is the encirclement of the active site achieved through extensive interactions between the finger domain loops ("fingertips") and thumb domain, to create an overall "closed-hand" conformation. The RNA-binding tunnel is located in the "front" of the polymerase and NTPs enters from the "back" of the polymerase. The interconnections between the fingers and thumb domains restrict large movements and conformational changes of the two domains when RNA, primer or NTP substrates bind in the template channel of RdRp.

1.6.3.1 Structural motifs of RdRps

All viral RdRps harbor polymerase catalytic motifs A-E in the palm domain and motifs F-G in the fingers domain, and each of the motifs assumes a specific and conserved fold. Motifs A, C and D are the most important elements in the polymerase and play crucial roles during catalysis. The conserved aspartic acid residues in motifs A and C are involved in coordinating two divalent metal ions that are critical for polymerase activity (88). During phosphodiester bond formation between incoming NTP and RNA, the Asp amino acid of motif C uses a metal ion to fix the α-phosphate of nucleotide and lowers the pK_a of 3'-hydroxyl group of the nascent RNA strand for nucleophilic attack (67). The β- and γ-phosphates of the pyrophosphate leaving group as well as the pentacovalent intermediate formed during phosphoryl transfer are in turn stabilized by the metal ion coordinated by the Asp of motif A. Biochemical analyses has shown that the transition state that occurs during deprotonation of the 3'-OH nucleophile for attack of the α-phosphate of incoming NTP and protonation of the pyrophosphate product during nucleotidyl transfer reaction is the rate-limiting step in nucleic acid synthesis (89). Motif D is less conserved in sequence and contains a lysine or histidine amino acid that is possibly protonated in the active site environment. The protonation state of this residue modulates conformation changes required for active site closure and mutation of the lysine (K359R) in poliovirus (PV) RdRp altered catalytic efficiency and nucleotide incorporation fidelity of the polymerase reaction (90). Moreover, this conserved amino acid (K359 of PV RdRp and K220 of HIV RT) was demonstrated to function as a general acid to protonate the pyrophosphate leaving group in nucleotidyl transfer (91). The Lys or His residue facilitates Asp of motif A in coordinating β-phosphate of incoming nucleotide, and can transfer a proton to pyrophosphate when it moves near the β-phosphate group. Substitution of the lysine to leucine resulted in a single proton transfer during polymerase-catalyzed nucleotidyl transfer reaction. In addition, one group had suggested that motif D could be involved in exporting pyrophosphate group

from the active site after catalysis (92). They also showed the collaborative movement of motifs A and D through interactions between residues from the two motifs, supporting an earlier work that both motifs in the palm domain undergo significant structural rearrangements during the open and closed states of the RdRp active site (93).

Motif B is involved in binding the template and incoming NTP through direct interactions between the base and its conserved residues ($3D^{pol}$ residues G289, S293, G294 and T298 of encephalomyocarditis virus (EMCV)), as revealed in several solved structures of picornaviral catalytic complexes (93-95). Conserved aspartic acid of motif A (D240 of EMCV $3D^{pol}$ and D245 of foot-and-mouth disease virus (FMDV) 3D) and motif B residues (N302 and S293 of EMCV $3D^{pol}$ and N307 of FMDV 3D) could rearrange their side chains for rNTP selection and proper positioning of the sugar in the ribose-binding site via hydrogen bonding to the 2'-hydroxyl group of the NTP ribose (94, 96). Another study on poliovirus $3D^{pol}$ demonstrated the importance of conformational flexibility of a highly conserved loop within the motif B (comprising residues 288-292) in mediating RNA translocation process following catalysis (97). In their work, they showed that the loop can adopt two stable orientations and mutation of residues within the loop, particularly S288, G289 and C290, affected RNA binding, processive elongation activity and translocation competency. The conformational dynamics of the flexible loop within motif B could likely apply to other RdRps from plus-sense RNA viruses since it exhibits high sequence and structural conservation among viral RdRps.

Motif E contains positively charged residues (S710 and R729 of DENV RdRp) that interact with the γ-phosphate of incoming rNTP through salt bridge and hydrogen bonding, as well as residues (H712, H714 and C728 of DENV RdRP) that coordinate one zinc atom (86). Substitution of the equivalent motif E residues in bovine viral diarrhea virus (BVDV) polymerase and hepatitis C virus (HCV) RdRp to other amino acid strongly impacted *de novo* initiation of RNA synthesis (98, 99). Thus, the residues in motif E play essential roles in *de*

novo RNA initiation by the polymerase and the zinc atom located nearby could modulate this activity.

Motifs F and G are found in the fingers domain of RdRp and are functionally important for polymerase activity. A number of basic amino acids of motif F are involved in coordinating the negatively-charged triphosphate of incoming NTP, implying its role in modulating NTP binding (88, 100). This motif orientated differently in the absence and presence of NTP in the JEV FL NS5 and RdRp structures, respectively (101, 102). Without binding of nucleotide, residue F467 from this motif interacts with residue P113 from the N-terminal protein domain. Binding of nucleotide in RdRp causes motif F to flip downwards and establish interactions with the triphosphate moiety of GTP via residues R460, K463, K471 and R474. Additionally, motif F could be involved in promoter-dependent initiation of RNA synthesis in DENV as alanine mutation of K456 and K457 (F1 motif residues) inhibited RNA production dependent on SLA promoter (103). Motif G could regulate access of ssRNA substrate to the entrance of template tunnel (86). Poliovirus $3D^{pol}$ showed that motif G in the pinky finger runs relatively parallel to the RNA strand with residues inserting at the +1/+2 backbone kink of the template (93).

1.6.3.2 Two distinct initiation mechanisms adopted by plus-sense ssRNA viruses

RdRps for viruses with plus-sense ssRNA genome can be categorized into two main classes based on their initiation mechanism of RNA replication – (i) *Picornaviridae* (e.g. poliovirus and FMDV) and *Caliciviridae* (e.g. Norwalk virus) utilize a virally encoded peptide as a primer for RNA synthesis (104), and (ii) *Flaviviridae* (e.g. dengue virus and WNV) uses initiating NTP to form the first phosphodiester bond in a primer-independent manner (100). The structure and size of the thumb domain is different between these two classes in which RdRps from *Picornaviridae* and *Caliciviridae* have smaller thumb and larger RNA-binding site to bind both template and a primer. On the contrary, RdRps from *Flaviviridae* have a priming element

integrated into their thumb domain that can protrude into the active site to stabilize initiating NTP and accommodate only ssRNA template in the narrower RNA-binding tunnel.

(i) Primer-dependent initiation

Primer-dependent viral RdRps like the PV $3D^{pol}$ utilize a terminal protein VPg (viral protein genome-linked, a 22-amino acid peptide) or its uridylylated forms to initiate RNA synthesis (105, 106). The viral RdRp is first synthesized as a 3CD precursor protein and undergoes a cleavage event to produce protease 3C and polymerase 3D. The 3D protein is responsible to catalyze attachment of VPg to the genome preceding elongation to generate genome progeny. RNA synthesis starts with uridylylation of VPg by $3D^{pol}$ to create a protein primer. The second nucleotide (adenosine) is initiated and not the 3'-terminal adenosine of the template, and a UTP is covalently linked to the hydroxyl group of a conserved tyrosine residue (Tyr3) in VPg to form VPg-pU. This VPg-pU then uses a back-slide mechanism on adenosine residues and base pair with the 3'-terminal nucleotide before the polymerase incorporates the second UTP to form VPg-pUpU (107). The VPg-pUpU primer can hybridize to the 3' polyA tail of the plus-strand genome and be elongated to synthesize the complete complementary minus-strand RNA. The VPg-pUpU molecule to synthesize plus-strand RNA is proposed to be produced from the cis-acting replication element (CRE), a 61-nucleotide stem-loop RNA structure in the coding region of protein 2C (108). Adenosine in the loop of CRE serves as a template to uridylylate VPg. Mutations in the CRE region prevented VPg uridylylation and positive-strand RNA synthesis but not negative-strand RNA synthesis. It remains unclear how the RdRp differentiates between the two types of VPg-pUpU for plus- and minus-sense RNAs production. Furthermore, VPg-pUpU primer uridylated at the CRE would require dissociation in the middle of the genome and reassociation at the 3'-end of the negative-strand template. The mechanism on how the 3D polymerase terminates RNA synthesis at VPg-pUpU and how this primer is transferred to the 3'-terminus of the genome is still undefined.

Crystal structures of 3D polymerase and its RdRp-VPg complexes from several members of the *Picornaviridae* and *Caliciviridae* families have been reported (106, 109, 110). The structure of FDMV 3D polymerase did not revealed large conformational changes induced by VPg binding and only small rearrangements in the side chain of residues R179 and D338 which participate in the uridylylation process were observed (106). VPg fits the RNA binding pocket and projects the key amino acid Tyr3 into the active site close to the catalytic Asp (D245 of motif A and D338 of motif C). Remarkedly, the 3D-VPg-UMP complex shows that VPg-pU positions itself analogously to the primer terminus in nucleotidyl transfer reaction and Mn^{2+} and Mg^{2+} divalent ions participate in the uridylylation reaction, similar to the two-metal-ion mechanism for stabilizing the transition state of the nucleotidyl transfer reaction that is common to all nucleic acid-synthesizing polymerases (67). Mn^{2+} binds to the carboxylic group of D338 of the catalytic GDD motif in the active site and the O^- of VPg Tyr3 side chain that is covalently attached to the α-phosphate of UMP. Mg^{2+} interacts with the carboxylic group of D245, oxygen of α-phosphate and the hydroxyl group of S298 side chain. Numerous residues in motif F of the fingers domain (R168, K172 and R179) together with residues of the thumb domain (T407, A410 and I411) and Y336 of motif C play important roles in stabilizing the Tyr3, VPg and UMP in the active site cavity for catalysis. Structure-based mutational analyses of amino acids involved in VPg uridylylation such as R168A, R179A and D338A of 3D and Y3F of VPg showed a negative impact in the uridylylation activity. Likewise, substitution of critical residues of enterovirus 71 (EV71) $3D^{pol}$ involved in VPg interaction to alanine resulted in impaired VPg uridylylation and lethal replication (110). It is still not clear on how VPg or its uridylylated forms is employed in the RNA-directed polymerase initiation and would be better understand if crystal structure of the ternary RdRp-VPg-RNA complex is available.

(ii) Primer-independent (*de novo*) initiation

Viruses from the *Flaviviridae* family synthesize RNA-dependent RNA polymerase at the C-terminal of the translated protein. Hepatitis C virus (Hepacivirus) NS5B polymerase has the smallest size of approximate 60 kDa among RdRps in the family without any additional domain fused to it. Pestivirus NS5B polymerase consists an extra N-terminal domain of unknown function. Flavivirus NS5 comprises of an N-terminal methyltransferase domain linked to a C-terminal RdRp, both of which are involved in genome replication process.

RdRps of *Flaviviridae* utilize a *de novo* mechanism to initiate RNA synthesis in which the second NTP enters the active site and forms a phosphodiester bond with the first initiating NTP without the need of a primer. Genome replication starts at the 3'-end of the plus-sense RNA and the polymerase can copy the entire length of the template without dissociation. The newly-synthesized minus-sense RNA then serves as a template to make multiple copies of plus-strand progeny. The formation of a stable *de novo* initiation complex for precise and efficient initiation is challenging as base pairing of the two NTPs with positions +1 and +2 of the template is inadequate to ensure correct positioning for catalytic reaction. Thus, polymerases employ several techniques to selectively accommodate its substrates and stabilize their interaction.

Crystal structures of the polymerase domains from all three members of the *Flaviviridae* family have been reported, providing the structural bases for how RNA initiation is achieved with the help of a priming element (86, 111-115). The priming element located at the C-terminal motif in the thumb domain is structurally diverse across various viruses, represented by an extended loop in flavivirus NS5, a β-hairpin in hepatitis C virus NS5B, and a β-strand and connecting loop in pestivirus NS5B. This element protrudes from the thumb domain into the active site, allowing only ssRNA access to the template-binding tunnel during *de novo* initiation. The importance of the priming element for efficient initiation and precise start site selection was highlighted when deletion of the β-hairpin caused HCV NS5B to use dsRNA substrates and initiate RNA synthesis from internal sites of the template (116). Moreover, mutation of

hydrophobic and charged amino acids within HCV 5B priming element significantly reduced *in vitro* RdRp *de novo* initiation activities and enhanced primer extension capabilities (117). Elongation of the template-primer after the *de novo* step would require conformation change of the thumb domain to an "open" form via movement of the C-terminal motif out of the template-binding channel to accommodate the growing dsRNA product.

De novo initiation of RNA synthesis requires a high concentration of GTP as a cofactor, regardless of the terminal nucleotides of the genome (118, 119). In BVDV RdRp, the primer loop is assisted with a GTP, possibly to stabilize the initiation NTP (114). The structure of BVDV polymerase complexed with GTP reveals that the nucleotide resides 6 Å away from the catalytic GDD motif and establishes interactions with residues from all three polymerase domains. Alanine mutations of residues within the GTP-binding sites (including C497, S498 and R517) severely impacted *de novo* RNA synthesis (98), indicating that the GTP-binding pocket is vital for the *de novo* step. Superimposition of a φ6 polymerase-NTP template structure onto the BVDV polymerase-GTP structure shows the ribose triphosphate moiety of GTP to be positioned as might be expected for an "i – 1" site of the synthesized RNA strand (114). The 3'-OH of GTP ribose is found close to the α- and β-phosphates of the NTP at the "i" priming site, probably to help in positioning the 3'-hydroxyl of initiating NTP for nucleophilic attack on the α-phosphate of incoming nucleotide at "i + 1" catalytic site. Nucleotide GTP also plays a role in stimulating *de novo* RNA synthesis by JEV RdRp (102) that is distinct from its role in BVDV polymerase. In JEV polymerase, GTP binds in a novel pre-initiation conformation that orders the conserved motif F and occludes NTP entry channel. In addition, binding of GTP to RdRp lowers its affinity for RNA template which may be resolved by addition of Mn^{2+} ions. These findings suggest that the pre-initiation state serves as a checkpoint to limit non-templated RNA synthesis by JEV RdRp during initiation and ensures only *de novo* template-dependent RNA production when Mn^{2+} is present.

Pestivirus and flavivirus polymerases have an additional N-terminal domain that may function during RNA synthesis. The polymerase of BVDV in the genus Pestivirus contains another 130 residues at its N-terminus with no known function. Mutational study demonstrated that deletion of the first 90 residues did not resulted in a loss of polymerase activity whilst truncation of the first 106 residues reduced both *de novo* and elongation reaction by 90% (98), denoting that residues 91-106 of the N-terminal domain may participate in both phases of RNA synthesis. Unique to flavivirus within the *Flaviviridae*, the viral genome contains a 5' cap structure and thus requires additional capping enzymes for genome replication. Flavivirus NS5 has an N-terminal methyltransferase domain connected to the C-terminal RdRp that is capable for methylations of both N7 position of guanine in the cap and ribose 2'-OH position of the first nucleotide of the RNA to form a type I cap structure (120). The presence of two enzymatic domains in a single polypeptide chain proposes the coupling of RNA synthesis and capping for efficient genome replication. The mechanisms for viral RNA capping would be described in the next section. Moreover, the respective functions of individual MTase and RdRp domains as well as possible inter-molecular interactions between the two domains in NS5 on flaviviral replication, particularly one of its members i.e. dengue virus (the main focus of my thesis), would be discussed in more details in later sections.

1.7 RNA capping process

In the eukaryotic cell, nascent cellular mRNAs are modified co-transcriptionally involving 5'-5' triphosphate linkage of a 7-methylguanosine (m^7G) moiety to the first nucleotide of the transcript (121). The presence of the cap enables protection of mRNA against degradation by 5'-3' exonucleases, efficient recognition of mRNA by ribosomal protein eIF4E for translation, and RNA splicing and export from the nucleus (122-124). RNA transcripts with unprotected 5' ends are degraded in cytoplasmic granules known as the processing bodies (P-bodies) (125). Nascent viral RNAs that are uncapped may be identified as "non-self" by the host cell, leading

to activation of antiviral innate immune response (126). In order to disguise self RNA and ensure efficient translation of proteins, viruses have evolved several strategies such as 5'-end RNA capping to generate the same cap structure as that of cellular mRNAs. Two viruses, vaccinia virus (from the dsDNA *Poxviridae* family) and orthoreovirus (from the dsRNA *Reoviridae* family), played a major role in the discovery and structural characterization of the RNA cap as well as in the mechanistic dissection of RNA capping event that is the same as that of their eukaryotic host (127-130).

1.7.1 Conventional viral RNA capping mechanisms

In the conventional pathway, capping reactions consists of (i) hydrolysis of the γ-phosphate of the primary transcript by an RNA 5'-triphosphate (RTPase), (ii) addition of guanosine 5'-monophosphate to the 5'-diphosphate RNA by a guanylyltransferase (GTase), and (iii) methylation at the N7 position of guanine by a cap-specific S-adenosyl-L-methionine (AdoMet)-dependent guanine N7-methyltransferase (N7 MTase), to generate the minimal cap-0 ($m^7GpppNp$) (131). Further methyl transfer reaction by ribose 2'-O-methyltransferases (2'-O MTases) can occur on nucleotides of the original transcript to produce cap-1 ($m^7GpppNm_{2'-O}$) and cap-2 ($m^7GpppNm_{2'-O}pNm_{2'-O}p$) structures respectively.

Cap structures can be incorporated to viral transcripts via several means. The first method consists of utilizing the host capping machinery by viruses such as majority of the DNA viruses as well as RNA viruses (ss(+)RNA *Retroviridae* and ss(-)RNA *Bornaviridae*) that synthesize their mRNA using cellular DNA-dependent RNA polymerase RNA pol II. The second mechanism includes using the "cap-snatching" strategy to obtain cap structures from host mRNAs by ss(-)RNA viruses from *Orthomyxoviridae*, *Arenaviridae* and *Bunyaviridae* families. The third way encompasses synthesizing the RNA cap using virally encoded capping machinery by ssRNA viruses. Viruses which encodes their own set of capping enzymes can

employ the conventional pathway by sequential action of RTPase, GTase and MTase, or the unconventional pathway that deviates from the eukaryotic mRNA-capping system.

Vaccinia virus follows the conventional RNA-capping mechanism and expresses a multifunctional mRNA capping enzyme, a heterodimer of D1 and D12 subunits, that functions as RTPase, GTase and N7 MTase (132). The N-terminal domain of D1 contains RTPase and GTase activities (133, 134) whilst the C-terminal of D1 harbors N7 MTase activity (135). Individual D1 protein exhibits weak intrinsic MTase activity and requires association with D12 subunit for optimal activity (136, 137). This heterodimer is also involved in termination of early transcription and transcription of intermediate genes (138-140). Cap formation is completed when viral VP39 protein catalyses 2'-O-methylation to generate cap 1 structure; VP39 is a dissociable subunit of viral poly(A) polymerase (VP55) that forms long poly(A) tails (141). ss(+)RNA viruses from the genus flavivirus (including DENV, YFV, WNV and JEV) also utilize the conventional RNA-capping pathway to synthesize the cap structure on its RNA. The RTPase activity was encoded in the multifunctional NS3 (protease-helicase) protein (142) and the GTase activity was proposed to be located at the N-terminal MTase domain of NS5 (143). Moreover, both N7 MTase and 2'-O MTase activities were assigned to the N-terminal domain of NS5 and they share the same cofactor-binding site for methyl transfer reaction (144, 145). Substrate repositioning is necessary to sequentially methylate N7 atom of guanine preceding 2'-O ribose of the first nucleotide. RNA secondary structures are important for both methylation processes whereby N7 MTase needs a long substrate with a specific stem loop structure and 2'-O MTase can methylate short RNAs (145).

dsRNA viruses from Reoviridae family produce multi-domain and -function proteins (including VP4 of bluetongue virus, λ2 of mammalian orthoreovirus and VP3 of cytoplasmic polyhedrosis virus) that are physically associated in an inner capsid which constitutes an assembly line that is able to carry out all the four reactions in the canonical pathway to yield

the cap-1 structure (146-148). The RNA substrate is shuttled from one domain to another during the sequential stages of cap synthesis and this process needs to be tightly regulated and coordinated by the various domains of the assembly line to attain complete cap formation.

Interestingly, some ss(+)RNA viruses from the *Picornaviridae*, *Caliciviridae* and *Astroviridae* families do not possess a cap moiety at the 5'-terminus of their mRNAs or genomic RNAs and use alternative strategies to direct mRNA translation. The 5' UTR of PV and EMCV in the *Picornaviridae* family can recruit the 43S preinitiation complex in a 5'-cap-independent manner, assisted by an IRES domain (149). In contrast, viruses from the *Caliciviridae* covalently attach their RNA 5' end to VPg protein which binds to the cap-binding protein eIF4E for translation initiation (150).

1.7.2 Unconventional viral RNA capping pathways

Viruses from the Mononegavirales order and *Togaviridae* family are capable of synthesizing viral RNA cap that is equivalent to host RNA cap via two distinct mechanisms. The Mononegavirales order comprises minus-sense non-segmented RNA viruses such as vesicular stomatitis virus (VSV) and rabies virus (from *Rhabdoviridae* family), measles virus (from *Paramyxoviridae* family), bornavirus (from *Bornaviridae* family) and Ebola virus (from *Filoviridae* family), that can cause serious illness in humans. These viruses encode a multifunctional L protein harbouring both RdRp and RNA capping activities. Different from the eukaryotic capping enzymes, the L protein from VSV (151, 152), spring viremia of carp virus (153), human respiratory syncytial virus (154) and chandipura virus (155) were shown to transfer GDP instead of GMP to the 5'-termini of the nascent transcript. During cap formation, an as-yet-unknown NTPase hydrolyzes GTP to GDP. The L protein contains GDP polyribonucleotidyl transferase (PRNTase) activity to transfer the 5'-monophosphorylated viral mRNA start sequence to GDP, producing GpppA capped RNA through a covalent enzyme-pRNA intermediate (156). The covalent bond with pRNA involves a conserved

catalytic histidine (H1227 of VSV) within the HR motif (157), different from the lysine residue used by conventional GTases (155). Mutagenesis study showed that the HR motif and a basic residue (R1221) nearby the motif are essential for PRNTase activity of VSV L protein at the step of enzyme-pRNA intermediate formation (157). The sequence of methylation is also not the same as the conventional pathway. The VSV MTase, located in domain VI of L protein (158, 159), transfers a methyl group to the ribose 2'-O position of the first nucleotide then to the guanine N-7 atom to form a cap-1 structure (160-162). The structure of VSV L protein was determined by electron cryomicroscopy (cryoEM), revealing three enzymatic domains (RdRp, PRNTase and MTase) and two structural domains (connector domain and C-terminal domain) (163). The RdRp resembles other polymerases, adopting a right-hand architecture with fingers, palm and thumb subdomains. The PRNTase (capping) domain contains two conserved motifs, GxxT and HR, at the active site for guanosine nucleotide binding and covalent RNA linkage respectively. Interestingly, a loop between residues 1157 and 1173 of PRNTase domain inserts into the catalytic site of the polymerase domain, suggesting coupling of capping to initiation of polymerization. The MTase domain of VSV can be superimposed on the MTases of flavivirus which has similar dual N7 and 2'-O methylation activities (145, 164, 165).

Alphavirus, a group of ss(+)RNA viruses such as Semliki Forest virus (SFV), sindbis virus and chikungunya virus within the *Togaviridae* family, synthesizes RNA cap-0 structure through a non-conventional mechanism. The nonstructural protein Nsp2 functions as RTPase to cleave the β-γ phosphate bond at the 5' end of viral RNA to form ppN-RNA (166). Nsp1 harbors N7 MTase and GTase activities to methylate the N-7 atom of a GTP molecule to produce m^7GTP before forming a covalent m^7GMP-enzyme complex involving a conserved catalytic histidine residue (H38 of SFV) that is only required for GTase reaction and not MTase activity (167, 168). The m^7GMP is then transferred to ppN-RNA to create the type-0 cap m^7GpppN-RNA. This capped RNA is not methylated at ribose 2'-O position of the first nucleotide. Conversely,

a methyl group is attached to the exocyclic N2 position of the cap structure as shown in SFV and Sindbis virus (169, 170), but the role of this methylation is not known. Since alphavirus RNA is not methylated at 2'-O ribose, it is uncertain on how the virus subverts host innate immune response during viral infection.

1.7.3 Cap-snatching mechanism

The three human pathogen families, *Arenaviridae*, *Bunyaviridae* and *Orthomyxoviridae*, contain ss(-)RNA that is segmented and do not encode a cap-synthesizing machinery. However, they have evolved alternative strategy for cap formation by seizing caps from host mRNAs to prime their own viral replication (171-173). Cap snatching begins by binding of 5'methylated cap structure of cellular mRNA to viral polymerase, followed by endonucleolytic cleavage of capped oligonucleotides from the 5'-termini of the mRNA and the short RNA is used as a primer for complementary viral RNA synthesis. The sequence, length and structure of the capped primer extensions on viral mRNAs can be heterogeneous amidst different viruses (174-180). The host mRNAs that lose its cap are targeted for degradation, leading to downregulation of cellular RNAs.

Cap snatching for influenza virus (from the *Orthomyxoviridae* family) serves as an example for viruses of the *Arenaviridae* and *Bunyaviridae* families, albeit it should be noted that the proteins involved in the pathway and the lengths of acquired sequences are different. The polymerase complex comprises of three subunits, namely PA, PB1 and PB2. The centre of PB2 lies the cap-binding domain to bind cellular mRNAs (181) which is subsequently snipped by the endonuclease domain at the N-terminus of PA (182, 183). The active site of PA contains a metal-coordinating histidine and acidic residues that are conserved and can bind two Mn^{2+} ions in a configuration comparable to other two-metal-dependent PD(D/E)XK endonucleases. On the other hand, both arenaviruses and bunyaviruses harbor a single L protein that exhibits polymerase and cap-snatching activities (184). Crystal structures of the endonuclease domain

in complex with Mn^{2+} ions for both Hantaan virus (from *Bunyaviridae* family) and Lassa virus (from *Arenaviridae* family) were solved and they displayed high structural homology. However, there are subtle changes in their active sites which cause the divalent ions to bind differently and impact *in vitro* nuclease activity. The endonuclease domain of hantavirus L protein shares the same active site configuration involving the characteristic catalytic histidine as the La Crosse bunyavirus and influenza A virus (orthomyxovirus) and demonstrated efficient endonuclease activity in isolation. Mutation of any active site residues influenced ion binding and dramatically reduced catalytic activity. For Lassa virus, the active site of the endonuclease domain contains E51 that replaces the conserved histidine in bunya- and orthomyxoviruses. This residue is unable to coordinate metal ions in the canonical way and the isolated enzyme showed a lack of endonuclease activity. Substituting E51 to histidine did not improve the activity as compared to wild-type enzyme. These findings suggest that the endonuclease of Lassa virus may require active site rearrangements or involvement from other parts of the L protein to achieve canonical ion binding for activity. The crystal structure and functional assay of Lassa nucleoprotein (NP) revealed that the C-terminal domain harbours 3'-5' exonuclease activity that participates in suppressing interferon induction and the N-terminal domain contains a deep cavity to bind m7GpppN cap structure, possibly involved in stealing cap from host mRNA (185). Similarly, the nucleocapsid protein (N) of hantavirus was proposed to play a role in cap acquisition by binding to and protecting capped mRNAs in cytoplasmic processing bodies (P bodies) (186). Notably, not all related nucleoproteins have the same features described above; the nucleoprotein (N) of Rift Valley fever virus (from *Bunyaviridae* family, now reclassified as *Bunyavirales* order) which encapsidates the viral RNA does not present any of these characteristics in the structure.

1.8 DENV RNA replication

DENV RNA replication requires three main components, namely the *cis*-acting factors, *trans*-acting elements (both viral and cellular proteins) and viral-induced membranes. The *cis*-acting elements refer to the structures in the vicinity of or found within both the 5' and 3'UTRs of the viral genome as mentioned in the text above (Section 1.4). At the 5' terminus, the 5'SLA binds to the viral polymerase to promote RNA replication and the cHP directs the selection of translation start region and replication of RNA (25, 26). At the 3' terminus, the variable region (VR) in domain I and the conserved 3'SL also participate in RNA synthesis (36, 42, 187). Importantly, the inverted complementary nucleotides present at both 5' and 3' ends, specifically the UAR, CS and DAR, mediate RNA-RNA interactions for the genome circularization. In this orientation, the polymerase which interacts with the SLA at the 5'UTR is close to the 3'end and is able to initiate negative-strand RNA production. RNA replication process takes place within a membrane-bound compartment for efficient production of RNA and viral morphogenesis. Positive immunolabeling of DENV-induced membranes with calnexin (a chaperone protein residing in the ER membrane), CLIMP-63 (a transmembrane protein of the rough ER), and synthaxin 17 (specifically localizes to the smooth ER) indicated that these membranes are derived from the ER (188, 189). In addition, membrane fractions extracted from cells infected with DENV demonstrated that the viral non-structural proteins NS1, NS2A, NS3, NS4A, NS4B and NS5 are colocalized to sites of RNA replication (188, 190-192). Non-structural proteins NS2A, NS2B, NS4A and NS4B are hydrophobic transmembrane proteins without reported enzymatic activities, but are shown to act as antagonists to inhibit type I interferon (IFN) signalling (65). Although it is still unclear on the specific part played by these proteins in virus replication and pathogenesis, they are crucial for the formation of active replication complex (RC). Trans-complementarity experiments revealed that NS1 functions early during RNA replication (193, 194), and that NS1-NS4A genetic interaction is necessary for replicase function (192). It could be probable that NS1 and

NS4A serve as structural components to anchor the complexes to ER-derived membranes. Moreover, yeast two-hybrid, biochemical pull-down and immunoprecipitation assays showed that the helicase domain of NS3 physically interacts with NS4B (195). This interaction dissociated NS3 from single-stranded RNA (ssRNA) and enhanced double-stranded RNA (dsRNA) unwinding activity, suggesting that NS4B regulates virus replication through its association with NS3. Within the functional centre of the RC are the multifunctional and multidomain NS3 and NS5 that contain several catalytic activities. The NS3 protein is an N-terminal serine protease, which together with its cofactor, NS2B, cleaves peptide bonds between viral proteins after translation, and its C-terminal domain exhibits RNA triphosphatase and helicase activities important for viral replication (142, 196-206). On the other hand, NS5 protein harbors a methyltransferase (MTase) at its N-terminal and a RNA-dependent RNA polymerase (RdRp) at its C-terminal for the capping and synthesis of viral RNA genome (83, 86, 164, 207, 208). Beside viral proteins, several host cellular factors such as elongation factor-1α (EF-1α), polypyrimidine tract binding protein (PTB), Y Box binding protein-1 (YB-1), T-cell intracellular antigen-1 (TIA-1) and the related protein (TIAR), as well as La, were identified using electrophoretic mobility shift assay (EMSA), UV-crosslinking and immunoprecipitation analyses to bind to viral genomic RNA and could also be involved during viral replication (209-214). Cellular proteins EF-1α, PTB and YB-1 can bind to the 3'SL region of DENV, but their precise function is unknown. It was hypothesized that PTB can positively modulate translation and replication during infection since increasing its expression level augments viral RNA levels (215-217). In contrast, YB-1 protein elicits an antiviral effect on DENV replication through translational repression (214). Colocalization of both TIA-1 and TIAR with dsRNA and NS3 in the perinuclear site of DENV-infected cells also advocates their roles in RNA synthesis (218). Another host factor, the La protein, can bind to both terminus of the DENV genome and be immunoprecipitated with NS3 and NS5 (219). However, *in vitro*

biochemical assay revealed that this protein blocks production of RNA in a dose-dependent way, implying its regulatory role in DENV replicative cycle.

Replication process initiates by *de novo* synthesizing the genome-length negative-sense intermediate RNA which appears as early as 3 hours after virus infection (194). The resultant dsRNA replicative form (RF) is then used as a template to produce additional plus-sense progeny RNA via a replicative intermediate (RI) complex. Pulse chase studies have identified RF and RI RNAs as precursors to genome RNA (220). RNA replication can be illustrated as asymmetric and semiconservative with the synthesis and accumulation of plus strands in approximately ten-fold in excess over the minus template strands (220, 221). The positive-sense genomic RNA is then packaged to form new progeny virus.

1.9 NS5 protein

Within the viral replication complex, NS5 is the best characterized and most conserved protein and performs its multifunctional roles in genome replication to synthesize both negative and positive-strand RNAs. Being the largest non-structural protein made up of 900 amino acid residues, the 103 kDa NS5 contains an N-terminal S-adenosyl-L-methionine (SAM)-dependent methyltransferase (MTase) and a C-terminal RNA-dependent RNA polymerase (RdRp) for the catalytic synthesis of viral RNA (222, 223). Besides its enzymatic functions in the RC, NS5 was shown to play a part in viral pathogenesis. This protein can exist free in the cytoplasm associated with NS3 protein or get phosphorylated and dissociate from NS3 to transport into the nucleus (224). The function of NS5 inside the nucleus is still not defined, however it could potentially interact with host factors and modulate host gene expression. Previous studies have shown that NS5 of specific flaviviruses could impair interferon-stimulated Janus kinase/signal transducers and activators of transcription (JAK-STAT) signaling, induce interleukin-8 transcription and secretion, as well as inhibit IFN-α signal transduction by blocking the phosphorylation of signal transducer and activator of transcription 2 (STAT2) (225-230).

Given the multiple roles played by NS5 during infection, it constitutes a valuable target for the development of antiviral drug.

1.9.1 The methyltransferase domain

The N-terminal region of the NS5 protein (residues 1-262 in DENV-3) functions as a dual methyltransferase (MTase) for catalyzing both guanine-N7 (N-7) and nucleoside-2'-*O* (2'-*O*) methylations in a sequential manner during the 5' end genome capping processes with the use of SAM as the donor of methyl group (144, 165, 207, 231). The formation of cap structure is crucial for maintaining the stability of mRNA and enabling efficient translation by host ribosomes (127, 232). The mRNA of DENV harbors a type I cap structure (5'-$^{7me}G_{ppp}A_{2'\text{-}O\text{-}me}$-G) (22) that is formed through four consecutive enzymatic reactions (Figure 1.6): (i) hydrolysis of the 5'-γ-phosphate of the nascent RNA by the RNA triphosphatase activity of NS3 protein (206, 233, 234), (ii) capping of the RNA 5'-diphosphate end with guanosine monophosphate (GMP) in a 5'-5'-triphosphate linkage by a guanyltransferase (GTase), possibly NS5 itself (143, 235), NS5 MTase methylates (iii) the N7 position of guanosine and (iv) ribose 2'-*O* atom of adenosine, sequentially forming a type 0 ($^{7me}G_{ppp}A$-G) (145, 165) followed by a type 1 ($^{7me}G_{ppp}A_{2'\text{-}O\text{-}me}$-G) cap structure (164, 222). Furthermore, NS5 MTase could methylate internal adenosines of the viral RNA and host ribosomal RNAs at the ribose 2'-OH moiety (236).

The two distinct methylation activities are independent, in which guanine N-7 precedes ribose 2'-*O* methylation ($G_{ppp}A$-RNA → $^{m7}G_{ppp}A$-RNA → $^{m7}G_{ppp}A_m$-RNA) (144, 145). Since flavivirus MTase bears one SAM binding site and another GTP pocket in its crystal structure (Figure 1.7) (205, 237, 238), repositioning of the RNA substrate must occur in order to accept methyl groups from SAM at the two different sites (239). The guanine N-7 of the RNA is first placed proximal to the SAM methyl donor to undergo N-7 methylation. This m7-capped RNA is then accommodated in the GTP-binding site to allow the first adenosine to be at close proximity to SAM for efficient 2'-*O* methylation. Structure and sequence alignments of

flavivirus MTase revealed a conserved K_{61}-D_{146}-K_{182}-E_{218} catalytic tetrad at the active site for methyl transfer reaction (164). Mutagenesis studies have demonstrated that the entire motif is imperative for 2'-*O* methylation whilst N-7 methylation only entails D_{146}, suggesting that the two processes employ different mechanisms (145, 165). In the context of WNV luciferase-expressing replicon, mutations within the catalytic motif substantially decreased or inhibited virus replication in cells. In the context of WNV virus, it has been shown that N-7 activity is vital for RNA replication (165, 239), while defects in 2'-*O* activity yielded attenuated viruses (165). As 2'-*O*-methylated viral RNA cap is required to subvert the IFN-mediated innate immune system, a loss in 2'-*O* activity would probably render the defective RNA to be eliminated in host cells and still allow viral replication to occur (75).

Earlier studies have demonstrated that different biochemical assay components and viral RNA elements are necessary for specific N-7 and 2'-*O* MTase activities (231). N-7 methylation needs RNA constructs containing 5' stem-loop structure with a minimum length of 74 nucleotides and specifically G and U bases at the second and third positions respectively. On the contrary, 2'-*O* methylation could be carried out using short RNA templates. The binding of short RNA substrates to DENV-2 MTase was enhanced in the presence of the first two authentic nucleotides (A and G bases) and they can be 2'-*O* methylated (120, 240). Optimizing the *in vitro* conditions for WNV MTase testing had shown that the best N-7 activity was achieved at neutral pH 7 with NaCl in the absence of $MgCl_2$, whereas 2'-*O* activity needs pH 10 with $MgCl_2$ in the absence of NaCl (165). A streptavidin bead-based scintillation proximity assay (SPA) was developed to detect *in vitro* DENV 2'-*O* MTase activity. Maximal level of 2'-*O* methylation was observed at physiological pH 7-8 in the presence of monovalent and divalent cations. The availability of this robust SPA assay makes it possible to conduct high-throughput screening of compounds targeting 2'-*O* methylation. In the past, two screening efforts were carried out with the use of SPA assay and another fluorescent polarization (FP)

assay (241), albeit no specific hits were identified (242). It is challenging to develop MTase inhibitors that are only selective towards viral MTase and do not target host MTases which are critical to methylate host protein and mRNA cap for their cellular functions (243). Since viruses incapable of 2'-*O* methylation are still replicative, they could be employed for live attenuated vaccine design to generate strong protective immune response against dengue infections (244, 245).

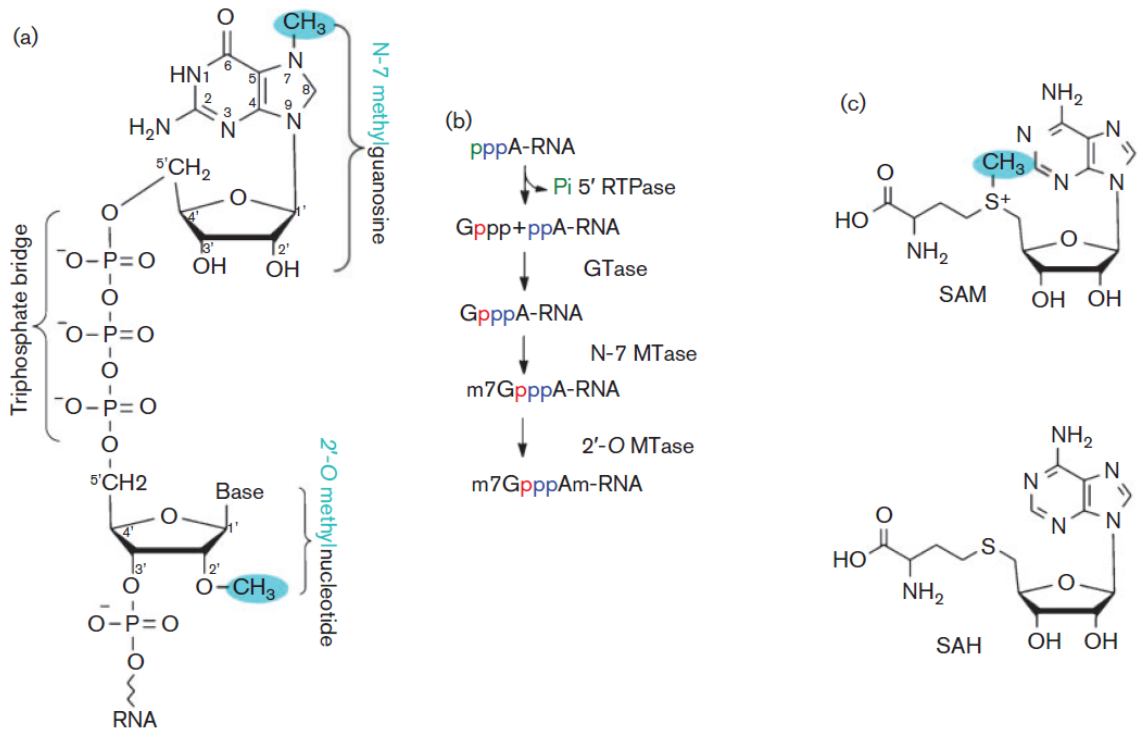

Figure 1.6 Mechanism of 5' cap formation. (a) The cap structure consists of an N-7 methylguanosine, a triphosphate bridge and a 2'-*O* methylnucleotide (adenosine in flavivirus). The N-7 and 2'-*O* methyl groups are indicated in blue. (b) The mechanism of cap formation. Four enzymes required for the formation of cap structure are denoted: RNA 5'-triphosphatase (5'RTPase), GTase, N-7 MTase and 2'-*O* MTase. Phosphates are colored to show their origins. (c) Structures of the methyl donor SAM and by-product SAH of methylation reaction. The transferred methyl group of SAM is colored in blue. Adapted from (75).

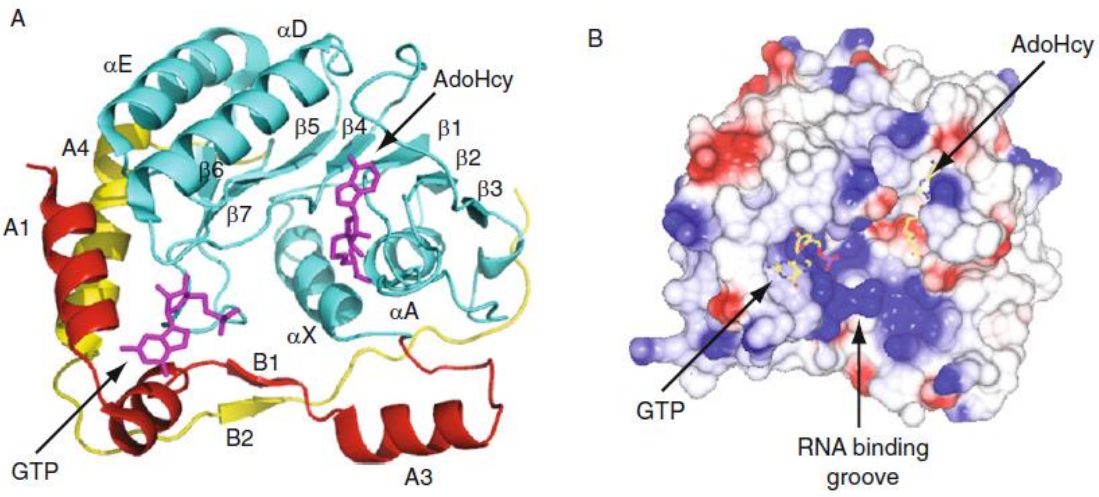

Figure 1.7 Structure of the DENV-2 MTase domain. (A) A schematic representation of the X-ray crystal structure of DENV-2 MTase (amino acids 1-296) in complex with GTP and AdoMet determined at 2.4 Å (PDB code: 2P1D). The N-terminal, core MTase and C-terminal subdomains are colored in red, cyan and yellow respectively. (B) A surface representation of the DENV-2 MTase shown in (A). Positively, neutral and negatively charged amino acids are presented in blue, white and red respectively. The predicted RNA binding groove is arrowed. Adapted from (164).

1.9.2 The RNA-dependent RNA polymerase domain

The C-terminal RNA-dependent RNA polymerase (RdRp) of NS5 (residues 273-900 in DENV-3) is capable of initiating *de novo* RNA synthesis without a viral RNA primer, and is able to carry out subsequent elongation activity to produce transient double-stranded replicative RNA intermediates in which the newly-generated negative strand RNA is used as a template to produce progeny positive-strand genome (83). Earlier studies using cytoplasmic extracts from DENV-2-infected cells and recombinant DENV-2 full-length NS5 and RdRp domain proteins resulted in the production of two predominant *in vitro* RNA products, namely the 1x and 2x products, from a subgenomic template containing 5' and 3' ends (83, 246, 247). Analysis by denaturing agarose gel electrophoresis revealed that the 1x product was a dsRNA composing of a newly synthesized minus strand RNA complementary to the input template, whilst the 2x product was a dsRNA hairpin generated by "copy-back" mechanism whereby the 3' end of the template folds back on itself to serve as a primer for minus strand RNA synthesis. This finding indicated that DENV polymerase can synthesize RNA without using a primer. The importance of genome cyclization, where complementary sequences in both 5' and

3'UTRs participate in long-range interactions, for synthesizing negative strand from the 3' end has been mentioned in earlier text. Another study further examined the template requirements for RNA synthesis and found that mutations in the complementary regions had no effect on plus strand RNA synthesis using negative-strand template, but affected minus strand RNA production using positive-strand template, suggesting that the cyclization of viral RNA is a prerequisite for negative-strand RNA synthesis (248). Moreover, the physical interaction between the polymerase and SLA present in the 5'UTR as demonstrated by atomic force microscopy and RNA binding assays (25, 27) brings the polymerase to the 3' initiation site via cyclization. SLA acts as a promoter for NS5 docking during viral replication. Mutations that disrupt the stem or top loop of SLA severely decreased viral replication whilst mutations that still maintain the structure did not significantly affect viral replication (25).

The crystallographic structure of DENV-3 RdRp (amino acids 273-900) has been solved and structural comparison with other RdRp structures from the *Flaviviridae* members showed that the overall fold is well conserved. The overall architecture of these polymerases is similar as they adopt a right hand closed conformation comprising a finger, thumb and palm subdomains (Figure 1.8) (86, 115). Extensive interactions were observed between the thumb and fingers subdomains to completely enclose the active site on the palm subdomain. Two perpendicular tunnels were observed in the structure. One runs vertically amid the thumb and fingers subdomains to allow access of ssRNA substrate to the catalytic site, another is situated at "the back" of the structure (Figure 1.8) to allow diffusion of incoming nucleoside triphosphates (NTPs) to the active site. The palm domain is highly conserved and contains the active site for catalysis. The GDD catalytic motif C comprises two strictly conserved aspartic acid amino acids, Asp-663 and Asp-664, which coordinate two Mg^{2+} metal ions and catalyze phosphodiester bond formation.

Since the bases at the ends of Flavivirus genomes are strictly conserved, there should be certain mechanisms to ensure nucleotide conservation at the terminus. In an earlier study, DENV RdRp was shown to possess unique structural and mechanistic features to modulate specificity and selectivity for nucleotide incorporation (249). The T794-A799 priming loop is required to enable precise *de novo* initiation and to shape the ATP-specific priming site. Deletion of residues in the priming loop forced the polymerase to incorporate GTP as the first nucleotide and to perform primer-dependent RNA synthesis. Residue H798 provides an initiation platform for stabilizing the stacking interaction between the priming ATP and the RNA template, although it does not differentiate between adenine and guanine (250). Interestingly, even without any RNA template, the polymerase could exclusively generate dinucleotide pppAG in the presence of Mn^{2+} rather than Mg^{2+} as a catalytic ion. In the presence of Mn^{2+}, the polymerase was also able to generate and elongate cognate dinucleotide by strongly discriminating against erroneous templates. It is possible that these mechanisms of maintenance, facilitated by the polymerase alone, could be applicable to viruses with conserved genomic RNA ends and to polymerases carrying out *de novo* viral RNA synthesis.

Following the production of short oligonucleotide, the RdRp opens up for elongation of double-stranded template-primer (83). These conformation changes require the priming loop to move out of the catalytic site, providing space for the polymerase to harbor and subsequently egress the nascent dsRNA.

As RdRp activity is necessary to synthesize viral RNA and is absent in human host cells, it constitutes an attractive target for antiviral therapeutic intervention. In subsequent section 1.10.2, past attempts to develop inhibitors targeting the viral polymerase are reported. Despite continuous concerted efforts, the development of effective antiviral drugs has not been successful so far. Perhaps one of the key challenges for NS5 is to understand the possible intra-

molecular interaction, inter-regulations and cooperativity between MTase and RdRp as a natural fusion protein that may provide novel insights for drug discovery and design.

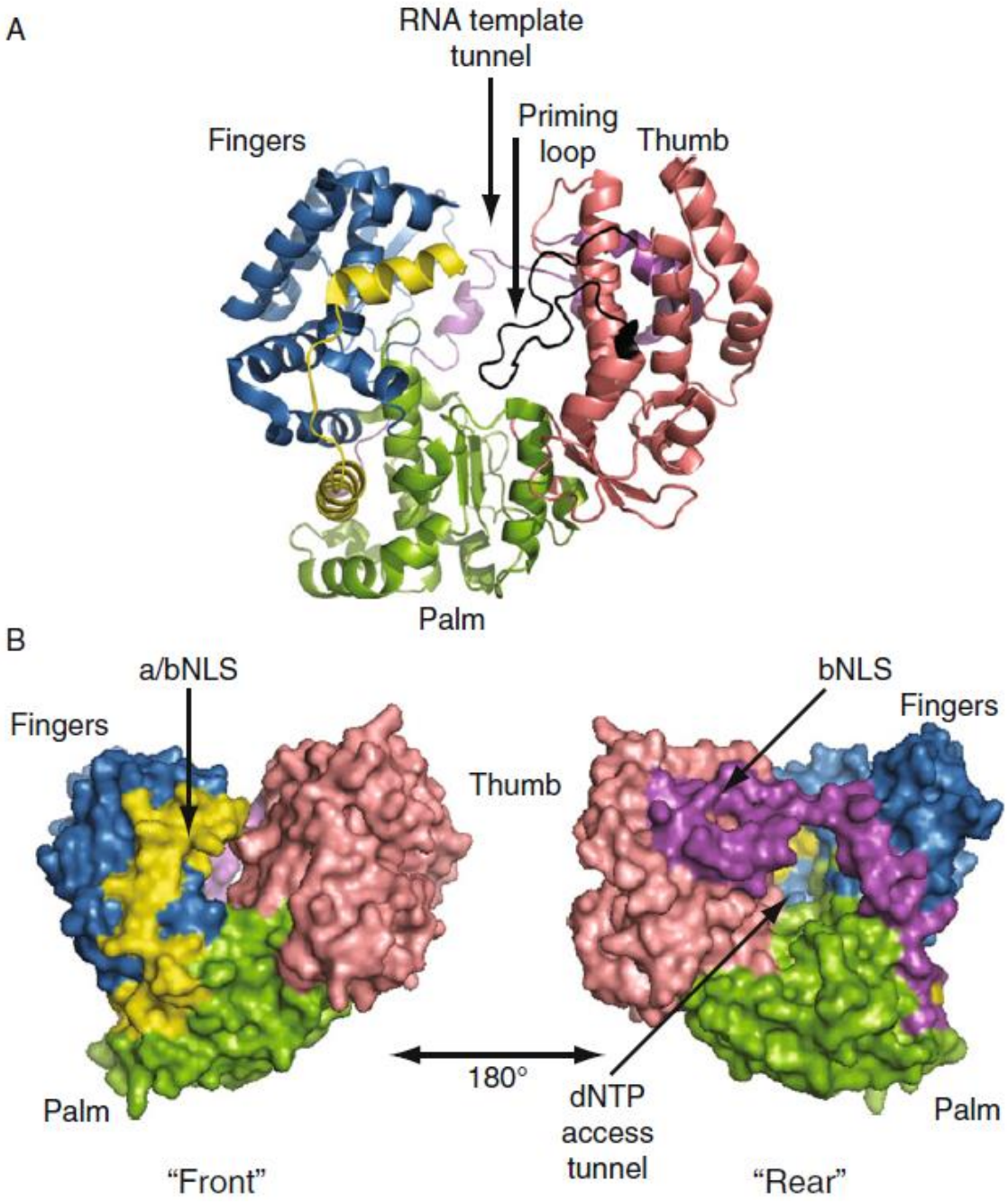

Figure 1.8 Structure of the DENV-3 RdRp domain. (A) A schematic representation of the X-ray crystal structure of DENV-3 RdRp (amino acids 273-900) determined at 1.85 Å (PDB code: 2J7U). The fingers, palm and thumb subdomains are colored in blue, green and salmon respectively. The priming loop is colored in black and arrowed. (B) Front and rear surface view of the DENV-3 RdRp structure. Adapted from (86).

1.9.3 NS5 inter-domain interactions

The viral replication processes carried out by NS5 not only require its interactions with viral RNA, viral proteins and host cellular proteins within the replication complex, but also involves

intramolecular conformational changes of NS5. Since both MTase and RdRp domains are physically linked within a single NS5 protein, it was suggested that RNA-cap formation is coupled to viral RNA replication. Both domain proteins are enzymatically active in isolation, albeit several studies have provided evidence of MTase and RdRp intra-molecular interactions and that their conformation or enzymatic function could affect each other.

Mutations of three surface exposed, charged residues Lys-46/Arg-47/Glu-49 to Ala in the DENV-2 MTase domain failed to produce infectious virus and resulted in a compensatory substitution of Leu to Val at residue position 512 of the RdRp domain which restored virus replicative ability (115). *In silico* docking of WNV MTase and RdRp domains revealed MTase Lys-46/Arg-47/Glu-49 loop fitted into a groove situated between the thumb and finger subdomains of RdRp (115). Similarly, the presence of genetic interaction between WNV MTase and RdRp was supported by mutagenesis analysis whereby the change of Asp-146 to Ser produced compensatory mutations of Lys-61 to Gln in the MTase domain which enhanced N-7 methylation activity, and Trp-751 to Arg in the RdRp domain which improved polymerase activity (251). Moreover, western blot analysis confirmed that recombinant WNV MTase co-immunoprecipitated with RdRp, providing direct evidence of the specific interaction between the two domains (252). Remarkably, a recent study showed that the presence of MTase in full-length (FL) NS5 mediates a higher RdRp activity by augmenting both *de novo* initiation and elongation as compared to NS5-RdRp alone (253). The enhancement of RdRp activity is probably attributed to an increased affinity of NS5 for ssRNA and priming nucleotide ATP during initiation, and also a greater affinity for primer-template RNA and an increased catalytic efficiency upon elongation. Together, these studies suggest that MTase domain makes dynamic and transient interactions with RdRp domain through a flexible linker, as supported by an earlier SAXS analysis which demonstrated that DENV-3 NS5 FL can adopt multiple conformations in solution (254).

1.10 Inhibitors of Flavivirus replication

1.10.1 Inhibitors of RNA capping

The RNA capping machinery can be targeted for anti-flaviviral drug discovery, particularly the essential enzymes involved in the conventional cap synthesis pathway. RNA triphosphatases (RTPases) catalyze the first step of cap formation by hydrolyzing the RNA 5'-γ-phosphate and can be found in flavivirus NS3 which also carries helicase and NTPase activities to unwind dsRNA. The RTPase active site can be superimposed onto NTPase active site containing DEAD/H sequence and providing energy for helicase movement along RNA (203). Inhibition at this site should be bi-functional, suppressing both RTPase/NTPase and helicase activities. A few groups have reported inhibitors targeting the NS3 helicase via structure-based approach, *in vitro* enzymatic or cell-based assays (255-257). High throughput molecular docking had identified two compounds that significantly reduced unwinding activity of JEV NS3 helicase and inhibited JEV propagation in cells (255). The EC50s of the compounds were 25.67 μM and 23.50 μM, and they exhibited low cytotoxicity. These compounds were shown to bind the RNA unwinding channel using simulated docking, in line with the results of enzyme inhibition assay and amino acids involved in the interactions could be used to facilitate future compound optimization. A widely-used anti-helminthic drug, Ivermectin, was discovered by *in silico* docking to bind in the NS3 ssRNA binding pocket and exerted inhibitory effects on the helicase activity and replication of several flaviviruses such as YFV, TBEV and DENV, albeit to different extents (258). High-throughput screening using a whole-virus assay detected a novel benzoxazole inhibitor, ST-610, that presented antiviral effects on DENV replication *in vitro* and *in vivo* (257). A virus variant conferring compound resistance was found to harbor a mutation (A263T) in the NS3 helicase domain, and molecular-beacon-based helicase assay supported the specific inhibition of ST-610 on helicase as the compound suppressed helicase RNA unwinding activity. Another group showed that ML283 can potently inhibit NS3 helicase

and HCV replication without significant cytotoxicity (259). They further analyzed a small library of ML283 analogues and pyrrolones, and confirmed that ML283 analogues inhibited DENV3 NS3-catalyzed RNA unwinding and replication whilst inhibitors with pyrrolone scaffold substantially reduced both DENV and WNV replication in cells (256). Besides targeting the domains of NS3, the interaction between NS3 protease and its cofactor NS2B important for catalytic processing of viral polyprotein could also be targeted for antivirals development. Several studies have identified non-peptidic inhibitors including flavonoids (260), diaryl (thio)ethers (261), thiadiazaoloacrylamide derivatives (262) and SK-12 (263) which demonstrated low micro-molar IC50 or EC50 against DENV NS2B-NS3pro. For these inhibitors, their binding pattern were predicted and further development would be greatly accelerated by the elucidation of cocrystal structures to validate the putative interactions. Recently, crystal structure of ZIKV NS2B-NS3pro in complex with a peptidomimetic boronic acid inhibitor, cn-716, revealed that the inhibitor fits in the substrate-binding site and forms a cyclic diester with glycerol as well as establishes interactions with residues (D83, D129 and S135) of NS2B (264). This compound reversibly inhibited ZIKV NS2B-NS3pro at IC50 of approximately 0.25 μM and K_i of 0.04 μM, and was not cytotoxic in cells. Thus, the crystal structure serves as a good starting point to facilitate the design of more specific and potent drugs for anti-ZIKV inhibition.

The second step of RNA capping reaction to attach a GMP molecule onto the pre-mRNA is performed by guanylyltransferases (GTases). In flaviviruses, the GTase activity was proposed to lie at the N-terminus of NS5 protein which also carries MTase activities to form cap structure (143). The MTase domain of NS5 contains a GTP-binding pocket and earlier studies have reported the ability of ribavirin (guanine nucleotide analogue) and 2-thioxothiazolidin-4-one analog, BG-323, to displace GTP from the DENV capping enzyme (265, 266). BG-323 was shown to decrease guanylation activity *in vitro*, present antiviral efficacy in DENV replicon

assay and inhibit replication of WNV and YFV. Moreover, resistance of WNV to the compound was not detected after long-term culture experiment (267). However, it is probable that the antiviral effect detected may be attributed to the compound interfering with the MTase activity of the capping enzyme or intervening with aldose reductase since BG-323 has a structure that resembles the known FDA-approved drug, Epalrestat, that targets this cellular protein for improving the conditions of patients with diabetic neuropathy (268). Additional experiments need to be carried out to confirm the mechanism of action for this series of compounds. The same group tested the antiviral effects of BG-323 in murine model and observed a lack of *in vivo* efficacy which may be due to its short half-life ($T_{1/2}$) in mice and human plasma protein binding (267). Future studies would be necessary to ameliorate the effects of plasma protein binding and improve compound stability and half-life *in vivo*. Ribavirin is a broad-spectrum antiviral agent used to treat infection caused by RNA viruses such as hepatitis C virus (HCV) (269-271). Similar to BG-323, ribavirin 5'-triphosphate (RTP) and its analogues compete against GTP for binding to DENV NS5 MTase (266). Crystal structure of DENV NS5 MTase in complex with RTP showed that the RTP molecule binds in the previously identified GTP-binding site (164) and forms atomic contacts with MTase similar to GTP. In the enzyme inhibition assay, RTP moderately reduced RNA 2'-*O*-methyltransferase activity of DENV at IC50 of about 101 μM. These findings suggest that RTP may compete with viral RNA cap structure to bind the GTP/RNA cap binding site of NS5 MTase, thereby preventing efficient cap 2'-*O* methylation.

The NS5 methyltransferase (MTase) domain mediates both guanine N-7 and ribose 2'-O methylations at the third and fourth steps of RNA capping pathway and uses the same SAM-binding site for the two methyl transfer reactions (145, 164). The inhibition of N-7 MTase activity is expected to cause a detrimental effect on viral replication as it prevents viral RNA translation, and this notion is corroborated by previous studies in which mutation (D146A of

WNV) that impaired N-7 activity abolished viral replication (145, 165). On the contrary, mutagenesis study indicates that inhibition of 2'-O activity yielded attenuated viruses in cells (165). Nonetheless, since a loss of methyl group at the ribose 2'-O atom induces type I interferon expression through MDA5-mediated sensing (272), this exemplifies the importance of 2'-O methylation. The SAM-binding pocket of MTase can be targeted and SAM analogues such as sinefungin, a broad-spectrum MTase inhibitor, has been shown to bind to this pocket of several flaviviruses (235, 237, 273). The binding mode of this ligand is similar to SAM without having extra contacts with the protein. Yet, the affinity for sinefungin is higher than SAM (274) which is translated to better inhibitory efficacy as compared to SAH in N7 and 2'-O assays (275). Nevertheless, this compound cannot be used as an antiviral drug as it lacks specificity towards viral MTase. Thus, rational design approaches were carried out to modify SAH by adding substituents to the adenine ring (276). SAH derivatives harboring hydrophobic extensions from the N6 position of adenine moiety showed improved potency and selectivity against human DNA, RNA and histone MTases. Crystal structure of DENV MTase-compound 10 complex revealed that the N6 benzyl ring fits into a unique cavity located above the SAM-binding site in flavivirus MTases and generates conformational changes in the residues (F133 and R163 of DENV-3) lining the pocket. Although this compound produced good inhibitory profile *in vitro*, improvement in cell permeability is required to achieve antiviral activity in cell culture. Several groups have performed virtual screening and docking method to identify potential binders against flavivirus NS5 MTase that were subsequently assayed *in vitro* to examine activity (277-281). Some molecules demonstrated inhibitory properties at micromolar IC50. Remarkably, two potent compounds, NSC306711 and NSC610930, inhibited viral MTase with low cytotoxic effects (281). The high potency of NSC306711 may be due to extra interactions of this larger compound with residues outside the SAM-binding pocket, thus improving the specificity towards flavivirus but not host MTase proteins. An interesting

approach was used recently to link fragment hits obtained from fragment-based X-ray crystallography screening targeting DENV MTase, leading to the production of a novel series of inhibitors that showed improved potency compared to the initial hits (282). In the past, two screening efforts were carried out to look for inhibitors of DENV MTase, as briefly mentioned in section 1.9.1. The first screen utilized the scintillation proximity assay (SPA) to assess N7 and 2'-O activities (240, 275) for approximately 60,000 compounds, but failed to identify any specific hits. It is possible that expanding the number of compounds for screening would increase the chance of obtaining specific inhibitors. However, further screening was not executed due to the high costs of reagents required for the assay. The second screen employed a fluorescent polarization assay (241) to measure 2'-O activity for 250,000 compounds, and was also unsuccessful in getting any specific hits. Given the unsatisfactory outcomes of enzymatic activity-based screens, it may be more feasible to obtain hits via structure-guided strategies, as evidenced by the success in discovery and design of potent inhibitors illustrated earlier. The availability of cocrystal structures with bound inhibitors would greatly facilitate optimization of compounds to achieve enhanced potency and specificity towards flaviviral MTases.

1.10.2 Inhibitors of RNA synthesis

The RNA-dependent RNA polymerase (RdRp) plays a central role in viral RNA synthesis and represents the most attractive drug target for antiviral research. There are two classes of viral polymerase inhibitors, i.e. nucleoside/nucleotide analog inhibitors (NIs) and non-nucleoside inhibitors (NNIs). NIs must be transformed into active triphosphates intracellularly before competing with natural NTP substrates and acting as RNA chain terminator to stop elongation. Some NIs, such as ribavirin, can be added into a growing RNA chain without termination and subsequently cause mutations in the daughter RNAs (283, 284). Ribavirin 5'-triphosphate (RTP) is a guanosine analog and is described in previous section 1.10.1 to interfere with viral

RNA capping. Here, poliovirus polymerase ($3D^{pol}$) was shown to be able to incorporate RTP in the viral RNA opposite either cytosine or uracil without any significant difference in its incorporation efficiency facing the two complementary bases (283). Similarly, CMP and UMP can be incorporated into a template containing ribavirin and the rate of their incorporation was about 500-fold more rapid than incorporation of RMP facing cytidine and uridine. In addition, $3D^{pol}$ was capable of extending the RNA chain after the position of RTP incorporation, proving that ribavirin is not a chain terminator. Cell-based assays showed that ribavirin drastically impaired virus production, but only moderately affected RNA replication since levels of poliovirus RNA was comparable to wild-type levels. Sequence analyses of cloned cDNA of capsid protein from virus grown in poliovirus-infected cells in the presence of ribavirin revealed that the genomes contain an increase in G-to-A and C-to-U transition mutations caused by incorporation of RTP as a GTP analog during plus- and minus-strand RNAs synthesis, respectively. Thus, ribavirin is a powerful mutagen that may exert its antiviral effects through introducing replicative errors. Notably, this drug has proven to be effective in treating infections caused by influenza virus (285), Lassa fever virus (286) and Hantaan virus (287), but has weak activity against flaviviruses (288-290). Prophylactic ribavirin treatment of rhesus monkeys infected with DENV-1 virus had little or no effect on viremia (288). However, ribavirin analogues such as 5-ethylnyl-1-β-D-ribofuranosylimidazole-4-carboxamide (EICAR) exhibited higher activity than ribavirin against YFV and DENV, as measured by a 20- to 35-fold improvement in EC50 (289). Correspondingly, EICAR was able to compete with GTP for binding to DENV NS5 MTase and could possibly also inhibit RNA 2'-O-methyltransferase activity like RTP (266). Hence, derivatives of ribavirin constitute potential drug candidates for anti-flaviviral activity and further exploration of their mechanism of action in either MTase or RdRp may lead to the development of more selective and potent inhibitors.

NIs represents the largest class of approved antiviral drugs and present several advantages for drug development. In the case of DENV, nucleoside analogs targeting RdRp should be broad-spectrum and exhibit pan-serotype inhibition. Also, they should display a higher barrier for resistance emergence since the residues at the active site of polymerase are mostly conserved. Nevertheless, there are challenges in the development of nucleoside analogs for therapeutics. It is difficult to predict the structure-activity relationship (SAR) of NIs as they depend on host kinases to convert into active triphosphates. Hence, potent NIs are usually discovered serendipitously. Additionally, mitochondrial toxicity is a common side effect as toxicity is unpredictable and is frequently missed out *in vitro*. This usually involved inhibition of the human DNA polymerase gamma which leads to a reduction in mitochondrial DNA level, especially for NIs used for treating HIV-1 infection (291). Thus, animal toxicological studies would be required to investigate potential side effects of compounds. Many NIs of DENV were derived from anti-HCV drugs as the two viruses belongs to the same *Flaviviridae* family. The 2'-C-methyl-substituted ribonucleosides which was active against HCV RdRp also harbors anti-flaviviral activity (292). Inhibition of several flaviviruses such as DENV, YFV and BVDV by 2'-C-methyladenosine ranges from an EC50 of 1.6 to 5.1 μM. However, this compound displayed susceptibility to get converted to 2'-C-methylinosine by host adenosine deaminase and had limited oral bioavailability in the rat (293). Incorporation of 7-deaza modification into 2'-C-methyladenosine resulted in the discovery of MK-0608 that exhibited improved pharmacokinetic properties as deamination of the compound was reduced, however there was an EC50 shift to 15 μM (294). Potency was regained to EC50 of 0.64 μM by replacing the 2'-C-methyl with 2'-ethylnyl group to produce NITD-008 (295). This adenosine analogue functions as a chain terminator during RNA polymerization and strongly blocked DENV replication both *in vitro* and *in vivo* (242, 243, 295). Besides DENV, it also demonstrated antiviral activity against other flaviviruses such as HCV. This compound entered preclinical

animal safety studies, but was terminated due to severe side-effects observed in both rats and dogs. For guanosine analogues, 2'-C-methylguanosine inhibited several members of flavivirus such as DENV and WNV at weak EC50 of 13.6 and 30 μM respectively (292) whereas its modified derivative, INX-08189, significantly increased potency in nano-molar range with no mitochondrial toxicity (296). Besides adenosine and guanosine analogues, cytosine analogue also showed anti-viral activity *in vitro* (297, 298). Balapiravir (an ester prodrug of cytidine analogue, 4'-azidocytidine) was originally developed for HCV treatment but its clinical development was discontinued due to serious adverse effects observed in patients (299). Moreover, treatment of dengue patients with this drug did not reduced viremia, NS1 production and fever duration although it was well tolerated (300). Chronic HCV infection can be treated with sofosbuvir, a marketed anti-HCV prodrug which demonstrated excellent safety and efficacy profile (301). Recent study reported good *in vitro* inhibition of DENV polymerase using this prodrug with EC50 of 0.4 μM (302), indicating the potential of sofosbuvir as an anti-DENV inhibitor. This drug also showed inhibitory effects towards zika virus (ZIKV) polymerase (303), suggesting that the same enzyme inhibitor could be used to treat infections caused by members from one family since the viruses share same morphology and replication mechanism. In all, the results demonstrated proof of concept in the potential of NIs to be developed for flavivirus therapy.

Another class of viral polymerase inhibitors is the NNIs which are usually non-competitive and bind to allosteric sites in the polymerase, blocking conformational changes crucial for its enzymatic functions. Highly specific NNIs could reduce off-target inhibitions and lower cytotoxicity. However, the difficulties related to NNIs include the emergence of resistant viruses and to have cross-serotype inhibitory properties as there is a lesser tendency to retain the residues lining the allosteric pockets. For instance, escape mutation that arose from benzimidazole-containing inhibitors was mapped to proline 495 of the HCV NS5b polymerase

thumb domain, conferring resistance to this class of compounds (304, 305). NNIs are mostly discovered in high-throughput screening campaigns using RdRp biochemical assays. One compound identified through elongation scintillation proximity assay (SPA), NITD-2, which likely inhibits polymerase activity by targeting the RNA tunnel of DENV RdRp, could not be advanced due to poor cell permeability (242, 306). *N*-sulfonyl-anthranilic acid derivatives, optimized from a hit discovered via primer extension-based RdRp assay, were also found to bind the RNA template tunnel and inhibit DENV RdRp at IC50 of 0.7 μM (306). The inhibitory effect of this compound was specific to DENV and not to other polymerases from *Flaviviridae* family or the host cell. Another NNI identified through fluorescent-coupled elongation assay (307), NITD-107, binds to the RNA binding groove but exhibited only weak antiviral activity against DENV polymerase and replicon (308). Furthermore, several NNIs of HCV NS5B such as tegobuvir (of unidentified binding site) and filibuvir (thumb domain site II inhibitor) progressed to clinical testing but did not produce desired outcomes (309). The challenges in developing NNIs highlighted the importance to validate the biological relevance of these allosteric pockets which might provide new insights to obtain better inhibitors.

1.11 Next challenges in Flavivirus RNA capping and RNA replication research

The flavivirus NS5 is a naturally fused protein comprising a methyltransferase (MTase) and a RNA-dependent RNA polymerase (RdRp), in which both are essential for virus replication in the host cell. Little is known about how the viral polymerase coordinates their nucleotide synthesizing activity with the 5'-capping activity of methyltransferase in the overall scheme of genome synthesis. The crystallographic structures of individual domains have been solved providing a structural basis for the design of drugs that may alter the enzyme's dynamics (86, 164). Subsequently, cocrystal structures of these domain proteins in complex with small-molecule inhibitors were obtained and are useful to understand the mode of actions of these antiviral compounds (266, 276, 308, 310). However, drug discovery efforts have not yielded

suitable leads and could be impeded due to the lack of a crystallographic structure of the full-length NS5 protein to understand the *in cis* regulation on RdRp by their N-terminal MTase domain. Elucidation of this structure would shed light on the possible interplay between the two domains in viral cap formation and genome replication as well as NS5-related molecular interactions for viral replication and pathogenesis during infection.

Another active area of research is to understand how the viral RNA substrate is recognized by the two enzymatic domains of NS5 to get replicated and capped. The mechanism for flavivirus guanylyltransferase and methyltransferase activities of the capping enzyme have been extensively studied ever since the structure of this enzyme was determined (164, 165, 231, 239). The N-terminus of NS5 was speculated to possess guanylyltransferase activity based *in vitro* experiments which showed that WNV NS5 was able to form a covalent enzyme-GMP intermediate in the presence of GTP as a substrate and has the ability to transfer GMP to RNA transcript containing diphosphate 5'-end (143). Likewise, Wesselsbron virus MTase becomes covalently linked to GMP via a lysine residue K38 following incubation with GTP molecule (235), hinting possible successive event to transfer the guanine group to diphosphate end of an acceptor RNA. The same domain with putative GTase function is also responsible to carry out N7 and 2'-O methylations for type I cap formation. Crystal structure of DENV-3 MTase in complex with a 5'-capped RNA octamer was solved and it shows the cap moiety of RNA ligand docking in the GTP binding pocket but the rest of the substrate did not extend in the putative basic RNA binding groove (238). This structure may represent the product of guanylylation step prior to the N7 and 2'-O methylation processes that require conformational rearrangements to bring the RNA substrate near to the SAM donor site for methyl transfer reaction. Therefore, in order to understand how flavivirus guanylyltransferase works, it would be necessary to dissect the mechanism of how the capping enzyme binds to diphosphorylated RNA substrate. Furthermore, trapping the capping enzyme in a catalytically relevant complex with its

substrates would open up new structural and functional insights on GTase, N7 and 2'-O MTase activities.

The flavivirus RdRp is responsible to copy the viral genetic code via *de novo* initiation followed by processive elongation of RNA synthesis. Major challenges remain in deciphering the mechanism of polymerase catalysis, translocation on the RNA template and the conformational changes involving the priming element during the transition from initiation to elongation phase. Remarkably, the stalled ternary structures of HCV NS5B in both primed initiation and elongation states have been determined, revealing conserved residues in the active site play a role in positioning the primer for nucleophilic attack on the incoming NTP as well as the different orientations of the thumb domain β-loop and C-terminal membrane-anchoring tail, from occupying the active site cavity in apo state to retraction during primed initiation formation and subsequently leaving the active site to accommodate the nucleic acid during elongation (311). Crystal structures of stalled elongation complexes (EC) of poliovirus, coxsackievirus and rhinovirus also provided molecular details associated with nucleotide selection and catalysis (93, 95). Therefore, in order to expand our knowledge on flaviviral RNA replication and to unravel the structural changes that occur during various steps of RNA synthesis, it is important to elucidate catalytically-relevant polymerase ternary complexes with its substrates which may in turn provide possibilities for the discovery and development of new inhibitors. Moreover, we still lack information about the macromolecular organization in the replication complex comprising of viral and cellular components in genome synthesis. Molecular interactions were illustrated between NS3 and NS5 proteins (224) that may be important for their coordinated activities in the individual steps of RNA synthesis and 5'-RNA cap formation (312), as well as between NS3 and NS4B for enhancement of the helicase activity of NS3 (195, 313). These interactions may account for the anchoring of viral replication machinery to ER membranes owing to the integral membrane association of NS4B

and NS2B (cofactor of NS3 for its protease function). Distinct spatial arrangements of the proteins in the replication complex may exist to allow coupling of dsRNA winding, RNA polymerization and capping of the newly-synthesized RNA. Future studies could look at how the membrane-bound replication complex is assembled and how this complex synchronizes the individual events of genome replication.

1.12 Aims of this thesis

My PhD research aims to reveal valuable information on the functions and dynamics of NS5 protein along with its molecular interactions with substrates and inhibitors, and to validate it as an attractive target for the development of anti-flaviviral drugs. There are four objectives to my project and they are described below.

(i) To examine how dengue virus NS5 performs its versatile, multi-functional roles in viral replication

This study was aided by the resolution of the first crystal structure of the DENV-3 FL NS5 which occurred when I first embarked on my PhD research. The functional significance of intra-molecular/domain interactions and the flexible interdomain linker for viral replication, growth and infectivity was explored using the following techniques.

Experimental work

- Site-directed mutagenesis was carried out to generate interdomain interface and linker mutations in the context of recombinant DENV-2 or -4 NS5 FL protein, DENV-2 or -4 subgenomic replicon and DENV-4 infectious clone.
- Biochemical and biophysical assays: Thermal stability, MTase and RdRp activities of mutant proteins were measured using thermo-fluorescence assay, scintillation proximity assay (SPA) and fluorescence-based alkaline phosphatase-coupled polymerase assays (FAPA), correspondingly. Steady-state kinetic measurement was also performed to determine mechanism of altered RdRp activity using FAPA.

- Cell-based assays: Replicon and virus growth fitness were examined using *renilla* luciferase assay, immunofluorescence assay (IFA), plaque assay and qRT-PCR.

(ii) To understand specific viral RNA recognition and 2'-*O* methylation by DENV NS5

Following the structure determination of DENV-3 FL NS5, the crystal structure of a ternary complex between DENV-3 NS5 protein, an authentic cap-0-viral RNA substrate and SAH was determined representing a catalytically-competent complex for methylation. The importance of amino acids lining the RNA binding groove as well as interacting nucleotide of the RNA substrate for specific viral RNA recognition and 2'-*O* methylation by DENV NS5 MTase was investigated as follows.

Experimental work

- Site-directed mutagenesis was carried out to generate mutations of NS5 MTase residues in the context of recombinant DENV-4 MTase and NS5 FL proteins and DENV-2 infectious clone, as well as mutations of the second nucleotide of viral RNA using capped-DENV-4 5' UTR 1-110 nt RNA template and in DENV-2 infectious clone.
- Biochemical and biophysical assays: Thermal stability, MTase 2'-*O* and RdRp enzymatic activities of mutants were measured using thermo-fluorescence, SPA and FAPA assays, respectively.
- Cell-based assays: Virus growth fitness was examined using plaque assay, qRT-PCR and IFA.

(iii) To examine biological relevance of allosteric binding pockets of DENV RdRp inhibitors

In-house (conducted at NITD) compound screening campaign and fragment-based screening exercise in combination with structure-guided approach targeting the DENV RdRp identified several non-nucleoside inhibitors that bound to allosteric pockets by X-ray crystallography. One class of the inhibitors bound at the thumb/palm interface near the enzyme active site

(termed “N pocket”), whilst another interacted with the finger-thumb interconnecting loops, resulting in an ordered F1 motif. The relevance of these inhibitor binding sites in the RdRp for viral replication and the mechanism of action of these compounds were assessed using the following approaches.

Experimental work

- Site-directed mutagenesis was performed to generate alanine mutations of residues lining the pockets in the context of recombinant DENV-4 NS5 FL protein and DENV-4 subgenomic replicon.
- Resistant mutations raised using N-pocket compounds were also engineered into DENV-2 subgenomic replicon and DENV-2 infectious clone.
- Biochemical and biophysical assays: Thermal stability, RdRp activity and *dn*I IC50 of mutants were measured using thermo-fluorescence and FAPA assays. The inhibition mode of N-pocket compounds was studied using order-of-reagent addition and steady-state kinetic competition experiments.
- Cell-based assays: Replicon and virus growth fitness were examined using *renilla* luciferase assay, IFA, cell viability assay, plaque assay and qRT-PCR.
- Co-crystallization of DENV-3 FL NS5 in complex with N-pocket compounds was carried out to examine the binding mode as compared to the polymerase domain.

(iv) To obtain a co-crystal structure of an elongation complex of DENV RdRp bound to dsRNA

Further dissection of the interactions between NS5 RdRp and viral RNA would be informative in elucidating how the viral RNA is recognized and replicated, and possibly facilitate drug discovery and design targeting the RdRp. A systematic approach was taken from assembling an active elongation complex, to profiling numerous dsRNA templates and selecting those with good binding and elongation profile, and finally generating stable polymerase-RNA elongation

complexes for crystallization.

Experimental work

- Development of fluorescence polarization (FP)-based assay to measure binding affinity and elongation activity of DENV NS5 protein with various distinct RNA constructs
- Assembly of functional elongation complexes and crystallization of these complexes using commercial screening kits
- Optimization of buffer conditions with observed crystals

2 MATERIALS AND METHODS

2.1 Cells

For transfection, baby hamster kidney cells (BHK-21-US) were maintained in Dulbecco's modified Eagle's medium (DMEM; Gibco) supplemented with 10% fetal bovine serum (FBS) and 1% penicillin/streptomycin (P/S) in 5% CO_2 at 37°C. For plaque assay, baby hamster kidney cells (BHK-21-NITD) were propagated in Roswell Park Memorial Institute (RPMI) 1640 (Gibco) supplemented with 10% FBS and 1% P/S in 5% CO_2 at 37°C.

2.2 Construction of DENV replicon cDNAs

2.2.1 Generation of DENV-4 NS5 interface mutant replicons

Mutations K95A, K95A/N96A (K95A/K96A in DENV-3), Y119A, R263A (R262 in DENV-3), E268A (E267 in DENV-3), E270A (E269 in DENV-3), R353A (R352 in DENV-3), R362A (R361 in DENV-3) and K596A (K595 in DENV-3) in the DENV-4 NS5 sequence were engineered into the subclone, pACYC-DENV4-F shuttle vector, using QuikChange II XL site-directed mutagenesis (SDM) kit according to the manufacturer's protocol (Stratagene). This plasmid harbours nucleotides 5351-10652 (from NS3 to 3'UTR) from the DENV-4 MY01-22713 strain, followed by Hepatitis delta virus ribozyme (HDVr) sequence. After sequence verification, the plasmids were digested with NotI and KpnI restriction enzymes and inserted with a PCR product comprising nucleotides 1-5350 downstream of the T7 promoter in which the region from nucleotides 217-2331 has been replaced by renilla luciferase and foot-and-mouth disease virus 2A protease cDNAs. DENV-4 replicon with R_{luc} reporter (pACYC-I-DV4 Rep; Figure 2.1) was used to study the effects of mutations on viral replication. After cloning, all constructs were checked by DNA sequencing again to ensure the presence of correct mutations before proceeding to subsequent experiments. A list of primers used for mutagenesis and cloning is available in Table 2.1 and 2.2.

2.2.2 Generation of DENV-4 NS5 3_{10}-helix mutant replicons

Mutations S264A (H263 in DENV-3), V265A (V264 in DENV-3), S266A (N265 in DENV-3) and T267A (A266 in DENV-3) in the DENV-4 NS5 sequence were introduced into pACYC-DENV4-F shuttle vector using QuikChange II XL SDM kit. Subsequent steps to generate replicon cDNA were performed as per section 2.2.1. A list of primers used for mutagenesis is available in Table 2.3.

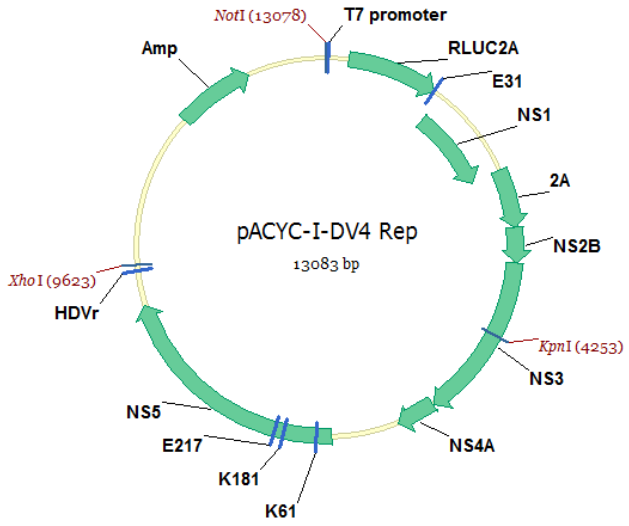

Figure 2.1 DENV-4 replicon cDNA. The plasmid map of DENV-4 replicon is shown.

2.2.3 Generation of DENV-2 NS5 linker mutant replicons

Mutations consisting 4 amino acids (aa264-267) in DENV-2 NS5 inter-domain linker swapped with corresponding Flavivirus amino acids (L4) were engineered into the subclone, TA-DENV2 NGC-E shuttle vector, using QuikChange II XL SDM kit according to the manufacturer's protocol (Stratagene). The primers used for mutagenesis are listed in Table 2.4. Mutations consisting 9 amino acids (aa264-272) in DENV-2 NS5 inter-domain linker swapped with corresponding Flavivirus amino acids (L9) were generated by overlap PCR using TA-DENV2 NGC-E shuttle vector. The overlapped PCR products were digested with AccI and PmlI restriction enzymes, following by cloning into TA-DENV2 NGC-E shuttle vector at these two sites. The primers used for overlap PCR reaction are shown in Table 2.5. To construct DENV2 NGC replicon, the mutants were cloned into pACYC-DENV2 NGC RLUC vector at BspEI and MluI restriction sites (Figure 2.2). The DENV2 NGC RLUC plasmid contains a T7

promoter and HDVr sequence at 5' and 3' ends respectively and the structural genes had been replaced by renilla luciferase and foot-and-mouth disease virus 2A protease cDNAs. All constructs were verified by DNA sequencing before proceeding to the subsequent experiments.

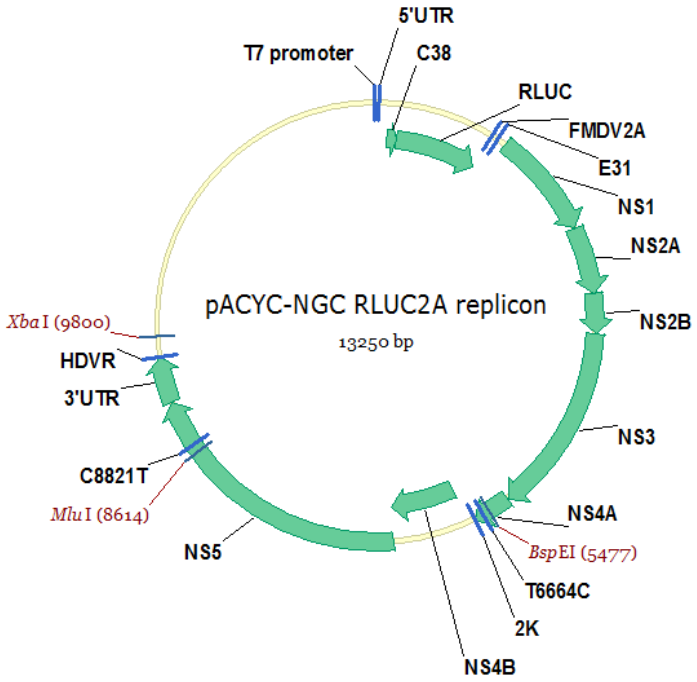

Figure 2.2 DENV-2 replicon cDNA. The plasmid map of DENV-2 replicon is shown.

2.2.4 Generation of DENV-4 NS5 F1 motif mutant replicons

Mutations N453A (N452 in DENV-3), K457A (K456 in DENV-3), R458A (R457 in DENV-3), K457A/R458A, E459A (E458 in DENV-3), F465A (F464 in DENV-3), W475A (W474 in DENV-3) and K579A (K578 in DENV-3) in the DENV-4 NS5 sequence were engineered into pACYC-DENV4-F shuttle vector using QuikChange II XL SDM kit. Subsequent steps to generate replicon cDNA were performed as per section 2.2.1. A list of primers used for mutagenesis is available in Table 2.6.

2.2.5 Generation of DENV-4 NS5 N-pocket mutant replicons

Mutations C710A (C709 in DENV-3), S711A (S710 in DENV-3), H801A (H800 in DENV-3) and Q803A (Q802 in DENV-3) in the DENV-4 NS5 sequence were engineered into pACYC-DENV4-F shuttle vector using QuikChange II XL SDM kit. Subsequent steps to generate

replicon cDNA were performed as per section 2.2.1. A list of primers used for mutagenesis is available in Table 2.7.

2.3 Construction of DENV infectious clones

2.3.1 Generation of DENV-4 NS5 interface mutant infectious clones

DENV-4 NS5 mutations were cloned into subclone, pACYC-DENV4-E shuttle vector, by subjecting DENV-4 NS5 mutant replicon cDNAs to KpnI and SalI restriction digestion. The pACYC-DENV4-E plasmids which now contain NS5 mutations were double digested with BsrGI & XhoI, followed by gel extraction to obtain the 8476 bp fragment comprising nucleotides 2246 to 10652 (contains NS1, 2A, 2B, NS3, 4A, 4B, NS5 and 3'UTR). Another subclone, pACYC-DENV4-A1 shuttle vector, was double digested with SacII and BsrGI, followed by gel extraction to obtain the 2268 bp fragment comprising the T7 promoter followed by nucleotides 1 to 2245 (contains 5'UTR, C, prM and E). The two fragments were *in vitro* ligated with T4 DNA ligase and purified through illustra MicroSpin G-25 column (GE Healthcare) and phenol-chloroform extraction. The purified ligated cDNAs (Figure 2.3) were resuspended in nuclease-free water.

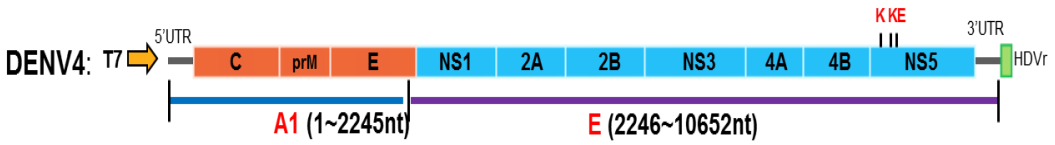

Figure 2.3 DENV-4 infectious clone. The structure of DENV-4 infectious clone is depicted. The infectious clone was generated by ligating the 8476 bp fragment from pACYC-DENV4-E shuttle vector and the 2268 bp fragment from pACYC-DENV4-A1 shuttle vector.

2.3.2 Generation of DENV-2 NS5 E111 and G_2 mutant infectious clones

DENV-2 full-length cDNA clones bearing NS5 E111A, E111Q and E111R substitutions were generated using pACYC-NGC FL and TA-NGC (shuttle E) plasmids as illustrated previously (314). The pACYC-NGC infectious clone vector contains a long DNA fragment comprising a T7 promoter, the DENV2 NGC genome, followed by the HDVr sequence (Figure 2.4). The shuttle vector harbors sequences from NS3 to 3'UTR-HDVr (nucleotides 5427 to 10955) from

the pACYC-NGC FL plasmid. All mutations were introduced into the shuttle E vector using QuikChange II XL SDM kit (Stratagene). The primers used for mutagenesis are available in Table 2.8. After sequence verification, the mutants were cloned into the FL infectious clone at *BspEI* and *MluI* restriction sites.

DENV2 full-length cDNA clones with mutations at the second nucleotide G_2 of the viral genome were constructed by PCR using Phusion DNA Polymerase under standard procedures. Table 2.9 shows the primers used for engineering 5' UTR mutations. The PCR products were purified and checked by DNA sequencing before cloning into pACYC-NGC infectious clone at *NotI* and *NheI* restriction sites.

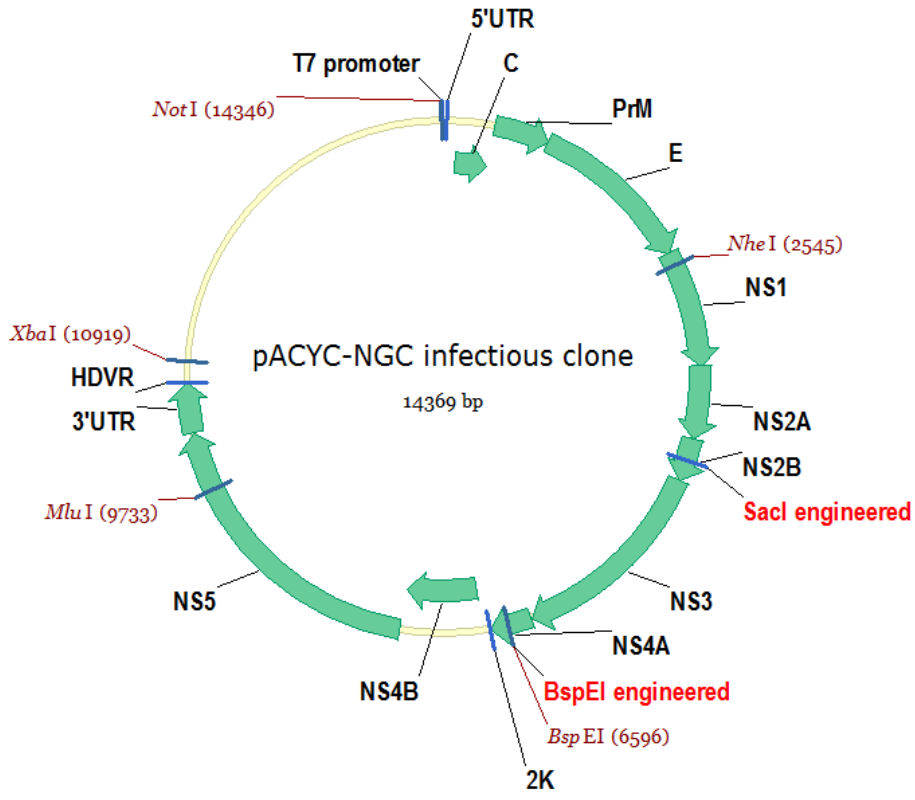

Figure 2.4 DENV-2 infectious clone. The plasmid map of DENV-2 infectious clone is shown.

2.4 RNA *in vitro* transcription and transfection

The DENV-4 and DENV-2 replicon cDNA plasmids were linearized with XhoI and XbaI respectively, whilst the full-length DENV-2 infectious cDNA clones were linearized with *XbaI*. These plasmids were purified with phenol/chloroform before carrying out *in vitro* transcription

(IVT) using T7 mMESSAGE mMACHINE kit according to the manufacturer's protocol (Ambion, U.S.A.). The genome-length DENV-4 interface mutant infectious cDNAs were *in vitro* transcribed similarly using T7 mMESSAGE mMACHINE kit. The resulting RNA was resuspended in RNase-free water and stored at -20°C before use. Approximately 10 µg replicon and DENV-2 infectious clone RNAs were electroporated into 8 x 10^6 BHK-21 cells in 0.8 ml Ingenio Electroporation Solution (Mirus) in a pre-chilled 0.4 cm cuvette, pulsing three times using Genepulser Xcell™ Electroporation System (Bio-Rad, U.S.A.) with 5-10 sec intervals at 850 V and 25 µF. Cells were recovered at room temperature (RT) for 3-5 min before mixing with 25 ml pre-warmed DMEM containing 10% FBS. The final cell number was 3.2 x 10^5 per ml. For DENV-4 interface mutant infectious clones, the RNA yield after IVT purification was relatively low so only about 2 µg RNA was electroporated into 4 x 10^6 BHK-21 cells in 0.4 ml Ingenio Electroporation Solution (Mirus). Cells were recovered at RT for 10 min before resuspending in 20 ml pre-warmed DMEM containing 10% FBS. The final cell number was 2 x 10^5 per ml.

2.5 Cell viability assay

Cell viability assay was performed using CellTiter-Glo kit (Promega, USA) following the manufacturer's protocols, and luminescence was measured using a microplate reader (Tecan).

2.6 *Renilla* luciferase assay

Replicon RNA transfection cells were seeded into 12-well plates at 0.5 ml per well (1.6 x 10^5 cells) and incubated in 5% CO_2 at 37°C. Duplicate wells were seeded for each time point. At 1, 4, 24, 48, 72, and 96 hour post-transfection (hpt), the medium was removed and the cells were washed with PBS twice before adding 250 µl lysis buffer to each well of 12-well plate and storing the plate at -80°C for subsequent luciferase assay. Luciferase activity was measured using the Clarity™ Luminescence Microplate Reader by adding 50 µl substrate to 20 µl lysate

in one well of 96-well white opaque plate. This assay was performed using *Renilla* Luciferase Assay System following the manufacturer's protocol (Promega, WI, U.S.A.).

2.7 Immunofluorescence assay (IFA)

Replicon RNA-transfected and DENV-2 genome-length RNA-transfected cells were seeded onto 8-well chamber slide at various amounts: 250 µl per well for 24 hpt harvesting (8 x 10^4 cells), 150 µl per well for 48 hpt harvesting (4.8 x 10^4 cells), and 100 µl per well for 72 and 96 hpt harvesting (3.2 x 10^4 cells), and were incubated in 5% CO_2 at 37°C. For DENV-4 interface mutant infectious clone, RNA-transfected cells were seeded onto 8-well chamber slide at 150 µl per well for 72 hpt harvesting (3 x 10^4 cells) and 100 µl per well for 120 hpt harvesting (2 x 10^4 cells). Note that at 24 hpt, the medium in the chamber slides for infectious clones was changed to DMEM containing 2% FBS and incubated in 5% CO_2 at 30°C. At designated time points, the medium was removed and the cells were washed with PBS twice before fixing in cold methanol for 30 min at -20°C. The fixed cells were washed with PBS three times and blocked with PBST (composed of 1% FBS (v/v), 1% bovine serum albumin (BSA) (g/v) and 0.05% Tween-20 (v/v) in PBS) for 1 hour at RT with gentle rocking to prevent non-specific binding of antibodies at later steps. After blocking, the cells were washed thrice with PBS and then incubated 1 hour at RT with primary antibodies – anti-NS3 helicase protein rabbit antibody (1:200 dilution with PBST; NITD), anti-DENV-4 RdRp rabbit antibody (1:100 dilution with PBST; NITD), anti-DENV2 NS5 rabbit polyclonal antibody (1:100 dilution with PBST; Genetex GTX103350), or anti-dsRNA mouse monoclonal antibody (1:100 dilution with PBST; clone J2, English & Scientific Consulting Kft., Hungary), with gentle rocking. Following primary antibodies staining, the cells were washed with PBS three times and then incubated in the dark with secondary antibodies – Alexa Fluor 568 donkey anti-mouse IgG (1:2000 dilution with PBST; Invitrogen, U.S.A.), Alexa Fluor 488 goat anti-rabbit IgG (1:2000 dilution with PBST; Invitrogen, U.S.A.), Alexa Fluor 568 goat anti-rabbit IgG (1:2000 dilution

with PBST; Invitrogen, U.S.A.), or FITC-labeled goat anti-mouse IgG (1:200 dilution with PBST; Sigma, USA), for 1 hour at RT with gentle rocking. After PBS washing for three times, mounting agent containing 4′,6-diamidino-2-phenylindole (DAPI; Vector Laboratories, Inc.) was added to stain the nuclei and seal the coverslip. The slide was visualized under a fluorescence microscope and cell images were captured on camera at 20x magnification.

2.8 Plaque assay

Virus stock was generated by harvesting the supernatant of genome-length RNA-transfected BHK-21 cells grown in T75 flask (Corning) at 24, 48, 72, 96, and 120 hpt, and virus titer and morphology were determined by standard plaque assay. Briefly, a series of 10-fold dilutions was produced by first diluting 50 µl virus stock with 450 µl RPMI 1640 with 2% FBS to obtain 10^{-1} dilution and then diluting further until 10^{-6} dilution was achieved. Confluent BHK-21 cells (8×10^4 seeded per well two days in advance) grown in 24-well plate was added with 200 µl of each dilution into each well. Duplicate wells were seeded for each time point and dilution factor. The infection was allowed to take place at 30°C for 1 hour. After an hour, the medium was removed and 500 µl 0.8% methyl-cellulose overlay (containing RPMI, 2% FBS, 1% P/S, 0.05% $NaHCO_3$, 25 mM Hepes, and 0.5% DMSO) was dispensed into each well. After 5 days of incubation in 5% CO_2 at 37°C, the cells were fixed in 3.7% formaldehyde and stained with 1% crystal violet. The virus titer was calculated as plaque-forming unit (PFU) per ml.

2.9 Intracellular and extracellular virus RNA extraction and quantification

DENV-4 and DENV-2 genome-length RNA-transfected BHK-21 cells were seeded into 6-well plate at 2×10^5 cells and 3.2×10^5 cells per well respectively, and incubated in 5% CO_2 at 37°C. Note that at 24 hpt, the medium was changed to DMEM containing 2% FBS and the plate was incubated in 5% CO_2 at 30°C. At designated time points (6.5/6, 24, 48, 72, 96, and 120 hpt), the medium was removed and the cells were washed once with PBS before lysing with 1 ml TRIzol Reagent (Invitrogen). The subsequent steps for RNA extraction was followed according

to the manufacturer's instruction. For intracellular viral RNA quantification, 100 ng of extracted RNA was subjected to qRT-PCR using iScript enzyme one-step RT PCR with SYBR and run with iQ™5 Multicolor or Bio-Rad CFX96 Real-Time PCR Detection System. The primers used of DENV-4 viral RNA are forward, 5'-GCTTACGCCCAGATGTGG-3', and reverse, 5'-CGTTGGAACTGCTGAGCAT-3', targeting the DENV-4 NS5 region. The primers used of DENV-2 viral RNA are forward, 5'-CGTCGAGAGAAATATGGTCACACC-3', and reverse, 5'-CCACAATAGTATGACCAGCCT-3', targeting the DENV-2 NS5 MTase region. The protocol for qRT-PCR reaction is as follows: (i) 52°C for 10 min, (ii) 95°C for 5 min, (iii) 95°C for 10 sec, (iv) 60°C for 30 sec, (v) repeat steps iii and iv for another 44 times, (vi) 95°C for 1 min, (vii) 55°C for 1 min, (viii) 0.5°C increment for 10 sec from 55°C to 95°C. To generate a standard curve for quantification of viral genome copy number, DENV-4 replicon WT IVT RNA and DENV-2 NGC WT FL IVT RNA were serially diluted 3-fold for 10 times and subjected to qRT-PCR similarly as described above (Appendix 1 and 2).

For extracellular viral RNA quantification, supernatant of DENV-2 genome-length RNA-transfected BHK-21 cells was collected at 24, 48, 72, 96, and 120 hpt, and clarified prior to addition of TRIzol LS reagent (Invitrogen). RNA extraction was performed and the extracted RNA was subjected to qRT-PCR as depicted above. To ensure that the engineered mutations were still present after transfection, the extracted RNA at 24 and 120 hpt were also used for RT-PCR by using several overlapping primers covering the complete NS5 gene. The RT-PCR products were then purified with gel extraction kit and sent for DNA sequencing.

2.10 Construction of DENV WT and mutant FL NS5 plasmids

2.10.1 Generation of DENV-4 WT and interface mutant FL NS5 plasmids

DENV-4 WT and interface mutant FL NS5 cDNAs were PCR amplified from the respective WT and mutant pACYC-DENV4-F shuttle plasmids and cloned into pET28a vector using NheI

and XhoI restriction sites (Figure 2.5). The primers used for PCR amplification can be found in Table 2.10.

2.10.2 Generation of DENV-4 WT and 3_{10}-helix mutant FL NS5 plasmids

The S264A, V265A, S266A and T267A mutations in the DENV-4 NS5 sequence were engineered into pET28a-DENV4 FL NS5-MY22713 plasmid using QuikChange II XL SDM kit according to the manufacturer's protocol (Stratagene). This vector contains an N-terminal His-tag sequence upstream of the NS5 FL sequence. The primers used for mutagenesis are listed in Table 2.11.

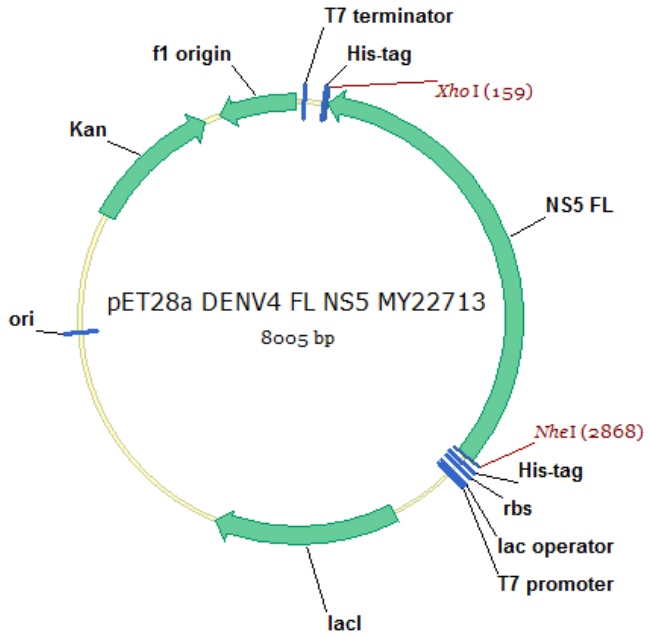

Figure 2.5 DENV-4 recombinant His-tag NS5 protein. The plasmid map of pET28a DENV-4 FL NS5 MY22713 is shown.

2.10.3 Generation of DENV-2 WT and linker mutant FL NS5 plasmids

DENV-2 WT FL NS5 protein plasmid was constructed by PCR amplifying the DENV-2 FL NS5 cDNA from TA-DENV2 NGC-E shuttle vector and cloning them into pET28a vector (Stratagene) using the NheI and XhoI restriction sites. The L4 mutations in the DENV-2 NS5 sequence were engineered into pET28a-DENV2 FL NS5 plasmid using QuikChange II XL SDM kit according to the manufacturer's protocol (Stratagene). This vector contains an N-

terminal His-tag sequence upstream of the NS5 FL sequence. The primers used for cloning and mutagenesis are listed in Table 2.12 and 2.4. To generate pET28a-DENV2 FL NS5 L9 mutant plasmids, the respective L9 mutant TA-DENV2 NGC-E shuttle plasmids were digested and cloned into pET28a-DENV2 FL NS5 plasmid at StuI and PmlI restriction sites.

2.10.4 Generation of DENV-4 WT and E111 mutant FL NS5 plasmids

The E111A, E111Q, E111R mutations in the DENV-4 NS5 sequence were introduced into pET28a-DENV4 FL NS5-MY22713 plasmid using QuikChange II XL SDM kit (Stratagene). This vector contains an N-terminal His-tag sequence upstream of the NS5 FL sequence. The primers used for mutagenesis are listed in Table 2.13.

2.10.5 Generation of DENV-4 WT and F1 motif mutant FL NS5 plasmids

The N453A, K457A, R458A, K457A/R458A, E459A, F465A, W475A and K579A mutations in the DENV-4 NS5 sequence were introduced into pET28a-DENV4 FL NS5-MY22713 plasmid using QuikChange II XL SDM kit (Stratagene). This vector contains an N-terminal His-tag sequence upstream of the NS5 FL sequence. A list of primers used for mutagenesis can be found in Table 2.14.

2.11 Construction of DENV WT and mutant MTase plasmids

The R38A, K42A, R57A, R84A, E111A, E111Q, E111R, R212A, S214A and T215A mutations in the DENV-4 NS5 sequence were generated using QuikChange II XL SDM kit (Stratagene) into the plasmid pGEX-4T-1+D4(MY22713)+SAM272 which bears DENV-4 genome sequence encoding amino acids 1 to 272 of the NS5 MTase protein (Figure 2.6). Table 2.13 shows the primers employed for mutagenesis.

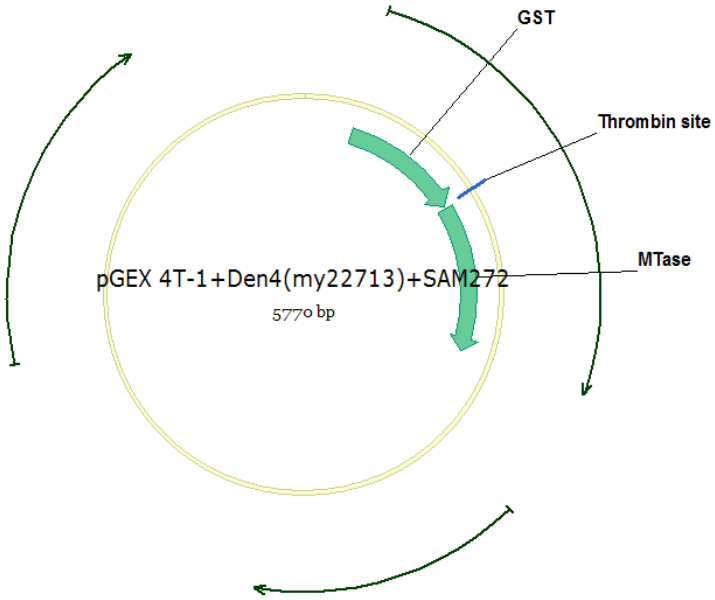

Figure 2.6 DENV-4 recombinant GST-tag MTase protein. The plasmid map of pGEX-4T-1+D4(MY22713)+SAM272 is shown.

2.12 Expression and purification of DENV WT and mutant proteins

2.12.1 Expression and purification of DENV-4 and DENV-2 WT and mutant FL NS5 proteins

Expression plasmids for all recombinant NS5 proteins fused with N-terminal His-tag sequence were transformed into *Escherichia coli* BL21 cells and grown on LB medium with 30 µg/ml kanamycin (Kan^{30}) agar plates for incubation at 37°C overnight. Colonies were scraped and inoculated into two 400 ml 2xYT medium with Kan^{30} per protein at 37°C with shaking at 180 rpm until an absorbance optical density at 600 nm of 0.6 to 0.8 was reached. The cultures were gradually cooled to 16°C before adding 0.4 mM isopropyl-β-D-thiogalactopyranoside (IPTG) for inducing protein expression at 16°C overnight with shaking at 180 rpm. After overnight growth, OD_{600} reached 2.0 and above and the cells were harvested by centrifugation at 6,000 rpm at 4°C for 10 min. Cell pellets were resuspended and sonicated in buffer A (20 mM Tris-HCl at pH 7.5, 550 mM NaCl, 5% glycerol, 5 mM β-mercaptoethanol (β-ME)) supplemented with 0.01% 3-[(3-Cholamidopropyl)dimethylammonio]-1-propanesulfonate (CHAPS), and protease inhibitor cocktail tablet (Roche). The lysates were clarified by centrifugation at 18,000

rpm for 40 min at 4°C and the supernatants were purified using nickel-nitrilotriacetic acid (Ni-NTA) agarose (Qiagen) by washing unbound protein with buffer A. Recombinant His-tag NS5 proteins were eluted with buffer B (buffer A supplemented with 400 mM imidazole), pooled and concentrated using Amicon Ultra centrifugal filter (Millipore, U.S.A.) with a molecular weight cut-off of 30 kDa. Further purification by size-exclusion chromatography was performed with the use of Superdex 200 10/300 GL column (GE Healthcare Life Sciences). Peak fractions were analysed on 10% sodium dodecyl sulphate-polyacrylamide gel electrophoresis (SDS-PAGE) gel before the desired His-tag NS5 FL proteins of size ~100 kDa were pooled, concentrated and stored at -80°C before use.

2.12.2 Expression and purification of DENV-4 WT and mutant MTase proteins

Expression plasmids for all recombinant MTase proteins fused with N-terminal GST-tag sequence were transformed into *Escherichia coli* BL21 cells and plated onto LB medium with 100 µg/ml ampicillin (Amp^{100}) agar plates for incubation at 37°C overnight. Colonies were scraped and inoculated into 2 ×YT medium containing Amp^{100} at 37°C with shaking at 180 rpm to ~0.6-0.8 absorbance optical density at 600 nm (OD_{600}). The cultures were gradually cooled to 16°C before adding 0.4 mM IPTG for inducing protein expression at 16°C overnight with shaking at 180 rpm. After overnight growth, OD_{600} reached 2.0 and above and the cells were harvested by centrifugation at 6,000 rpm at 4°C for 10 min. Cell pellets were resuspended and sonicated in buffer A (20 mM Tris-HCl at pH 7.5, 0.5 M NaCl, 2 mM β-ME, 5% glycerol) supplemented with 0.01% CHAPS, and protease inhibitor cocktail tablet (Roche). The lysates were clarified by centrifugation at 18,000 rpm for 40 min at 4°C and the supernatants were loaded on a GSTrap™ FF column (GE Healthcare) pre-equilibrated with buffer A. Overnight cleavage at 4°C using thrombin was carried out to remove the GST-tag. The desired DENV-4 MTase protein was further purified through both the GSTrap™ FF and HiTrap™ Benzamidine

FF columns (GE Healthcare) and analysed on 10% SDS-PAGE gel before concentrated and stored at -80°C.

2.13 Construction of mutant $^{m7}G_{0ppp}$-DENV4 5'UTR nt-110 RNAs for 2'-*O* MTase assay

DENV-4 5' UTR nt-110 DNA with mutations at the second position G_2 was generated by Phusion PCR kit (New England Biolabs; NEB). The primers used for engineering 5' UTR substitutions are shown in Table 2.15. Purification and sequencing of the PCR products were carried out before using MEGAshortscript T7 Transcription Kit (Life Technologies) for *in vitro* transcription (IVT). The transcription reaction was added with ^{m7}GpppA cap analog to obtain RNA containing the cap structure. The IVT RNAs were subsequently purified and resuspended in RNase-free water.

2.14 Thermo-fluorescence assay

A 20 µl reaction mixture comprising of 2.5 µM protein, with or without 50 µM 5'-$^{m7}G_{ppp}$AGUUGUU-3' RNA (Trilink) and SYPRO Orange dye (Invitrogen) in 1x assay buffer (50 mM Tris-Cl at pH 7.5, 100 mM KCl, 0.001% Triton X-100, 0.1 mM $MnCl_2$ and 0.1 mM $MgCl_2$) was prepared in a 96-well white opaque plate (Bio-Rad). Duplicate wells were prepared for each protein. The plate was sealed and centrifuged briefly before heated at 0.5°C increments from 25°C to 85°C using iQ5 Multicolor or CFX96 Touch Real-Time PCR Detection System (Bio-Rad, Hercules, U.S.A.). Fluorescence was detected at $excitation_{max}$ and $emission_{max}$ wavelengths of 485 nm and 625 nm respectively, and signals were recorded as relative fluorescence unit (RFU) with respect to temperature. The derivatives (-dRFU/dT) were plotted using Graphpad® Prism software.

2.15 DENV NS5 N-7 and 2'-*O* methyltransferase assays

DENV scintillation proximity-based N-7 and 2'-*O* methyltransferase assays were carried out similarly as described previously (240, 275, 276). For testing DENV-4 NS5 methyltransferase

activity, the 25 µl N-7 assay reaction mixture comprised of 25 nM protein, 240 nM biotinylated GTP-capped DENV-4 nucleotide 1-110 (includes 5'UTR and 66 nucleotide of the core sequence) IVT RNA, and 320 nM Adenosyl-L-Methionine/[^{3}H-methyl]-SAM (Perkin Elmer, USA) in 50 mM Tris at pH 7.5, 20 mM NaCl, and 0.05% CHAPS. The 25 µl 2'-*O* reaction mixture comprised of 25 nM protein, 40 nM m7-Gppp-DENV4 5'UTR nt-110 RNA or GpppA-7mer RNA (Trilink), and 320 nM [^{3}H-methyl]-SAM in 50 mM Tris at pH 7.5, 10 mM KCl, 2 mM $MgCl_2$, and 0.05% CHAPS. For testing DENV-2 NS5 methyltransferase activity, the N-7 MTase reaction comprised 25 nM protein, 240 nM Gppp-DENV4 5'UTR nt-110 RNA and 125 nM [^{3}H-methyl]-SAM (American Radiolabeled Chemicals, Inc., USA) in 50 mM Tris-HCl at pH 7.5, 75 mM NaCl and 0.001% Triton X-100. The 2'-*O* MTase reaction comprised 25 nM protein, 40 nM m7-Gppp-DENV4 5'UTR nt-110 RNA or 5'GpppAGAACCUG-3' RNA (Trilink) and 125 nM [^{3}H-methyl]-SAM in 50 mM Tris-HCl at pH 7.5, 10 mM KCl, 2 mM $MgCl_2$, and 0.05% CHAPS. The reaction was set up in a 96-well half-area white opaque plate (Corning Costar, Acton, MA) by first mixing buffer, RNA substrate and enzyme, followed by adding the [^{3}H-methyl]-SAM to initiate the reaction. Duplicate wells were prepared for each protein. The N-7 and 2'-*O* reactions were incubated at RT for 15 min and 1 hour respectively before stopping the reactions with 2x stop solution (50 mM Ethylenediaminetetraacetic acid (EDTA), 100 mM Tris at pH 7, 300 mM NaCl, 4mg/ml or 2 mg/ml streptavidin-SPA beads, and 62.5 µM cold SAM). The plate was shaken at 750 rpm for 20 min at RT and centrifuged at 1,200 rpm for 2 min, and subsequently read in a Trilux microbeta counter (PerkinElmer, Boston, MA) at 1 min/well. All data points were collected in duplicate wells.

2.16 DENV NS5 polymerase *in vitro* FAPA assays

DENV polymerase *de novo* initiation (*dn*I)/elongation and elongation fluorescence-based alkaline phosphatase-coupled polymerase assays (FAPA) were performed similarly as demonstrated earlier (307, 315). In general, the 15 µl *dn*I reaction comprised of 100 nM protein,

100 nM IVT DENV-4 5'UTR-3'UTR RNA (Trilink), 20 µM ATP, 20 µM GTP, 20 µM UTP, and 5 µM Atto-CTP (Trilink Biotechnologies) in assay buffer (50 mM Tris-Cl at pH 7.5, 0.3 mM $MnCl_2$, 0.001% Triton X-100, 10 mM KCl, 1 mM $MgCl_2$, and 10 µM cysteine). The 15 µl elongation reaction comprised of 100 nM protein, 100 nM IVT 244 nucleotide heteropolymeric RNA (repeats of $(UCAG)_{20}(UCCAAG)_{14}(UCAG)_{20}$), 200 nM four primers (C1 primer: 3'-AGUCAGCAGUCGUGU-biotin-5', A1 primer: 3'-GUCAGUCAGUCAGUCUC-biotin-5', G1 primer: 3'-UCAGUCAGUCAGUCAGCA-biotin-5', and U1 primer: 3'-CAGUCAGUCAGUCAGAG-biotin-5') (316), 2 µM ATP, 2 µM GTP, 2 µM UTP, and 0.5 µM Atto-CTP in assay buffer (50 mM Tris-Cl at pH 7.5, 0.5 mM $MnCl_2$, 0.001% Triton X-100, 10 mM KCl, and 10 µM cysteine). Before the reaction, RNA was pre-annealed to the four different sets of primers at 95°C for 3 min, followed by 65°C for 20 min and 37°C for 20 min, cooled and mixed together. All the reactions were incubated at RT for up to 3 hours. At designated time points, 10 µl of 2.5x STOP buffer (200 mM NaCl, 25 mM $MgCl_2$, 1.5 M DEA, pH 10; Promega) containing 25 nM calf intestinal alkaline phosphatase (CIP; New England Biolabs) was added to the wells to terminate the reactions. The plate was centrifuged at 800 rpm and shaken briefly, followed by incubation at RT for additional 60 min. The released AttoPhos was measured by reading on a Tecan Saffire II microplate reader at $excitation_{max}$ and $emission_{max}$ wavelengths of 422 nm and 566 nm respectively. All data points were performed in triplicate wells in 384-well black opaque plates (Corning).

2.17 Measurement of steady-state kinetic parameters in FAPA assays

Michaelis-Menten constant (K_m) and V_{max} of Atto-CTP and RNA substrates were determined in both *de novo* initiation (*dn*I) and elongation FAPA. A range of substrate concentrations were obtained by serially diluting Atto-CTP and RNA two-fold for up to 10 times. In *dn*I FAPA, Atto-CTP concentrations tested ranged from 20 to 0.03 µM (at a fixed RNA concentration of

200 nM and the three other individual NTP concentrations of 20 μM), while RNA concentrations tested ranged from 500 to 0.73 nM (at fixed individual NTP concentrations of 20 μM). In elongation FAPA, Atto-CTP concentrations tested ranged from 20 to 0.03 μM (at fixed annealed RNA concentration of 200 nM and the three other individual NTP concentrations of 5 μM), while RNA concentrations tested ranged from 400 to 0.59 nM (at fixed individual NTP concentrations of 5 μM). To measure K_m of Atto-CTP, 5 μl of the serially diluted Atto-CTP was added to their respective wells, followed by 5 μl of RNA and NTPs mix to all reaction wells. For K_m measurement of RNA, 5 μl of the serially diluted RNA was added to their respective wells, followed by 5 μl of NTPs mix to all reaction wells. The reaction was initiated upon adding 5 μl of enzyme at a concentration of 100 nM. After incubation at RT for 120 minutes, 10 μl of 2.5x STOP buffer was added to terminate the reactions. The plate was centrifuged at 800 rpm and shaken briefly, followed by incubation at RT for additional 60 min and read on a Tecan Saffire II microplate reader at $excitation_{max}$ and $emission_{max}$ wavelengths of 422 nm and 566 nm respectively. All data points were performed in triplicate wells in 384-well black opaque plates (Corning) and the experiments were performed two times. A standard curve consisting of 10-points of 2-fold serially diluted Atto-Phos substrate (2′-[2-benzothiazoyl]-6′-hydroxybenzothiazole phosphate or BBT-Pi; Promega) with concentrations ranged from 1000 to 1.95 nM was generated for calculating the amount of Atto-Phos released from Atto-CTP incorporation. K_m and V_{max} values were obtained by plotting the observed BBT production (nM/min or velocity, v) as a function of Atto-CTP or RNA concentrations, and the data were fitted to the equation: $v = V_{max} \times [S]/(K_m + [S])$ for Michaelis-Menten model or $v = V_{max} \times [S]/(K_m + [S] \times (1+[S]/K_i))$ for substrate inhibition model, where [S] is the substrate concentration for Atto-CTP or RNA, using Graphpad Prism software.

2.18 Determination of IC_{50} using *De Novo* FAPA assay

IC_{50} values for F1 motif inhibitors were determined in DENV-4 *de novo* initiation FAPA assay by dose response testing of compounds (10-point, 3-fold serially diluted compounds from 0-2 mM or 0-10 mM), from one experiment with WT and mutant enzymes. Briefly, compounds were incubated for 20 min with enzyme alone, after which reactions were started with addition of ssRNA and nucleotide substrates, and allowed to proceed for 3 hr (317). Reactions were stopped by addition of 2.5X STOP buffer with 25 nM CIP, re-incubated at RT for 60 min and read on a Tecan Safire II microplate reader ($excitation_{max}$ and $emission_{max}$ wavelengths 422 nm and 566 nm). Data was fitted to the four parameter logistic equation and IC_{50} curves were plotted using GraphPad Prism software. Average IC_{50} values and hill slopes were obtained. All data points were measured in duplicates.

2.19 Co-crystallization of compounds with DENV-3 FL NS5

Co-crystallization of compounds 27 and 29 with DENV-3 FL NS5 was performed by vapor diffusion hanging drop method according to conditions from (318). Basically, 1 µl of mother liquor (0.2 M Magnesium Formate, 16-18% PEG 3350) was mixed with 1 µl of protein mixture (10 mg/ml of protein supplemented with 2 mM TCEP and with a final compound concentration of 2.5 mM diluted in 5% DMSO) and incubated at 18°C. Crystals obtained were cryo-protected in crystallization solution supplemented with 25% glycerol and 5 mM compound.

2.20 Order-of-reagent addition experiment

DENV-4 FL NS5 *de novo* initiation FAPA assay was performed with 10-point, 2-fold serially diluted compounds from 0-2.5 µM for compound 29 and 0-25 µM for compound 27. Compounds were incubated for 20 min with 100 nM enzyme alone, pre-formed enzyme-ssRNA complex or enzyme-dsRNA complex (comprising ssRNA and newly-synthesized RNA products – AGAA or AGAACC), followed by reaction initiation with corresponding missing ssRNA and/or NTP components for 2 hours. 100 nM DENV-4 5'-3' UTR IVT RNA, 20 µM ATP, 20 µM GTP, 20 µM UTP and 5 µM Atto-CTP were used. After 2 hours of incubation,

reactions were stopped by addition of 2.5X STOP buffer with 25 nM CIP and re-incubated at RT for 60 min before reading on a Tecan Safire II microplate reader ($excitation_{max}$ and $emission_{max}$ wavelengths 422 nm and 566 nm). Data was fitted to the four parameter logistic equation and IC_{50} curves were plotted using GraphPad Prism software. Average IC_{50} values and hill slopes were obtained. All data points were measured in duplicates.

2.21 Inhibition kinetic characterization of compound 29

DENV-4 *de novo* initiation FAPA assay was performed in increasing concentration of compound 29 (obtained by 2-fold serial dilution from 1 μM) with a range of substrate concentrations (obtained by 2-fold serial dilution of RNA and GTP for up to 10 times). RNA concentrations tested ranged from 500 to 0.98 nM (at fixed ATP, GTP and UTP concentrations of 50 μM and Atto-CTP concentration of 5 μM), while GTP concentrations tested ranged from 50 to 2.5 μM (at a fixed RNA concentration of 100 nM, ATP and UTP concentrations of 50 μM, and Atto-CTP concentration of 5 μM). For competition of compound with RNA, 100 nM enzyme was first added to compound-spotted plate followed by addition of the serially diluted RNA to their respective wells and NTPs mix to all reaction wells. For competition of compound with GTP, 100 nM enzyme was first added to compound-spotted plate followed by addition of the serially diluted GTP to their respective wells and RNA-NTPs mix to all reaction wells. After incubation at RT for 120 minutes, 10 μl of 2.5x STOP buffer was added to terminate the reactions. The plate was centrifuged at 800 rpm and shaken briefly, followed by incubation at RT for additional 60 min and read on a Tecan Saffire II microplate reader at $excitation_{max}$ and $emission_{max}$ wavelengths of 422 nm and 566 nm respectively. All data points were performed in duplicate wells in 384-well black opaque plates (Corning). Lineweaver-Burk and Michaelis-Menten plots were derived from non-linear regression curve fitting using Graphpad Prism software.

2.22 Optimization of DENV NS5 or RdRp elongation complex formation

The elongation complex was formed by incubating 250 nM DENV-4 FL NS5 or RdRp (aa266-900) and 50nM T18/FAM-labeled-P8 at RT for 1 min in 50 mM Tris-Cl at pH 7.5, 0.5 mM $MnCl_2$, 0.001% Triton X-100, 10 mM KCl, and 10 µM cysteine. Reaction was started by adding UTP at varying concentrations (0.017 to 1000 µM) and was terminated after 15 min using 50 mM EDTA. For buffer optimization, various concentrations of divalent cations (0.25, 0.5, 1, 2 and 5 mM $MnCl_2$/$MgCl_2$) and monovalent salts (2-fold dilutions of KCl/NaCl from 250 mM for 10 times) as well as pH values (5.0 to 9.0) were tested during complex assembly and reaction. The reaction was composed of 250 nM DENV-4 RdRp (aa266-900), 50nM T18/FAM-labeled-P8 and 100 µM UTP, incubated at RT for 8 min. All the elongation reactions were added with 2X loading dye (Ambion) and heated at 65 °C for 15 min before running on 23% Urea-PAGE gel. The gel was scanned on a Typhoon phosphor/fluorescence imager and band intensity was determined using ImageQuant TL software (GE Healthcare Life Sciences) to calculate the percentage of incorporation.

2.23 Fluorescence polarization RNA binding assay

RNA binding assay was performed using 5 nM 6-FAM (6-carboxyfluorescein) labelled RNAs (ordered from Sigma-Aldrich or TriLink BioTechnologies; pre-annealed before use) in 50 mM Bis-Tris at pH 7.25, 0.5 mM $MnCl_2$, 0.001% Triton X-100, 10 mM KCl and 10 µM cysteine. Purified WT DENV-2, -3 or -4 FL NS5 proteins (additional 20 mM NaCl from protein storage buffer) was titrated into the RNA mix giving a range of protein concentrations from 0.1 nM to 10 µM. The binding reaction was incubated at room temperature for 10 min before FP data was collected using the BIOTEK Synergy 4 Multi-Detection Microplate Reader at excitation and emission wavelengths of 495 nm and 520 nm respectively. RNA dissociation constant (K_d) was determined by curve fitting the data to a one-site specific binding isotherm using Graphpad Prism Software.

2.24 Fluorescence polarization polymerase elongation assay

Polymerase elongation assay was performed by incubating DENV-4 or -3 NS5 FL protein (at K_d concentration with respect to the RNA substrate) and 5 nM FAM-labelled RNA in 50 mM Bis-Tris at pH 7.25, 0.5 mM $MnCl_2$, 0.001% Triton X-100, 10 mM KCl and 10 μM cysteine at RT for 1 min. Next, nucleotides were added to a final concentration of 100 μM each for elongation. At indicated time points, the reaction was stopped with 300 mM NaCl or 50 mM EDTA and added to each well of a 384-well black opaque plate (Corning) before FP data was collected using the BIOTEK Synergy 4 Multi-Detection Microplate Reader at excitation and emission wavelengths of 495 nm and 520 nm respectively. The elongation reaction was also run on 23% Urea-PAGE gel and scanned on a Typhoon phosphor/fluorescence imager to monitor nucleotide incorporation.

2.25 Steady-state kinetic measurements of DENV elongation complexes

Single nucleotide incorporation assay was performed by incubating 250 nM DENV-4 NS5 FL or RdRp (266-900) protein, 50 nM annealed RNA/labelled-primer (Table 2.16) and 0.2 U/uL RNasin ribonuclease inhibitor (Promega) in 50 mM Bis-Tris at pH 7.25, 0.5 mM $MnCl_2$, 0.001% Triton X-100, 10 mM KCl and 10 μM cysteine at RT for 1 min. After this, NTP substrate at varying concentrations (4-fold dilutions from 1000 μM to 0.015 μM) was added to initiate elongation. After 15 min of incubation, the reaction was terminated with 50 mM EDTA. The elongation reaction was added with 2X loading dye (Ambion) and heated at 65 °C for 15 min before running on 23% Urea-PAGE gel. The gel was scanned on a Typhoon phosphor/fluorescence imager and band intensity was determined using ImageQuant TL software (GE Healthcare Life Sciences). In order to determine amount of incorporation, a standard curve was established by first loading a range of FAM- primer samples with known concentrations onto Urea-PAGE gel, followed by measuring the band intensity for each sample and obtaining a linear regression of band intensity versus substrate concentrations (Appendix 3). Amount of single nucleotide incorporation from this assay was calculated based on the

standard equation and plotted against varying concentrations of NTP substrate. Michaelis-menten constant K_m and k_{cat} values were obtained from non-linear regression curve fitting using Graphpad Prism software.

2.26 Crystallization attempts of DENV polymerase-RNA and elongation complexes

DENV polymerase-RNA complex was assembled by incubating DENV-3 FL NS5 and pre-annealed RNA (T18/P8, T12/P8, T10/P6 and 12-7) at 1:1.5 molar ratio in binding buffer (50 mM Bis-Tris pH 7.25, 2.5 mM $MnCl_2$, 0.001% Trx-100, 10mM KCl, 10uM cysteine) on ice for 15 min. The complexes (each with different RNA substrate) were clarified by centrifugation before purification by size exclusion chromatography on a Superdex 200 10/300 GL gel filtration column (GE Healthcare Life Sciences), buffer exchanged with 20 mM Hepes pH 7.5, 150 mM NaCl, 1 mM TCEP reducing agent and 10% glycerol. The peak fractions were spectrophotometrically analyzed for nucleic acid purity and those with 260/280 nm ratio of approximately 1.20 to 1.70, possibly consisting of both protein and RNA, were pooled and concentrated (Figure 6.7). Crystallization screens were carried out using commercial kits from Hampton Research and Molecular Dimensions at 18°C.

Additionally, DENV3 NS5-T12/P8 and NS5-T10/P6 were incubated with nucleotides (GTP and 3'dCTP, or CTP and GTP) to form +1 or +2 elongation complexes. All the crystals were cryoprotected with the same crystallization buffer and sent to Swiss Light Source (SLS) for data collection.

Formation of a more stable elongation complex was carried out by incubating DENV-3 and DENV-4 FL NS5 and pre-annealed RNA (T18/P8 and T10/P6) at 1:1.2 molar ratio in binding buffer (50 mM Bis-Tris pH 7.25, 2.5 mM $MnCl_2$, 0.001% Trx-100, 10 mM NaCl, 10 µM cysteine) at RT for 15 min. The protein-RNA complexes were either not elongated and screened directly, or added with (i) UTP, GTP, ATP and 3'dCTP to elongate T18/P8 by +4 bases, or (ii) GTP and CTP to elongate T10/P6 by +2 bases during overnight incubation at RT.

All the complexes were centrifuged to remove precipitants and the supernatants were used for screening with commercial crystallization kits at 18°C.

Table 2. List of primers used for mutagenesis, cloning and assay

Mutation(s)[a]	Primer	
	Orientation[b]	Sequence
K95A	For	GTCCTATTACATGGCGACACTCGCAAACGTGACTGAAGTGAAAGGAT
	Rev	ATCCTTTCACTTCAGTCACGTTTGCGAGTGTCGCCATGTAATAGGAC
K95A/N96A	For	GGATGGTCCTATTACATGGCGACACTCGCAGCCGTGACTGAAGTGAAAGGATATACAAA
	Rev	TTTGTATATCCTTTCACTTCAGTCACGGCTGCGAGTGTCGCCATGTAATAGGACCATCC
Y119A	For	ATGAAGAACCAATCCCCATGGCTACTGCAGGCTGGAATTTGGTCA
	Rev	TGACCAAATTCCAGCCTGCAGTAGCCATGGGGATTGGTTCTTCAT
R263A	For	GATCTTGGGGCAGGAACGGCAAGTGTCTCCACTGAAAC
	Rev	GTTTCAGTGGAGACACTTGCCGTTCCTGCCCCAAGATC
E268A	For	CGAGAAGTGTCTCCACTGCAACAGAAAAACCAGACAT
	Rev	ATGTCTGGTTTTTCTGTTGCAGTGGAGACACTTCTCG
E270A	For	GAAGTGTCTCCACTGAAACAGCAAAACCAGACATGACAATTAT
	Rev	ATAATTGTCATGTCTGGTTTTGCTGTTTCAGTGGAGACACTTC
R353A	For	CAACCCCTTTTGGGCAACAAGCAGTGTTCAAGGAGAAGGT
	Rev	ACCTTCTCCTTGAACACTGCTTGTTGCCCAAAAGGGGTTG
R362A	For	CAAGGAGAAGGTGGATACCGCAACACCACAACCAAAACCC
	Rev	GGGTTTTGGTTGTGGTGTTGCGGTATCCACCTTCTCCTTG
K596A	For	GTAATGGACATTATATCCAGGGCAGACCAAAGAGGTAGTGGACA
	Rev	TGTCCACTACCTCTTTGGTCTGCCCTGGATATAATGTCCATTAC

Table 2.1 Primers used for site-directed mutagenesis (SDM) to generate interface mutants in pACYC-DENV4-F plasmid

[a] Mutations generated using QuikChange II XL SDM kit.

[b] For, forward; Rev, reverse.

Primer	Orientation[a]	Sequence
DV4-Rep-NotI-FOR	For	GTATCACATATTCTGCGGC
DV4-Rep-KpnI-REV	Rev	ATCCATCACTATGAGGTTAT

Table 2.2 Primers used for PCR of T7pro-LUC-NS3 cDNA cassette from pACYCI DV4-WT replicon

[a] For, forward; Rev, reverse.

Mutation(s)[a]	Primer	
	Orientation[b]	Sequence
S264A	For	GATCTTGGGGCAGGAACGAGAGCAGTCTCCACTGAAACAGAAAAA
	Rev	TTTTTCTGTTTCAGTGGAGACTGCTCTCGTTCCTGCCCCAAGATC
V265A	For	GGCAGGAACGAGAAGTGCATCCACTGAAACAGAAA
	Rev	TTTCTGTTTCAGTGGATGCACTTCTCGTTCCTGCC
S266A	For	GGCAGGAACGAGAAGTGTCGCAACTGAAACAGAAAAACCAG
	Rev	CTGGTTTTTCTGTTTCAGTTGCGACACTTCTCGTTCCTGCC
T267A	For	GGAACGAGAAGTGTCTCCGCTGAAACAGAAAAACCAG
	Rev	CTGGTTTTTCTGTTTCAGCGGAGACACTTCTCGTTCC

Table 2.3 Primers used for SDM to generate 3_{10}-helix mutations in pACYC-DENV4-F plasmid

[a] Mutations generated using QuikChange II XL SDM kit.

[b] For, forward; Rev, reverse.

The positions of the mutated amino acids are underlined.

Mutation(s)[a]	Primer	
	Orientation[b]	Sequence
d1-L4	For	CTCGGAAGCGGAACCCGCCATGTGGCAGTAGAAAGTGAGATACCAAAC
	Rev	GTTTGGTATCTCACTTTCTACTGCCACATGGCGGGTTCCGCTTCCGAG
d3-L4	For	CTCGGAAGCGGAACCCGCCATGTCAATGCGGAAAGTGAGATACCAAAC
	Rev	GTTTGGTATCTCACTTTCCGCATTGACATGGCGGGTTCCGCTTCCGAG
d4-L4	For	CTCGGAAGCGGAACCCGCAGTGTCTCCACTGAAAGTGAGATACCAAAC
	Rev	GTTTGGTATCTCACTTTCAGTGGAGACACTGCGGGTTCCGCTTCCGAG
JV-L4	For	CTCGGAAGCGGAACCCGCGCCGTGGGAAAGGAAAGTGAGATACCAAAC
	Rev	GTTTGGTATCTCACTTTCCTTTCCCACGGCGCGGGTTCCGCTTCCGAG
ZV-L4	For	CTCGGAAGCGGAACCCGCGCGGTGGTTAGCGAAAGTGAGATACCAAAC
	Rev	GTTTGGTATCTCACTTTCGCTAACCACCGCGCGGGTTCCGCTTCCGAG

Table 2.4 Primers used for SDM of DENV-2 NS5 inter-domain linker amino acids (L4) in TA-DENV2 NGC-E and pET28a-DENV2 FL NS5 plasmids

[a] Mutations generated using QuikChange II XL SDM kit.

[b] For, forward; Rev, reverse.

The positions of the mutated amino acids are underlined.

Mutation(s)[a]	Primer	
	Orientation[b]	Sequence
DV2-AccI	For	CAATGAGACACAAGAAAGCCA
DV2-PmI	Rev	CCTACTATCTTCAACAGCCTC
d1-L9	For	GGAACCAGAGGTAGCCAACCTAGACATAATCGGG
	Rev	GGCTACCTCTGGTTCCACTGCCACATGGCGGGTTCCGCTTCCG
d3-L9	For	CGGAACCAGAAACACCCAACCTAGACATAATCGGG
	Rev	GGGTGTTTCTGGTTCCGCATTAACATGGCGGGTTCCGCTTCCG
d4-L9	For	CGGAAACCGAAAAACCGAACCTAGACATAATCGGG
	Rev	CGGTTTTTCGGTTTCCGTACTGACAGAGCGGGTTCCGCTTCCG
JV-L9	For	AGGGAGAAGTCCATAGCAACCTAGACATAATCGGG
	Rev	TGCTATGGACTTCTCCCTTTCCCACGGCGCGGGTTCCGCTTCCG
ZV-L9	For	GCTGCGCGGAGGCGCCGAACCTAGACATAATCGGG
	Rev	TCGGCGCCTCCGCGCAGCTAACCACCGCGCGGGTTCCGCTTCCG

Table 2.5 Primers used for overlap PCR reaction to generate DENV-2 NS5 inter-domain linker amino acids mutations (L9) in TA-DENV2 NGC-E shuttle plasmid

[a] Mutations generated using overlap PCR.

[b] For, forward; Rev, reverse.

Mutation(s)[a]	Primer	
	Orientation[b]	Sequence
N453A	For	AGGAAGGAAAATGTGAATCGTGTGTCTATGCCATGATGGGAAAACGT
	Rev	ACGTTTTCCCATCATGGCATAGACACACGATTCACATTTTCCTTCCT
R457A	For	AATGTGAATCGTGTGTCTATAACATGATGGGAGCACGTGAGAAAAAATTAG
	Rev	CTAATTTTTTCTCACGTGCTCCCATCATGTTATAGACACACGATTCACATT
R458A	For	GAATCGTGTGTCTATAACATGATGGGAAAAGCTGAGAAAAAATTAGGAGA

	Rev	TCTCCTAATTTTTTCTCAGCTTTTCCCATCATGTTATAGACACACGATTC
K457A/R458A	For	GGAAAATGTGAATCGTGTGTCTATAACATGATGGGAGCAGCTGAGAAAAAATTAGGAGAGT
	Rev	ACTCTCCTAATTTTTTCTCAGCTGCTCCCATCATGTTATAGACACACGATTCACATTTTCC
E459A	For	GTCTATAACATGATGGGAAAACGTGCAAAAAAATTAGGAGAGTTTGGTAGGG
	Rev	CCCTACCAAACTCTCCTAATTTTTTTGCACGTTTTCCCATCATGTTATAGAC
F465A	For	GTGAGAAAAAATTAGGAGAGGCTGGTAGGGCCAAGGGAAGC
	Rev	GCTTCCCTTGGCCCTACCAGCCTCTCCTAATTTTTTCTCAC
W475A	For	GGGAAGCCGAGCAATCGCCTACATGTGGCTGGGGG
	Rev	CCCCCAGCCACATGTAGGCGATTGCTCGGCTTCCC
K579A	For	CTATCAAAACAAAGTGGTGGCAGTCCTCAGACCCACACCG
	Rev	CGGTGTGGGTCTGAGGACTGCCACCACTTTGTTTTGATAG

Table 2.6 Primers used for SDM to generate F1 motif mutations in pACYC-DENV4-F plasmid

[a] Mutations generated using QuikChange II XL SDM kit.

[b] For, forward; Rev, reverse.

The positions of the mutated amino acids are underlined.

Mutation(s)[a]	Primer	
	Orientation[b]	Sequence
C710A	For	GAAAAACTGGCAAGAGGTTCCTTTTGCCTCCCACCATTTTC
	Rev	GAAAATGGTGGGAGGCAAAAGGAACCTCTTGCCAGTTTTTC
S711A	For	GCAAGAGGTTCCTTTTTGCGCCCACCATTTTCACAA
	Rev	TTGTGAAAATGGTGGGCGCAAAAAGGAACCTCTTGC
H801A	For	CATGGTCGATCCACGCTGCACACCAGTGGATGACCAC
	Rev	GTGGTCATCCACTGGTGTGCAGCGTGGATCGACCATG
Q803A	For	GTCGATCCACGCTCATCACGCATGGATGACCACTGAAGACA
	Rev	TGTCTTCAGTGGTCATCCATGCGTGATGAGCGTGGATCGAC

Table 2.7 Primers used for SDM to generate N-pocket mutations in pACYC-DENV4-F plasmid

[a] Mutations generated using QuikChange II XL SDM kit.

[b] For, forward; Rev, reverse.

The positions of the mutated amino acids are underlined.

Mutation(s)[a]	Primer	
	Orientation[b]	Sequence
E111A	For	GAGGACCAGGACATGCAGAACCCATCCCCAT
	Rev	ATGGGGATGGGTTCTGCATGTCCTGGTCCTC
E111Q	For	AGGAGGACCAGGACATCAAGAACCCATCCC
	Rev	GGGATGGGTTCTTGATGTCCTGGTCCTCCT
E111R	For	CAAAAGGAGGACCAGGACATAGAGAACCCATCCCCATGT
	Rev	ACATGGGGATGGGTTCTCTATGTCCTGGTCCTCCTTTTG

Table 2.8 Primers used for SDM to generate DENV-2 NS5 E111 mutations in TA-DENV2 NGC-E plasmid

[a] Mutations generated using QuikChange II XL SDM kit.

[b] For, forward; Rev, reverse.

Mutation(s)[a]	Primer

	Orientation[b]	Sequence
G2A	For	TTCTGCGGCCGCTAATACGACTCACTATAGAATTGTTAGTCTAC
	Rev	GCTGAAGCTAGCTTTGAAGGGGATTC
G2U	For	TTCTGCGGCCGCTAATACGACTCACTATAGATTTGTTAGTCTAC
	Rev	GCTGAAGCTAGCTTTGAAGGGGATTC
G2C	For	TTCTGCGGCCGCTAATACGACTCACTATAGACTTGTTAGTCTAC
	Rev	GCTGAAGCTAGCTTTGAAGGGGATTC

Table 2.9 Primers used to generate G2 mutations at 5' UTR of pACYC-NGC FL plasmid

[a] Mutations generated using Phusion PCR reaction.

[b] For, forward; Rev, reverse.

Primer	Orientation[a]	Sequence[b]
D4 FL-NheI-FOR	For	GCTAGCTAGCGGAACTGGGACCACAGGAG
D4 FL-XhoI-REV	Rev	CTCACTCGAGTTACAGAACTCCTTCACTCT

Table 2.10 Primers used for PCR of NS5 FL mutant cDNA cassettes from pACYCI DV4-F mutant Rep plasmids

[a] For, forward; Rev, reverse.

[b] Restriction enzyme sequences are underlined.

Mutation(s)[a]	Primer	
	Orientation[b]	Sequence
S264A	For	GGGGCAGGAACGAGAGCGGTCTCCACTGAAACAGAAAAA
	Rev	TTTTTCTGTTTCAGTGGAGACCGCTCTCGTTCCTGCCCC
V265A	For	GGAACGAGAAGTGCCTCCACTGAAACAGAAAAACC
	Rev	GGTTTTTCTGTTTCAGTGGAGGCACTTCTCGTTCC
S266A	For	CGGGTACGCGCTCTGTCGCTACGGAAACCGAAAAAC
	Rev	GTTTTTCGGTTTCCGTAGCGACAGAGCGCGTACCCG
T267A	For	GGGTACGCGCTCTGTCAGTGCGGAAACCGA
	Rev	TCGGTTTCCGCACTGACAGAGCGCGTACCC

Table 2.11 Primers used for SDM to generate 3_{10}-helix mutations in pET28a-DENV4 FL NS5-MY22713 plasmid

[a] Mutations generated using QuikChange II XL SDM kit.

[b] For, forward; Rev, reverse.

The positions of the mutated amino acids are underlined.

Primer	Orientation[a]	Sequence[b]
DENV2 NS5 FL-NheI-FOR	For	GCTAGCTAGCGGAACCGGTAACATAGGAGAGACG
DENV2 NS5 FL-XhoI-REV	Rev	CTCACTCGAGCTACCACAGGACTCCTGCC

Table 2.12 Primers used for PCR amplification of DENV-2 FL NS5 from TA-DENV2 NGC-E shuttle plasmid into pET28a vector

[a] For, forward; Rev, reverse.

[b] Restriction enzyme sequences are underlined.

Mutation(s)[a]	Primer	
	Orientation[b]	Sequence
R38A	For	AAGTGGAATACTAGAAGTGGATGCAACTGAAGCCAAGTCTGCCCT
	Rev	AGGGCAGACTTGGCTTCAGTTGCATCCACTTCTAGTATTCCACTT
K42A	For	GAAGTGGATAGGACTGAAGCCGCATCTGCCCTAAGAGATGGATCT
	Rev	AGATCCATCTCTTAGGGCAGATGCGGCTTCAGTCCTATCCACTTC

R57A	For	ATCAAGCATGCGGTGTCCGCAGGGTCTAGTAAGATCAG
	Rev	CTGATCTTACTAGACCCTGCGGACACCGCATGCTTGAT
R84A	For	CGTGGATCTTGGTTGTGGGGCAGGAGGATGGTCCTATTACA
	Rev	TGTAATAGGACCATCCTCCTGCCCCACAACCAAGATCCACG
E111A	For	GGAGGTCCAGGACATGCAGAACCAATCCCCATG
	Rev	CATGGGGATTGGTTCTGCATGTCCTGGACCTCC
E111Q	For	AAGGAGGTCCAGGACATCAAGAACCAATCCCC
	Rev	GGGGATTGGTTCTTGATGTCCTGGACCTCCTT
E111R	For	CAAAAGGAGGTCCAGGACATAGAGAACCAATCCCCATGG
	Rev	CCATGGGGATTGGTTCTCTATGTCCTGGACCTCCTTTTG
R212A	For	CTCGTCAGATGCCCGCTATCCGCAAATTCTACTCATGAGATGTAT
	Rev	ATACATCTCATGAGTAGAATTTGCGGATAGCGGGCATCTGACGAG
S214A	For	CAGATGCCCGCTATCCAGGAATGCAACTCATGAGATGTATTG
	Rev	CAATACATCTCATGAGTTGCATTCCTGGATAGCGGGCATCTG
T215A	For	CCCGCTATCCAGGAATTCTGCACATGAGATGTATTGGGTGT
	Rev	ACACCCAATACATCTCATGTGCAGAATTCCTGGATAGCGGG

Table 2.13 Primers used for SDM to generate MTase mutations in pET28a-DENV4 FL NS5-MY22713 and pGEX-4T-1+D4(MY22713)+SAM272 plasmids

[a] Mutations generated using QuikChange II XL SDM kit.

[b] For, forward; Rev, reverse.

Mutation(s)[a]	Primer	
	Orientation[b]	Sequence
N453A	For	GAAGGCAAATGCGAATCTTGTGTGTATGCCATGATGGGTAAACG
	Rev	CGTTTACCCATCATGGCATACACACAAGATTCGCATTTGCCTTC
R457A	For	ATGCGAATCTTGTGTGTATAACATGATGGGTGCACGTGAGAAAAAACTG
	Rev	CAGTTTTTTCTCACGTGCACCCATCATGTTATACACACAAGATTCGCAT
R458A	For	CTTGTGTGTATAACATGATGGGTAAAGCTGAGAAAAAACTGGGCG
	Rev	CGCCCAGTTTTTTCTCAGCTTTACCCATCATGTTATACACACAAG
K457A/R458A	For	GCGAATCTTGTGTGTATAACATGATGGGTGCAGCTGAGAAAAAACTGGGCG
	Rev	CGCCCAGTTTTTTCTCAGCTGCACCCATCATGTTATACACACAAGATTCGC
E459A	For	TATAACATGATGGGTAAACGTGCAAAAAAACTGGGCGAATTCGGTC
	Rev	GACCGAATTCGCCCAGTTTTTTTGCACGTTTACCCATCATGTTATA
F465A	For	CGTGAGAAAAAACTGGGCGAAGCCGGTCGTGCAAAAGGTAG
	Rev	CTACCTTTTGCACGACCGGCTTCGCCCAGTTTTTTCTCACG
W475A	For	CAAAAGGTAGTCGCGCTATTGCATACATGTGGCTGGGCGC
	Rev	GCGCCCAGCCACATGTATGCAATAGCGCGACTACCTTTTG
K579A	For	GTACCAAAACAAAGTTGTCGCAGTTCTGCGCCCGACCC
	Rev	GGGTCGGGCGCAGAACTGCGACAACTTTGTTTTGGTAC

Table 2.14 Primers used for SDM to generate F1 motif mutations in pET28a-DENV4 FL NS5-MY22713 plasmid

[a] Mutations generated using QuikChange II XL SDM kit.

[b] For, forward; Rev, reverse.

The positions of the mutated amino acids are underlined.

Mutation(s)[a]	Primer	
	Orientation[b]	Sequence
G2A	For	GCGGCCGCTAATACGACTCACTATTAATTGTTAGTCTGTGTGGAC
	Rev	TGGTTCATTTTTCCAGAGATCTGC
G2U	For	GCGGCCGCTAATACGACTCACTATTATTTGTTAGTCTGTGTGGAC
	Rev	TGGTTCATTTTTCCAGAGATCTGC
G2C	For	GCGGCCGCTAATACGACTCACTATTACTTGTTAGTCTGTGTGGAC
	Rev	TGGTTCATTTTTCCAGAGATCTGC

Table 2.15 Primers used to generate G2 mutations at 5' UTR of DENV-4 5'UTR nt-110 DNA

[a] Mutations generated using Phusion PCR reaction.

[b] For, forward; Rev, reverse

RNA/primer	Sequence (5'-3')
Primer	$N_1N_2N_3N_4N_5N_6N_7N_8$
A-RNA template	$N_{18}N_{17}N_{16}N_{15}N_{14}N_{13}GCAUN_8N_7N_6N_5N_4N_3N_2N_1$
C-RNA template	$N_{18}N_{17}N_{16}N_{15}N_{14}N_{13}CAUGN_8N_7N_6N_5N_4N_3N_2N_1$
G-RNA template	$N_{18}N_{17}N_{16}N_{15}N_{14}N_{13}UAGCN_8N_7N_6N_5N_4N_3N_2N_1$
U-RNA template	$N_{18}N_{17}N_{16}N_{15}N_{14}N_{13}GUCAN_8N_7N_6N_5N_4N_3N_2N_1$

Table 2.16 RNA and primer used for single nucleotide incorporation assay

The primer contains FAM fluorophore conjugated at the 5' end and sequences complementary to the RNA template (highlighted in blue). A, C, G, U-RNA templates represent the identity of the first nucleotide to be incorporated into the strand by pairing with the bases underlined in red.

3 RESULTS AND DISCUSSION

3.1 Functional Characterization of the DENV-3 FL NS5 Protein

The crystal structure of DENV-3 FL NS5, encompassing amino acids 6-895, was determined at a resolution of 2.3 Å bound to SAH and GTP (318). This structure revealed a well-ordered linker region consisting of a short 3_{10}-helix (residues 263-266) and an inter-domain interface formed by mostly polar residues (Figure 3.1). The interface is composed of two contact areas involving amino acid residues from the putative linker region (residues 263-272), the finger subdomains of RdRp, and MTase domain (Figure 3.1). The polar interaction network is established via water-mediated hydrogen bonding as well as directly between charged side-chains. In the first cluster (Figure 3.1C), the side chain of E267 from the linker region interacts with Y119 and R262 from the MTase domain via hydrogen bonding, while E269 from the linker region makes salt bridge interaction with the guanidinium side chain of R361 as well as interacts with K595 from the RdRp domain. Additionally, MTase amino acids K95-K96 form several electrostatic interactions with E296-K300 from the RdRp domain. The second cluster (Figure 3.1D) features numerous contacts including water-mediated hydrogen bonding between amino acids from the MTase domain and residues F348 to K357 of helix α5 which is part of the βNLS motif of the RdRp domain. At the center of this helix, the guanidinium functional group of R352 forms various electrostatic interactions with E67, E252 and Q63. A salt bridge is also formed between K357 and D256. The only hydrophobic contacts comprise stacking interactions between W64, R68, F348 and P582. Most of the interface residues are highly evolutionarily conserved in DENV (Figure 3.1E), indicating their functional importance in NS5. By employing a combination of biochemical and reverse genetic approaches, the biological relevance of intra-molecular interactions and the flexible interdomain linker in the DENV-3 NS5 FL structure was elucidated. The details of these experimental results are described in following Sections (3.1.1 and 3.1.2).

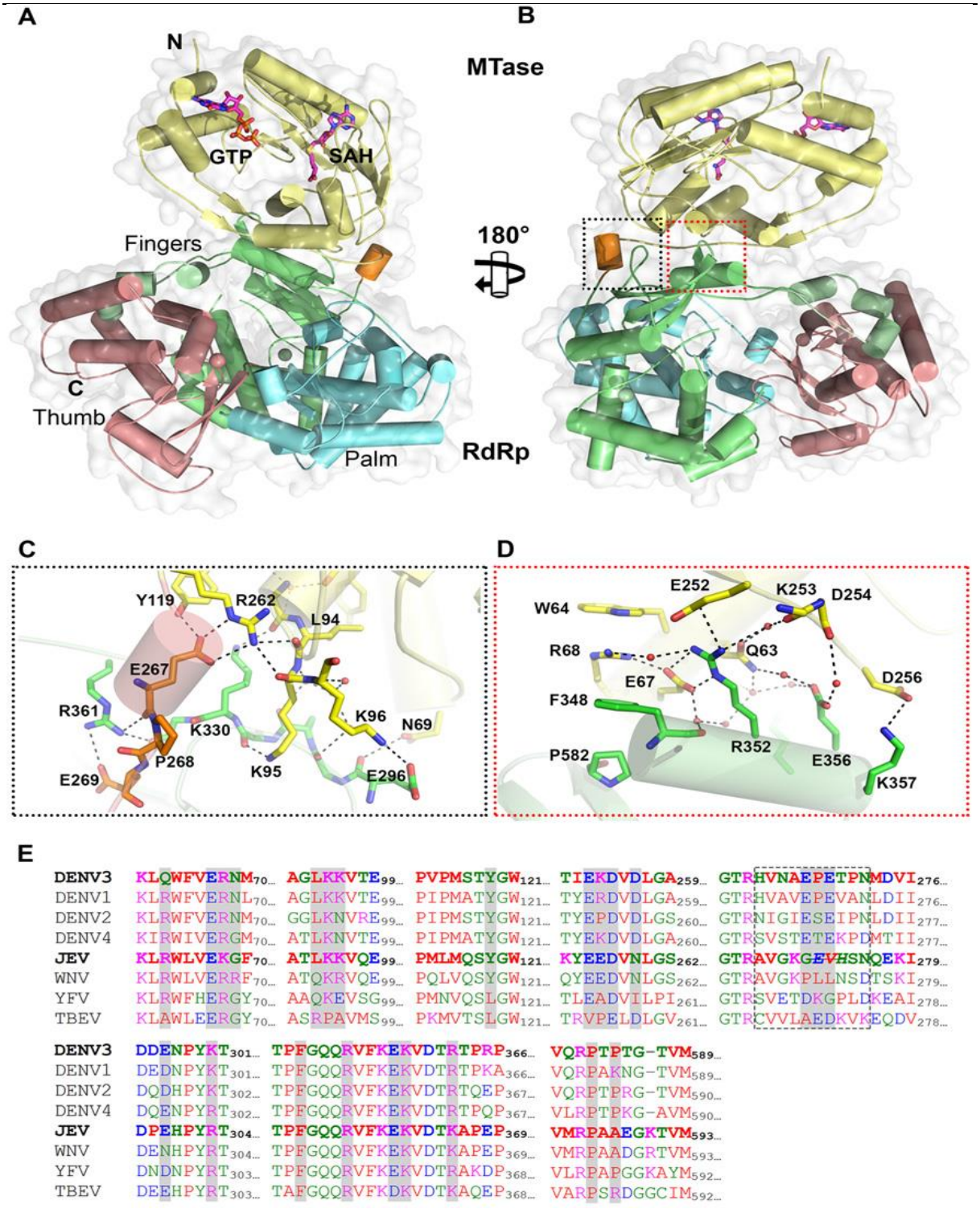

Figure 3.1 Crystal structure of DENV-3 FL NS5. (A) Overall structure of DENV-3 NS5 FL protein in cartoon representation viewing from the bottom of RdRp. MTase, RdRp fingers, palm and thumb domains are colored yellow, green, blue and salmon respectively. The linker helix (residues 263-267) is colored orange. GTP and co-factor SAH are represented as sticks and labelled. Zinc ions are shown as spheres. (B) 180° rotation of the NS5 FL molecule around a vertical axis as in (A). The two inter-domain interface regions as indicated in (B) are boxed and shown in (C) and (D). Key residues for intra-molecular interactions are shown as sticks and labeled. (E) Multiple sequence alignment of flavivirus NS5 proteins. Interface residues are shaded in gray. The linker residues from 263-272 are boxed. Adapted from (318).

3.1.1 Functional importance of the intra-molecular interactions

Several conserved interface residues were selected for structure-guided site-directed mutagenesis (SDM). The effect of mutations on viral replication was studied using *in vitro* enzymatic assays, transient luciferase-expressing subgenomic-replicon system and virus infectious clones.

3.1.1.1 The interface mutants differentially affect NS5 activities in vitro

To investigate the functional relevance of amino acids involved in inter-domain interactions on MTase and RdRp enzymatic activities, individual alanine mutations of the residues K95, K95/N96 (K95/K96 in DENV-3), Y119, R263 (R262 in DENV-3), E268 (E267 in DENV-3), E270 (E269 in DENV-3), R353 (R352 in DENV-3), R362 (R361 in DENV-3) and K596 (K595 in DENV-3) were introduced into DENV-4 NS5 FL and the recombinant proteins were expressed. The mutations were introduced into DENV-4 NS5 protein and not DENV-3 which was used for structural determination because DENV-3 NS5 protein is unstable *in vitro* and not robust for enzymatic activity measurement. Residues K95, N96, Y119 and R263 are localized within the MTase core domain, whilst residues E268 and E270 reside in the putative linker region and residues R353, R362 and K596 are found in the RdRp core domain. Note that the amino acids chosen for mutations are conserved across all serotypes of DENV except for N96 and K596, but not across other flaviviruses except for R263 and R353 (Figure 3.1E). The substitution of these charged residues except for Y119 that is polar, hydrophobic, and N96 that is polar, uncharged, with alanine could induce a non-complementary charge and disrupt inter-domain interactions, allowing us to study their biological functions. Thermo-fluorescence assay showed that WT protein and all the mutant proteins exhibited comparable stability, indicated by only ±1.5°C difference in their T_m values, denoting that the proteins were properly folded (Table 3.1).

The MTase activities of the proteins were assessed by N-7 and 2'-*O* methylation assays, while the RdRp activities were examined using *de novo* initiation (*dn*I)/elongation and elongation fluorescence-based alkaline phosphatase-coupled polymerase assays (FAPA) as illustrated in Materials & Methods. The *dn*I assay employs a viral UTR sequence as template to initiate new RNA synthesis, whereas the elongation assay uses a heteropolymeric RNA template annealed to four primers to carry out RNA extension. The enzymatic activities of the mutant proteins were compared against WT protein (Table 3.1).

In general, none of the alanine substitutions induced significant impairment in MTase activity except for Y119A which displayed less than 50% N-7 activity and minimal 2'-*O* activity, and R263A in which both N-7 and 2'-*O* activities were almost abolished (Table 3.1 and Figure 3.2C and 3.2D). These two residues are part of the MTase core domain, and thus are important for MTase activity of NS5.

In the RdRp assays, only E270A which resides at the putative linker region showed key reduction of 40-50% in *de novo* initiation/elongation activity and 20-30% in elongation activity (Table 3.1 and Figure 3.2A and 3.2B). Its interacting partner in the RdRp domain, K596A, displayed a moderate decrease in both polymerase activities by 30-40%. The remaining mutants either exhibited comparable or higher RdRp activities as compared to WT. The alanine mutation of MTase domain residue K95 seems to have resulted in an active RdRp with approximately 2-fold increase in both RdRp activities as compared to WT. Additionally, its double mutant, K95A/N96A, displayed two times enhancement in the *de novo* initiation/elongation activity and about 60-90% increase in the elongation activity. Interestingly, R353, which is part of the helix α5 of the βNLS motif and plays a central role in forming transverse polar contacts with interacting residues at the second cluster of the interface (Figure 3.1D), when substituted with alanine, exhibited 2-fold higher in the elongation activity while maintaining *de novo* initiation/elongation activity similar to WT. In contrast, R362A

mutant that also belongs to part of the βNLS region and is present at the first interaction cluster demonstrated a 2-fold increase in the *de novo* initiation/elongation activity and no change in the elongation activity.

The only mutant that displayed minor changes in both MTase and RdRp activities is E268A in which 70% of both MTase activities were retained, elongation activity was similar to WT, and the *de novo* initiation/elongation activity was about 30% higher than WT (Table 3.1, Figure 3.2A-D).

% FL NS5 activity	***De novo* initiation/elongation**			**Elongation**			**N-7 MTase**	**2'-*O* MTase**	***Thermo-fluorescence***	**Location in NS5**
Time (hr)	**1**	**2**	**3**	**1**	**2**	**3**	**0.25**	**1**	***Tm* (ºC)**	
WT	100	100	100	100	100	100	100	100	37	
K95A	189.9 ± 4.0	198.4 ± 9.5	171.9 ± 3.7	194.0 ± 3.9	200.6 ± 1.0	182.3 ± 13.1	85.6 ± 15.0	82.4 ± 1.0	37	MTase domain
K95A/N96A	214.4 ± 1.2	209.1 ± 17.2	197.5 ± 8.9	166.1 ± 6.5	185.2 ± 1.9	168.5 ± 8.3	92.6 ± 4.2	117.6 ± 12.0	36	
Y119A	149.5 ± 11.4	144.3 ± 22.1	149.9 ± 12.1	113.0 ± 3.3	110.2 ± 1.1	114.5 ± 0.5	46.3 ± 0.8	8.3 ± 0.4	38	
R263A	151.3 ± 2.5	142.9 ± 5.0	135.7 ± 5.0	103.9 ± 4.8	105.0 ± 0.5	112.4 ± 0.8	4.0 ± 0.3	3.2 ± 0.3	37	
E268A	129.0 ± 4.6	128.3 ± 8.3	135.2 ± 8.2	92.7 ± 2.5	87.6 ± 2.8	98.3 ± 3.2	71.9 ± 2.6	70.4 ± 2.5	37	Putative linker region
E270A	56.0 ± 3.7	62.3 ± 5.4	57.4 ± 5.5	71.7 ± 2.4	70.1 ± 1.8	77.9 ± 1.5	74.1 ± 10.2	65.1 ± 0.4	37	
R353A	107.0 ± 3.1	92.0 ± 3.4	94.3 ± 2.5	193.1 ± 2.9	198.1 ± 25.1	206.4 ± 15.0	106.3 ± 6.7	97.7 ± 4.4	38	RdRp domain
R362A	194.2 ± 12.6	185.5 ± 5.0	198.5 ± 15.4	101.9 ± 2.0	104.3 ± 4.2	119.6 ± 3.4	126.0 ± 0.9	81.2 ± 2.6	37	
K596A	59.5 ± 12.8	84.9 ± 2.8	78.6 ± 3.2	67.4 ± 2.3	75.0 ± 3.0	62.7 ± 10.9	N.D.	N.D.	35.5	

Table 3.1 Enzymatic activities and thermo-stabilities of DENV-4 NS5 FL WT and interface mutant proteins. The polymerase *de novo* initiation and elongation activities of DENV-4 WT and interface mutant FL NS5 proteins were measured in FAPA assays. Results shown are the average percentage activity compared against DENV-4 WT FL NS5 protein derived from average relative fluorescence units (RFU) obtained for each protein from one experiment. N-7 and 2'-*O* MTase activities of DENV-4 WT and interface mutant FL NS5 proteins were measured in SPA assays. Results shown are the average percentage activity compared against DENV-4 WT FL NS5 protein derived from average corrected counts per minute (CCPM) obtained for each protein. All data points were performed in triplicate (RdRp activities) or duplicate (MTase activities) wells. Thermo-stability was assessed using thermo-fluorescence assay. N.D. denotes not determined.

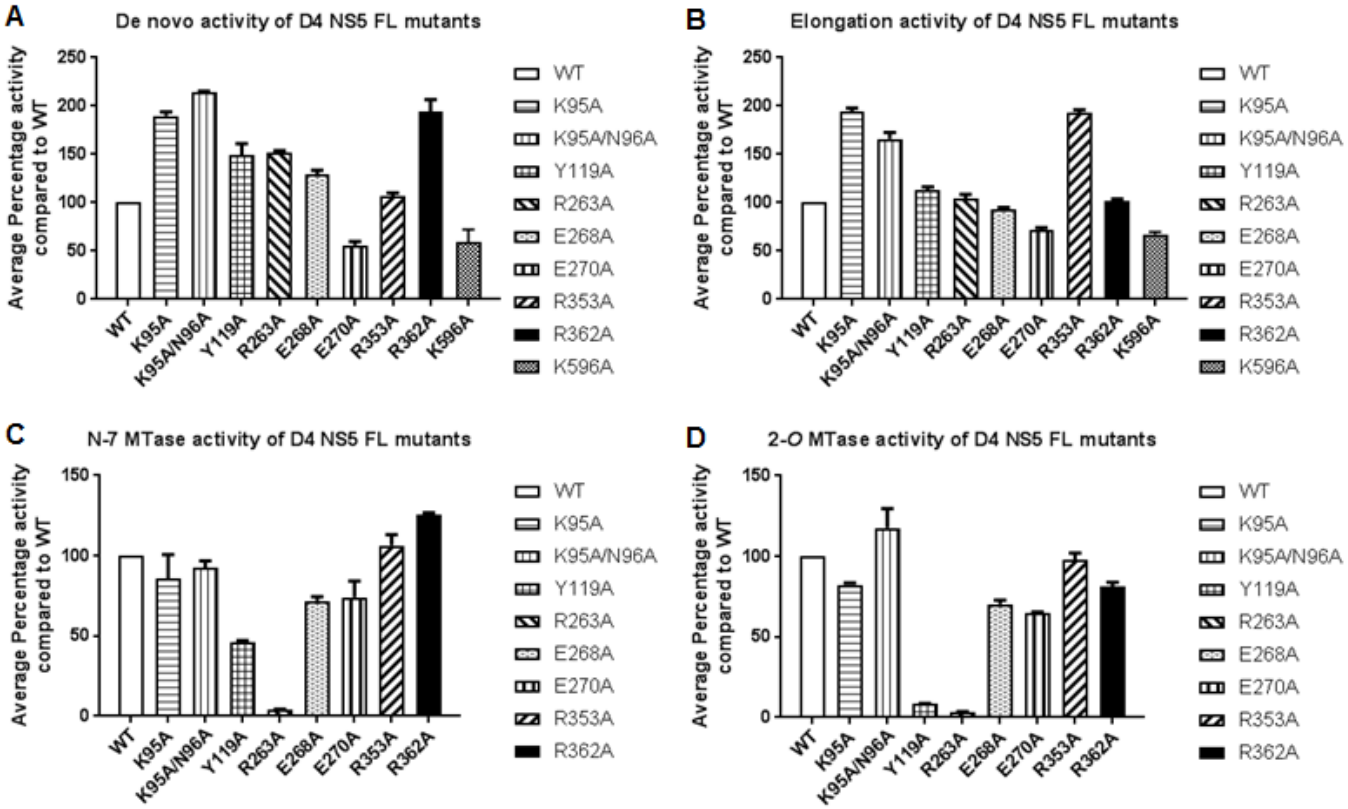

Figure 3.2 *In vitro* enzymatic activities of DENV-4 NS5 FL WT and interface mutant proteins. (A) De novo initiation/elongation activities, (B) elongation activities, (C) N-7 MTase, and (D) 2'-*O* MTase activities of DENV-4 WT and interface mutant FL NS5 proteins. The graphs in (A) and (B) show the average percentage activity of the mutants as compared to WT at 1 hr.

3.1.1.2 Increased RdRp activities could be correlated to a higher affinity of NS5 towards nucleotide and RNA substrates

To better understand the mechanism for enhanced RdRp activity, steady-state kinetic measurements were performed with K95A that showed 2-fold increase in both RdRp activities, R353A that displayed 2 times better in the elongation activity, and R362A that exhibited double enhancement in the *de novo* initiation/elongation activity, and were compared with WT NS5 FL protein (Table 3.2). Both *dn*I and elongation FAPA were employed to measure K_m, K_{cat} and V_{max} of Atto-CTP and RNA substrates. Relatively consistent with the results from RdRp activity testing, K95A demonstrated about 1.8-fold lower K_m and 2.1-fold higher K_{cat} resulting in about 3.7-fold higher catalytic efficiency for Atto-CTP upon *dn*I, as well as comparable catalytic efficiency for Atto-CTP and RNA as WT upon elongation. This result suggests that

K95A stimulates higher RdRp activity by slightly increasing affinity and turnover for Atto-CTP during *dn*I, and sustains elongation capability similar to WT for Atto-CTP incorporation and affinity towards RNA. Likewise for R362A, the observed increase in the *de novo* initiation/elongation activity could be accounted for by a marginally better affinity (K_m about 1.8-fold lower) and catalytic efficiency (2.2-fold higher) for Atto-CTP during *dn*I, For R353A mutant, the double increase in the elongation activity was not reflected on the kinetic measurements whereby only a partially better affinity for RNA (K_m about 1.5-fold lower) was observed during elongation.

FAPA *dn*I	**Atto-CTP**				**RNA**	
Average	**V_{max}^{app} (nM/min)**	**K_m^{app} (μM)**	**K_{cat}^{app} (min-1)**	**k_{cat}^{app}/K_m^{app} (min^{-1} μM^{-1})**	**K_m^{app} (nM)**	**K_{cat}^{app} (min-1)**
DENV4 NS5 FL WT	2.225 ± 0.071	1.370 ± 0.296	0.022 ± 0.001	0.017 ± 0.004	39.050 ± 7.449	0.031 ± 0.014
DENV4 NS5 FL K95A	4.816 ± 0.101	0.759 ± 0.057	0.048 ± 0.001	0.064 ± 0.006	38.065 ± 0.064	0.043 ± 0.002
DENV4 NS5 FL R362A	2.776 ± 0.602	0.726 ± 0.025	0.028 ± 0.006	0.038 ± 0.010	48.495 ± 2.510	0.034 ± 0.005
FAPA elongation	**Atto-CTP**				**RNA**	
Average	**V_{max}^{app} (nM/min)**	**K_m^{app} (μM)**	**K_{cat}^{app} (min-1)**	**k_{cat}^{app}/K_m^{app} (min^{-1} μM^{-1})**	**K_m^{app} (nM)**	**K_{cat}^{app} (min-1)**
DENV4 NS5 FL WT	0.861 ± 0.114	0.163 ± 0.002	0.009 ± 0.001	0.053 ± 0.006	61.620 ± 5.558	0.010 ± 0.000
DENV4 NS5 FL K95A	1.199 ± 0.112	0.188 ± 0.024	0.012 ± 0.001	0.065 ± 0.014	45.500 ± 4.384	0.011 ± 0.001
DENV4 NS5 FL R353A	1.018 ± 0.051	0.317 ± 0.013	0.010 ± 0.001	0.032 ± 0.003	40.425 ± 11.264	0.013 ± 0.003

Table 3.2 Kinetic constants for DENV-4 NS5 FL WT and interface mutant proteins derived using FAPA *dn*I and elongation assays. V_{max}, K_m and k_{cat} values were obtained using Graphpad Prism 6 software as described in Materials and Methods. Results shown in the table are the average values obtained for each protein from two independent experiments. All data points were performed in triplicate wells.

3.1.1.3 The MTase-RdRp interface is essential in modulating viral replication

A systematic mutagenesis analysis was performed by engineering alanine substitutions at key positions K95, K95/N96 (K95/K96 in DENV-3), Y119, R263 (R262 in DENV-3), E268 (E267 in DENV-3), E270 (E269 in DENV-3), R353 (R352 in DENV-3), R362 (R361 in DENV-3) and K596 (K595 in DENV-3) in a DENV-4 subgenomic RNA replicon, harboring a R_{luc} reporter (in place of the viral structural genes), to examine whether amino acids at the interface

are essential for virus replication. The same amounts of WT and mutant replicon RNAs were electroporated into BHK-21 cells and luciferase activities were measured at 1, 4, 24, 48, 72 and 96 hour post-transfection (hpt) (Figure 3.3A). The luciferase activity for DENV-4 WT replicon reached a peak level at about 24 to 48 hpt and the signal gradually dropped from 48 to 96 hpt. For DENV-4 mutant replicons Y119A, R263A, E270A, R362A and K596A, only background or low luciferase signal level was observed from 24 to 96 hpt, implying that they were unable to replicate. This finding was supported by the substantial decrease in the MTase or RdRp activities observed for Y119A, R263A, E270A and K596A (Table 3.1 and Figure 3.2A-D). Surprisingly, the results from enzymatic assays for R362A did not account for the defective viral replication observed here. Mutant replicons K95A, K95A/N96A and E268A exhibited roughly equal levels of luciferase signal that are comparable to WT replicon at 48 hpt, albeit they showed some delay at the first 24 hrs.

Interestingly, R353A mutant replicon replicated at a lower level as compared to WT replicon at earlier hours (about 13-fold lower at 24 hpt), but the level of luciferase signal increased subsequently and maintained at about 2.5-fold higher than WT replicon throughout 48 to 96 hpt. This observation is in accordance with the previous data whereby R353A mutant showed a 2-fold increase in the elongation activity while maintaining its *de novo* initiation/elongation activity and MTase activity (Table 3.1 and Figure 3.2A-D).

Immunofluorescence assay (IFA) was also carried out to detect NS3 helicase protein and viral RNA expression in transfected cells, and only images at 48 hpt were shown in Figure 3.3B. Consistent with the results in *Renilla* luciferase assay, K95A and E268A produced IFA-positive cells comparable to WT, while R353A produced more IFA-positive cells than WT. Also, no IFA-positive cells were seen in Y119A, R263A, E270A, R362A and K596A-transfected cells, suggesting that these residues play a vital role in viral replication. Overall, the data from both *Renilla* luciferase assay and IFA provided evidence that the conserved residues in the MTase-

RdRp interface are essential for regulating virus replication and mutations of critical residues resulted in defective replication ability.

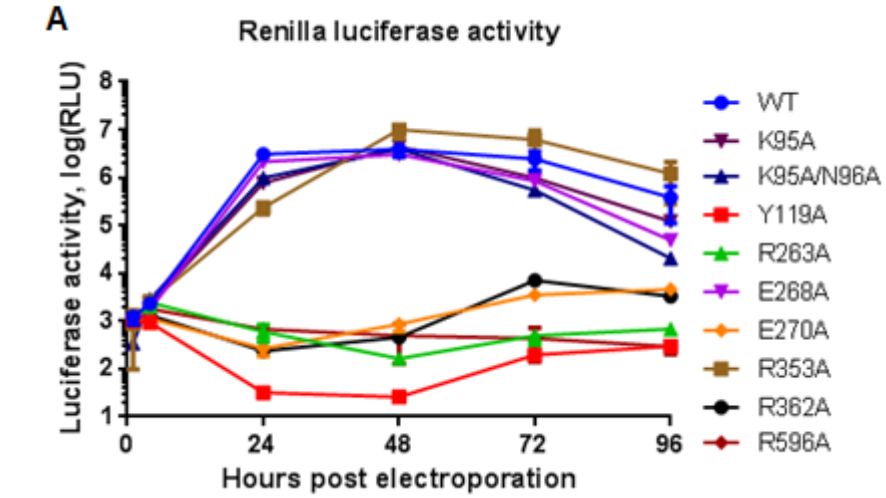

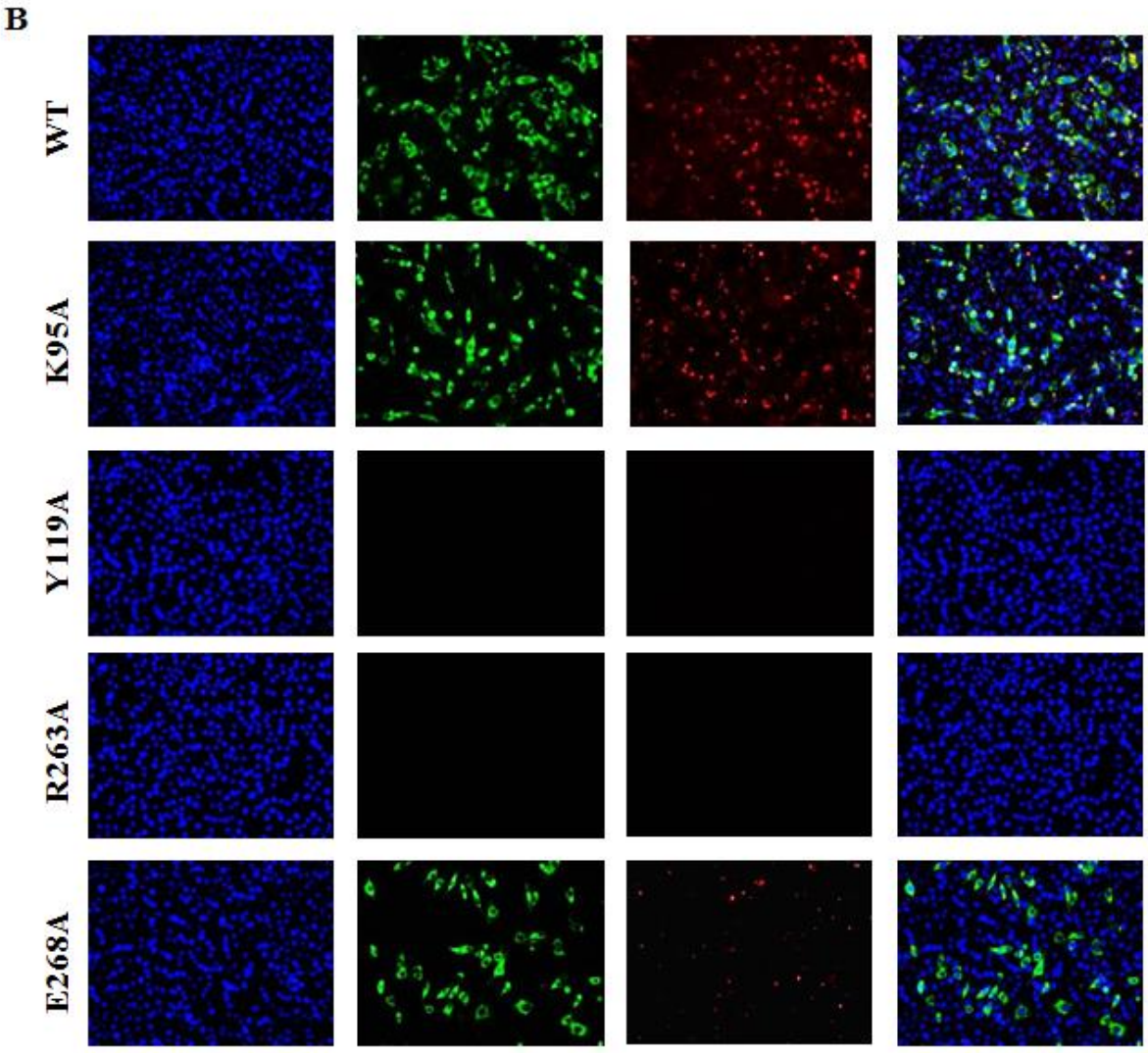

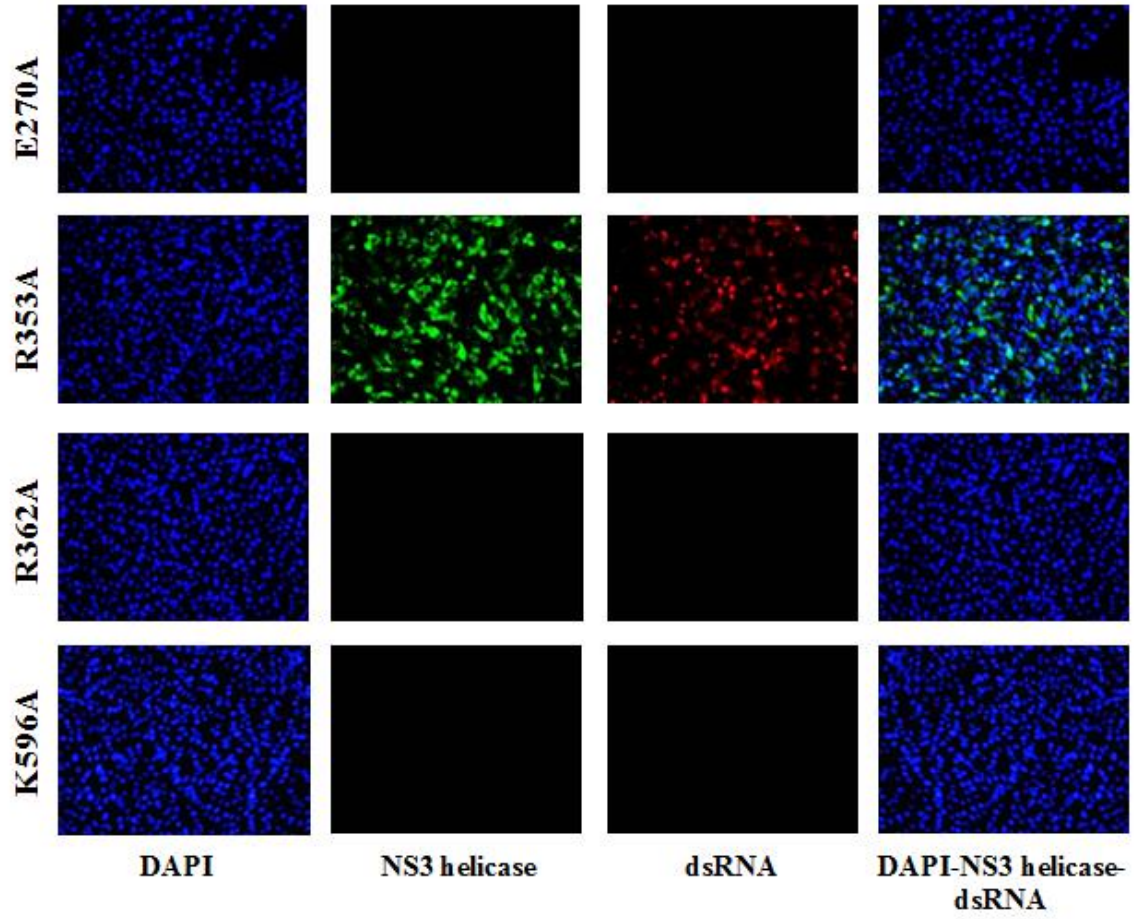

Figure 3.3 Replicon analysis of NS5 interface mutants. (A) DENV-4 subgenomic RNA replicon was used to assess the effects of interface mutations on viral RNA replication. Equal amounts of WT and mutant replicon RNAs were electroporated into BHK-21 cells and assayed for luciferase activity at the designated time points post transfection. The y-axis shows the log10 value of *Renilla* luciferase activity (relative light units, RLU) and the x-axis shows the time post electroporation (hr). Each data point is the average for two replicates, and error bars indicate the standard deviations. (B) Immunofluorescence analysis of DENV-4 subgenomic RNA replicon replication containing NS5 interface mutations in BHK-21 cells at 48 hpt. Primary antibodies used were anti-NS3 helicase protein rabbit polyclonal antibody and anti-dsRNA mouse monoclonal antibody (J2), while secondary antibodies used were Alexa Fluor 488-conjugated goat anti-rabbit IgG and Alexa Fluor 568-conjugated donkey anti-mouse IgG.

3.1.1.4 The importance of the MTase-RdRp interface in DENV-4 virus production

To further explore the biological importance of the MTase-RdRp interactions in viral replication, K95A, Y119A, E268A (E267 in DENV-3), and R353 (R352 in DENV-3) alanine mutations were introduced into DENV-4 infectious clone. Immunofluorescence assay (IFA) was carried out to monitor viral RNA and RdRp protein expression in transfected cells, and only images at 72 and 120 hpt were shown in Figure 3.4A. Plaque assay and qRT-PCR were also carried out for quantification of virus productions and intracellular viral RNA at indicated

time points post transfection respectively (Figure 3.4B and 3.4C). Similar to the replicon data (Figure 3.3A), Y119A mutant failed to produce infectious virus or increased intracellular RNA, further confirming its critical role in viral replication. K95A mutant virus displayed lower replicative ability than WT with lesser IFA-positive cells, virus production and intracellular RNA as compared to WT at the first 4 days. Strangely at 120 hpt, K95A mutant expressed higher intracellular RNA level than WT which is not reflective of the lesser IFA-positive cells and lower virus production observed.

For E268A mutant, virus production was detected at 96 and 120 hpt consistent with the plaque formation observed at 120 hpt, although no IFA-positive cells and increased intracellular RNA were seen. This observation is relatively in line with the results from enzymatic assays and replicon experiments whereby E268A did not exhibit significant changes in both MTase and RdRp activities (Table 3.1 and Figure 3.2A-D), and it replicated similarly as WT (Figure 3.3A), indicating that E268 does not play essential roles in the enzymatic activities of NS5 as well as in viral replication and infectivity. R353A did not produce any IFA-positive cells and viable virus as shown by no plaque formation and no increase in intracellular RNA. This result did not match the replicon data in which its luciferase signal sustained at a higher level than WT replicon from 48 to 96 hpt and more IFA-positive cells were generated (Figure 3.3A), suggesting that R353 play important but non-enzymatic role in viral replication, growth and infectivity.

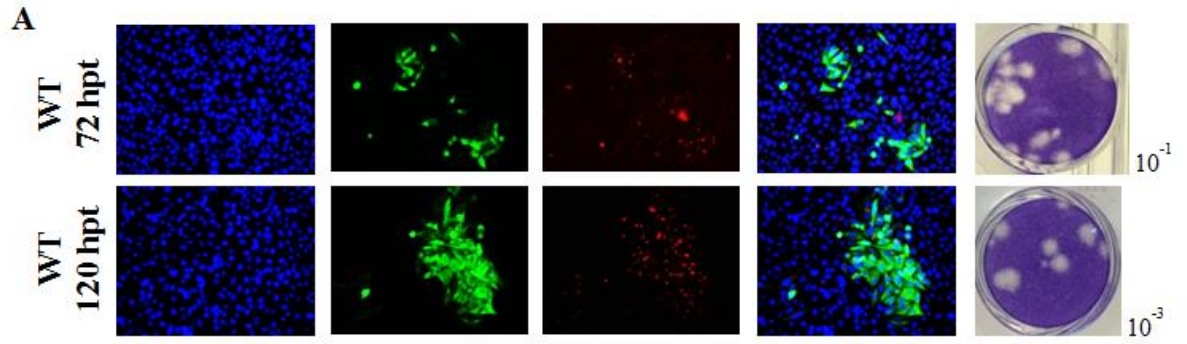

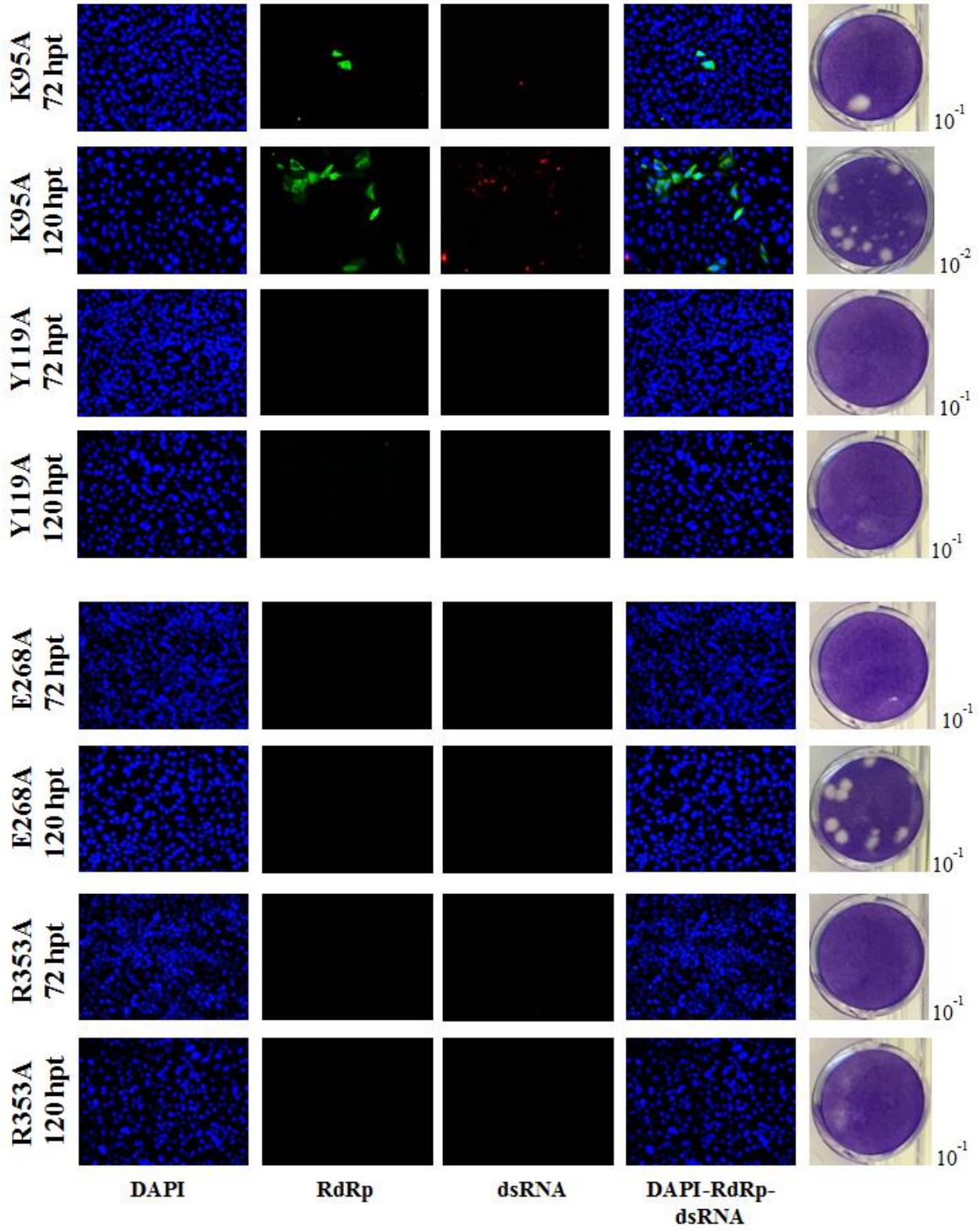
K95A 72 hpt
K95A 120 hpt
Y119A 72 hpt
Y119A 120 hpt
E268A 72 hpt
E268A 120 hpt
R353A 72 hpt
R353A 120 hpt
10-1
10-2
DAPI
RdRp
dsRNA
DAPI-RdRp-dsRNA

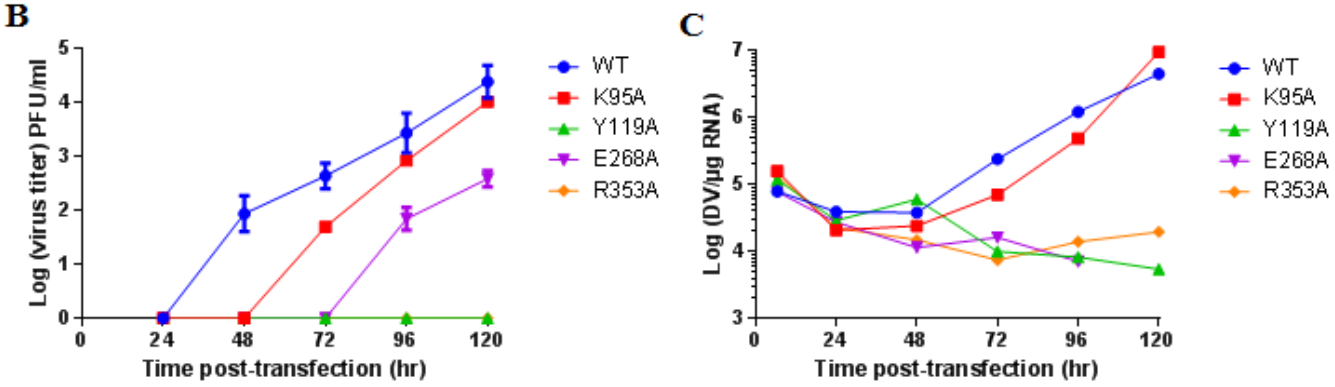

Figure 3.4 Functional analysis of NS5 interface mutations in DENV-4 infectious cDNA clone. (A) Immunofluorescence analysis and plaque morphology of DENV-4 genome-length viral RNA replication containing NS5 interface mutations in transfected BHK-21 cells at 72 and 120 hpt. Primary antibodies used were anti-DENV-4 RdRp rabbit polyclonal antibody and anti-dsRNA mouse monoclonal antibody (J2), while secondary antibodies used were Alexa Fluor 488-conjugated goat anti-rabbit IgG and Alexa Fluor 568-conjugated donkey anti-mouse IgG. Plaque morphogy of WT and mutant viruses was determined using supernatants collected at 72 and 120 hpt. The dilution factor where countable plaques were observed is indicated. (B) Virus production of the transfected cells at each time point post-transfection was observed by plaque assay, and the visible plaques were used to calculate titers of DENV-4 WT and NS5 interface mutants. (C) Viral replication in transfected BHK-21 cells was monitored over a course of 5 days. Intracellular viral RNA replication was detected by qRT-PCR as described in Materials and Methods.

3.1.2 Functional importance of the interdomain linker region

The importance of the linker region in NS5 was highlighted earlier using alanine mutagenesis for *in vitro* enzymatic and cellular-based viral replication studies whereby mutation of critical linker residues affected polymerase activities and impaired viral replication in cells (315, 318, 319).

Since the DENV-3 NS5 FL structure presented a well-ordered linker with clear electron density, the boundaries of the RdRp domain was carefully delineated and the linker region was precisely defined as 4-amino acids long from residues 263 to 266 (318). The least evolutionarily conserved short linker folds into a compact 3_{10}-helix, allowing the formation of a MTase-RdRp interface. The functional relevance of the short 3_{10}-helix residues in viral replication was explored using biochemical and reverse genetic approaches. The linker in DENV-2 NS5 was also swapped with corresponding flavivirus sequences to examine the biological relevance of amino acid composition of the linker region in viral replication.

3.1.2.1 The residues of the 3_{10}-helix are important for viral replication

To characterize the enzymatic function of the short 3_{10}-helix residues, individual alanine mutations of the residues S264A (H263 in DENV-3), V265A (V264 in DENV-3), S266A (N265 in DENV-3) and T267A (A266 in DENV-3) were introduced into the DENV-4 NS5 FL protein and the enzymatic activities of polymerase were compared against WT protein (Figure 3.5A and 3.5B). Note that the amino acids chosen for mutations are highly variable across all serotypes of DENV and other flaviviruses (Figure 3.6). Thermofluor assays confirmed that all the mutant proteins exhibited comparable stability as WT NS5 FL, suggesting that they were properly folded (Table 3.3). The RdRp activity of WT and mutant proteins was examined using both the coupled *de novo* initiation/elongation and elongation FAPA assays as illustrated previously (315, 318). S264A exhibited about 40% increase in *de novo* initiation/elongation activity compared to WT protein, whilst V265A demonstrated comparable *de novo* initiation/elongation and elongation activities to WT protein. In contrast, S266A and T267A displayed differential effects on both polymerase activities. Their elongation activities were about 50-60% higher than WT protein whereas their *de novo* initiation/elongation activities showed 30-40% reduction. These results indicated that the last two amino acids of the 3_{10}-helix are important for regulating both the *de novo* initiation and elongation steps of RNA synthesis. We next assessed whether the mutants could have an effect on viral replication in cells.

The same individual alanine mutations were introduced in a DENV-4 subgenomic replicon, bearing a renilla luciferase reporter. All WT and mutant DENV-4 replicon RNAs were electroporated into BHK-21 cells at equal amounts and luciferase activities were assayed at 1, 4, 24, 48, 72 and 96 hour post-electroporation (Figure 3.5C). After 24 hours, mutant replicons S264A and V265A were less replicative competent as compared to WT replicon. However, growth of S264A was comparable to WT at 48 and 72 hour, and V265A showed less than 1 log reduction in luciferase signals from 48-96 hour post-electroporation. On the other hand,

little or no luciferase activity was detected for mutant replicons S266A and T267A throughout the four days following transfection. Together, these data indicated that the first two residues of the short 3_{10}-helix are less important for viral replication whereas the third and fourth residues are essential for virus replication in cells. These results are in line with the observed impacts of these mutations on *in vitro* NS5 polymerase activities.

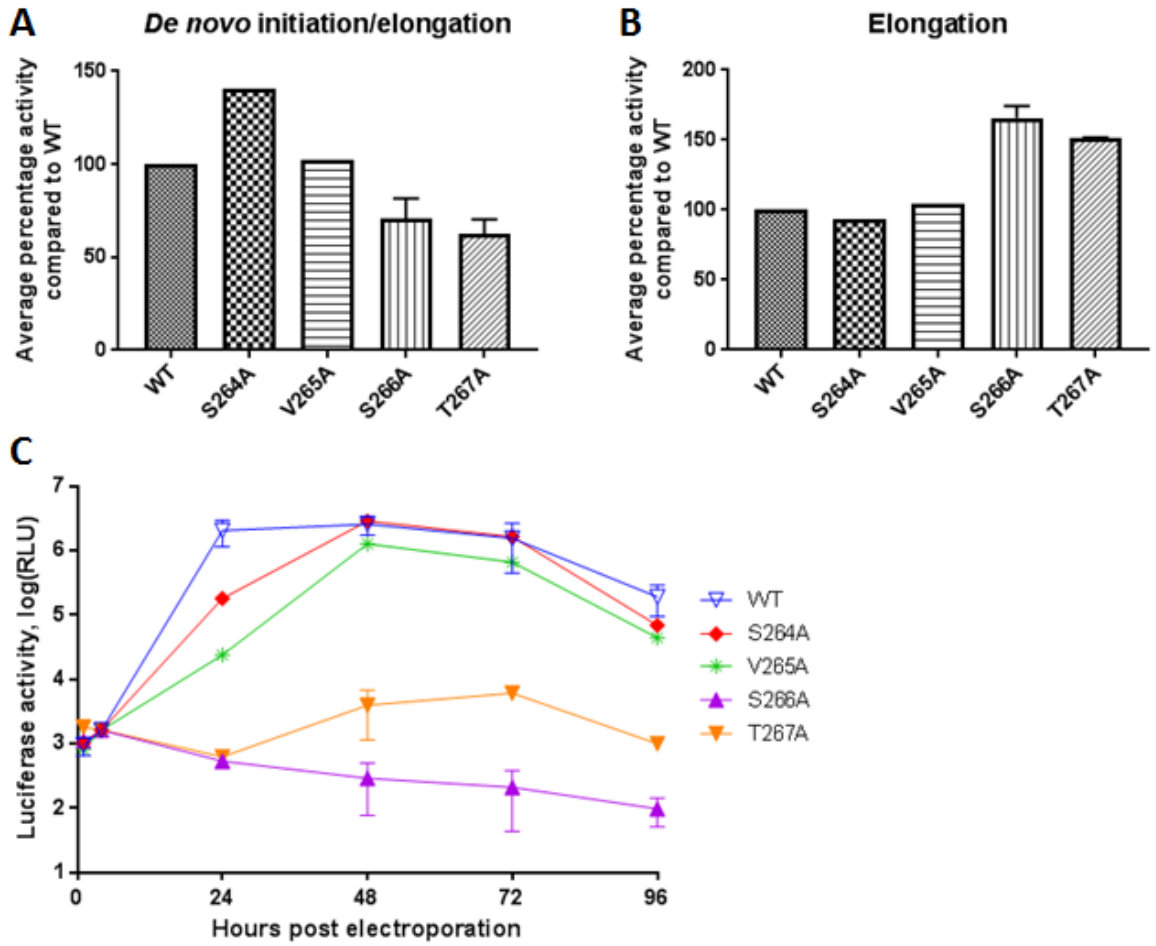

Figure 3.5 Polymerase activities and replication profiles of DENV-4 WT and 3_{10}-helix mutant NS5 FL proteins and replicons. (A) A polymerase *de novo*/elongation assay was performed using viral untranslated region (UTR) sequence as the RNA template as described previously (242, 306). (B) Elongation assay was performed with a heteropolymeric RNA template annealed with four primers as described previously (316, 318). Results shown are the average percentage activity compared against DENV-4 WT NS5 FL protein at t=1hr derived from average relative fluorescence units (RFU) obtained from each protein from one experiment. Two independent experiments were carried out in triplicate wells. (C) Renilla luciferase activities of DENV-4 WT and mutant replicons. Equal amount of replicon RNA were electroporated into BHK-21 cells and luciferase activities were assayed at indicated time points. The y axis shows the log10 value of Renilla luciferase activity (RLU). Each data point is the average for two replicates, and error bars show the standard deviations. **Note that the effects of alanine mutation of S264 and V265 on polymerase de novo initiation activities were previously studied (315) and are included here for comparison.*

% D4 NS5 activity	De novo initiation/elongation	Elongation	Thermo-fluorescence Tm (°C)
WT	100	100	37
S264A	*140.6 ± 10.9	93.3 ± 6.6	37
V265A	*102.0 ± 1.7	104.0 ± 3.2	37
S266A	70.9 ± 10.9	165.9 ± 8.5	37
T267A	62.5 ± 7.9	151.3 ± 0.6	37

Table 3.3 Enzymatic activities and thermo-stabilities of DENV-4 WT and 3_{10}-helix mutant NS5 FL proteins. The polymerase *de novo* initiation and elongation activities of DENV-4 WT and 3_{10}-helix mutant NS5 FL proteins were measured in FAPA assays with 1 hour incubation at RT. Results shown are the average percentage activity compared against DENV-4 WT NS5 FL protein derived from average relative fluorescence units (RFU) obtained for each protein from one experiment. Two independent experiments were performed for each assay in triplicate measurements. Thermo-stability was assessed using thermo-denaturation assay. **Note that the effects of alanine mutation of S264 and V265 on polymerase de novo initiation activities were previously studied (315) and are included here for comparison.*

Flavivirus	Sequence
DENV-1	$_{263}$HVAVEPEVAN$_{272}$
DENV-2	$_{264}$NIGIESEIPN$_{273}$
DENV-3	$_{263}$HVNAEPETPN$_{272}$
DENV-4	$_{264}$SVSTETEKPD$_{273}$
JEV	$_{266}$AVGKGEVHSN$_{275}$
ZIKV	$_{265}$AVVSCAEAPN$_{274}$

Figure 3.6 Sequences of flavivirus NS5 linker. Shown here are the NS5 linker sequences of the four DENV serotypes (DENV-1, 2, 3 and 4) as well as Japanese Encephalitis Virus (JEV) and Zika Virus (ZIKV). Swapping of the 3_{10}-helix amino acids (aa264-267 in DENV-2 numbering) and the entire inter-domain linker (aa264-272 in DENV-2 numbering) in DENV-2 NS5 with corresponding Flavivirus sequences was carried out to generate L4 and L9 mutants. Residues in DENV-3 linker that make interactions with MTase or RdRp are highlighted in red. Residues that are underlined means that they are predicted to have a higher preference for α-helix formation. CFSSP online tool was used to predict the helix propensity of different linker sequences.

3.1.2.2 Biological relevance of the unique amino acid composition of linker

To investigate the relevance of amino acid composition of the linker region, the 3_{10}-helix amino acids (aa264-267 in DENV-2 numbering; L4) as well as the entire inter-domain linker (aa264-272 in DENV-2 numbering; L9) in DENV-2 NS5 were swapped with corresponding Flavivirus sequences. Note that there is low sequence conservation of the linker region across the four DENV NS5 serotypes as well as JEV and ZIKV (Figure 3.6). The enzymatic activities and

viral replicative abilities of these mutations were studied in the context of DENV-2 NS5 FL protein and DENV-2 subgenomic RNA replicon respectively. With the exception of d4-L9 (DENV-2 entire linker amino acids replaced by DENV-4) protein which has a slightly higher melting temperature (Tm) than WT NS5 FL, all the other purified mutant proteins exhibited comparable stability to WT as determined by the thermofluor assay (Table 3.4A and 3.4B). FAPA assays mentioned above were employed to examine the ability of mutant proteins to carry out *de novo* initiation/elongation and elongation activities (Figure 3.7A-D). In general, the L4 and L9 mutants were able to elongate RNA to similar extent or better than WT (< 40 % change in activity compared to WT protein).

Substituting DENV-2 NS5 with DENV-1 linker residues (d1-L4 and d1-L9) did not influence its *de novo* initiation nor elongation activities significantly (< 30% change). Substitution with DENV-3 and ZIKV linker residues (d3- or ZV-L4 and d3- or ZK-L9) decreased DENV-2 *de novo* initiation activity somewhat (~40% reduction in d3- and ZV-L9) and did not affect its NS5 elongation activity. Likewise, JEV linker residues, JV-L4 and JV-L9 also reduced DENV-2 *de novo* initiation activity by ~40 % and ~60 % respectively, without changing its elongation activity. On the other hand, DENV-4 linker residues (d4-L4 and d4-L9) did not impact DENV-2 *de novo* initiation but enhanced its elongation activity (~70% in d4-L9). In summary, replacing DENV-2 interdomain linker residues with those from other Flaviviruses had a stronger impact on its *de novo* initiation activity compared to elongation activity. Of the 5 sequences investigated, DENV-2 *de novo* initiation activity was most strongly suppressed by JEV linker residues whilst its elongation activity was found to be most highly augmented by DENV-4 linker residues.

In order to examine the biological importance of these mutants in viral replication, the same mutations engineered in DENV-2 subgenomic RNA replicon harboring a renilla luciferase reporter were electroporated into BHK-21 cells and measured for luciferase levels at indicated

time points (Figure 3.8A and 3.8B). DENV-1 and DENV-3 substitutions displayed marginally poorer viral replication compared to WT, whilst the most similar DENV-4 sequence, demonstrated comparable viral replicative ability as DENV-2. This is in agreement with their observed *in vitro de novo* initiation and elongation activities. The better *in vitro* elongation activity of DENV2-d4-L9 NS5 protein did not translate to better viral growth properties. The linker residues of JEV and ZIKV which have the least sequence identity with DENV-2 exhibited poorest replicative abilities. When the entire inter-domain linker amino acids of DENV-2 was substituted with JEV and ZIKV sequences, virus replication was completely abolished whilst changing the shorter 3_{10}-helix amino acids of DENV-2 to JEV and ZIKV sequences still allowed low levels of viral replication. The lethal phenotype observed for JV-L9 and ZV-L9 mutant replicons could not be attributed entirely to an impact in their *in vitro* polymerase activity since they still retained 40% and 60% *de novo* initiation activity respectively as well as WT levels of elongation activity. Moreover, since JV-L4 and ZV-L4 mutants produced comparable luciferase signals throughout the four days post-electroporation, we would have expected similar *de novo* initiation and elongation activities in *in vitro* enzymatic assays. However, ZV-L4 enzyme displayed 60% higher *de novo* activity than JV-L4. Since JV and ZV mutant proteins generated differential enzymatic results and the *in vitro* data could not match the observed replicative abilities of the mutants in cells, it may be possible that the linker residues also play non-enzymatic roles in viral replication. The unique amino acid composition of the linker may be crucial for serotype/virus-specific inter-domain interactions between MTase and RdRp which are necessary for viral replication.

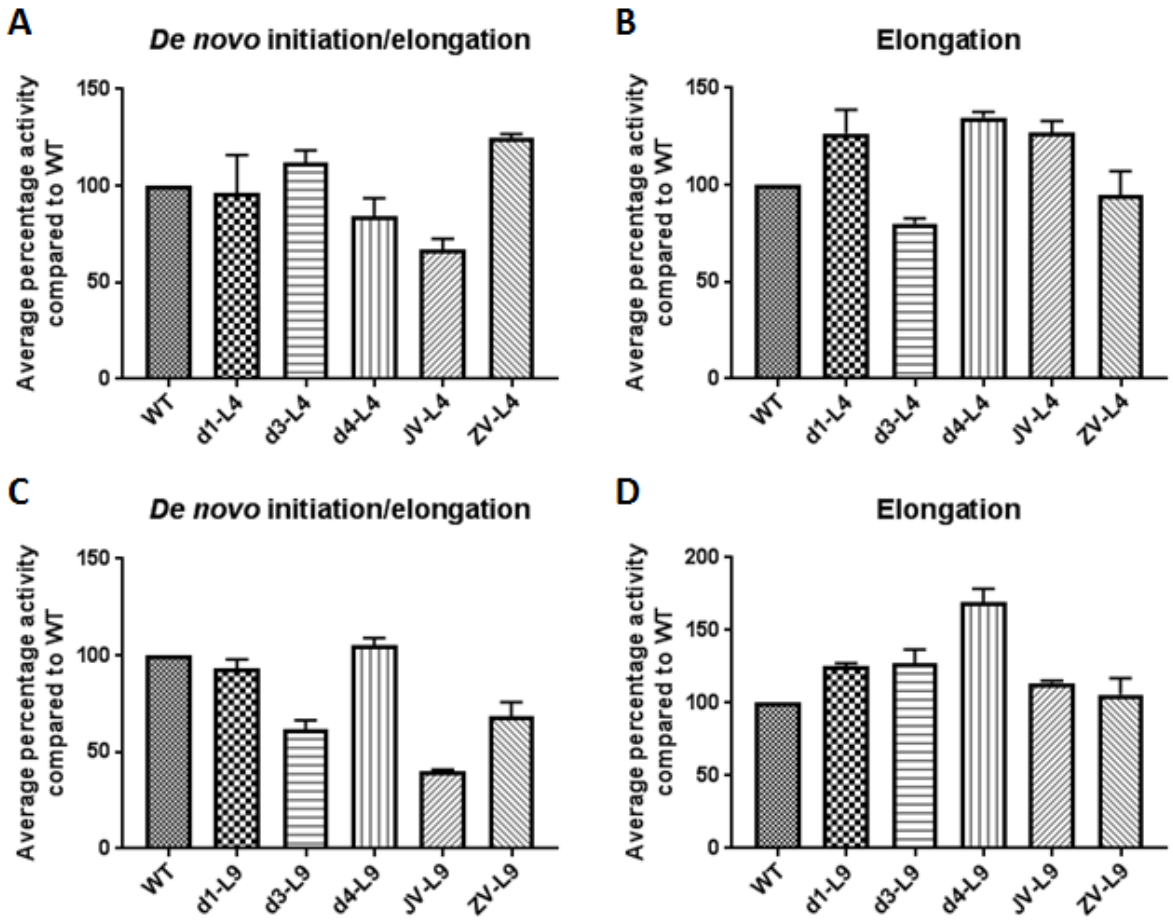

Figure 3.7 Polymerase activities of DENV-2 WT and linker mutant NS5 FL proteins. (A) Polymerase *de novo*/elongation and (B) elongation assays were carried out using DENV-2 NS5 FL WT and L4 mutants. (C) Polymerase *de novo*/elongation and (D) elongation assays were performed using DENV-2 NS5 FL WT and L9 mutants. DENV-2 linker amino acids replaced by DENV-1, 3, 4, JEV and ZIKV are denoted as d1, d3, d4, JV and ZV on the diagrams. Results shown are the average percentage activity compared against DENV-2 WT NS5 FL protein at t=1hr derived from average relative fluorescence units (RFU) obtained from each protein from one experiment. Two independent experiments were carried out in triplicate wells.

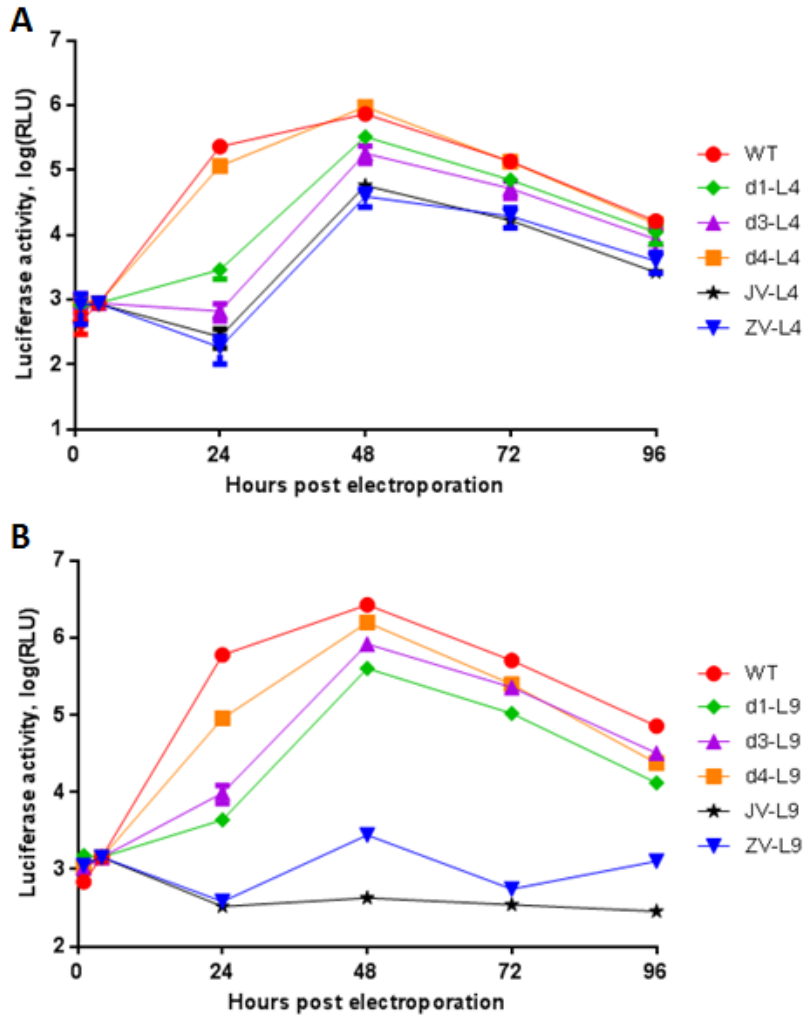

Figure 3.8 Replication profiles of DENV-2 WT and linker mutant replicons. Renilla luciferase activities of DENV-2 WT and linker mutant replicons - (A) DENV-2 3_{10}-helix amino acids swapped with corresponding Flavivirus sequences (L4) and (B) DENV-2 entire inter-domain linker swapped with corresponding Flavivirus sequences (L9). DENV-2 linker amino acids replaced by DENV-1, 3, 4, JEV and ZIKV are denoted as d1, d3, d4, JV and ZV on the diagrams. Equal amount of replicon RNA were electroporated into BHK-21 cells and luciferase activities were assayed at indicated time points. The y axis shows the log10 value of Renilla luciferase activity (RLU). Each data point is the average for two replicates, and error bars show the standard deviations.

% D2 NS5 activity	De novo initiation/elongation	Elongation	Thermo-fluorescence Tm (°C)
WT	100 ± 0	100 ± 0	37.5
d1-L4	96.1 ± 16.2	126.7 ± 9.9	37.5
d3-L4	112.2 ± 4.4	80.2 ± 1.8	37.5
d4-L4	84.0 ± 7.9	135.0 ± 2.2	38
JV-L4	66.9 ± 4.7	126.9 ± 5.0	38
ZV-L4	125.0 ± 1.3	94.7 ± 8.8	38

Table 3.4A Enzymatic activities and thermo-stabilities of DENV-2 WT and L4 mutant NS5 FL proteins.

% D2 NS5 activity	De novo initiation/elongation	Elongation	Thermo-fluorescence Tm (°C)
WT	100 ± 0	100 ± 0	37.5
d1-L9	93.4 ± 3.2	125.5 ± 1.3	39
d3-L9	62.0 ± 3.2	127.4 ± 6.8	38
d4-L9	105.3 ± 2.6	169.1 ± 6.7	41
JV-L9	40.0 ± 0.7	114.0 ± 0.9	37
ZV-L9	68.6 ± 5.1	105.7 ± 8.1	37

Table 3.4B Enzymatic activities and thermo-stabilities of DENV-2 WT and L9 mutant NS5 FL proteins. Polymerase activities DENV-2 WT, (A) L4 and (B) L9 mutant NS5 FL proteins measured in *de novo* initiation/elongation and elongation FAPA assays with 1 hour incubation at RT. Results shown are the average percentage activity compared against DENV-2 WT NS5 FL protein derived from average relative fluorescence units (RFU) obtained for each protein from one experiment. Two independent experiments were performed for each assay in triplicate. Thermo-stability was assessed using thermo-denaturation assay.

3.1.3 Discussion

The first high-resolution crystal structure of DENV-3 NS5 FL assumes a compact conformation in which the MTase domain is positioned on top of the finger subdomain of the RdRp (318). In this conformation, NTP and RNA entry channels of the RdRp domain remain accessible. This structure also reveals an inter-domain interface made up of numerous polar, electrostatic interactions as well as a well-ordered linker consisting of a short 3_{10}-helix (residues 263-266). By comparing the DENV-3 NS5 crystal structure with that from Japanese Encephalitis Virus (JEV), it was shown that the relative arrangements of MTase and RdRp domains are different (101). The MTase domain of JEV is situated at the back of the RdRp partially blocking the NTP entry tunnel and the inter-domain interactions are mainly hydrophobic. Since these interface residues are highly conserved, it suggests that NS5 protein from various flaviviruses may have evolved to assume distinct orientations stabilized by unique inter-domain interfaces, thereby resulting in different mechanisms for regulating their catalytic functions. Previous study using small-angle X-ray scattering (SAXS) demonstrated that the full length NS5 from DENV-3 could adopt multiple conformations in solution, from compact to more extended forms (254). The ability to assume various conformers could be attributed to

the flexibility of the ten-residue linker. With the use of a combination of established biochemical and reverse genetic approaches, the functional significance of intra-molecular interactions and linker region to virus replication, growth and infectivity was explored by structure-guided mutagenesis.

3.1.3.1 The polar interface modulates virus replication, growth and infectivity

The intra-molecular interactions between the two domains in the dengue NS5 FL structure is believed to be of utmost importance for NS5 to perform its versatile, multi-functional roles in genome replication. The presence of MTase-RdRp interface possibly brings the two domains close to each other for inter-domain regulations of the essential enzymatic activities of this naturally fused protein.

The DENV-3 NS5 MTase-RdRp interface is composed of two contact regions, one of which comprises residues from the well-ordered linker region making polar interactions with amino acids from both domains (Figure 3.1C). This interaction network is not observed in the FL JEV NS5 structure whereby the flexible linker is disordered (101). In this first cluster of residues involved in inter-domain interactions, the side chain of E267 from the linker region interacts with Y119 and R262 from the MTase domain via hydrogen bonding. The substitutions of DENV-4 Y119 and R263 (R262 in DENV-3) to alanine severely affected both MTase activities (Table 3.1 and Figure 3.2C-D), and impaired viral replication and reinfection (Figure 3.3 and 3.4), indicating that Y119 and R262 which belong to MTase core domain, are critical for the NS5 MTase activity and also viral replication. On the contrary, alanine substitutions of DENV-4 E268 (E267 in DENV-3) provoked only minor changes in both MTase and RdRp activities – about 70% of both MTase activities are retained, elongation activities are comparable to WT, and the *de novo* initiation/elongation activity are 30% higher than WT (consistent with the *dn*I activity data for alanine mutant for E267 in (315)). In addition, this mutant replicated similarly as WT and was able to produce viable virus, suggesting that E267 does not play critical roles

in the enzymatic activities of NS5 as well as in viral replication and infectivity, probably due to conformational flexibility of NS5 at its inter-domain linker region.

Also in the first cluster, salt bridge interaction is established between the carboxylate group of E269 and the guanidinium side chain of R361 from the DENV-3 RdRp domain (Figure 3.1C). Residue E269 also forms hydrogen bonding with the main-chain nitrogen amide of K595. Interestingly, residue 595 is either a lysine or an arginine in DENV-1 to -4 whilst E269 and R361 are strictly conserved across the four serotypes of DENV. Thus, the K595-E269-R361 interactions are also likely to be conserved across all the serotypes and could constrain the mobility of the linker. Consistent with the hypothesis, alanine mutations of DENV-4 E270 (E269 in DENV-3), R362 (R361 in DENV-3) and K596 (K595 in DENV-3) resulted in defective viral replication (Figure 3.3A), possibly caused by reduction in both polymerase activities due to a loss in its ability to assume functional conformation for catalysis. A previous study (315) reported that DENV-4 E270A mutant demonstrated approximately 2-fold reduction in *dn*I activity which is in line with our enzymatic data (Table 3.1 and Figure 3.2A), due to about 2-fold poorer turnover of NTP and RNA substrates. Mutant K596A also displayed a decrease in both *de novo* initiation and elongation activities by 30-40%. On the contrary, the results from enzymatic assays for R362A did not account for impaired viral replication. A double enhancement in the *de novo* initiation/elongation activity was detected with no change in the elongation activity, and only slight changes in both MTase activities (Table 3.1 and Figure 3.2A-D). It is possible that R362A mutation causes NS5 conformation modifications, influencing its ability to bind to the viral protease/helicase, NS3, as well as nuclear transport receptor, importin-β. This residue belongs to part of the βNLS region containing amino acids 320-368 whereby yeast two-hybrid system and pull-down assays showed that NS3 and importin-β bind competitively with NS5 at this region (320). Indirect immunofluorescence revealed that the hyperphosphorylated NS5 was distributed predominantly in the nucleus

during DENV infection (224), and importin-β was proposed to interact with NS5 for its nuclear import (321, 322). The importance of the region containing NLS and importin-β binding domain was evidenced by a mutagenesis study in which mutations in this region caused a severe reduction in viral titer in cultured cells, thus implying that NS5 translocation into the nucleus is vital for virus fitness and virulence (323). The dengue pathogenesis could be explained by another study in which they showed that DENV-2 infection triggered chemokine interleukin-8 gene expression, presumably through activation of CAAT/enhancer binding protein (227). Besides importin-β binding, NS3 can also interact with NS5 at the βNLS region, localizing NS5 in the cytoplasm necessary for viral replication (224). The relevance of the βNLS has now been questioned and the true NLS (recognized by importin) has recently been proposed to lie at the C-terminal end of NS5 (324). The amino acid crucial for NS3 binding is K330 that is within the α3 helix of the RdRp domain (325). Surface plasmon resonance (SPR) assay demonstrated that K330A mutation reduced NS5-NS3 interaction. Also, K330A retained *in vitro* RdRp activity but abolished viral replication in an infectious clone. Thus, NS5-NS3 association may facilitate NS3 helicase activity for dsRNA unwinding during RNA synthesis, as well as aid in NS5 stimulation of nucleotide triphosphatase (NTPase) and RNA triphosphatase (RTPase) activities of NS3 for viral RNA replication and capping respectively (326). Therefore, the inability of NS5 to bind to importin-β or NS3 due to perturbation at the βNLS region of the RdRp domain could render drastic effects on virus replication and infectivity. In all, these three residues form important charged interactions within NS5 in which a loss of these interactions crippled viral replication either enzymatically or non-enzymatically. Several polar interactions exist between MTase residues K95-K96 and RdRp residues E296-K300 in the first cluster (Figure 3.1C). Alanine substitutions of K95 and K96 resulted in an active RdRp with almost 2-fold increase in both RdRp activities without impacting N-7 and 2'-*O* MTase activities (Table 3.1 and Figure 3.2A-D). Analogously, transverse polar interactions

occur between the guanidinum functional group of R352 and E67, E252 and Q63 in the second cluster (Figure 3.1D). DENV-4 R353A (R352 in DENV-3) mutant also demonstrated 2-fold higher in the elongation activity (Table 3.1 and Figure 3.2B). However, these hyperactive enzymes were not beneficial for the virus. Replicon assay showed that they displayed delayed viral replication at the first 24 hour (Figure 3.3A), while K95A produced lesser viable virus and R353A was completely lethal in virus production (Figure 3.4). It could be possible that these mutations induce dynamic NS5 conformational changes that impact its ability to form competent viral replication complex with viral and host cofactors, as in the case of R362A mentioned above. Moreover, R352 and residues F348 to K357 of helix α5 is part of the βNLS motif of the RdRp domain present in the second interaction cluster, making numerous interactions with residues from the MTase domain. Like R361, these residues may also bind to NS3 and importin-β for virus replication and infectivity. This notion is supported by the crystal structure of DENV-3 RdRp in which R352, F354, E356 and K357 are properly positioned to interact with importin-β (86). It is expected that alanine mutation of these residues would likely give the same results as observed for R353A (R352 in DENV-3).

Taken together, these findings showed that the conserved amino acids at the inter-domain interface of DENV NS5 are important for virus replication, growth and infectivity, and that the inter-domain regulations and cooperativity of the essential enzymatic activities of NS5 could be elegantly modulated by the presence and dynamics of MTase-RdRp interface.

3.1.3.2 Hydrophobic contacts at the interface are critical for viral replication

The only hydrophobic contacts formed in the inter-domain interface of the DENV-3 NS5 FL structure comprise stacking interactions between W64, R68, F348 and P582 at the second cluster. These four residues are strictly conserved across flavivirus except for residue 68 which is a lysine instead of arginine at this position for JEV, denoting their functional relevance in NS5. Recent elucidation of the JEV NS5 FL structure revealed a conserved interface containing

a hydrophobic network and GTP sequence (101). The hydrophobic network is composed of three residues P113, L115, and W121 from the MTase domain, and three residues F467 (ring), F351 (index/βNLS core helix), and P585 (middle) from the RdRp finger subdomains, arranged in an alternating pattern at the heart of the interface. A comparison between the hydrophobic amino acids of DENV-3 and JEV NS5 FL structures found two residues, F348 (F351 in JEV) and P582 (P585 in JEV), which coincided in the two structures.

Mutagenesis analysis was carried out by the group by substituting each of the six hydrophobic residues with Arginine (R), Aspartic Acid (D) and Serine (S) in JEV infectious clone to disrupt the hydrophobic network (327). In general, most of the mutations impacted viral replication to different extent, with P113S, L115R/D/S, W121S, F351R/D/S, and P585S capable of virus production, albeit much lower than WT. In the same study, corresponding mutations (P113D, P115D, W121D, F349D, F465D, and P583D) in DENV-2 infectious clone yielded similar results whereby P113D, W121D and F465D-transfected cells did not produce IFA-positive cells, and both F349D and P583D produced lesser viable virus than WT. This finding provides functional validation of the biological relevance of the two hydrophobic residues, F348 and P582, at the interface of the DENV-3 NS5 FL structure. It would not be surprising if mutations of the other two residues, W64 and R68, involved in the hydrophobic stacking interactions also lead to viral replication impairment. The group further examined revertant viruses in the same study and they identified L322F adaptive mutation derived from P113D and F467D which is situated outside the interface and could rescue the replication defect of P113D and F467D mutations in MTase and RdRp, respectively. It could be possible that this residue also plays critical roles in viral replication during DENV life cycle.

In all, the analysis of the hydrophobic network at the interface of JEV NS5 FL structure suggested that the hydrophobic interactions at the interface of the DENV-3 NS5 FL structure could also be important for viral replication. Further functional and mechanistic investigations

by reverse genetic approaches and *in vitro* enzymatic assays would be necessary to gain more detailed understanding of the inter-domain hydrophobic interactions in regulating viral replication and would likely open up new opportunities for drug discovery and development.

3.1.3.3 The linker confers inter-domain flexibility to attain necessary distinct functional conformations of NS5 for catalysis and viral replication

The flexible linker facilitates the formation of inter-domain interface important in mediating inter-regulations and cooperativity of the essential enzymatic activities of NS5 for virus replication, growth and infectivity. Simple addition of NS5-MTase to NS5-RdRp in trans was not sufficient to bring the two domains close enough to each other in order to reconstitute a stimulatory interface for *de novo* initiation (253), suggesting the existence of a linker for high inter-domain affinity and interface formation. In addition, DENV-3 RdRp comprising residues from the putative linker region (residues 265 to 900) exhibited improved thermostability and polymerase *dn*I activity as compared to the shorter catalytic domain (residues 272 to 900), pointing that the linker residues are critical for viral replication (315). Furthermore, DENV-2 NS5 exhibited enhanced *dn*I and elongation activities than NS5-RdRp domain, suggesting that the MTase domain makes dynamic interactions with RdRp domain to modulate RNA synthesis (328).

In the crystallographic structure of DENV-3 NS5 (318), the linker amino acids H263, V264, N265 and A266 folds into a short 3_{10}-helix and probably acts as a swivel, making structural transition to allow the formation of distinct inter-domain interfaces and enable the MTase and RdRp domains to adopt various orientations for cross-talk during viral replication. It is possible that this short linker may experience structural transition and convert to a more extended conformation for re-positioning of the two domains of NS5 for their respective or cooperative enzymatic functions during viral replication.

In this study, it was shown that the first two residues S264 and V265 (DENV-4 numbering) are less important for viral replication whilst the third and fourth residues S266 and T267 (DENV-4 numbering) modulate polymerase *de novo* initiation (*dn*I) activity for viral replication in cells. Previously, our group had characterized the residue V264 in the context of DENV-3 NS5 protein and DENV-2 infectious clone (319) and discovered that substitution of this residue to glycine substantially reduced the *de novo* initiation RdRp activity and produced slightly attenuated viruses. This finding supported our results here in which V265A still retained the ability to replicate in cells. It could be possible that the change of valine to smaller amino acids such as glycine and alanine did not affect the flexibility of the linker to regulate necessary NS5 conformational modifications. However, mutation of this residue to proline had a dramatic effect on viral replication (319). It severely decreased the *de novo* initiation RdRp activity and failed to generate any viable viruses. The replacement of valine to proline could rigidify NS5 structure and dynamics, deterring the formation of functional orientations between the two domains during viral replication. The importance of the third and fourth residues was corroborated by a recent research done using small-angle X-ray scattering (SAXS) to examine the flexibility of DENV-4 NS5 S266N/T267A and $\Delta S_{266}T_{267}$ proteins (329). Mutations S266N/T267A whereby polar residues S266 and T267 from DENV-4 were reverted to asparagine and alanine from DENV-3, as well as $\Delta S_{266}T_{267}$ whereby these two residues were deleted, both displayed enlarged dimensions and larger flexibility alike to wild-type DENV-3 NS5. This result provided an indication that these two residues are vital for the compactness of DENV-4 NS5 and mutations may cause structural perturbations to the NS5 protein, impacting its specific interaction with viral RNA and its enzymatic ability to synthesize RNA in a *de novo* manner.

Several linker residues downstream of the 3_{10}-helix from 267 to 272 are also essential to regulate NS5 conformational flexibility and form extensive interactions with RdRp domains

(315, 318). For instance, the main-chain carbonyl oxygen of E267 makes a hydrogen bond with the side-chain amino group of R361. The side-chain of R361 is also involved in a salt bridge linkage with the carboxylate group of E269 which in turn forms hydrogen bonding with the main-chain nitrogen amide of K595. The importance of the electrostatic interactions between these three residues was emphasized earlier in Section 3.1.3.1. The side-chain amino group of K595 also interacts with the main-chain carbonyl oxygen of T270. In addition, the main-chain carbonyl group of N272 establishes contacts with the main-chain amide of V275. The residue at position 270 (DENV-3 numbering) was shown to be essential for maintaining the compactness of DENV-4 NS5 since mutation of K271 in DENV-4 NS5 to threonine in DENV-3 had the same effect as S266N/T267A and $\Delta S_{266}T_{267}$ proteins mentioned earlier (329) whereby the mutant protein exhibited higher flexibility comparable to wild-type DENV-3 NS5. A former study further confirmed the relevance of these amino acids as paired mutations E270A/K271A and R595A/K596A in DENV-4 completely inhibited virus replication in cells (323). Residue P268 that does not interact with any residues from the RdRp domain in DENV-3 may establish critical interactions in DENV-4 context as DENV-4 infectious virus exhibited selective pressure to retain threonine residue at position 269 of the linker region (315). Thus, linker residues downstream of the 3_{10}-helix also play critical roles during viral replication.

The recent comparison of all four DENV NS5 FL proteins using SAXS shed light into their similarities and diversity in terms of compactness and dynamics, which may influence their conformation for catalysis and ensemble formation within the replication machinery (330). DENV-3 NS5 FL was revealed to be flexible in nature with the MTase domain forming multiple conformations in solution which are essential for its sequential steps of capping RNA after synthesis. On the other hand, DENV-4 NS5 demonstrated greater compaction as compared to DENV-1 to DENV-3 NS5. Remarkably, swapping the ten-residue linker from DENV-3 into DENV-4 NS5 FL increased the compactness of the protein, possibly caused by

changes in the amino acid partners in the linker region and residues of the MTase and RdRp domains. The newly-substituted residues were postulated to be involved in different or additional interactions that may aid in stabilization of the preferential molecular conformation. Further mutagenesis and solution studies carried out by the same group had identified residues S266, T267 and K271 in DENV-4 NS5 to be critical for the maintaining the compact form of the protein (329). This finding was in line with our reverse genetic work described earlier whereby DENV-4 replicons with S266A and T267A mutations significantly reduced polymerase *de novo* initiation activity and inhibited viral replication. The importance of the linker for NS5 conformational regulation was also confirmed when we swapped the linker amino acids in DENV-2 NS5 with other Flavivirus sequences. Their ability to replicate in cells decreases as the sequences became more non-homologous to DENV-2, indicating that the unique amino acid composition of the linker controls the formation of diverse inter-domain interactions in a serotype/virus-specific manner and contributes to the difference in flexibility and dynamics of the NS5 protein.

In conclusion, the linker of flaviviruses may have evolved to allow functional conformational plasticity of NS5 as well as to accommodate other host and viral partners in the replication complex, and is a valuable drug target for anti-flaviviral therapeutic development. Future research could involve the search for peptides, aptamers or small molecules to disrupt the degree of freedom of the overall molecular conformation of NS5 as part of the drug discovery effort towards antiviral therapy.

3.2 Functional Validation of the DENV-3 FL NS5 and 2'-*O* Methylated Capped-RNA Cocrystal

Previous studies have reported co-crystal structures of flavivirus MTases bound to S-adenosyl-L-homocysteine (AdoHcy/SAH; the product of methylation reaction) and GTP (164), to guanosine analog ribavirin 5'-triphosphate (RTP) (266), to short cap analogs (120, 235), and to a 5'-capped RNA octamer (238). These structures revealed a SAM methyl donor binding site, GTP-binding site, and a basic putative RNA binding groove, and also provided structural insights on the interactions between the substrates and MTase within their distinct pockets. The crystal structure of DENV MTase in complex with the 5'-capped RNA octamer does not represent a catalytically-competent complex for specific viral RNA methylation and may correspond to the product of guanylylation of the RNA genome preceding subsequent methylation events (238). Thus, determination of the structure of NS5 bound to viral RNA would be useful to understand RNA recognition, which may propose new strategies to the design of NS5 inhibitors targeting the catalytic site of NS5.

Following the resolution of the crystallographic structure of FL NS5 protein from the dengue virus, the crystal structure of a ternary complex between DENV-3 FL NS5 protein, an authentic octameric cap-0 viral RNA substrate (5'-$^{m7}G_{0ppp}A_1G_2U_3U_4G_5U_6U_7$-3'), and SAH was determined at a resolution of 2.6 Å (Figure 4.1) (331). This structure represents a catalytically-competent complex, in which it shows that the viral MTase is in the midst of transferring a methyl group to the 2'-*O* ribose of the first nucleotide of the viral genome. As seen from the electrostatic surface diagram in Figure 4.1B, the RNA moiety occupies a large basic area of the NS5 protein. Only the first four stacked bases $A_1G_2U_3U_4$ and the $^{m7}G_{0ppp}$ cap are ordered whereas $G_5U_6U_7$ extends beyond the binding groove and exhibits weak electron density (Figure 4.1C). This observation is in line with earlier RNase footprinting experiment whereby WNV MTase protected 4 nucleotides of the viral RNA during 2'-*O* methylation (239). The first base

adenosine A1 fits tightly in a pocket shaped by NS5 residues I147-G148-E149-S150 and SAH (Figure 4.1D), and its 2'-*O* atom sits next to the sulfur atom of SAH and adjacent to the side chain of residue K180 from the highly conserved K_{61}-D_{146}-K_{180}-E_{216} catalysis tetrad, positioned to accept a methyl group from a SAM methyl donor (Figure 4.1C and 4.2A). The second base guanosine G2 stacks with A1, and interacts with the carboxylic side chain of residue E111 via its N2 atom and with a water molecule coordinating the Mg^{2+} ion through hydrogen bonding (Figure 4.1E). In order to examine the functional implications of the ternary complex for virus replication, mutagenesis study targeting highly conserved residue E111 of NS5 and G_2 base of the RNA as well as several residues lining the RNA binding groove were executed. This work provides a molecular basis for specific 2'-*O* methyl transfer reaction and cap formation by the flavivirus MTase, and also rationalizes the interactions between the protein and viral RNA.

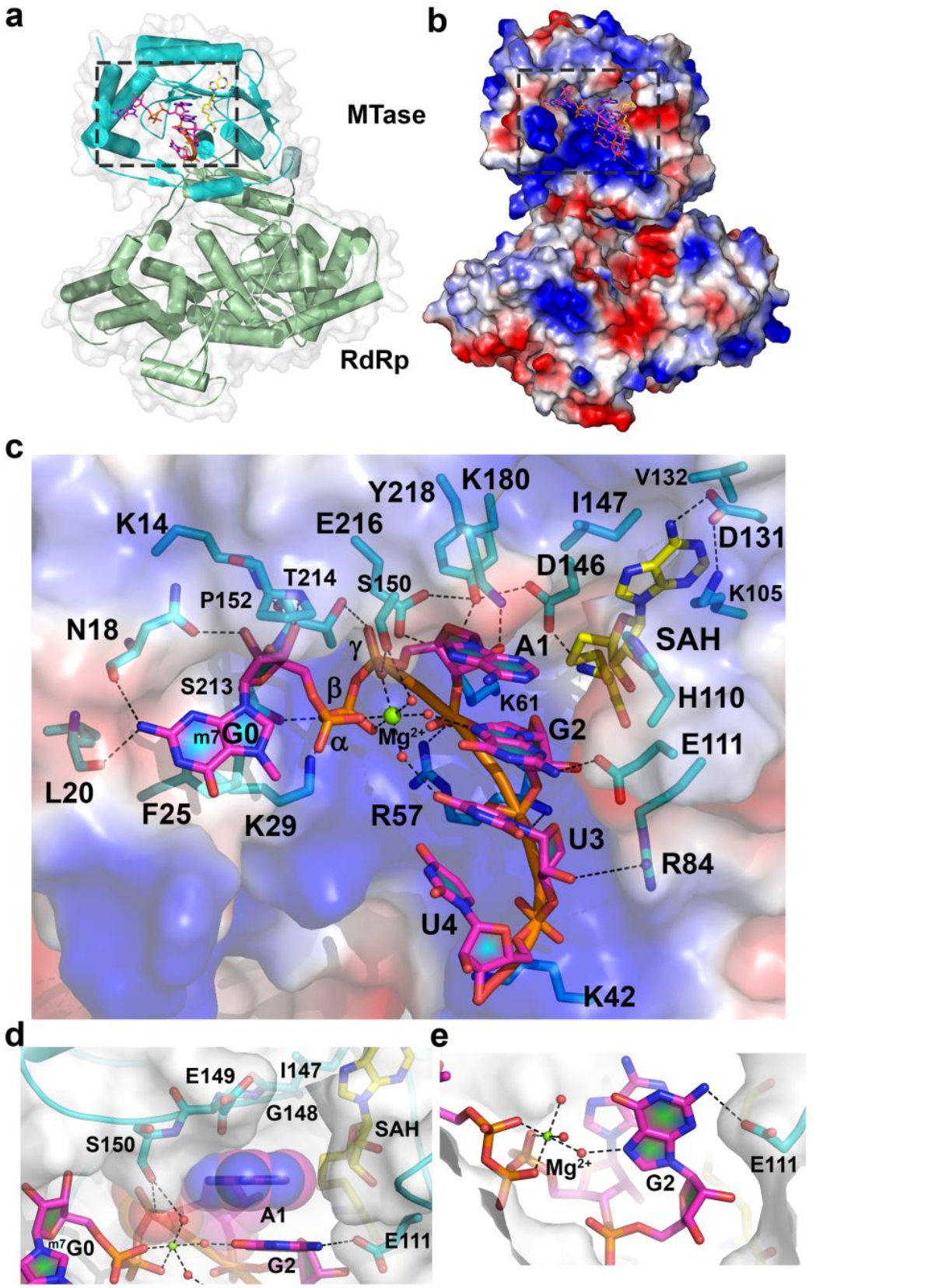

Figure 4.1 Crystal structure of ternary complex between DENV-3 FL NS5, capped RNA and SAH. (A) Crystal structure of DENV-3 NS5 (residue 6-895) bound to an authentic RNA substrate (5'-$^{m7}G_{0ppp}A_1G_2U_3U_4GUU$-3'). MTase and RdRp domains are colored cyan and green respectively. The RNA/SAH binding pocket is boxed. Capped RNA and SAH are represented as sticks and are in magenta and yellow colors

respectively. (B) Electrostatic-potential map of NS5 (positive charges are in blue and negative charges are in red). (C) Magnified view of the boxed RNA and SAH binding sites. Amino acid residues interacting with RNA or SAH are shown as sticks (cyan) and labeled. Polar interactions between capped RNA nucleotides and protein residues are indicated as dashed lines. Mg^{2+} ion and water molecules are depicted as green and red spheres correspondingly. (D) Tight shape complementarily with adenine A1 only within the RNA binding groove. (E) The second nucleotide G2 of the RNA substrate forms hydrogen bonding with residue E111 and Mg^{2+} ion. Adapted from (331).

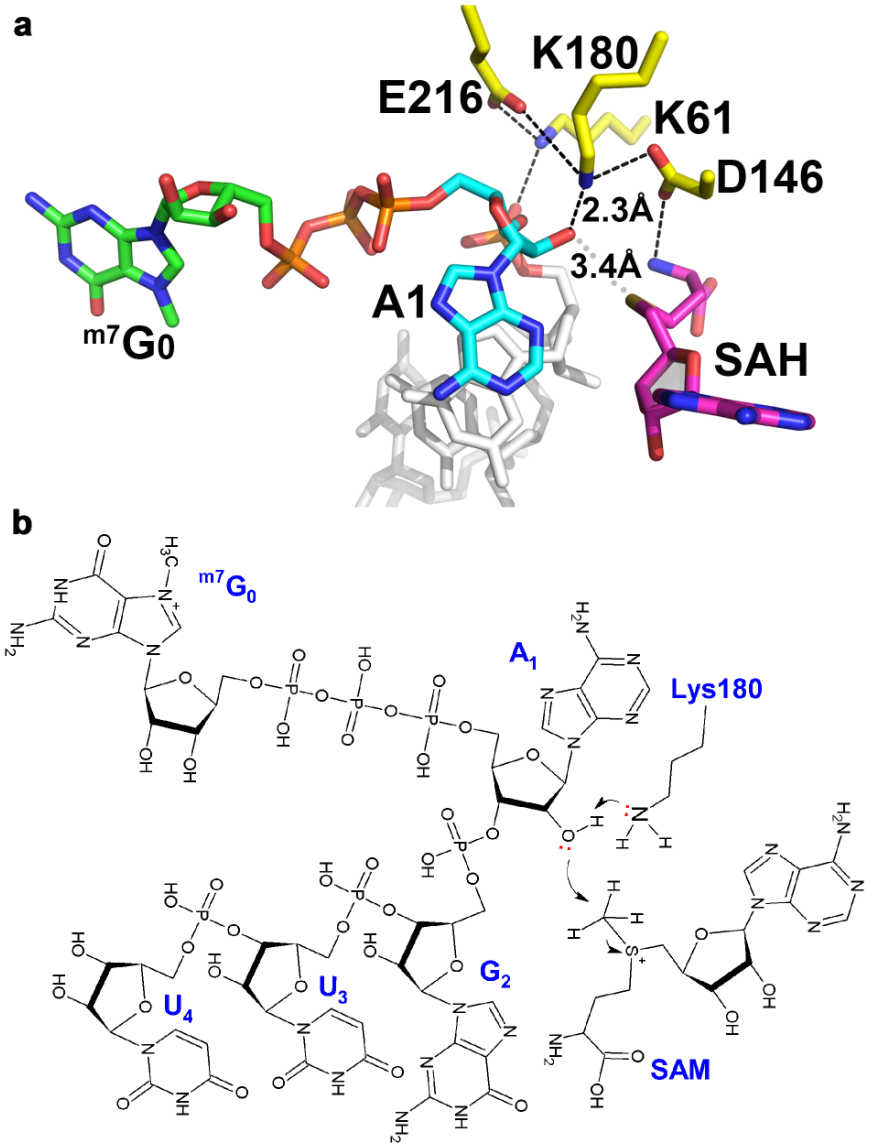

Figure 4.2 Proposed enzymatic mechanism for 2'-*O* methylation. (A) Close-up view of the MTase active site with the K_{61}-D_{146}-K_{180}-E_{216} enzymatic motif and SAH displayed as yellow and magenta sticks respectively. The close contacts and distances between the 2'-oxygen atom of adenine A1, the amino group of residue K180 and the sulfur group of SAH are indicated. (B) Schematic diagram of an active ternary complex formed by capped RNA and SAM, based on the present crystal structure. Adapted from (331).

3.2.1 Residue E111 of NS5 is important for virus replication

From the crystal structure of the ternary complex, it was revealed that the NS5 residue E111 makes sole direct specific polar interaction with the second nucleotide G_2 of the viral RNA

(Figure 4.1C and 4.1E). This residue is highly conserved across the four DENV serotypes and other flaviviruses, and was selected for mutagenesis into alanine (A), glutamine (Q) and arginine (R). These single mutations were engineered into DENV-4 MTase (aa1-272) and DENV-4 NS5 FL, and the recombinant proteins were expressed and tested for their effects on *in vitro* MTase 2'-*O* and RdRp enzymatic activities. All the purified mutant proteins were relatively stable as determined by thermo-fluorescence assay (Table 4.1 and 4.2). The 2'-*O* MTase activity was measured using SPA assay, whilst the RdRp activities were assessed by *de novo* initiation/elongation and elongation FAPA assays as mentioned before. The enzymatic activities of the mutant proteins were compared against WT protein (Figure 4.3A, Table 4.1 and 4.2).

Mutation E111R, which reversed the charge from negatively-charged glutamic acid to positively-charged arginine, resulted in a loss in 2'-*O* MTase activity (Figure 4.3A and Table 4.1). On the contrary, mutants E111A and E111Q, which either remove the charged group or still retain the oxygen atom for interaction with G_2 base respectively, exhibited >93% 2'-*O* MTase activity. Modelling NS5 protein carrying E111 to A and Q suggests that these mutations have limited impact on protein-RNA interaction whilst E111R mutation possibly introduces steric hindrance and influences the ability of the protein to bind cap-0 viral RNA (Figure 4.4A). The *in vitro* MTase and modelling results are consistent with thermo-stability measurements of FL NS5 WT and mutant proteins in the absence and presence of the cap-0-7mer-RNA whereby E111R mutant displayed the most reduced thermo-stability in its free state and in the presence of RNA ligand (Table 4.2).

The effects of E111 mutants were also evaluated in cell culture to investigate its role in viral replication. The three mutations, E111A, E111Q and E111R, were introduced into DENV-2 infectious clone to examine the growth kinetics of virus mutants. Plaque assay and qRT-PCR were carried out for quantification of virus productions, intracellular and extracellular viral

RNA levels from day 1 to 5 post-transfection (Figure 4.3B-E). Immunofluorescence assay (IFA) was also performed to detect viral RNA and RdRp protein expression in transfected cells (Figure 4.3F). Both E111A and E111Q mutants attenuated viral replication and yielded three to four times less infectious virus. On the other hand, E111R mutant did not produce any viable virus and IFA-positive cells. The severe impairment in virus replication for E111R could be attributed to several factors: this mutant is defective in 2'-*O* methylation, less thermostable as compared to WT protein (Table 4.1) and has 50-60% decrease in polymerase elongation activity than WT protein, likely due to its poor binding to RNA substrate (Table 4.2). Thus, these findings indicate that residue E111 of NS5 plays a crucial role in virus replication, growth and infectivity.

3.2.2 Conservation of terminal nucleotides in viral RNA

Previous study had demonstrated the strict conservation of nucleotides at the ends of the flaviviral genomes (249). The genome of flaviviruses always starts with an adenosine at position 1 (Figure 4.4B) and this base binds tightly in a pocket formed by residues 147 to 150 of NS5 and SAH as presented in the crystal structure of the ternary complex (Figure 4.1D). Modelling of RNA A_1 to G, U or C showed that the amine group of G_1 would sterically collide with the ribose ring of SAH molecule while pyrimidine bases U_1 and C_1 would leave an empty space energetically unfavourable for van der Waals interactions with the protein (Figure 4.4C), thus emphasizing the stringent requirement for an adenosine as the first nucleotide.

The relevance of guanosine as the second nucleotide of viral RNA was assessed by measuring the 2'-*O* methylation activity of DENV-4 MTase protein using capped-DENV-4 5' UTR 1-110 nt RNA template containing G_2 mutated to A, U, or C, and also in the context of DENV-2 infectious clone. Substitution of G_2 to A, U, or C lowered the 2'-*O* MTase activity of WT protein to 84%, 55% and 24% respectively (Table 4.1). This result is in line with the modelling of RNA G_2 which shows that other bases are incompetent to establish the same polar

interactions with the carboxylic group from E111 of the NS5 MTase domain, and introduce unfavorable electrostatic repulsion (Figure 4.4D). DENV infectious clones harboring mutants G2A, G2U, and G2C completely abolished viral replication as evidenced by the absence of IFA-positive cells and did not produce any viable virus shown by no plaque formation and no increase in intracellular and extracellular RNAs (Figure 4.3B-F), indicating that the virus does not tolerate changes at the second position of the genome. Since the G_2 mutations still retain 2'-*O* methylation activity to different extents, their impact on virus growth could possibly be ascribed to an influence in the *de novo* initiation step during polymerization, where strict conservation of the dinucleotides $pppA_1G_2$ at the 5' end of the flavivirus genome was observed (Figure 4.4B) (249).

Percentage of WT and mutant MTase activity		WT	E111A	E111Q	E111R
2'-*O* MTase activities using DENV4 5'UTR G0-1-110nt RNA	G2 (WT)	100 ± 0	93.9 ± 1.7	93.4 ± 10.4	0
	A2	83.9 ± 5.2	62.4 ± 5.7	69.7 ± 3.0	4.0 ± 0.8
	U2	55.4 ± 1.4	37.1 ± 8.0	47.9 ± 12.3	2.4 ± 0.1
	C2	24.4 ± 4.7	26.8 ± 6.1	11.1 ± 0.3	0
Protein thermo-stability, Tm (°C)		39.5	39.0	39.0	38.5

Table 4.1 *In vitro* 2'-*O* MTase activity and thermo-stabilities of DENV-4 WT MTase and E111 mutant proteins. SPA assay was performed using WT and mutant viral 5' UTR RNA templates. Results shown are normalized to the activity of WT MTase on WT RNA, which is set to 100%. All data points and standard deviations were derived from two independent experiments, each with duplicate measurements. Protein thermo-stability was determined from one experiment with duplicate measurements.

% NS5 activity	**De novo Initiation/Elongation**			**Elongation**			**Thermo-fluorescence (°C)**		
Time (hr)	**1**	**2**	**3**	**1**	**2**	**3**	**Tm, no RNA**	**Tm, +RNA**	**ΔTm with RNA**
WT	100 ± 0	100 ± 0	100 ± 0	100 ± 0	100 ± 0	100 ± 0	37.3 ± 0.3	41.0 ± 0	+3.7 ± 0.3
E111A	69.2 ± 5.2	67.9 ± 4.4	67.4 ± 10.3	30.9 ± 1.7	40.2 ± 5.4	38.5 ± 7.4	37.3 ± 0.3	38.5 ± 0	+1.2 ± 0.3
E111Q	116.5 ± 14.2	118.2 ± 21.8	119.7 ± 12.6	62.8 ± 0.8	71.5 ± 4.6	61.6 ± 7.0	36 ± 0	38.5 ± 0	+2.5 ± 0
E111R	92.8 ± 5.4	94.6 ± 2.8	101.2 ± 2.0	43.0 ± 0.9	51.3 ± 2.6	51.1 ± 1.3	35.5 ± 0	37.0 ± 0	+1.5 ± 0

Table 4.2 Polymerase *de novo* initiation/elongation and elongation activities and thermo-stabilities of DENV-4 FL WT NS5 and E111 mutant proteins. *De novo* initiation/elongation and elongation FAPA assays were employed to measure polymerase activities of DENV-4 FL WT and mutant proteins at 1, 2 and 3 hours after

incubation of the reaction at RT. Results shown are the average percentage activity compared against WT protein derived from average relative fluorescence units (RFU) obtained for each protein. Two independent experiments were carried out, each with triplicate measurements. Protein thermo-stabilities with or without cap0-7mer-RNA were determined from two independent experiments, each with duplicate measurements.

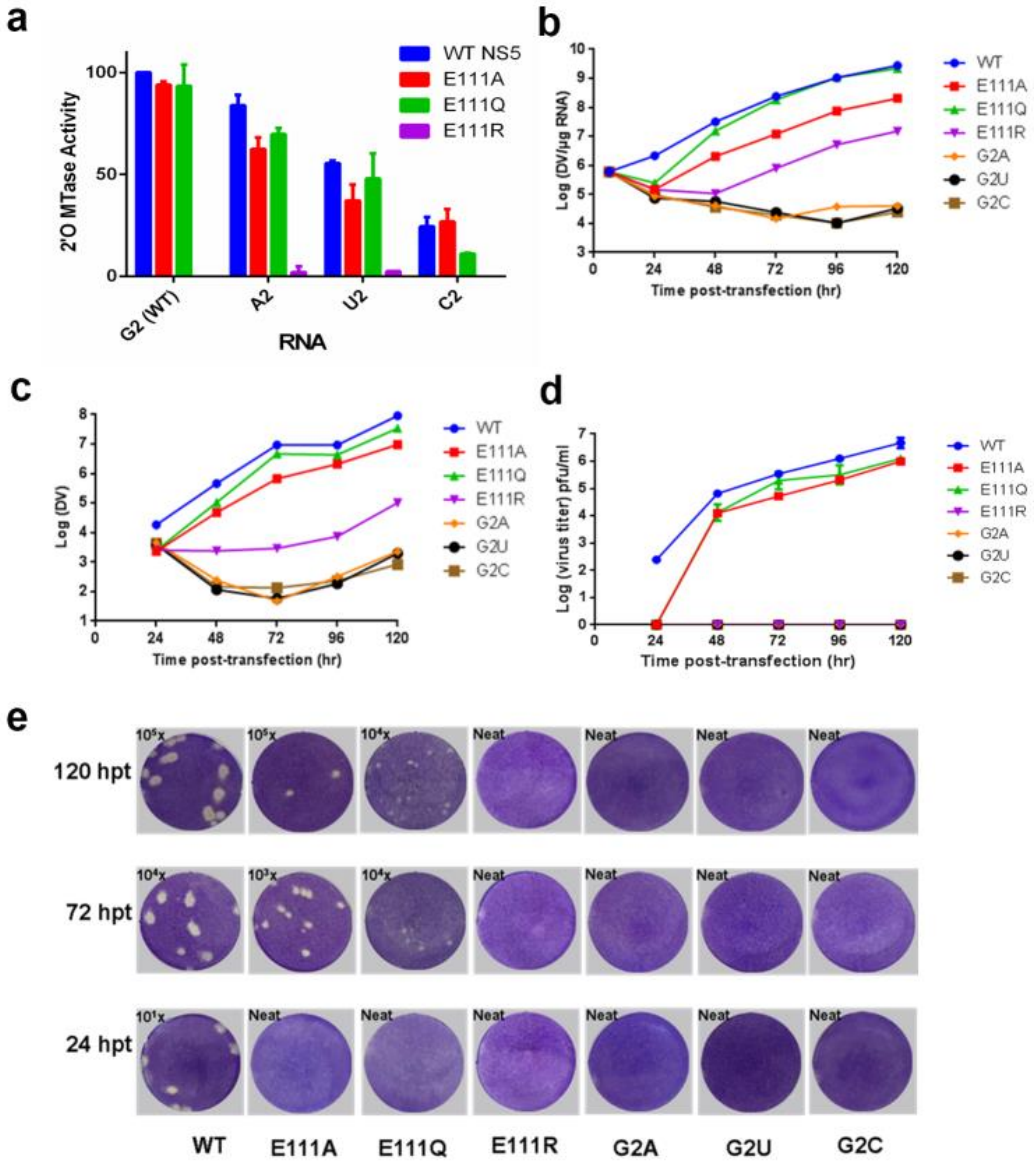

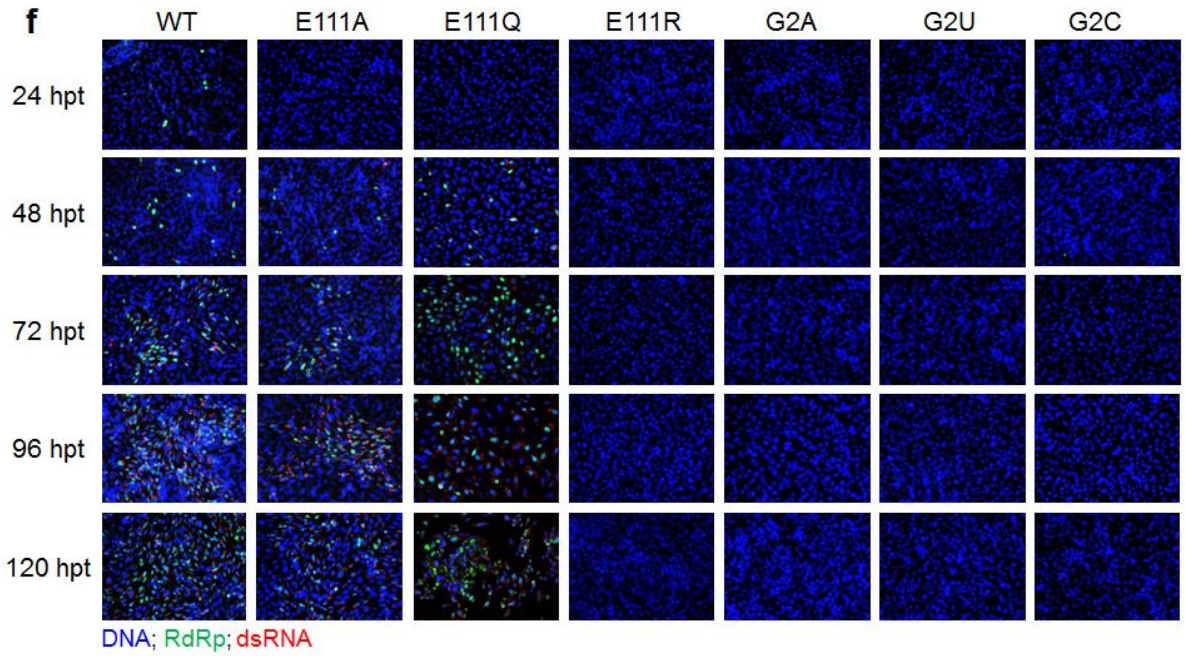

Figure 4.3 Specific recognition of the capped viral RNA by NS5 protein is important for virus replication. (A) 2'-*O* MTase activities of DENV-4 WT MTase and E111 mutants using WT and mutant viral 5' UTR RNA templates in SPA assay. Results shown are the average percentage activity of mutant MTase proteins compared against the activity of WT NS5 MTase on WT RNA, which is set to 100%. Each data point was derived from two independent experiments, and error bars denotes standard deviations. (B-F) IVT DENV-2 infectious clone RNAs were electroporated into BHK-21 cells and viral replication was monitored over a course of 5 days. (B) Intracellular viral RNA levels and (C) extracellular viral RNA levels in the supernatants were detected by qRT-PCR as illustrated in Materials and Methods. (D) Virus titers were calculated based on visible plaques observed by plaque assay shown in (E). (E) Plaque morphology for WT and mutant viruses was determined using supernatants collected at 24, 72 and 120 hour post transfection (hpt). The dilution factor where countable plaques were observed is indicated. (F) Immunofluorescence analysis at 24, 48, 72, 96 and 120 hpt. Primary antibodies used were anti-DENV-4 RdRp rabbit polyclonal antibody and anti-dsRNA mouse monoclonal antibody (J2), while secondary antibodies used were Alexa Fluor 488-conjugated goat anti-rabbit IgG and Alexa Fluor 568-conjugated donkey anti-mouse IgG.

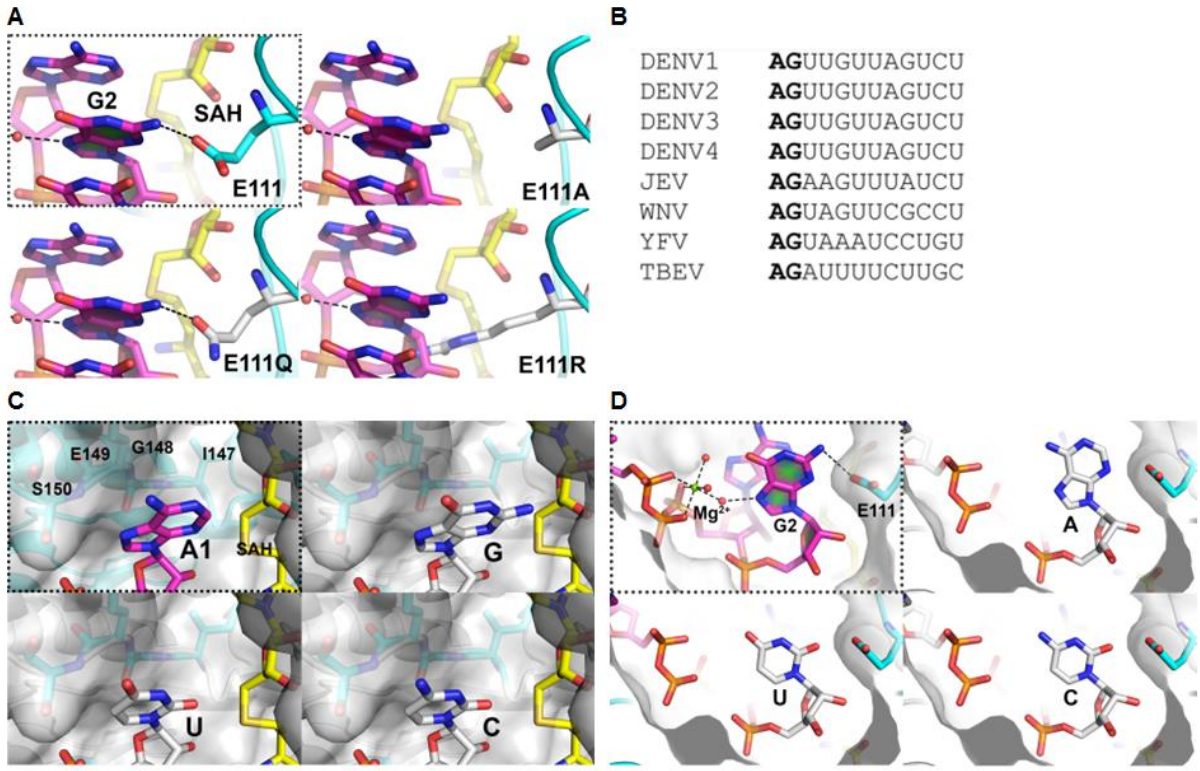

Figure 4.4 Local protein environment imposes strict requirement for adenine as the first base and preference for guanine as the second base. (A) Modeling E111A/Q/R mutations in the NS5-cap-0 RNA. (B) Multiple sequence alignment of the first 12 nucleotides of viral genome from various flaviviruses. (C) Modeling of X_1 = G, U, or C ($^{m7}G_{0ppp}X_1$-RNA) in place of A_1. (D) Modeling of X_2 = A, U, or C ($^{m7}G_{0ppp}AX_2$-RNA) in place of G_2. Adapted from (331).

3.2.3 Critical residues lining the RNA binding groove are vital for 2'-*O* methylation activity

The crystal structure of the ternary complex shows that several NS5 MTase residues lining the RNA binding groove forms key specific polar interactions with the RNA ligand (Figure 4.1C and Table 4.3). Alanine substitution of selected amino acids, R38, K42, R57, R84, R212 (R211 in DENV-3), S214 (S213 in DENV-3) and T215 (T214 in DENV-3), were engineered into DENV-4 MTase (aa1-272). These recombinant proteins were generated and assayed for 2'-*O* cap methylation. Note that these residues are conserved across all the four serotypes of DENV, and other flaviviruses except for K42 and T214. The 2'-*O* activity of these mutants was compared against WT protein (Table 4.3).

The alanine mutants exhibited varied reduction in their 2'-*O* methylation activity. DENV-4 R38A, R57A and R212A, which establish electrostatic contacts with G_2-U_3-U_4 of the RNA, demonstrated a detrimental effect on 2'-*O* MTase activity (0 to 9% of the WT level; Table 4.3), suggesting that these residues are critically important for 2'-*O* methylation. Located near the $^{m7}G_0$ cap, DENV-4 T215A decreased 2'-*O* methylation to 42% of the WT level whilst S214A still maintained 80% of the activity as compared to WT. Mutations of DENV-4 K42A and R84A, which are situated near the third and fourth bases of the RNA, resulted in minor decrease of about 20-30% in 2'-*O* MTase activity. The stability of mutant proteins was measured using thermo-fluorescence assay to show that the loss of 2'-*O* methylation for critical residue mutants was not due to instability of protein as shown by minimal difference in the Tm (Table 4.3). Although these mutations are not explored in DENV infectious clone, R38A, R57A and R212A mutants which displayed significant reduction in 2'-*O* methylation activity could probably impede virus replication and growth, similar to E111R mutant mentioned earlier (Figure 4.3). It may be possible that the other mutants, which still retain moderate *in vitro* 2'-*O* MTase activity, could attenuate virus growth and infectivity in cells, like the E111A and E111Q mutations.

D4 mutants	D3 NS5 aa interaction with RNA atom/base	% 2'-*O* activity	Thermo-fluorescence (°C)
WT	-	100.0 ± 0	39.5
R38A	R38 NH2 with U4-OP1	8.9 ± 2.2	40.5
K42A	K42 NZ with U4-OP1	76.7 ± 2.4	40
R57A	R57 NH2 with G2-OP1	0.0 ± 0	40.5
R84A	R84 NH1 with U3-2'O	68.4 ± 6.4	40.5
E111A	E111 OE1 with G2-N2	94.0 ± 1.7	39
R212A	R211 NH1 with H2O/U3-OP2	2.7 ± 3.8	41.5
S214A	S213 OG with G0-O2B	79.2 ± 11.7	37.5
T215A	T214 OG1 with G0-O2C	41.9 ± 10.7	36

Table 4.3 *In vitro* 2'-*O* MTase activity and thermo-stabilities of WT and mutant DENV-4 MTase proteins. SPA assay was performed using DENV-4 5' UTR $^{m7}G_0$-1-110nt RNA template. Results shown are normalized to

the activity of WT MTase, which is set to 100%. All data points and standard deviations were derived from two independent experiments, each with duplicate measurements. Protein thermo-stability was determined from one experiment with duplicate measurements.

3.2.4 Discussion

The ternary crystal structure presented here represents a catalytically-relevant complex for specific viral RNA recognition and 2'-*O* methylation by the DENV NS5. In this structure, the RNA ligand binds to an extended patch of positively-charged amino acids of the NS5 protein between residue F25 of the MTase GTP-binding site and the SAM methyl donor binding pocket, spanning an overall atomic distance of about 17 Å across the RNA binding groove (Figure 4.1B and 4.1C). This observation tallies with the crystal structure of WNV MTase (239) and DENV-3 MTase bound to a 5'-capped octameric RNA (238) in which F25 (F24 in WNV) is approximately 16 Å away from the SAM-binding pocket. Moreover, F25 was found to stack with the $^{m7}G_0$ base at the 5' end and the hydrogen bonds formed between $^{m7}G_0$ ring and residues K14, L17, N18 and L20 of the GTP-binding site were similar in the two DENV MTase-capped RNA structures as well as in other flaviviral structures in complex with short cap analogs (120, 332). Mutagenesis studies done earlier on DENV and WNV MTases have highlighted the importance of the aromatic ring at position 25 (24 in WNV) to form stacking interaction with the G_0 base for RNA cap recognition and 2'-*O* methylation (207, 239). Mutation of F25 (F24 in WNV) to alanine lowered the 2'-*O* activity of DENV-4 and WNV MTases down to 4% and 33% respectively, and attenuated WNV replication. In contrast, substitution of WNV F24 to other aromatic residues such as tryptophan (W) and tyrosine (Y) has a lesser impact on 2'-*O* activity whereby 61% and 90% of the WT level were retained, further supporting the notion that stacking between the guanine base and an aromatic residue at position 24 mediates methylation. Amino acids of the GTP-binding pocket also specifically function at the stage of 2'-*O* cap methylation as N18A (N17A in WNV) mutant moderately suppressed the 2'-*O* activity of DENV-4 and WNV MTases to 70% and 52% correspondingly, whilst K14A (K13A

in WNV) mutation resulted in a substantial decrease of >90% on the 2'-*O* activity of both DENV-4 and WNV MTases, and reduced virus replication.

Nonetheless, the previous DENV-3 MTase-capped RNA crystal structure does not correspond to a functional conformation for methylation. Despite the docking of cap moiety in the GTP-binding pocket, the remaining of the RNA chain does not extend into the putative basic RNA binding cleft and are instead stabilized by intra-molecular interactions. Since the N7 atom and 2'-*O* ribose of the RNA cap is not situated beside the methyl donor, RNA substrate repositioning must occur for successive methyl transfer reactions. In the present ternary crystal structure, the RNA ligand is bound in the catalytic site of MTase such that the 2'-oxygen atom of A_1 base is positioned adjacent to the SAH molecule, proposing that this complex is a representative of a particular stage during the 2'-*O* methylation cycle (Figure 4.2). The adenosine methyl acceptor is located near the K-D-K-E enzymatic motif of MTase which catalyzes 2'-*O* methyl transfer via an S_N2 reaction (333). All the four residues are essential for 2'-*O* methylation and can impact viral replication (165, 207, 239). It is hypothesized that 2'-*O* methyl transfer event occurs through first, activation of the 2'-OH of the adenosine ribose by the amino group of K180, followed by a nucleophilic attack on the methyl group of the positively-charged sulfur center of SAM by the active ribose 2'-O. As K180 sits in the middle of D146 and E216, the amino group of K180 could readily be protonated and deprotonated at different steps of the 2'-*O* methylation pathway. The carboxylic group of D146 acts to stabilize the electrophilic sulfur center and K180 upon ribose 2'-OH activation.

The negative charges of the 5'-5' triphosphate linkage between $^{m7}G_0$ and A_1 of the RNA are neutralized by a hexacoordinated Mg^{2+} ion and form contacts with S213 and S150 of the MTase protein (Figure 4.1C and Table 4.3). DENV-4 S214A (S213 in DENV-3) and S150A (207) mutants still maintained about 80% and 55% of the 2'-*O* activity respectively as compared to WT (Table 4.3), suggesting that the loss of a single bond would likely not introduce major

perturbation to the overall binding of RNA to the protein since various interactions would still be in place. The remaining of the cap-0 RNA sequence assumes an α-helical conformation perpendicular to the $^{m7}G_{0ppp}$ moiety (Figure 4.1C), revealing numerous protein surface residues that participate in polar interactions with the RNA.

Two groups had previously performed systematic Ala-scanning mutagenesis on amino acids within the putative RNA binding groove of DENV-4 and WNV MTases (207, 239). These distinct residues are selected as they shape the continuous positively-charged patch on the surface of MTase and are postulated to form critical interactions with RNA during cap methylation. Some of these selected amino acids coincide with our mutagenesis study targeting residues lining the RNA binding site presented in the 2'-*O* methylation ternary crystal structure, corroborating the electrostatic potential analyses of flavivirus MTase structures that the basic cleft is conserved (164, 165, 334, 335). Residues R38, R57 and R211 of the protein make electrostatic interactions with the phosphate backbone of G_2-U_3-U_4 nucleotides; mutations to alanine in the context of DENV-4 MTase enzyme drastically impaired their 2'-*O* MTase activities to 9%, 0% and 3% of WT level respectively (Table 4.3). This result is similar to the equivalent WNV R37A, R57A and R213A mutations in which 18%, 6% and 7% of the 2'-*O* MTase activity were exhibited (239). The reduction in methylation activity of these mutants is not due to poorer RNA binding since WNV R37A and R57A still displayed RNA-binding affinity comparable to WT. Instead, a critical single amino acid change may disrupt transient local RNA interactions, influencing methyl transfer reaction which could be translated to an impact on virus replication as evidenced by the lethal phenotype of WNV R37A infectious clone (239). Our mutagenesis work also revealed three other RNA-binding residues that do not play an essential role in 2'-*O* methylation. K42A, R84A and T215A substitutions moderately decreased the 2'-*O* MTase activity to 77%, 68% and 42% respectively in DENV-4 (Table 4.3), and to 90%, 100% and 104% in WNV (239). This result indicated that weakening of one

binding contact may be insufficient to block functional RNA-MTase complex formation, given that multiple interactions are established in the complex. Of these three mutants, R84A was introduced into WNV infectious cDNA to examine its biological relevance in cell culture because this mutation affected N7 but not 2'-*O* methylation, and no virus production was detected (239). This finding is consistent with an earlier observation that viruses inactive for N7 methylation alone was lethal while defect in 2'-*O* yielded attenuated viruses that can protect mice from later WT WNV challenge (165, 336).

This structure not only validated the specific recognition of viral RNA by NS5 MTase, but also supported an earlier study which showed that the nucleotides at the ends of the flaviviral genomes are strictly conserved (249). Modelling of the first nucleotide A_1 of the RNA has proven that other bases are unable to replace adenosine for the formation of favourable contacts with the protein (Figure 4.4C). In accordance, flavivirus NS5 specifically perform internal 2'-*O* methylation on polyA but not polyG/C/U RNA substrates (236). The four residues surrounding adenine A_1 are involved in methylation activity of NS5. Amino acid S150, which interacts with the α-phosphate of GTP as mentioned above, when mutated to alanine reduced 2'-*O* activity of DENV-4 and WNV MTases by 45% and 38% respectively (207, 239). Likewise, I147A and E149A significantly lowered their 2'-*O* MTase activity down to 15% and 5%, and 49% and 69%, as compared to WT correspondingly. Furthermore, E149A mutant did not produce viable WNV and recovered DENV with engineered mutation reverted back to WT sequence.

The second nucleotide G_2 of the RNA forms stacking interaction with A_1 and hydrogen bonds with the carboxylic group of E111 and with a water molecule coordinating Mg^{2+} ion (Figure 4.1E). Mg^{2+} ion was proposed to structurally and electrostatically stabilize the RNA-MTase complex (337, 338) and stimulate 2'-*O* activity of DENV NS5 (240). The functional significance of the polar interaction between G_2 base of RNA and NS5 residue E111 for viral

replication as well as the identity of guanosine for virus growth was highlighted by our enzymatic assays and virus work in this study. Mutations of E111 and G_2 to other amino acids or bases have varied effects on 2'-*O* activity of DENV-4 MTase (Table 4.1 and Figure 4.3A), albeit they either attenuated or completely inhibited virus replication (Figure 4.3B-F). The decrease of 2'-*O* methylation activity to 24% as measured for G2C mutation could be due to poorer RNA binding to MTase when G_{0ppp}AC-RNA was used rather than the consensus sequence G_{0ppp}AG-RNA of flaviviruses (120), substantiating the modelling analyses explained earlier. Consistently, functional studies of terminal nucleotides showed that WNV replicons carrying A1G and G2C substitutions replicated <1% as compared to WT, and its corresponding mutant infectious clones recovered infectious viruses with engineered mutations reversed to WT sequence on day 5 post-transfection (339). Collectively, these findings confirmed that flavivirus NS5 methylates cap-0 RNA substrate in a sequence-dependent manner and strictly conserves $pppA_1G_2$ dinucleotide at the 5' end of the genome (249). Similarly, residues projecting from the MTase surface along the RNA binding groove and form polar contacts with the first two nucleotides of RNA are also relatively conserved across flaviviruses.

In summary, our targeted mutagenesis work on both NS5 protein and viral RNA supports the functional relevance of the ternary structure to DENV replication and infection, and proposes novel strategies for the design of inhibitors targeting the catalytic site of NS5 MTase. As SAM-binding site is conserved among various MTases, toxicity issues may arise from inhibitors of both viral and host SAM-utilizing enzymes. In order to minimize off-target inhibition, one possibility would be to design more specific and potent inhibitors through extending SAM or GTP analog towards the RNA binding pocket. Inhibitors that disrupt viral RNA-MTase interactions without influencing host methylation reaction could also be developed for antiviral therapeutic intervention.

3.3 Genetic Validation of Inhibitor Binding Pockets of DENV NS5 RdRp

The NS5 RdRp enzyme is highly conserved amongst all four serotypes of DENV and *Flavivirus* (83) and is responsible for the catalyzing viral RNA synthesis without having any equivalent in the human host cell , thus constituting an ideal target for the design of anti-viral inhibitors to treat diseases caused by flaviviruses (205, 341). Compounds targeting RdRp may either directly inhibit its enzymatic activity or perturb its interaction with RNA and other proteins. Previous high-throughput screening efforts had identified non-nucleoside inhibitors (NNIs) that bound to allosteric sites of DENV RdRp, but they do not exhibit potency and lead-like properties good enough for development (306, 342, 343). Here, we reported novel NNIs that bound to two distinct allosteric pockets by X-ray crystallography. One class of the inhibitors bound at the thumb/palm interface near the enzyme active site whilst another interacted with the finger-thumb interconnecting loops, resulting in an ordered F1 motif. The relevance of these inhibitor binding pockets in the RdRp for viral replication and the mechanism of action of these compounds were assessed and described below.

3.3.1 Compound that binds to F1 motif of NS5 RdRp

Following a diverse screening campaign of two million compounds from the Novartis compound library using the FAPA assay, one compound was identified to bind to the finger domain of DENV RdRp by X-ray crystallography and impede *in vitro* polymerase *de novo* initiation activity at low micro-molar inhibitory concentration. The compound structure and co-crystal structure are not shown here as the information is proprietary. Several amino acid residues lining this pocket and are involved in specific interactions with this compound are N452, K456, R457, E458, F464, W474 and K578 of DENV-3 NS5 RdRp (Table 5.1). Residues W474 and K578 are located at the α10 region and β2 region of the finger subdomain respectively. Within the finger subdomain, amino acids 455-468 form the motif F and are missing from both the crystal structures of DENV-3 RdRp (aa273- 900) and FL NS5 (aa6-895)

(86, 318). Residue N452 is found upstream of this motif whilst K456, R457, E458 and F464 belong to part of the motif F. In order to understand the biological importance of this pocket for viral replication, these amino acids were selected for site-directed mutagenesis study. These residues are conserved in all four DENV serotypes and other flaviviruses such as YFV and WNV with an exception of K578 that is replaced by arginine in DENV-1 and DENV-2 serotypes (Figure 5.1), suggesting that they may play an important role in viral RNA replication. Moreover, there was an earlier study proposing that this motif is crucial for binding to the viral promoter, Stem Loop A (SLA), and for SLA-dependent RNA synthesis (103).

DENV-3 RdRp residue	**Amino acid interactions with compound**
N452	
K456	
R457	Side chain interacts with carboxylic acid and tetrazole in compound
E458	Side chain interacts with carboxylic acid in compound
F464	
W474	Hydrophobic interaction with tetrazole
K578	Side chain interacts with tetrazole in compound

Table 5.1 Interaction of DENV-3 NS5 RdRp amino acid residues with compound in F1 motif.

```
DENV3      (447) GSCVYNMMGKREKKLGEFGKAKGSRAIWYMWLGAR
DENV1      (447) ATCVYNMMGKREKKLGEFGKAKGSRAIWYMWLGAR
DENV4      (448) ESCVYNMMGKREKKLGEFGRAKGSRAIWYMWLGAR
DENV2      (448) ETCVYNMMGKREKKLGEFGKAKGSRAIWYMWLGAR
YFV        (449) RTCVYNMMGKREKKLSEFGKAKGSRAIWYMWLGAR
WNV        (450) HTCIYNMMGKREKKPGEFGKAKGSRAIWFMWLGAR

DENV3      (571) TYQNKVVKVQRPTPTG
DENV1      (571) TYQNKVVRVQRPAKNG
DENV4      (572) TYQNKVVKVLRPTPKG
DENV2      (572) TYQNKVVRVQRPTPRG
YFV        (573) TYKNKVVKVLRPAPGG
WNV        (574) TYRHKVVKVMRPAADG
```

Figure 5.1 Multiple sequence alignment of F1 motif residues across various flaviviruses. F1 motif residues which interact with the compound are highlighted in gray.

3.3.1.1 Residues in the F1 motif regulate de novo initiation process during viral RNA replication

The functional importance of residues in the F1 motif was examined by generating DENV-4 FL NS5 proteins with the seven amino acid residues singly mutated to alanine and assayed for their polymerase *de novo* initiation and elongation activities *in vitro* as described in Materials and Methods. All the purified mutant NS5 recombinant proteins demonstrated similar melting temperatures as WT, indicating that the stabilities of the protein structures were not compromised by alanine mutations (Table 5.2).

In general, the effects of alanine mutations were more evident in *de novo* initiation assay than in elongation assay (Table 5.2). The substitution of E459 (E458 in DENV-3) and W475 (W474 in DENV-3) to alanine impacted only the *de novo* initiation activity and still exhibited about 70-80% of the elongation activity, implying that these two residues may be more important in regulating the *de novo* process. However, alanine mutation of F465 (F464 in DENV-3), a residue within motif F, did not affect both the *de novo* initiation and elongation steps during RNA synthesis since the respective RdRp activities were about 6-22% and 24-39% more than WT. This suggested that F465 may not play an enzymatic role in viral RNA replication. Interestingly, an upstream F1 motif residue N453A (N452 in DENV-3) demonstrated a dramatic decrease in both polymerase activities to approximately 4-7% and 21-30%, indicating that this residue plays a crucial role in both *de novo* and elongation processes. On the contrary, K579A (K578 in DENV-3) mutant displayed 53-63% and 83-100% of *de novo* initiation and elongation activities respectively and may be moderately important for polymerase reaction. This residue in sequence is positioned far from the F1 motif but due to conformational folding of NS5, it comes into close proximity to the amino acids in the motif and plays a role in RNA synthesis. Another two amino acids within the F1 motif, K457A (K456 in DENV-3) and R458A (R457 in DENV-3), displayed about 40-60% reduction in polymerase *de novo* activity

whilst maintaining elongation activity comparable to WT. For the double mutant, no significant change was observed as relative to single mutations, thus there was no additive effect. Taken together, these findings advocated that residues in the F1 motif play a more important part in regulating *de novo* initiation process during viral RNA replication.

% NS5 activity	**De novo Initiation/Elongation**			**Elongation**			**Thermo-fluorescence (°C)**
Time (hr)	**1**	**2**	**3**	**1**	**2**	**3**	
WT	100 ± 0	100 ± 0	100 ± 0	100 ± 0	100 ± 0	100 ± 0	37
N453A	6.4 ± 3.9	4.4 ± 1.1	7.4 ± 1.4	21.0 ± 2.7	23.8 ± 2.7	29.6 ± 4.3	37
K457A	45.3 ± 16.3	44.0 ± 15.4	59.4 ± 10.5	88.7 ± 0.3	85.3 ± 4.2	97.1 ± 1.9	37
R458A	62.9 ± 0.5	51.1 ± 2.3	55.9 ± 8.8	115.9 ± 0.5	110.8 ± 1.0	123.7 ± 11.5	37
K457A /R458A	36.4 ± 11.0	33.9 ± 10.7	42.8 ± 12.7	64.2 ± 8.3	62.1 ± 10.9	72.6 ± 15.5	38
E459A	22.7 ± 3.4	18.3 ± 4.7	23.7 ± 8.2	77.1 ± 0.5	72.3 ± 5.7	79.7 ± 8.4	37
F465A	119.5 ± 27.8	106.2 ± 27.6	121.7 ± 40.6	126.5 ± 12.4	124.3 ± 4.6	138.8 ± 1.5	37
W475A	37.5 ± 9.0	42.7 ± 7.7	52.8 ± 7.7	73.9 ± 2.4	76.9 ± 1.9	85.8 ± 7.0	37
K579A	59.2 ± 12.1	53.0 ± 12.7	63.2 ± 18.2	83.4 ± 6.1	86.8 ± 8.6	100.1 ± 14.0	37

Table 5.2 Polymerase *de novo* initiation/elongation and elongation activities and thermo-stabilities of DENV-4 FL WT NS5 and F1 motif mutant proteins. *De novo* initiation/elongation and elongation FAPA assays were employed to measure polymerase activities of DENV-4 FL WT and mutant proteins. Results shown are the average percentage activity compared against WT protein derived from average relative fluorescence units (RFU) obtained for each protein. Activities less than 30% were colored red and activities less than 60% were colored blue. Four independent experiments were carried out, each with triplicate measurements. Protein thermo-stability was determined from one experiment with duplicate measurements.

3.3.1.2 Compound binding and inhibition are modulated by multiple interacting residues of the F1 motif

The non-nucleoside compound that binds to the F1 motif of NS5 interacts with specific amino acids residues to inhibit polymerase *de novo* initiation activity at a good half maximal inhibitory concentration (IC_{50}) of about 2 µM. To examine whether individual or double mutations of the F1 motif residues could have an effect on compound inhibition, IC_{50} of the hit compound (F1-cpd-1) and its analogs (F1-cpd-2, 3 and 4) were measured using *de novo* FAPA assay (Table 5.3). Mutants N453A and E459A were excluded from this study as they exhibited

dramatic decrease in *de novo* activity of less than 30% as compared to WT. F1-cpd-1 to -4 demonstrated varied potencies and had IC_{50} values ranging from 2 µM to 17 µM when tested with WT protein. Single or double mutants of the F1 motif (K457A, R458A, K457A/R458A F465A, W475A and K579A) did not render significant change in IC_{50} relatively to WT, indicating that one or two mutations alone had no substantial effect on compound inhibition and that multiple mutations may be required to influence compound binding and inhibition.

Compound	WT		K457A		R458A		K457A/R458A	
	IC_{50} (µM)	HS	IC_{50} (µM)	HS	IC_{50} (µM)	HS	IC_{50} (µM)	HS
F1-cpd-1	2.18	0.85	6.38	1.48	2.29	0.81	3.33	1.15
F1-cpd-2	2.69	1.00	4.17	1.23	2.94	0.94	4.57	1.47
F1-cpd-3	15.53	1.09	42.60	1.86	19.90	1.14	20.37	1.02
F1-cpd-4	4.97	1.58	7.57	1.87	5.43	1.46	6.93	1.63

Compound	WT		F465A		W475A		K579A	
	IC_{50} (µM)	HS	IC_{50} (µM)	HS	IC_{50} (µM)	HS	IC_{50} (µM)	HS
F1-cpd-1	2.87	0.99	1.88	0.77	2.36	1.19	3.39	0.84
F1-cpd-2	3.20	1.26	2.25	1.00	2.11	0.91	3.47	0.98
F1-cpd-3	17.38	1.12	23.46	0.98	20.10	1.05	28.81	1.08
F1-cpd-4	3.57	1.49	5.31	1.08	5.83	1.10	5.47	1.00

Table 5.3 *De novo* FAPA IC_{50} testing of DENV-4 FL WT NS5 and F1 motif mutant proteins. *De novo* initiation/elongation FAPA assay was employed to measure IC_{50} values of DENV-4 FL WT and mutant proteins when exposed to F1 motif inhibitors and are illustrated in Materials and Methods. Average IC_{50} values and hill slopes were shown in this table.

3.3.1.3 Critical residues of the F1 motif are vital for viral replication

To investigate whether the F1 motif residues interacting with the compound are important for replication fitness, the same alanine mutations were engineered into a DENV-4 luciferase-reporter subgenomic RNA replicon. WT and mutant replicon cDNAs were *in vitro* transcribed before electroporated into BHK-21 cells. After 1, 4, 24, 48, 72 and 96 hour post-electroporation, renilla luciferase activities were measured. Immunofluorescence assay (IFA) was also performed to detect viral dsRNA and NS3 protein expression at day 1, 2, 3 and 4 post-electroporation.

The luciferase activity in cells bearing DENV-4 WT replicon reached its peak level at 48 hour post-electroporation (Figure 5.2A). No luciferase activity was detected for DENV-4 mutant replicons N453A, K457A, R458A, K457A/R458A, E459A, F465A and W475A. K579A was the only mutant that demonstrated significant luciferase activity comparable to WT at 72 and 96 hours, albeit there was some delay at the first 48 hours. In accordance with the renilla luciferase assay results, the mutants that exhibited impaired viral replication did not yield IFA-positive cells whereas K579A produced IFA-positive cells (Figure 5.2B-C). Since K579A mutant still maintained moderate *de novo* initiation and elongation activities (Table 5.2), thus may explain its ability to replicate in cells. The lethal phenotype observed for N453A was not surprising as both of its RdRp activities were dramatically reduced. On the other hand, F465A did not influence both the *de novo* initiation and elongation activities but was lethal in viral replication. It was postulated that residue F465 may play a non-enzymatic part in viral replication, possibly involved in sustaining or regulating essential NS5 conformation for interaction with host and viral proteins during viral replication. Additionally, the loss of replicative abilities for K457A, R458A, K457A/R458A, E459A and W475A could be attributed to their severe decrease in RdRp *de novo* initiation activity of more than 50%. In all, most of the amino acid residues in the compound binding pocket regulates polymerase reaction especially during the *de novo* step and impacts growth fitness in cells.

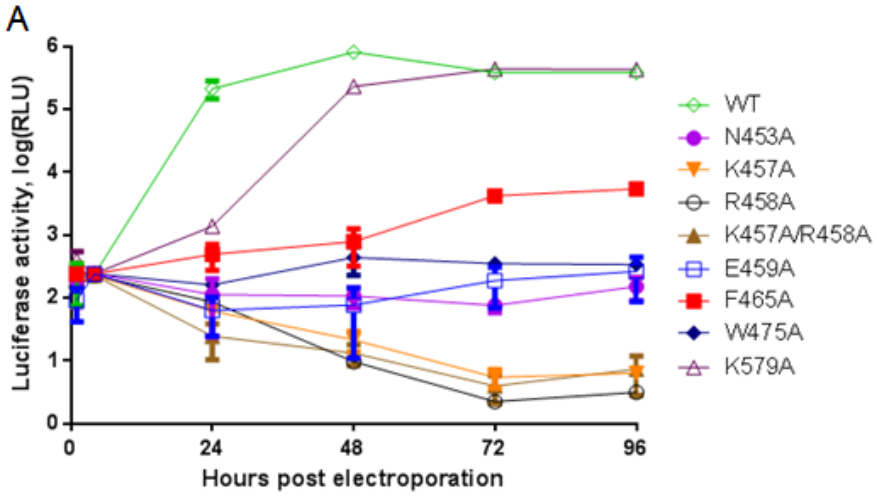

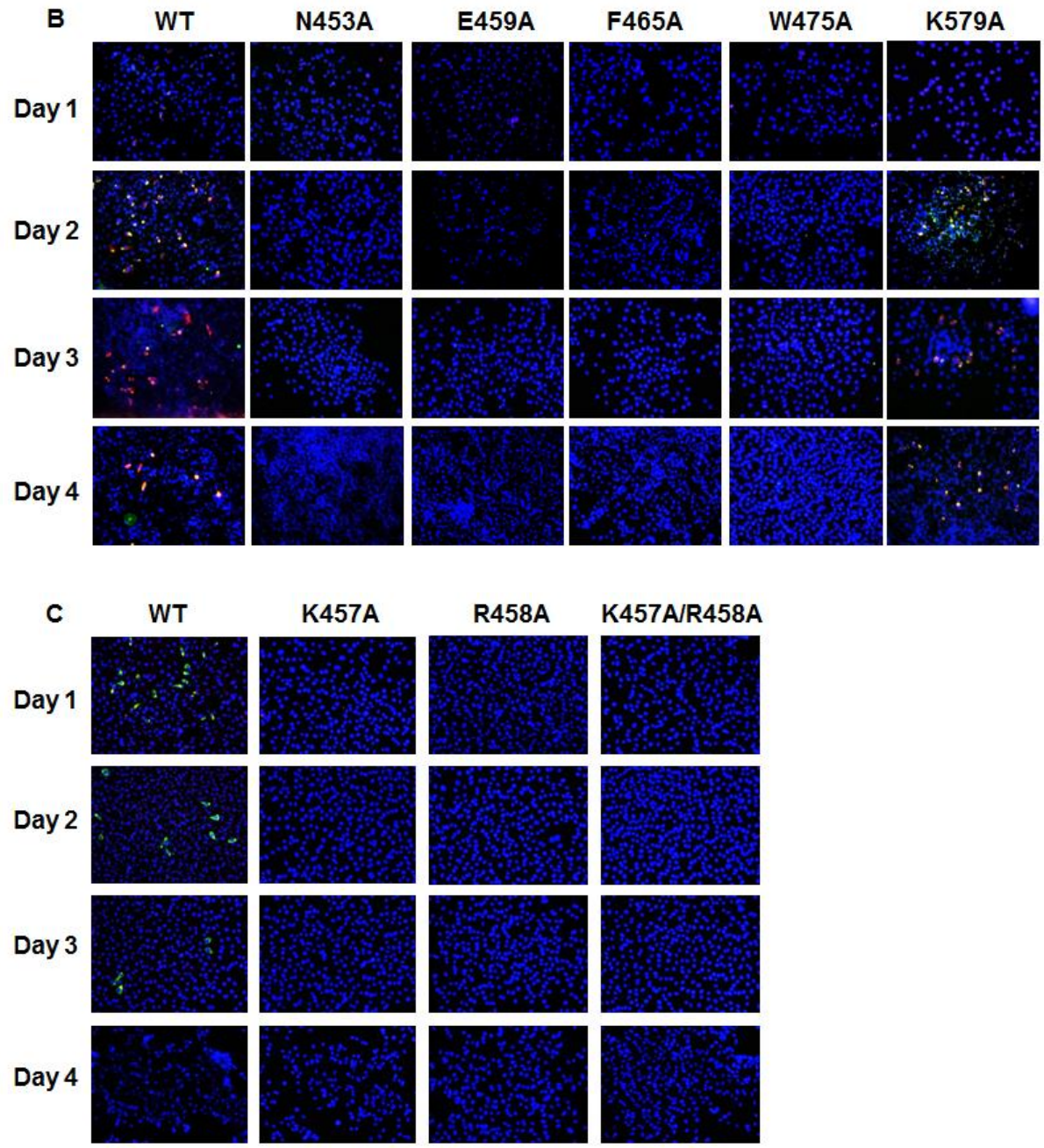

Figure 5.2 Replication profiles of DENV-4 luciferase-reporter subgenomic F1 motif mutant replicons. (A) Renilla luciferase activities of DENV-4 WT and mutant replicons. BHK-21 cells were electroporated with equal amount of replicon RNA and lysed at various time points for luciferase activity measurements. The y-axis denotes the log10 value of Renilla luciferase signal (RLU). Each data point is the average of duplicates, and error bars represent the standard deviations. (B) and (C) IFA images showing dsRNA and NS3 protein co-staining at day 1, 2, 3 and 4 post electroporation. In (B), NS3 protein was stained red in colour by Alexa Fluor 568 goat anti-rabbit IgG (Invitrogen, USA), dsRNA was stained green in colour by FITC-labeled goat anti-mouse IgG (Sigma, USA) and DAPI stained the nucleus blue in colour. In (C), NS3 protein was stained green in colour by Alexa Fluor 488 goat anti-rabbit IgG (Invitrogen, USA), dsRNA was stained red in colour by Alexa Fluor 568 donkey anti-mouse IgG (Invitrogen, USA) and DAPI stained the nucleus blue in colour.

3.3.1.4 Discussion

In this study, the compound binding pocket in the finger domain of RdRp was validated and the importance of F1 motif in viral replication by regulating *de novo* initiation process during RNA synthesis was highlighted. Selected DENV-4 residues N453, K457, R458, E459 and W475 when substituted to alanine, displayed severe reduction in RdRp *de novo* initiation activity and abolished viral replication. The only residue that did not affect RdRp polymerase activity but failed to replicate in cells, F465A, could be essential for other viral activities such as regulating NS5 conformation for interaction with host and viral proteins. The results observed for K457A and R458A were supported by previous enzymatic work whereby the group similarly tested the single and double mutants K456A/R457A (DENV-3 numbering) in polymerase assays using 5' DV RNA and poly(rC) as templates for *de novo* initiation and elongation respectively (103). Their results are in agreement with our data in which *de novo* RNA synthesis was greatly reduced to less than 20% and elongation activity was retained. In addition, DENV-2 infectious clones with these mutations impaired viral replication. Furthermore, they demonstrated that the F1 region is involved in SLA promoter-dependent initiation. Since amino acids 455-468 which form the motif F are disordered in both DENV-3 RdRp (aa273- 900) and FL NS5 (aa6-895) crystal structures (86, 318), suggesting that this region is highly flexible in solution when the protein is in its free state. It could be possible that during RNA synthesis, the dynamic F1 motif assumes a specific orientation in order for NS5 RdRp to bind the SLA promoter present at the 5' untranslated region of the RNA and be catalytically competent to perform *de novo* initiation activity. Thus, the compound likely inhibits polymerase activity by preventing the F1 motif to orientate correctly, leading to an impact in the *de novo* initiation process. In all, this work provides evidence for targeting F1 motif of the finger domain of DENV RdRp as a site for potent inhibitor design.

Additional studies should be done to examine the biological relevance of the F1 motif mutants on replication fitness in the context of the full-length infectious virus. Further revertant analysis

could be conducted to check for possible mutations that may restore replication defect of these alanine mutants. Kinetic studies could also be performed to dissect the mechanism of action for this series of compounds.

3.3.2 Compounds that bind to N-pocket of NS5 RdRp

Following fragment-based screening of ~1400 fragments from Novartis proprietary compound archive using X-ray crystallography, a single hit was identified to bind to a novel allosteric pocket at the interface of the thumb and palm subdomains of DENV-3 RdRp near its active site (termed the "N pocket") (344). This pocket is located close to the priming loop (aa782-809) of the polymerase and conserved across all four serotypes of DENV and other flaviviruses. The biphenyl acetic acid fragment 3 demonstrated an IC_{50} of 734 µM in DENV-4 RdRp *de novo* initiation assay (345). Subsequent growing and optimization of the fragment hit via structure-guided design yielded pan-serotype compounds with >1000-fold improvement in potency *in vitro* and antiviral activity at low micro-molar EC_{50} in cell-based assays. The lead candidate, 3-methoxyphenyl sulfonamide 27, is the most potent in inhibiting viral replication for all four serotypes at EC_{50} of 1.8-2.3 µM. On the other hand, the most active compound in this series, 8-quinolyl sulfonamide 29, displayed the highest biochemical potency with an IC_{50} of 0.013-0.038 µM and SPR binding affinity with a Kd of 0.007 µM (345, 346). Here, both compounds 27 and 29 were co-crystallized with DENV-3 FL NS5 and they showed similar binding mode as seen for the polymerase domain, revealing multiple interactions with amino acid residues lining the pocket (Figure 5.4). Several residues were selected for reverse genetic studies to explore their biological importance in viral replication. The inhibition mode of the compounds was also investigated by performing order-of-reagent addition and kinetic competition experiments using DENV *dn*I FAPA assay. Moreover, resistant mutants generated using the two compounds were mapped to the N-pocket and examined for replication fitness in the context of DENV-2 replicon and infectious full-length virus genome. The findings from this

study confirmed that the antiviral activity of the compounds was attributed to its binding to the N-pocket for specific inhibition of the polymerase and proven the successful use of structure-guided approach for designing potent DENV RdRp inhibitors.

3.3.2.1 Crystal structure of DENV-3 FL NS5 bound to compounds 27 and 29

DENV-3 FL NS5 co-crystal structures with compounds 27 and 29 were solved at a resolution of 1.65 Å and 1.99 Å respectively (Figure 5.3; Figure 3 and Table 1 in S1 Text of (346)). Both compounds were overlaid in the polymerase domain and they displayed closely superimposable conformations in which their thiophene ring and propargyl alcohol are completely overlapped, whilst the acyl-sulfonamide and solvent-exposed ring (methoxy-substituted phenol ring in 27 and 8-quinolinol ring in 29) assume distinct orientations (Figure 5.3A). Superimposition of the compound-bound FL NS5 and RdRp co-crystal structures revealed that the compounds bound in the same way in both polymerase domains without any conformational changes (Figure 5.3D-F). Both compounds made numerous polar interactions with neighbouring amino acid residues within the N-pocket of RdRp (Figure 5.4). The terminal propargyl alcohol projected deeply into a narrow cavity lined by residues W803, M761 and M765, and displaced a water molecule to form two hydrogen bonds with the backbone amide of H800/K800 and the side chain of Q802/E802 (DENV-3 and DENV-2 numberings respectively) (Figure 5.4D & 5.4E). The sulfur of the thiophene ring interacted non-covalently with the side-chain hydroxyl group of S796. At the mouth of the N-pocket, the acyl-sulfonamide moiety are surrounded by residues S710, R729 and R737 and formed H-bond interactions with the side chain of T794 and R729, as well as with the backbone amide of W795 in compound 27. The side chain of R729 established additional hydrogen bond with the 8-quinolinol ring of compound 29 that is absent in the compound 27 in which the methoxy-substituted phenol ring pointed towards the solvent away from R729. This favourable contact may render compound 29 to bind and stabilize

DENV RdRp better than compound 27, and was supported by higher binding affinity and melting temperature observed in SPR and thermo-denaturation analyses (346).

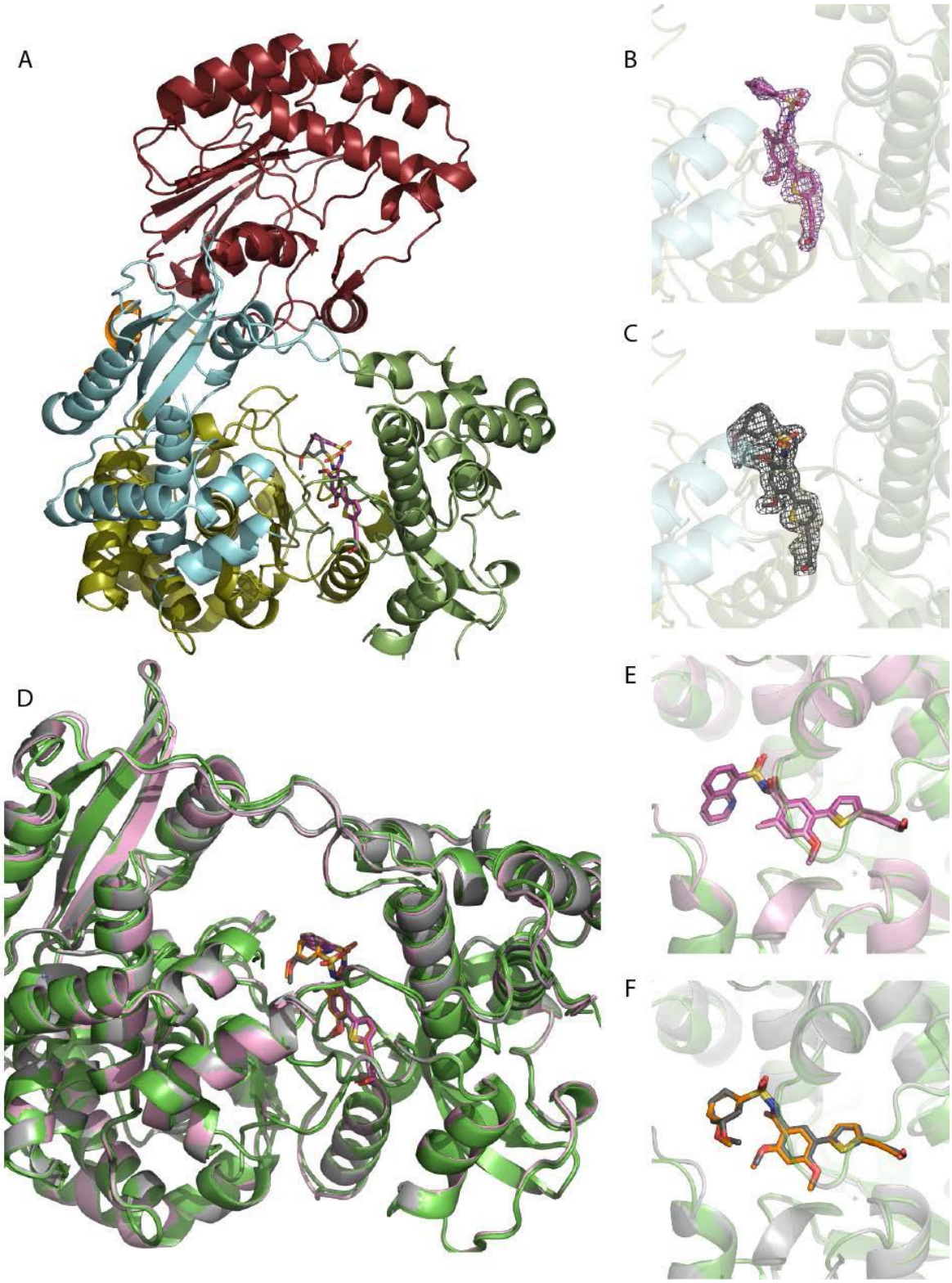

Figure 5.3 Crystal structures of DENV-3 FL NS5 with bound compounds 27 and 29. (A) Overall view of the DENV-3 FL NS5 structure in ribbon representation. MTase domain, linker region, palm, thumb and finger subdomains of RdRp are colored in red, orange, olive, green and blue respectively. Both compounds 27 and 29

are overlapped in the polymerase domain and shown as sticks in the diagram. Close-up views of compounds 29 (B) and 27 (C). (D) Superimposition of the polymerase domain from the co-crystal structures of FL NS5 (green ribbon) and RdRp (pink ribbon). Superimposition of compounds 29 (E) and 27 (F) bound to FL NS5 and RdRp. PDB codes for the crystal structures of DENV-3 FL NS5 with bound compounds 27 and 29 are 5JJS and 5JJR respectively. Adapted from (346).

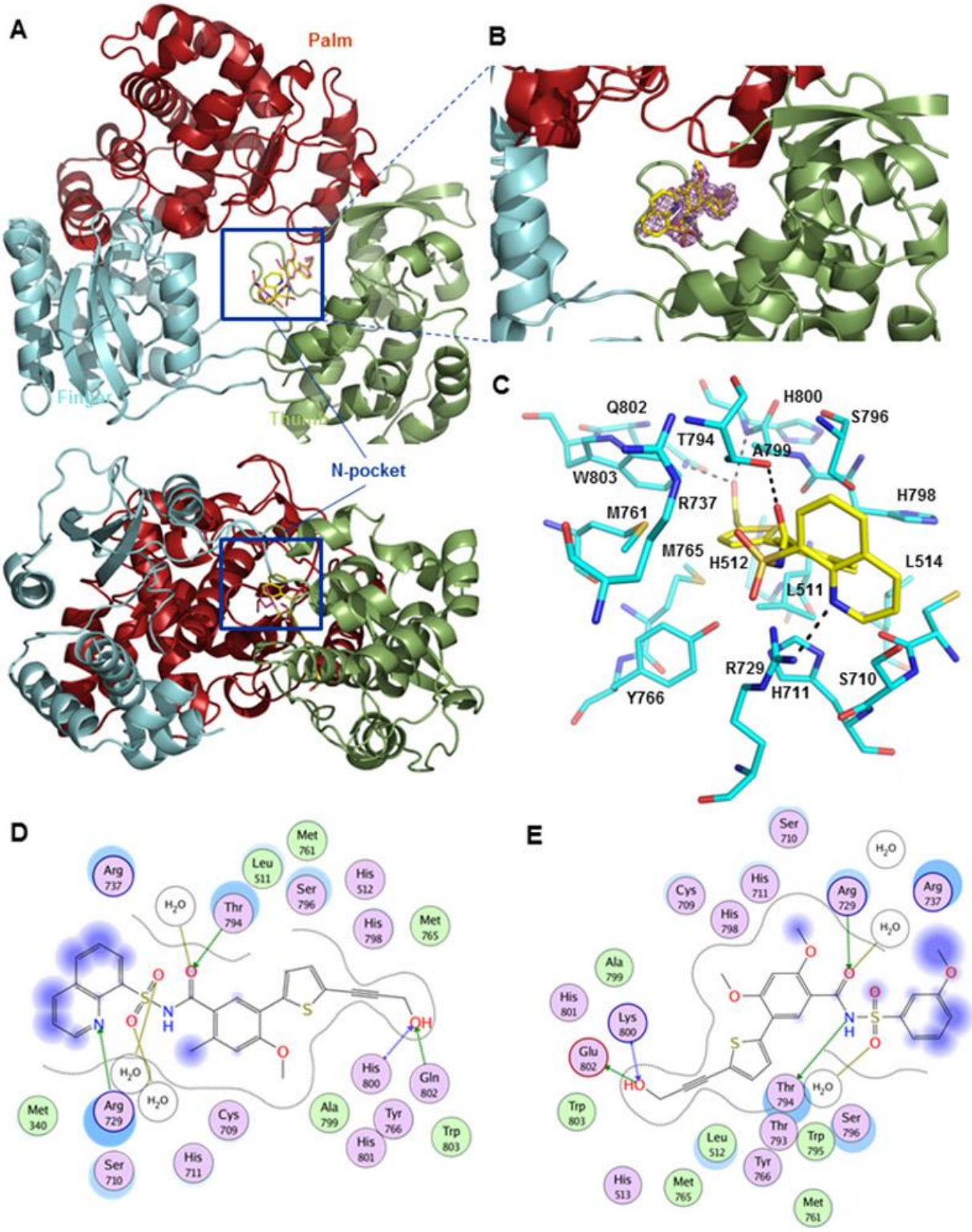

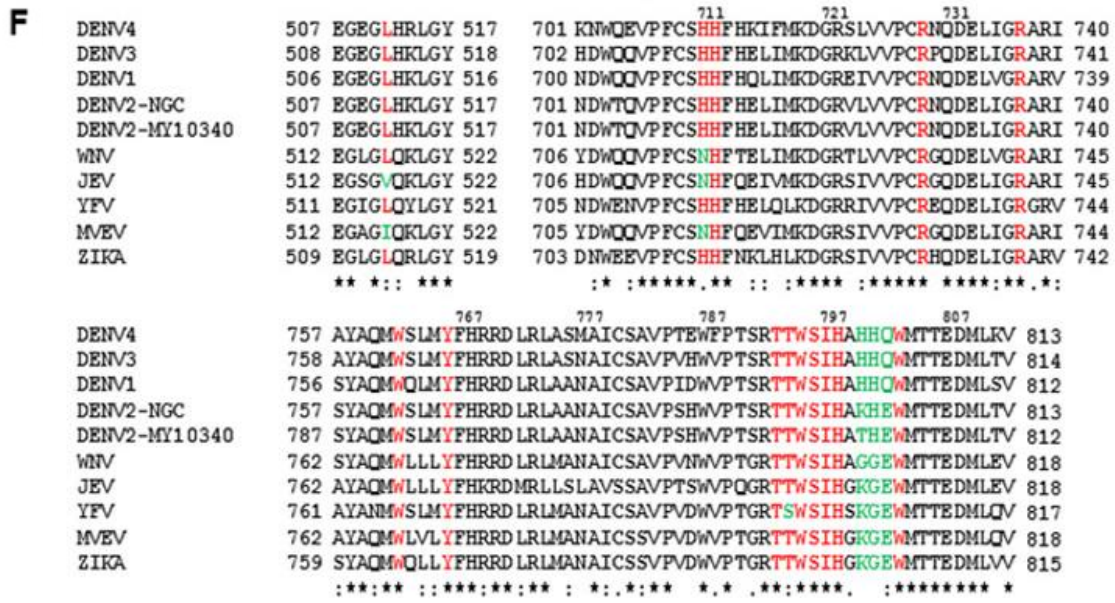

Figure 5.4 Crystal structures of RdRp with bound compounds 27 and 29. (A) Ribbon representation of the DENV-3 RdRp bound to compound 29 in the N-pocket (magnified view in (B)). Palm, finger and thumb subdomains of RdRp are colored in red, cyan and olive respectively. (C) Residues (labelled) lining the N-pocket with compound 29 are depicted as cyan and yellow sticks correspondingly. Dashed lines show the hydrogen bonding. (D) Binding of compound 29 to DENV-3 RdRp domain and (E) compound 27 to DENV-2 RdRp domain as shown in the two-dimensional ligand-interaction maps. Residues are colored light purple and green to represent polar and lipophilic respectively, and charged residues have an extra blue ring. The blue halos indicate the degree of solvent exposure. Hydrogen bonding with amino acid side chain or main chain is shown as green or blue arrows respectively, whilst water-mediated interactions are denoted as gold lines. (F) Multiple alignment of N-pocket residues across different members of the Flavivirus family. Adapted from (346).

3.3.2.2 Role of N-pocket residues for virus fitness

In order to understand the biological relevance of N-pocket binding site for virus replication, DENV-4 subgenomic replicon alanine mutants of selected residues were generated and their replicative profiles were explored in cell-based renilla luciferase assay (Table 5.4). All the chosen residues are conserved across all four DENV serotypes except for H801 and Q803 which are replaced by lysine and glutamic acid in DENV-2 NGC strain respectively (Figure 5.4F). The luciferase signals for all mutants at 72 hour post transfection were compared to WT replicon, which is set at 100%.

Almost all the mutant replicons were lethal for viral replication, as shown by the absence of luciferase activity. Only mutants T795A (T794 in DENV-3), S797A (S796 in DENV-3), H801A (H800 in DENV-3) and Q803A (Q802 in DENV-3) still demonstrated weak replication

of ≤30% comparative to WT. This result was in agreement with their poor *in vitro* RdRp enzymatic activities whereby most mutants have differential reduction in their NS5 polymerase activities with a bigger impact on *de novo* initiation than elongation (data published in (346)). Thus, amino acids residing in the N-pocket are important for virus replication, possibly through regulating the NS5 polymerase *de novo* initiation process.

DENV-4 alanine replicons	DENV-3 numbering	Fitness after 72 hr compared to WT (%)
WT	WT	100
C710A	C709	0
S711A	S710	0
R730A*	R729	0
R738A*	R737	0
Y767A*	Y766	0
T795A*	T794	30
S797A*	S796	30
H801A	H800	10
Q803A	Q802	13
W804A*	W803	0

Table 5.4 DENV-4 alanine substitution of N-pocket amino acid residues that interact with compounds 27 and 29. Equal amount of WT and mutant DENV-4 replicon RNAs were electroporated into BHK-21 cells and assayed for renilla luciferase activities at indicated time points post transfection. Results shown are the percentage replicon activities of mutants compared against WT at 72 hour post-transfection, derived from average relative light units (RLU) obtained from one experiment with duplicate measurements. Note that mutant replicons R730A, R738A, Y767A, T795A, S797A and W804A (indicated by asterisk) were generated by my colleague in NITD and their replicon results are included here for comparison. The data in this table was published in (346).

3.3.2.3 Kinetic studies of DENV RdRp inhibition by compounds 27 and 29

To better understand the inhibitory properties of compounds 27 and 29, order-of-reagent addition experiments were carried out using DENV *de novo* initiation FAPA assay (Table 5.5). This assay involved exposing the compounds to enzyme alone, enzyme-ssRNA complex, enzyme-dsRNA complex, followed by reaction initiation with corresponding missing ssRNA template and/or nucleotide components (317). When both compounds were exposed to pre-formed enzyme-ssRNA complexes before addition of nucleotides, compound 27 did not show much difference in IC_{50} value as compared to the IC_{50} generated by standard assay format, suggesting that this compound could bind to polymerase with the same affinity in the presence or absence of ssRNA. In contrast, compound 29 exhibited about 3-fold decrease in inhibitory potency, implying that it could discriminate between the apo-enzyme and ssRNA-bound

polymerase. Next, compounds were tested with elongated enzyme-dsRNA complexes (comprising of ssRNA substrate and newly synthesized short RNA products – AGAA or AGAACC) and they demonstrated a marked 8-15 fold reduction in inhibitory potencies. This result proposes that the compound binding pocket may undergo conformational changes and become inaccessible during the transition from initiation to elongation state as polymerase accommodates the growing dsRNA product. Elongation FAPA IC_{50} measurement of these compounds corroborated our findings in which a significant 19-23 fold decline in compound potencies were observed (Table 5.5) (346). Thus, this series of compounds was postulated to act and inhibit the enzyme at the *de novo* initiation step of polymerization reaction.

	Order of addition	**Compound 27**	**Compound 29**
de novo IC_{50} (µM) [fold change]	Enzyme + compound	0.172 ± 0.097*	0.023 ± 0.001*
	[Enzyme + RNA] + compound	0.20 ± 0.07 [0.84X]	0.073 ± 0.02 [3.2X]
	[Enzyme + RNA + ATP + GTP] + compound	2.2 ± 1.91 [9.3X]	0.338 ± 0.12 [14.7X]
	[Enzyme + RNA + ATP + GTP + ATTO-CTP] + compound	1.89 ± 1.56 [8X]	0.239 [10.4X]
Elongation IC_{50} (µM)	Enzyme + compound	5.46 ± 2.14 [23X]#	0.427 ± 0.013 [18.6X]#

Table 5.5 Inhibitory properties of DENV polymerase N-pocket compounds. Order-of-reagent addition experiments were carried out using DENV *de novo* initiation FAPA assay as illustrated in Materials and Methods. *De novo* IC_{50} values of compounds 27 and 29 measured via standard assay format (asterisk *) were used as a comparison to calculate fold change in compound inhibitory potencies in the order-of-addition experiments. Elongation IC_{50} values of compounds 27 and 29 (hash #) were obtained from (346). The data in this table was published in (346).

To determine the mechanism of inhibition for the most potent compound 29 against DENV polymerase, kinetic characterization using *de novo* initiation FAPA assay was performed. As expected, control 3'dGTP shows competitive inhibition with respect to GTP whereby both substrate and inhibitor compete for binding to the active site of the enzyme (Figure 5.5B and 5.5F), and non-competitive inhibition with respect to RNA substrate in which it does not interfere in the binding of RNA to the enzyme (Km is unaffected) but influence the progression to reaction products (Vmax is decreased with increasing concentration of 3'dGTP) (Figure 5.5A and 5.5E).

From Figure 5.5C and 5.5G, compound 29 was shown to be an uncompetitive inhibitor of RNA template, decreasing both Km and Vmax. On the other hand, compound 29 seems to display mixed inhibition profile with respect to GTP substrate (Figure 5.5D and 5.5H). Lineweaver-Burk plot revealed that this compound demonstrated an uncompetitive mode of inhibition for GTP, however at high GTP substrate concentrations this compound was a non-competitive inhibitor. Since the Km for GTP was higher during the rate-limiting initiating step as compared to the highly processive elongation phase of RNA synthesis (317), the mixed inhibition profile for compound 29 likely reflects the differential effects on these two processes of the polymerase activities. In consistence, compound 29 has substantially poorer inhibitory potency in elongation phase than in initiation phase (Table 5.5) (346).

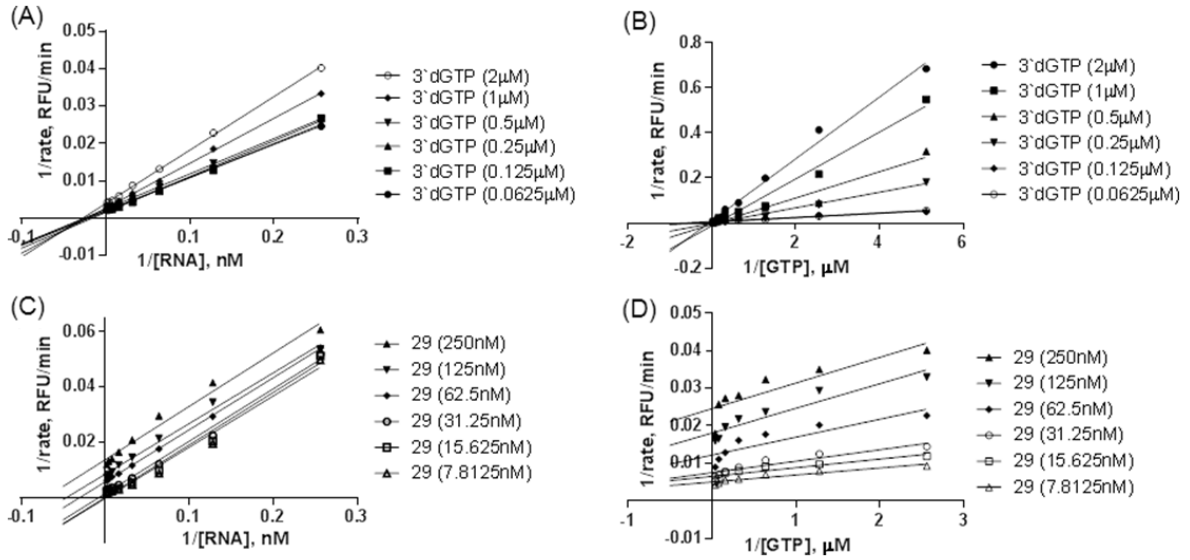

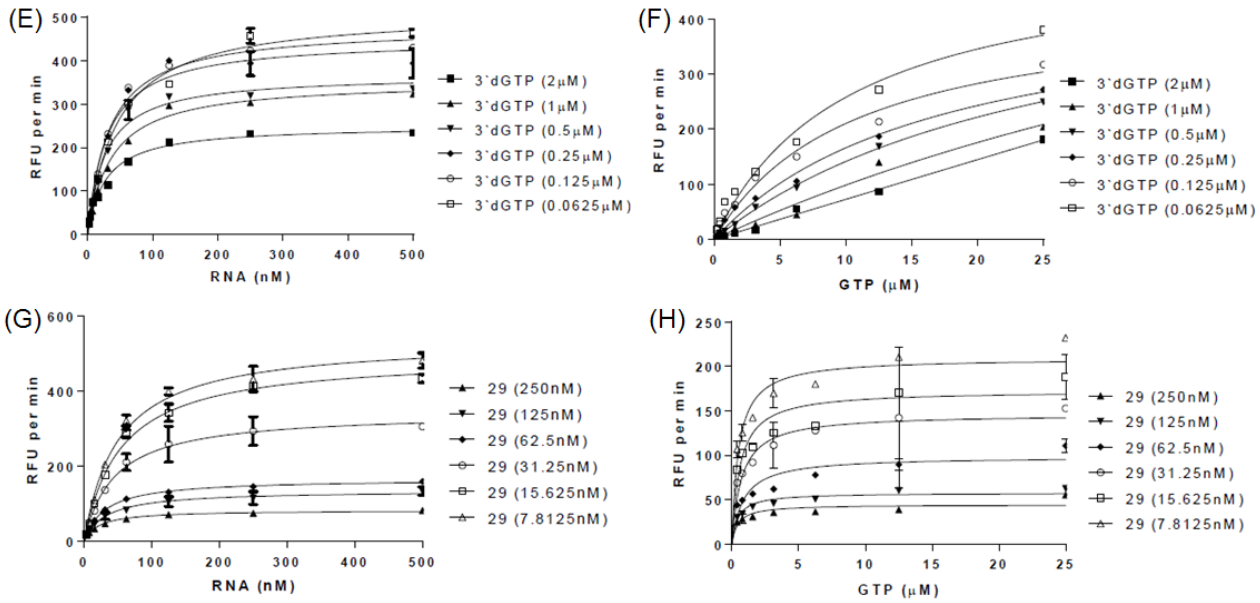

Figure 5.5 Enzyme inhibition kinetics of compound 29 against DENV polymerase. DENV *de novo* initiation FAPA assay was employed to understand the mechanism of inhibition by increasing concentration of 3'dGTP control (A, B, E, F) and compound 29 (C, D, G, H) with 0-500 nM RNA (A, C, E, G) or 0-50 μM GTP (B, D, F, H) substrates. Representative Lineweaver-Burk plots (A-D) and Michaelis-Menten plots (E-H) were derived from non-linear regression curve fitting using Graphpad Prism software. These results were published in (346).

3.3.2.4 Impact of resistant mutations on virus replication

To confirm that the antiviral activity exhibited by this series of compounds was attributed to specific binding to the N-pocket for inhibition of NS5 polymerase activity, resistant DENV-2 replicons were grown in the presence of compounds 27 and 29 (346). Genome-sequencing of compound-exposed replicons detected two resistant mutations, E802D and L511V, raised using compound 29, and only E802D mutation produced by compound 27. Interestingly, these two amino acid changes were mapped to the compound binding N-pocket. Notably, amino acid residue 802 is glutamic acid (E) in DENV-2 NGC and glutamine (Q) in DENV-3 (Figure 5.4F). From the crystal structures of DENV-3 RdRp bound to compound 29 and DENV-2 RdRp bound to compound 27 (Figure 5.4D and 5.4E), the hydroxyl group of the propargyl alcohol arm of both compounds forms hydrogen bonding with the side chain of residue Q802 and E802 in DENV-3 and DENV-2 respectively. Mutation of E802 to aspartic acid (D) shortens the negatively-charged side chain by one methyl group and possibly breaks this H-bond interaction. Additionally, van der Waals interactions were established between the hydrophobic residue

L511 and the thiophene ring of compound 29. Mutation of L511 to valine (V) removes one methyl group from the hydrophobic side chain and may weaken the interaction. Consequently, these structurally validated resistant mutants may result in a lower binding affinity of compounds 27 and 29 in the N-pocket, providing convincing evidence that both compounds specifically target the RdRp for replication impairment.

To investigate the effects of L511V and E802D amino acid changes on virus replication, individual and double mutations were engineered into DENV-2 subgenomic replicon and infectious full-length virus genome. Replication fitness of replicons and virus were determined using renilla luciferase activity and plaque assay respectively, over the course of four days (Figure 5.6). Electroporated BHK-21 cells containing WT and mutant replicons maintained similar proliferation rates and viability throughout the four days post transfection as detected by cell viability assay (Figure 5.6A). Overall, all three mutant replicons were more replicative and produced higher levels of luciferase signals, intracellular viral RNA and NS5 protein as compared to WT replicon (Figure 5.6B-C and 5.7A). The luciferase activity for L511V and L511V/E802D mutants reached the highest level at 24 hour, whilst it peaked at 48 hour for WT and E802D (Figure 5.6B).

For WT and mutant infectious clones, viral titers increased steadily over the four days post transfection (Figure 5.6D). Compared to WT virus, both E802D and L511V/E802D mutants produced more infectious virus particles and extracellular viral RNA whereas L511V yielded the least viable virus and extracellular viral RNA (Figure 5.6D-E). However, intracellular dsRNA and RdRp levels for mutant L511V were highest at day 4 post electroporation (Figure 5.7B). The discrepancy in viral replication profile for L511V is unclear and may be due to different impact of this mutation on replicon and virus. In all, these resistant mutations generated using the N-pocket compounds enhanced the ability of virus to replicate in cells.

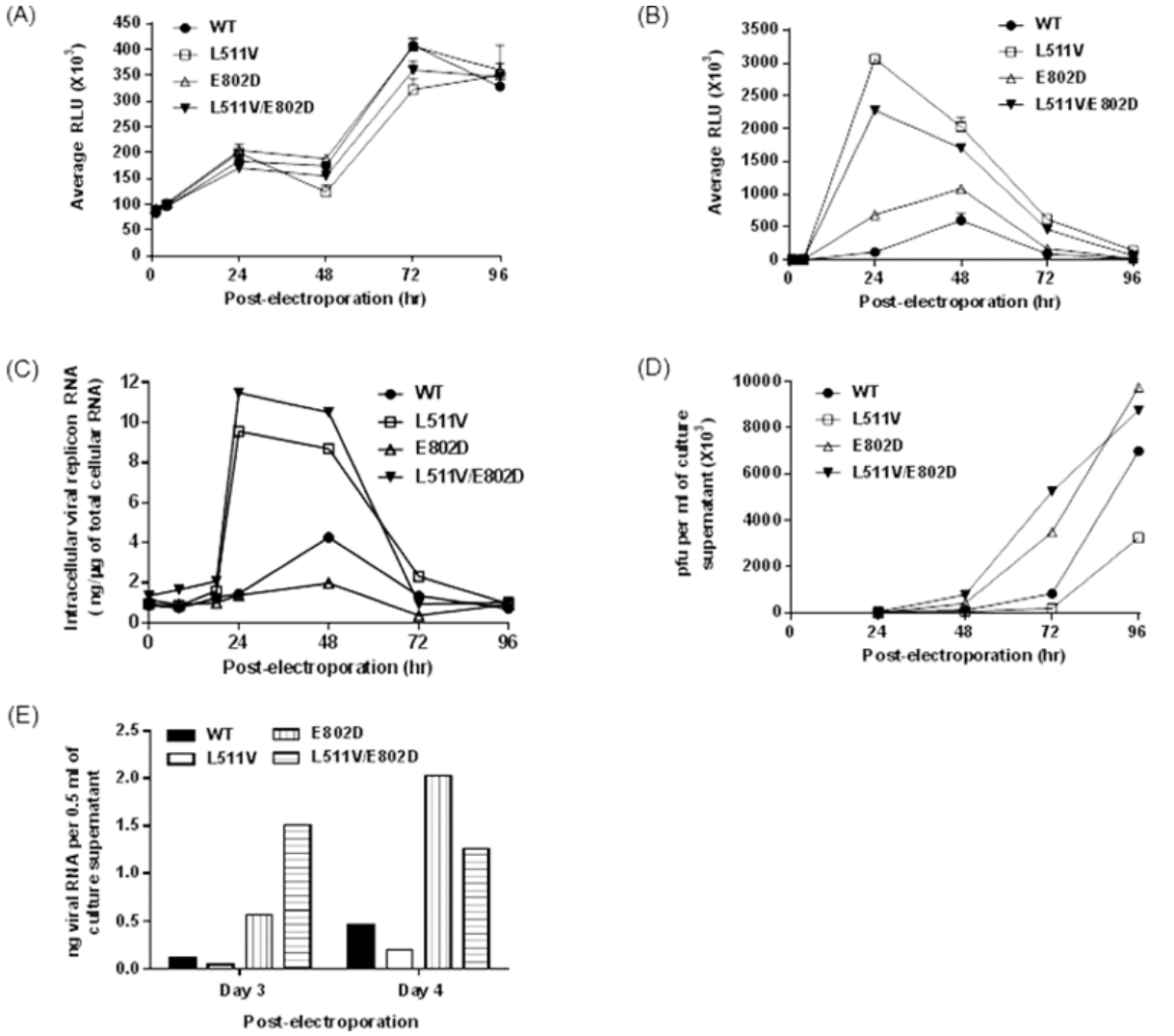

Figure 5.6 Growth kinetic profiles of DENV-2 replicons and full length genomic RNAs with resistant phenotype mutations. Equal amount of WT and mutant replicon RNAs were electroporated into BHK-21 cells, after which cell viability (A), renilla luciferase signals (B) and intracellular viral RNA levels (C) were measured at indicated time points. Equal amount of WT and mutant full length genomic RNAs were electroporated into BHK-21 cells, after which secreted infectious virus particles (D) and extracellular viral RNA levels (E) were detected using harvested culture supernatants from day 1 to 4. These results were published in (346).

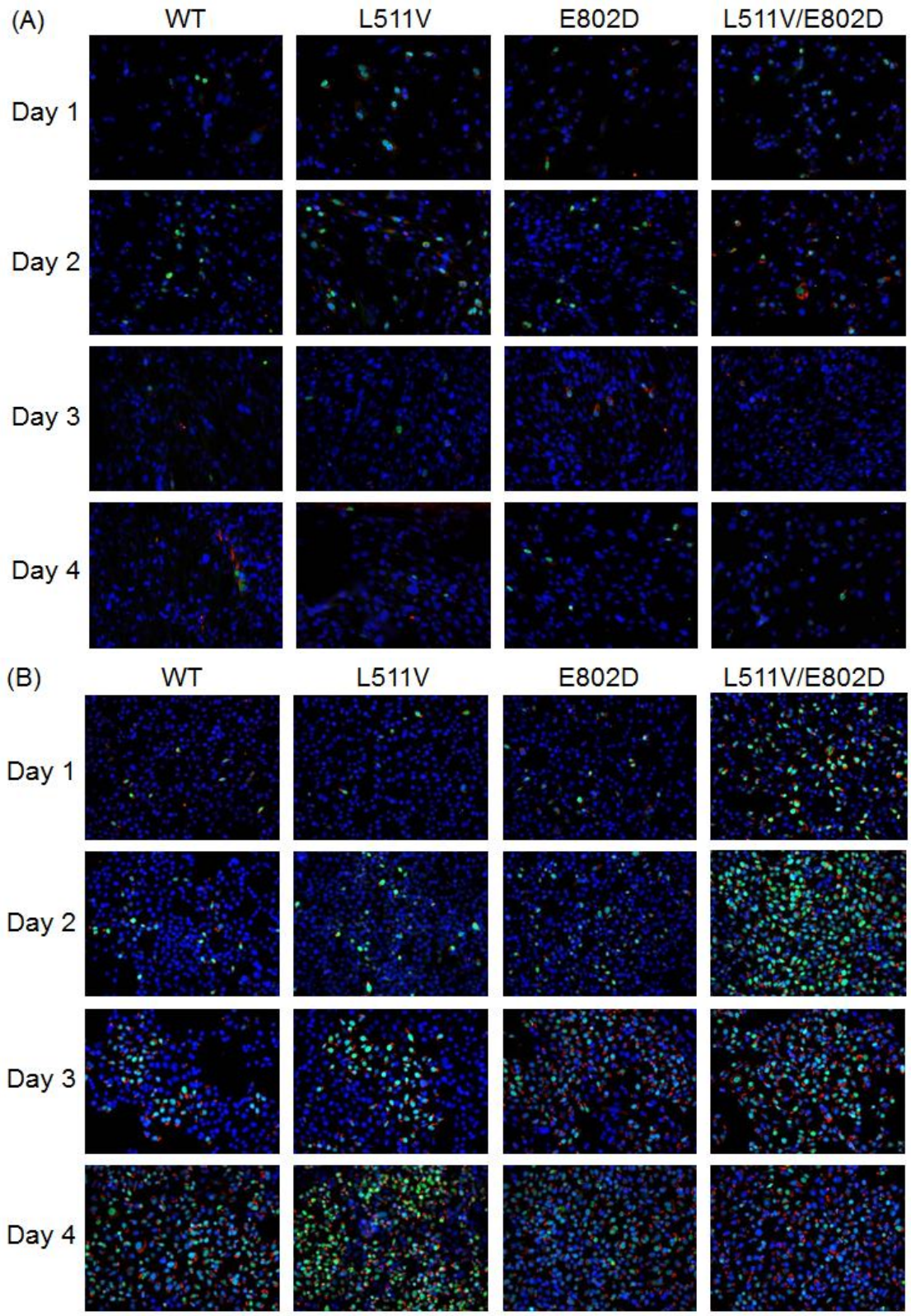

Figure 5.7 Analysis of viral RNA and NS5 protein expressions from DENV-2 WT and mutant replicons and viruses. Immunofluorescence assay (IFA) was performed on BHK-21 cells harboring WT and mutant (A) replicon and (B) full length genomic IVT RNAs. At indicated time point, the cells were fixed and stained with primary antibodies (anti-dsRNA mouse monoclonal antibody (J2), anti-DENV2 NS5 rabbit polyclonal antibody (GTX103350) for replicon and anti-DENV4 RdRp rabbit polyclonal antibody for virus) and secondary antibodies (Alexa Fluor 488-conjugated goat anti-rabbit IgG and Alexa Fluor 568-conjugated donkey anti-mouse IgG). These results were published in (346).

3.3.2.5 Discussion

Through a fragment-based screening approach via X-ray crystallography targeting the DENV-3 RdRp, a novel allosteric pocket (termed the "N pocket") was identified at the thumb/palm interface near the active site and priming loop of the enzyme, and is formed by amino acid residues conserved across all four DENV serotypes and other flaviviruses (Figure 5.4). This pocket was characterized and validated for their functional importance in NS5 polymerase *de novo* initiation activity and virus replication using alanine mutagenesis and reverse genetic studies (346). The fragment hit and related compounds generated by rational design were found to bind to this discrete site with high affinity and stabilize the RdRp melting temperature by 4-14 °C (344-346). The two most potent compounds in the series, 27 and 29, were efficacious in inhibiting viral replication in cells at single-digit micro-molar EC_{50} and *de novo* initiation activity *in vitro* at nano-molar IC_{50}, respectively. When these compounds were assayed with alanine mutants of N-pocket residues, their inhibitory properties were greatly impacted as they exhibited 13.5-107 fold shift in *de novo* IC_{50}. Exposure of DENV-2 replicon to compound 29 produced two resistant amino acid changes, E802D and L511V, mapped to the compound-binding N-pocket. These two residues were shown to form critical interactions with compounds 27 and 29 in the co-crystal structures (Figure 5.4D and 5.4E). Consistently, both E802D and L511V mutants were more replicative than WT in cells (Figure 5.6 and 5.7) and reduced compound potencies significantly in DENV RdRp enzymatic and cell-based assays (346). These findings confirmed that this class of compounds specifically target the N-pocket of RdRp for inhibition of viral replication.

Kinetic characterization revealed that compound 29 is an uncompetitive inhibitor of RNA template and demonstrated mixed inhibitory modes with respect to GTP substrate in *de novo* initiation FAPA assay (Figure 5.5C-D and 5.5G-H). As the *de novo* assay also measures elongation activity after *de novo* initiation step, this mixed inhibition profile plausibly denotes

the differential inhibitory effects on these two processes of the polymerase activities. In agreement, compound 29 has considerably weaker inhibitory potency in the elongation assay than in *de novo* initiation assay (Table 5.5), suggesting that this compound blocks the first step of RNA synthesis better than the second step. This finding was further supported by the order-of-reagent addition experiments whereby the inhibitory properties of compound were diminished when the polymerase was occupied with dsRNA and not by ssRNA. Since retraction of the priming loop from the active site occurs during elongation event to provide space for the newly synthesized duplex RNA and given that the N-pocket inhibitors interact with residues from the priming loop, it could be possible that compound binding may be affected by conformational modifications of the pocket. Thus, the proposed mechanism of action for this series of compounds could be to prevent RdRp conformational changes during the transition from initiation to elongation phase of RNA synthesis.

Taken together, the discovery of N-pocket and rational design of inhibitors targeting this allosteric site constitute a novel structure-based anti-viral pharmaceutical strategy. These inhibitors were proven to be potent for antiviral activity and are promising to be developed as drug candidate. Further optimization of the structure of these compounds could be carried out to improve their pharmokinetic properties and stabilities *in vivo*.

3.4 Crystallization Attempts of the DENV NS5 RdRp-RNA Complex

DENV NS5 initiates RNA synthesis by a *de novo* mechanism to form a starting dinucleotide primer followed by transition to a rapid, processive elongation state. The NS5 RdRp contains a highly conserved active site that is often targeted for antiviral drug development as nucleotide analogs could exhibit cross-serotype/viral inhibitory activity and confer a high barrier for resistance emergence. The clinically approved nucleotide prodrug, sofosbuvir (2'-modified uridine analog), is a successful example of a potent inhibitor of the Hepatitis C virus (HCV) NS5B polymerase and demonstrated good efficacy and safety for combination treatment against chronic HCV (347). Interestingly, sofosbuvir has antiviral activity against ZIKV as it inhibited virus replication and infection in different cell lines and prevented ZIKV-induced death in mice (303, 348, 349). However, a recent study has revealed that despite being structurally and functionally closely related to HCV NS5B, DENV and ZIKV NS5 exhibited differences in selectivity towards 2'-modified nucleotide analogs which could correspond to varied potency in infected cell cultures (350, 351). Moreover, a repurposing strategy to develop potent anti-DENV drugs from HCV inhibitors failed due to toxicity and efficacy issues (352). So far, high throughput screening or fragment based screening have primarily yielded compounds that block the *de novo* initiation activity of DENV NS5 RdRp (Section 3.3). Therefore, in order to design specific and effective nucleotide-based drugs for DENV, it is crucial to obtain structural information about the complete RdRp catalytic cycle (*de novo* initiation and elongation steps).

Over the past decade, crystal structures of polymerase-RNA complexes from FMDV (96, 106, 353), Norwalk virus (354) and HCV (311, 355) have been determined, and they mostly represented initiation phase complexes and revealed critical amino acids involved in viral RNA replication. However more recently, a series of distinct structures obtained from stalled elongation complex (EC) of several positive-strand RNA viruses such as poliovirus,

coxsackievirus and rhinovirus (93, 95), provided snapshots of the polymerase catalytic cycle and valuable insights into the molecular basis and structural changes in the polymerase for nucleotide selection, active site closure for catalysis and RNA duplex accommodation, as well as key interactions between polymerase and RNA strands in the active site. Following their strategy to obtain ternary crystal structure of DENV, we took a systematic approach from assembling an active elongation complex which allows the measurement of nucleotide incorporation using PAGE and fluorescence polarization (FP), to profiling numerous RNA templates and selecting those with good binding affinity and elongation activity, and finally generating and purifying stable polymerase-RNA elongation complexes for crystallization.

3.4.1 Formation of a functional DENV NS5 elongation complex

A functional elongation complex of DENV-4 FL NS5 or RdRp (aa266-900) was assembled using RNA template/primer (T18/P8; Figure 6.1A) whereby the 5'-end of the primer was labelled with 6-carboxyfluorescein (6-FAM), preincubated with the enzyme in buffer (50 mM Tris-Cl at pH 7.5, 0.5 mM $MnCl_2$, 0.001% Triton X-100, 10 mM KCl, and 10 µM cysteine; buffer composition same as in FAPA elongation assay). The concentrations of enzyme and RNA were kept at 250 nM and 50 nM respectively, and these two components were incubated at RT for 1 min before addition of UTP at varying concentrations to allow single nucleotide incorporation at +1 position for 15 min (Figure 6.1B). PAGE gel showed that RdRp and FL NS5 exhibited highest elongation activity of 9.3% and 42.3% using 111 µM and 333 µM UTP respectively. In addition, incubation with additional amounts of UTP substrate inhibited these two proteins, as seen from the non-linear fitting curve. Thus, NTP concentration used for subsequent complex formation was set at 100 µM.

Next, the effects of divalent cations on elongation complex formation were evaluated. Previously, it was reported that Mg^{2+} ion is required to form productive DENV elongation complex (356), albeit Mn^{2+} ion is commonly used in RdRp enzymatic assays for both initiation

and elongation. In this study, varying concentrations of the two divalent cations were tested for nucleotide incorporation (Figure 6.2A and 6.2B). The observed optimal concentration of $MnCl_2$ was 0.5-1 mM with no mismatch incorporation at position +2, even though it was shown to be highly possible when Mn^{2+} was used (357-359). On the other hand, $MgCl_2$ only weakly produced extended RNA. Moreover, a combination of both ions did not enhance elongation activity as compared to Mn^{2+} alone, and the absence of any ion also generated lesser product. These findings indicated that Mn^{2+} itself could stimulate assembly and reaction of active complex better than $MgCl_2$. Similar to the set up for testing divalent cations, the effects of KCl and NaCl salts on elongation complex formation were also examined (Figure 6.2A and 6.2C). Equivalent incorporation profile was observed for both KCl and NaCl whereby increasing the concentration of salt reduces the percentage of NTP incorporation, possibly due to instability of the elongation complex and dissociation of RNA from the polymerase. Thus, it would be desirable to maintain the concentration of salt as low as possible for active complex formation. Further investigation on pH dependence for elongation complex assembly and reaction was performed (Figure 6.2A and 6.2D). Our result revealed that the amount of incorporation was higher when the polymerase-RNA was incubated in Bis-Tris buffer, especially at pH 7.0 and 7.5 which gave 15.5% and 16.8% incorporation respectively. Taken together, the optimized final buffer condition for efficient elongation is 50 mM Bis-Tris at pH 7.25, 0.5 mM $MnCl_2$, 0.001% Triton X-100, 10 mM KCl and 10 µM cysteine.

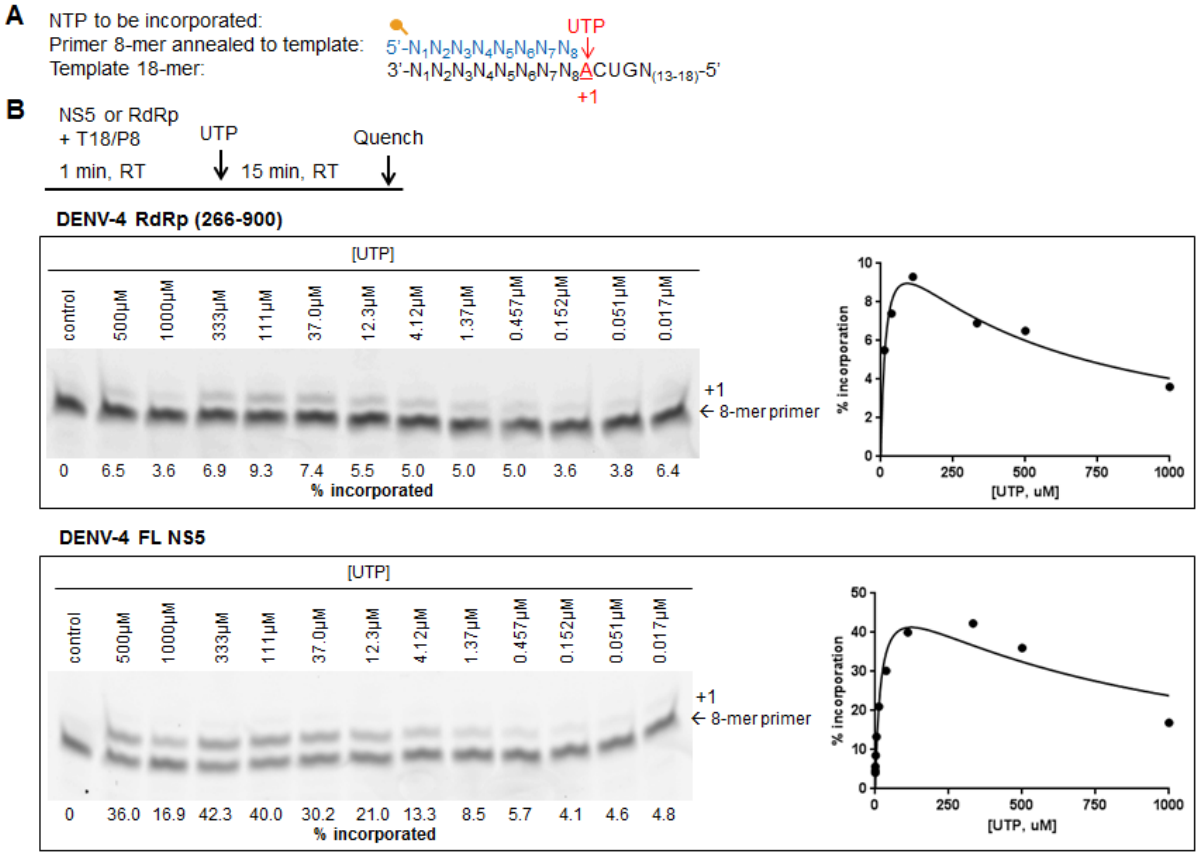

Figure 6.1 Single nucleotide incorporation of DENV-4 FL NS5 and RdRp. (A) Template/primer T18/P8 (8 nucleotides from primer complementary to the 18-mer template) was labelled with 6-carboxyfluorescein (6-FAM; orange ball) at the 5' end of the primer. Addition of UTP to preincubated DENV-4 FL NS5 or RdRp (aa266-900) and RNA mixture enabled formation of +1 RNA product which can be visualized using PAGE (B). The elongation reaction was quenched after 15 min and ran on 23% Urea-PAGE gel to monitor nucleotide incorporation. The percentage of incorporation was determined using ImageQuant TL software and was plotted against varying concentrations of UTP.

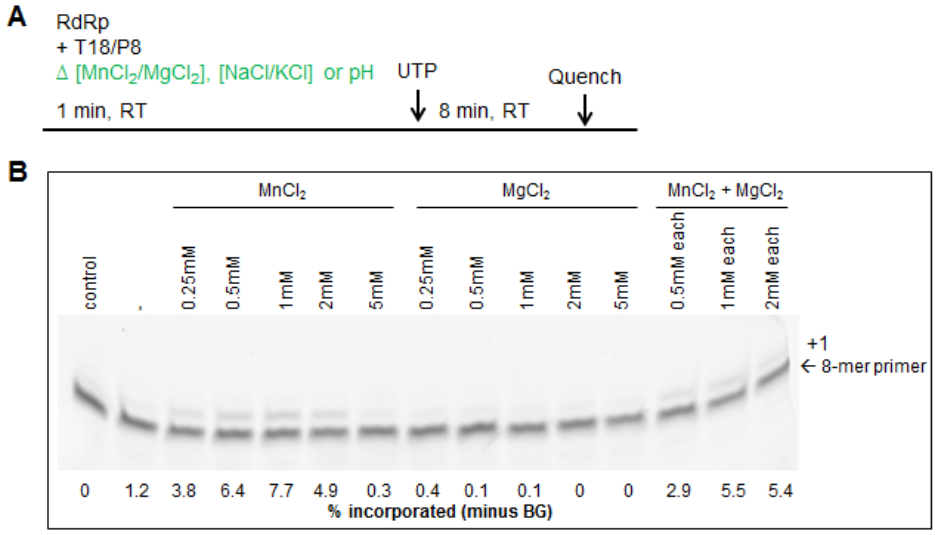

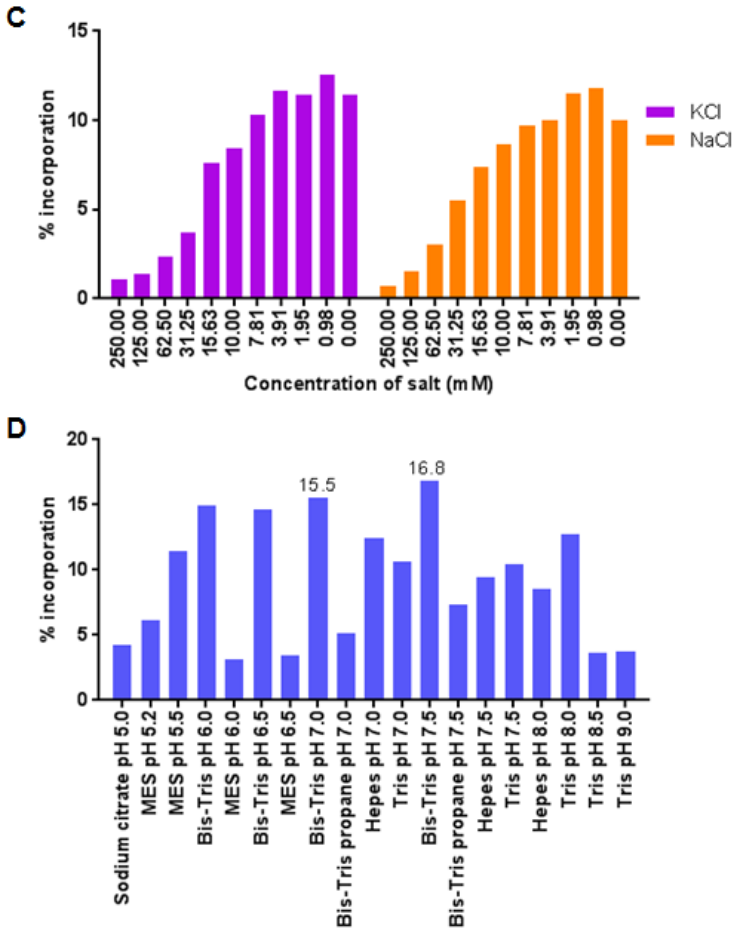

Figure 6.2 The effects of divalent cations, salts and pH on single nucleotide incorporation of DENV-4 RdRp. (A) DENV-4 RdRp (aa266-900) and T18/P8 was preincubated at RT for 1 min in buffer with different concentrations of divalent cations (B) and salts (C) as well as varied pH values (D). Reaction was initiated upon addition of UTP and quenched after 8 min prior to running on PAGE gel. The percentage of incorporation was determined using ImageQuant TL software.

3.4.2 Determination of DENV NS5-RNA binding and elongation activities by fluorescence polarization

A fluorescence polarization (FP) assay was developed to detect both DENV NS5-RNA binding and elongation activities. The principle of this assay is that when a fluorescent ligand is bound by a larger macromolecule, in this case binding of the fluorescent-labelled primer-template substrate to the polymerase, the probe is no longer free in solution and tumbles less rapidly, FP signal will increase (Figure 6.3). Addition of NTPs for elongation increases the molecular size of the complex and further reduces the mobility of the ligand, thus increasing the FP signal

even more. Hence, the degree of polarization is directly proportional to the amount of bound fluorophore and inversely related to molecular rotation.

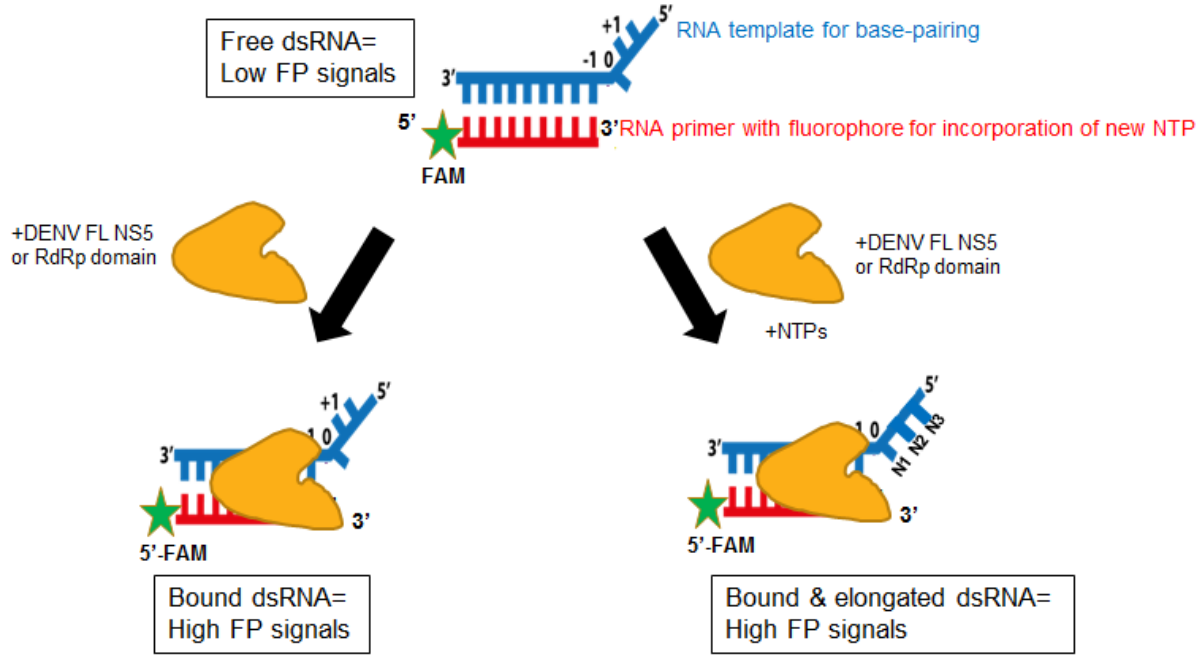

Figure 6.3 Principle of the fluorescence polarization (FP) assay. When a fluorescent-labeled primer-template substrate is free in solution, it tumbles rapidly leading to a low FP value. Binding of nucleic acid to the polymerase reduces tumbling and increases polarization. Addition of NTPs to the enzyme-nucleic acid complex for elongation further increases the overall molecular weight, resulting in a higher FP signal.

Using this FP-based assay, the binding of DENV-4 FL NS5 enzyme to FAM-conjugated RNA T18/P8 was examined (Figure 6.4A). The binding assay was performed by incubating a fixed concentration of RNA in increasing concentrations of NS5 protein for 10 min before measuring the FP signal. Low concentration of annealed T18/P8 at 5 nM was used in order to achieve good signal-to-noise for a quantitative measurement. RNA dissociation constant (K_d) obtained was 38 nM, indicating that the enzyme has high affinity for T18/P8 RNA.

The use of this RNA duplex T18/P8 as a substrate for polymerase elongation activity measured by FP was also carried out (Figure 6.4B). DENV-4 FL NS5 at K_d concentration of 38 nM was incubated with 5 nM RNA at RT for 1 min, followed by addition of all four nucleotides (100 µM each) to completely elongate the RNA by +10 bases. There was a clear gradual increase in

polarization from the start of the reaction to after incubation for 1 hour (ΔmP ~70) and the FP signal maintained for another hour, suggesting that the elongation complex was stable.

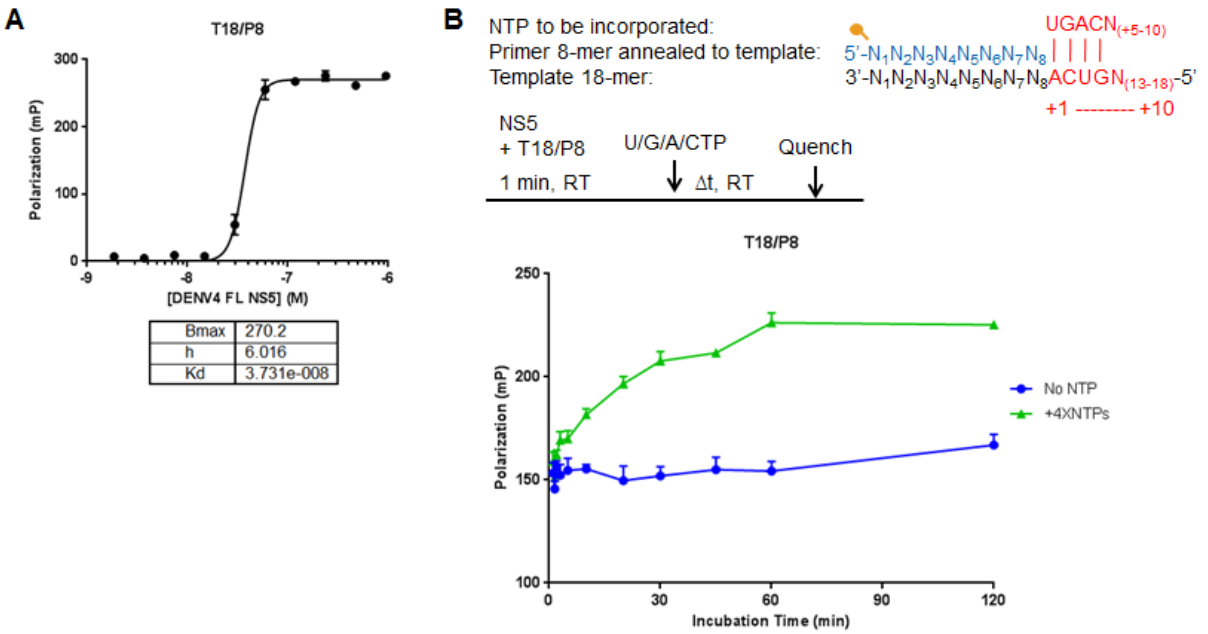

Figure 6.4 Binding and elongation activities of DENV-4 FL NS5 using T18/P8 RNA. (A) Binding assay was performed by varying the concentration of DENV-4 FL NS5 protein and fixing the concentration of T18/P8 substrate at 5 nM. RNA dissociation constant (K_d) was determined by curve fitting the data to a single-site binding isotherm using GraphPad Prism software. (B) Time-course measurement of FP signals after addition of all four nucleotides at 100 µM each to the polymerase-RNA complex for elongation.

The influence of divalent cations on RNA binding to DENV-4 FL NS5 RdRp and enzyme activity was explored using FP-based assays (Table 6.1). The divalent ions tested were Mn^{2+}, Mg^{2+}, Co^{2+}, Ca^{2+}, Zn^{2+}, Ni^{2+} and Cu^{2+} at fixed concentration of 0.5 mM in the buffer. All the reactions yielded similar K_d values of approximately 30 nM, but they displayed difference in polymerase elongation activity. The reaction containing $MnCl_2$ produced the best change in FP signal of 70 mP after 2 hours of incubation, followed by $CoCl_2$>$ZnCl_2$>$MgCl_2$. On the contrary, $CaCl_2$, $NiCl_2$ and $CuCl_2$ failed to promote elongation of RNA chain.

The four divalent ions $MnCl_2$, $CoCl_2$, $ZnCl_2$ and $MgCl_2$ were selected and further tested at a range of concentrations from 0.5 mM to 200 mM at three temperatures, RT, 30°C and 37°C, to assess whether there is any improvement in NS5 elongation complex formation (Figure 6.5A). Magnesium acetate and magnesium formate, which are one of the buffer components for crystallization of DENV-3 NS5 structure, were also included in this experiment. FP signals

were measured at three indicated time points, 1, 2 and 4 hours, after reaction initiation. Overall, there was no substantial difference in polarization with different temperatures. It was observed that RdRp was inactive in the presence of $ZnCl_2$, inconsistent with the previous result that 0.5 mM $ZnCl_2$ stimulated elongation activity by 30 mP. The biggest FP signal change of 60-80 mP was obtained with 50 mM $MnCl_2$, 5 and 10 mM $MgCl_2$, 5 mM $CoCl_2$, 10 mM magnesium acetate and 10 mM magnesium formate. Notably, magnesium chloride, acetate and formate at ≥50 mM inactivated polymerase elongation activity; however DENV-3 NS5 crystal grew in buffer containing 200 mM magnesium acetate or formate. Hence, it was postulated that the crystal of DENV elongation complex should form in crystallization buffer different from apo-DENV-3 NS5, probably in conditions with lower concentration of divalent cations. Next, FP binding assay was conducted in buffer harboring 50 mM $MnCl_2$, 10 mM $MgCl_2$ and 5 mM $CoCl_2$ to examine whether higher concentration of divalent ions could have an impact on polymerase binding to RNA substrate (Figure 6.5B). Higher concentration of Mn^{2+} and Mg^{2+} ions resulted in poorer K_d of 191 nM and 254 nM respectively, whilst Co^{2+} still retained low K_d of 27 nM. The difference in elongation activity of 0.5 mM $MnCl_2$ and 5 mM $CoCl_2$ was not significant, thus subsequent polymerase complex was still assembled using $MnCl_2$ and not $CoCl_2$.

Divalent ions	K_d	ΔmP at 120min	Comments
$MnCl_2$	37nM	70mP	Enzyme binds RNA and is most active
$MgCl_2$	32nM	10mP	Enzyme binds RNA and inactive
$CoCl_2$	34nM	50mP	Enzyme binds RNA and is active
$CaCl_2$	31nM	-	Enzyme binds RNA and is inactive
$ZnCl_2$	28nM	30mP	Enzyme binds RNA most tightly and is weakly active
$NiCl_2$	36nM	-	Enzyme binds RNA and is inactive
$CuCl_2$	35nM	-	Enzyme binds RNA and is inactive

Table 6.1 The effects of different divalent cations on binding and elongation activities of DENV-4 FL NS5 RdRp. The binding and elongation activities of DENV-4 FL NS5 protein to T18/P8 RNA substrate in buffer containing differing divalent ions was determined using FP assays. RNA dissociation constants (K_d) were determined by curve fitting the data to a single-site binding isotherm using GraphPad Prism software. Change in polarization (ΔmP) was calculated by deducting average FP signals obtained at 0 hour from average FP signals detected at 2 hour after addition of all four nucleotides to initiate elongation.

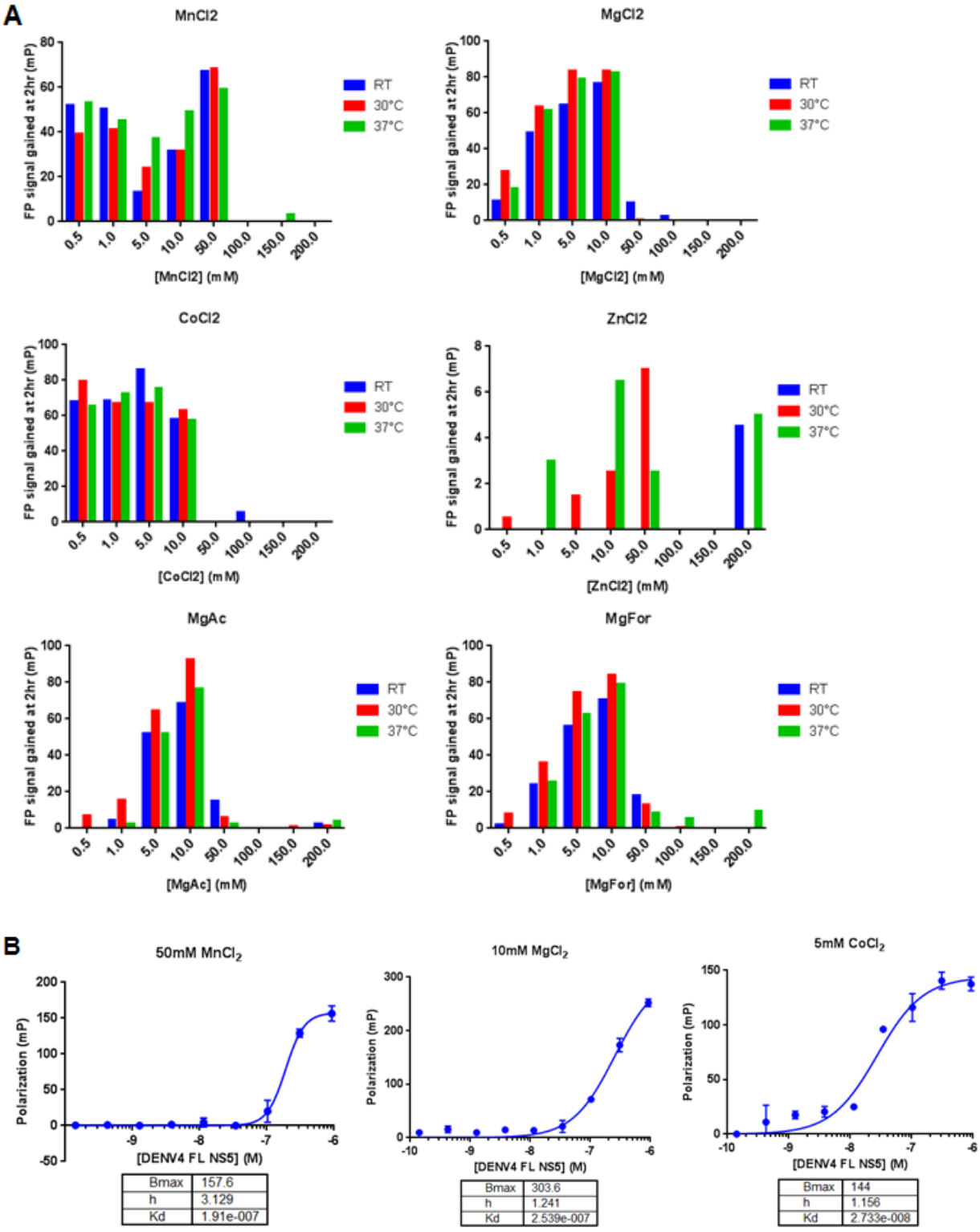

Figure 6.5 The effects of divalent cations and temperature on binding and elongation activities of DENV-4 FL NS5 RdRp. (A) DENV-4 FL NS5-T18/P8 RNA complex was assembled at three temperatures (RT, 30°C and 37°C) in buffer containing different divalent cations at varying concentrations from 0.5 mM to 200 mM. Elongation reaction was started by adding all four nucleotides at 100 µM each and terminated at indicated time points (1, 2 and 4 hour). FP signal gained at 2 hour was plotted against various concentrations of divalent ions. (B) Binding assay was performed in buffers containing higher concentration of $MnCl_2$, $MgCl_2$ and $CoCl_2$. RNA dissociation constant (K_d) was determined by curve fitting the data to a single-site binding isotherm using GraphPad Prism software.

3.4.3 Selection of RNA suitable for co-crystallization

The development of a novel FP-based assay to evaluate binding and elongation activities of DENV NS5-RNA enables rapid profiling of numerous RNA substrates for their suitability for co-crystallization. The binding of DENV FL NS5 enzyme to a series of different RNA substrates (Figure 6.6A) was examined (Table 6.2 and Figure 6.6B). These RNA-primed substrates were labelled with 6-FAM at the 5' end of either the primer or template strand. RNA dissociation constants (K_d) obtained for all RNA substrates bound to NS5 protein were low (≤50 nM), indicating that the enzyme has high affinity for all the RNAs.

Next, elongation complex was formed by addition of NTP(s) to a mixture containing DENV-3 or -4 FL NS5 and RNA-primed substrate. The incorporation of nucleotide(s) was detected using FP and on denaturing Urea-PAGE gel (Table 6.2 and Figure 6.6C-D). In general, all the RNAs have differential effects on polymerase elongation activity. The best polarization signal was achieved using RNA duplex T18/P8 (studied earlier) whereby an increase in FP values of 67 and 75.5 mP were obtained with DENV-4 and DENV-3 NS5 respectively, at 2 hours after addition of all four nucleotides. Denaturing PAGE analysis of the elongation reaction showed gradual accumulation of extended products from +1 to +10, with about 50% of the fluorophore-conjugated primer left unincorporated. Interestingly, addition of only UTP did not produce any difference in FP signal as compared to the control (no NTP added) even though RNA primer with UTP incorporated at +1 position was visible on PAGE gel, implying that our FP assay was not sensitive enough to measure one nucleotide incorporation. Also, as seen from the PAGE gel, there was no misincorporation of UTP as the second base even though a high concentration of UTP (100 µM) was added to comparatively lower concentration of RNA substrate (5 nM) and enzyme (38 nM). Steady-state kinetic measurements showed that each NTP has high turnover rate for incorporation and exhibited good Km value of 3-7 µM (Table 6.3). In addition, it was observed that beyond 100 µM NTP concentration, substrate inhibition

occurred (Figure 6.1B). Hence, the DENV polymerase was able to elongate the correct base and did not misincorporate non-cognate nucleotide even at high concentration of NTP substrate. Self-complementary RNAs 12-7 and 12-12, which contains 12 paired sequences and either 7 or 12 nucleotides in the single-stranded template, produced an increase in polarization of 24 and 36.5 mP correspondingly at 2 hours after adding all four nucleotides. The change in FP signal for these two substrates were weaker than T18/P8. Nevertheless, completely elongated RNA products were observed on PAGE gel, alongside with higher amount of partially extended products. This finding suggests that the elongation reaction was stalled halfway, thus may account for the lower FP signal detected. Additional elongation experiment performed in the presence of higher $MnCl_2$ concentration at 2.5 mM increased polarization of 12-12 RNA from 36.5 mP to 47 mP (results not shown). Hence, the use of buffer containing 2.5 mM $MnCl_2$ could be considered to assemble more elongation complex using less active RNA substrate.

Another two shorter RNA duplexes T12/P8 and T10/P6 exhibited a low change in FP value of 10.5 to 13.5 mP which could be explained by no or +2 nucleotides incorporation despite addition of the four NTPs. The reasons for the absence of elongation activity on T12/P8 as well as stalled elongation reaction for T10/P6 were unclear, although both RNAs could bind to NS5 RdRp with high affinity.

The idea of designing the dumbbell-type RNA used in this study was adopted from previous work which successfully crystallized the structures of poliovirus, coxsackievirus and rhinovirus ECs (93, 95). This RNA could establish coaxial stacking of upstream RNA duplexes with a flexible RNA-RNA junction. In our assays, this RNA gave the best K_d value of 19 nM and produced an FP gain of 10 mP after addition of CTP, UTP and GTP to elongate the strand by 5 bases. However, negative control (no NTP addition) also yielded an increase of FP by 10 mP, thus it was postulated that there was no nucleotide incorporation. As the fluorophore was

labelled on the template strand in this case, we could not monitor incorporation event by PAGE analysis.

Finally, a single-stranded 34-mer RNA that forms an intramolecular hairpin with a stem length of 6 bp was also employed in this study. This RNA was postulated to form a stable EC with DENV RdRp following the incorporation of +9 bases. However, PAGE gel revealed that the RNA was only extended by 2 nucleotides albeit elongation activity was rapid (about 25% of the RNA was elongated in 10 seconds). Additionally, FP signal was only mildly increased as opposed to a bigger change in FP value for the negative control.

Based on these results from both assays, we selected RNA constructs, T18/P8, 12-7, T12/P8 and T10/P6, which provided reasonable binding and elongation profiles for co-crystallization. RNA 12-7 was chosen instead of 12-12 because the length of the template was more alike to the best RNA substrate, T18/P8. The dumbbell-type RNA and 6-18 hairpin were eliminated from crystallization work since the FP signal of their negative control was unstable.

RNA	NS5	Binding affinity	Elongation activity			
		K_d (nM)	ΔmP at 1hr# or 2hr*	Nucleotides added	Expected nt incorporated	Actual nt incorporated
T18/P8	DENV-4	38	67*	4XNTPs	+10	+10
			0*	UTP	+1	+1
	DENV-3	41	75.5*	4XNTPs	+10	+10
	DENV-2	50	N.D.	-	-	-
12-7	DENV-3	35	24*	4XNTPs	+7	+7
12-12	DENV-3	38	36.5*	4XNTPs	+12	+12
T12/P8	DENV-3	48	10.5#	4XNTPs	+4	0
T10/P6	DENV-3	38	13.5#	4XNTPs	+4	+2
Dumbbell-type RNA	DENV-4	19	10*	CTP, UTP, GTP	+5	N.D.
6-18 hairpin	DENV-4	28	15*	CTP, UTP	+9	+2

Table 6.2 Binding and elongation activities of DENV FL NS5 using different RNA substrates. DENV-2, -3, or -4 FL NS5 proteins were tested with various RNA constructs in binding and elongation experiments using fluorescence polarization (FP). RNA dissociation constants (K_d) were determined by curve fitting the data to a single-site binding isotherm using GraphPad Prism software. Change in polarization (ΔmP) was calculated by deducting average FP signals obtained at 0 hour from average FP signals detected at 1 or 2 hour after addition of nucleotides to initiate elongation. Elongation reaction was also run on Urea-PAGE gel to visualize nucleotide incorporation. N.D. denotes not determined.

Steady-state kinetic parameters			
Constant	**Divalent ion**	**DENV-4 NS5**	**DENV-4 NS5-Pol**
K_m UTP (μM)	Mn2+	6.63±2.29	4.64±2.68

K_m ATP (μM)	Mn2+	N.D.	3.61±0.99
K_m CTP (μM)	Mn2+	N.D.	3.68±1.29
K_m GTP (μM)	Mn2+	N.D.	4.46±1.06
k_{cat} UTP (min^{-1})	Mn2+	0.0032±0.0006	0.0022±0.0004
k_{cat} ATP (min^{-1})	Mn2+	N.D.	0.0017±0.0002
k_{cat} CTP (min^{-1})	Mn2+	N.D.	0.0020±0.0005
k_{cat} GTP (min^{-1})	Mn2+	N.D.	0.0017±0.0000

Table 6.3 Kinetic constants of DENV-4 NS5 FL and RdRp (aa266-900) elongation complexes. Single nucleotide incorporation assay was performed and the product RNA was monitored on Urea-PAGE gel. Amount of incorporation was calculated based on band intensity and plotted against varying concentrations of NTP substrate. Michaelis-menten constant K_m and k_{cat} values were obtained using Graphpad Prism software. Results shown in the table are the average values obtained for each protein from two independent experiments. N.D. denotes not determined.

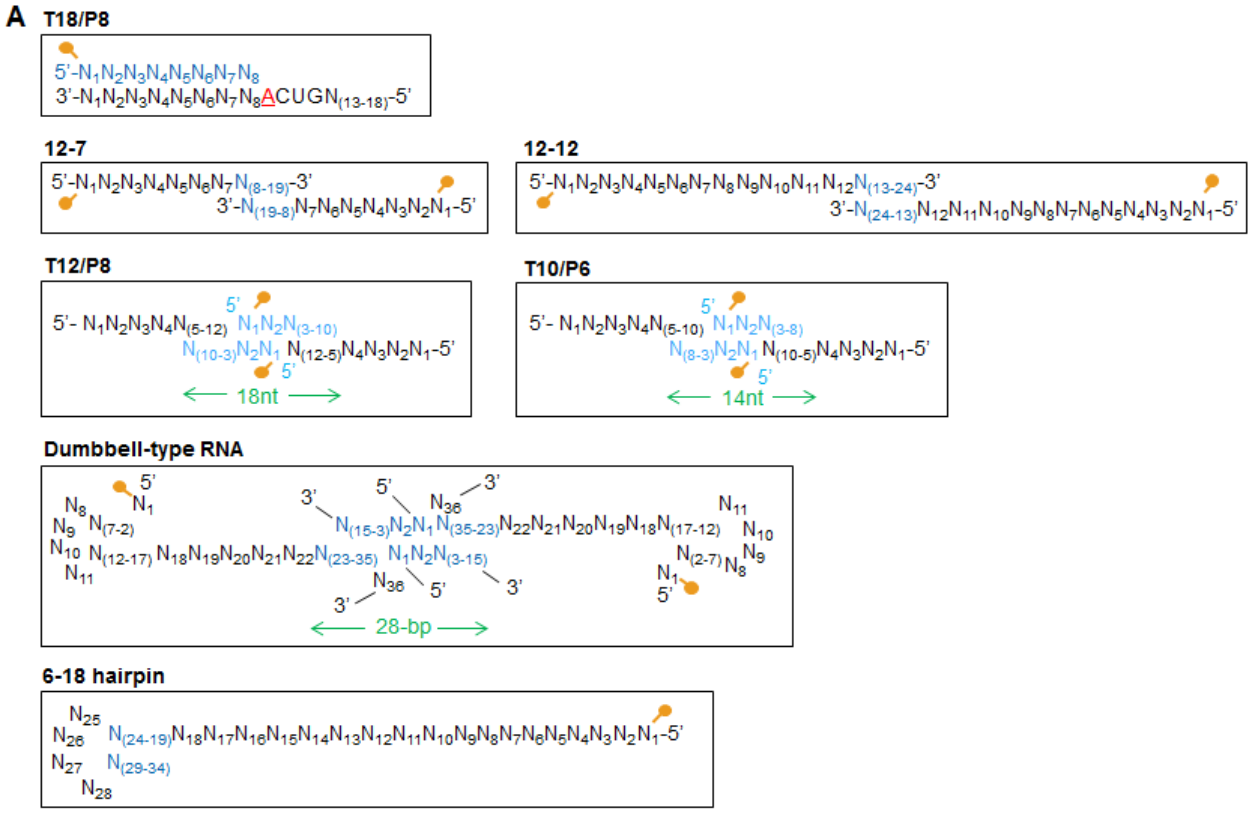

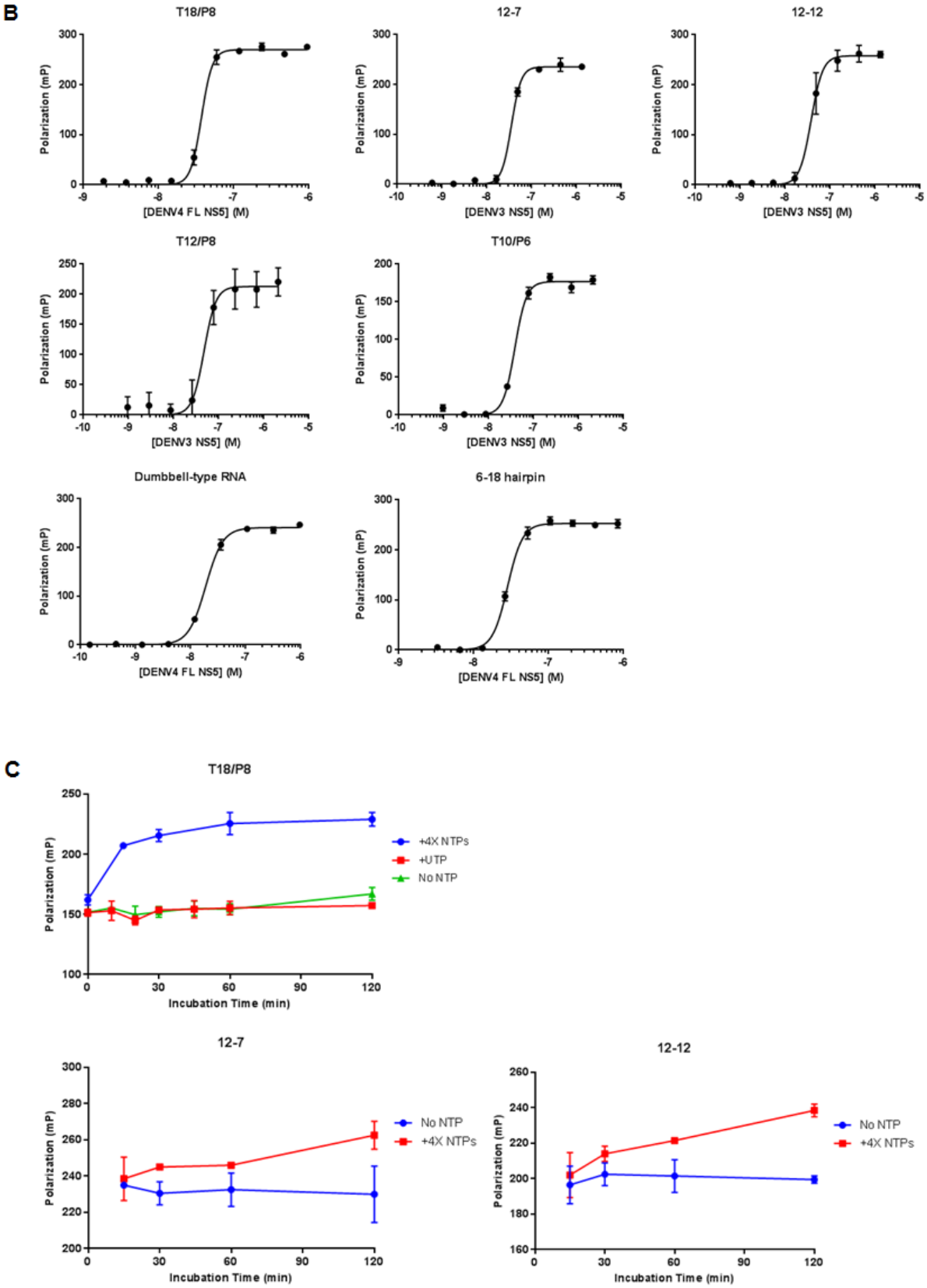
B
T18/P8
12-7
12-12
T12/P8
T10/P6
Dumbbell-type RNA
6-18 hairpin
Polarization (mP)
[DENV4 FL NS5] (M)
[DENV3 NS5] (M)
C
T18/P8
+4X NTPs
+UTP
No NTP
Incubation Time (min)
12-7
12-12
No NTP
+4X NTPs

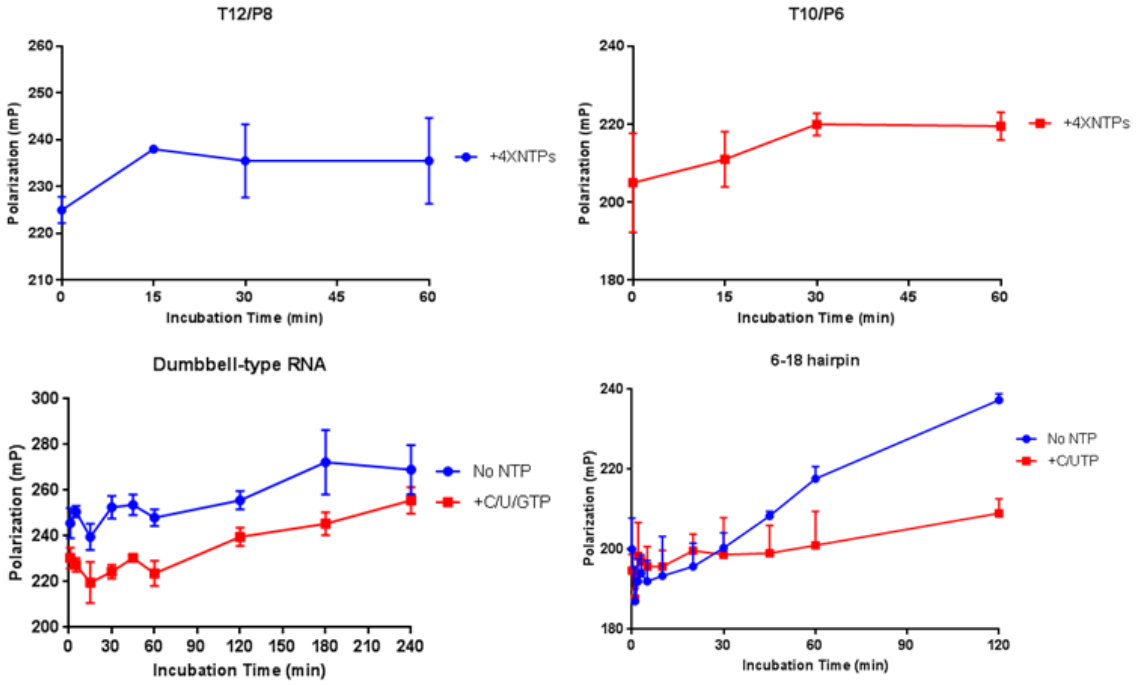
T12/P8
Polarization (mP)
Incubation Time (min)
+4XNTPs
T10/P6
Polarization (mP)
Incubation Time (min)
+4XNTPs
Dumbbell-type RNA
Polarization (mP)
Incubation Time (min)
No NTP
+C/U/GTP
6-18 hairpin
Polarization (mP)
Incubation Time (min)
No NTP
+C/UTP

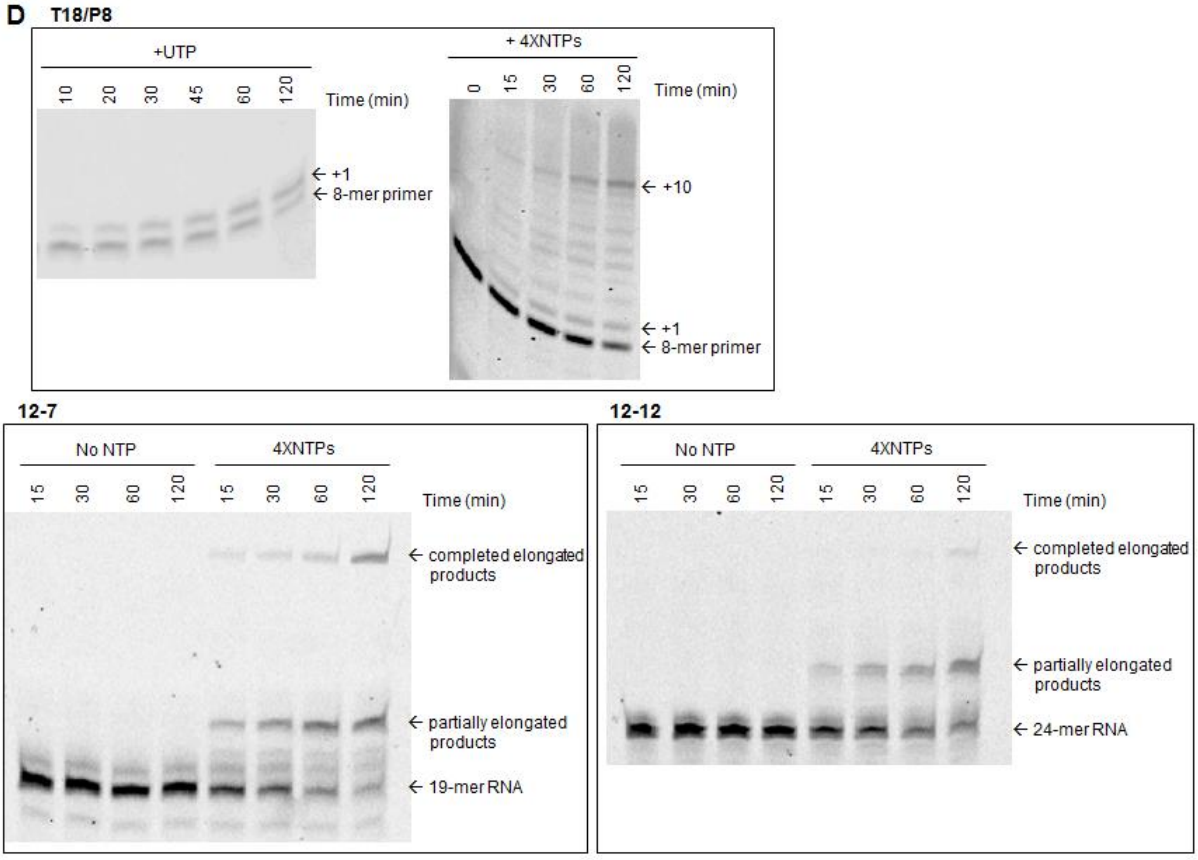
D
T18/P8
+UTP
Time (min)
← +1
← 8-mer primer
+ 4XNTPs
Time (min)
← +10
← +1
← 8-mer primer
12-7
No NTP
4XNTPs
Time (min)
← completed elongated products
← partially elongated products
← 19-mer RNA
12-12
No NTP
4XNTPs
Time (min)
← completed elongated products
← partially elongated products
← 24-mer RNA

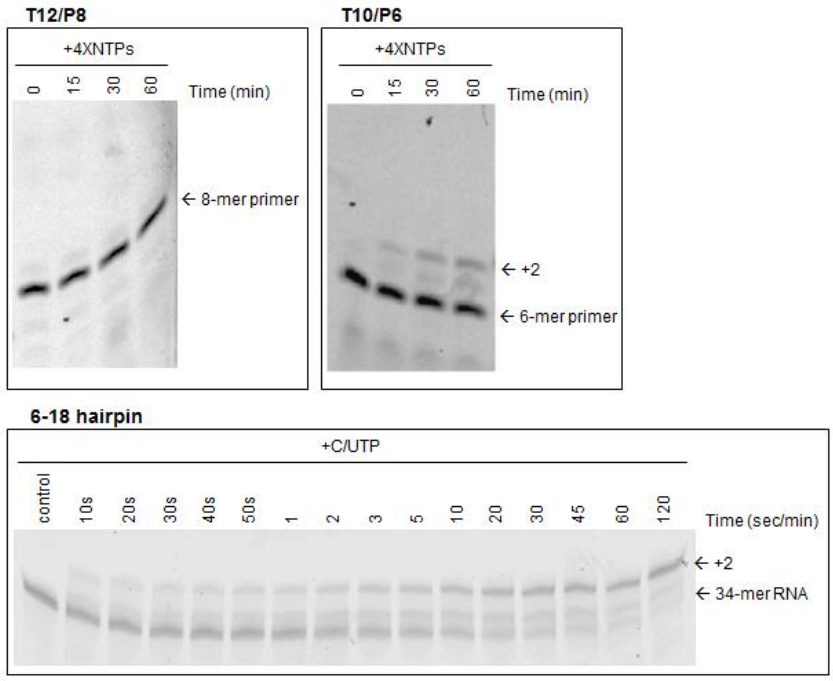

Figure 6.6 Binding and elongation activities of DENV FL NS5 using different RNA substrates. (A) RNA-primed substrates are labelled with 6-FAM (orange ball) at the 5' end of either primer or template strand to determine binding and elongation activities using fluorescence polarization (FP). (B) Binding assay was performed by varying the concentration of DENV FL NS5 protein and fixing the concentration of RNA substrate. RNA dissociation constants (K_d) were determined by curve fitting the data to a single-site binding isotherm using GraphPad Prism software. (C) Time-course measurement of FP signals after addition of nucleotide(s) to the polymerase-RNA complex for elongation. (D) Elongation reaction was run on 23% Urea-PAGE gel to monitor nucleotide incorporation.

3.4.4 Crystallization attempts of DENV polymerase-RNA and elongation complexes

Before assembling an elongation complex for crystallization, we started off with screening DENV polymerase-RNA complex (without NTP addition) for crystal formation. Briefly, DENV-3 FL NS5 and pre-annealed RNA (T18/P8, T12/P8, T10/P6 and 12-7) were incubated at 1:1.5 molar ratio on ice for 15 min. The assembled NS5-RNA complexes (each with different RNA substrate) formed mild precipitation despite the low incubation temperature and were clarified by centrifugation before purification by size exclusion chromatography to remove excess RNA (Figure 6.7). The purified complexes were subsequently screened using commercial crystallization kits.

A few positive hits were identified in three different crystallization buffer conditions. Crystals were detected in drops containing DENV3 NS5 apo protein, NS5-T18/P8, NS5-T12/P8, NS5-T10/P6 and NS5-12-7 complexes (Figure 6.8A-C). In order to reproduce the crystals,

polymerase-RNA complexes were assembled in the same way as before. In addition, elongation complexes were also formed by adding NTPs (3'dCTP or C/GTP) to elongate the RNA by +1 or +2 bases for 1 hour at RT. Precipitation occurred during the assembly of these complexes and were removed by centrifugation. The supernatants were used directly for crystallization set up without column purification. Similarly, condition A2 enabled crystal formation in drops containing DENV3 NS5-T12/P8 and NS5-T10/P6 as well as their corresponding elongation complexes (Figure 6.9A). Vast amount of small crystals was formed in the presence of RNA and NTPs, but no apo crystal was observed. Interestingly, condition D8 did not reproduce crystal in the drop consisting of DENV3-T18/P8 and instead generated crystals in drops containing DENV3-T12/P8 and its elongated counterpart (Figure 6.9B). These crystals were thin and clustered together, and no crystal for apo protein was detected. Overall, all the crystals grew quite rapidly within 2 to 3 days after crystallization set up. The crystals generated from initial screening as well as those reproduced were sent for data collection, but either they did not diffract or no RNA was found in the structure. The failure to obtain a crystal structure with RNA bound to the enzyme could be attributed to instability of the complex whereby RNA gets dissociated from the polymerase during incubation, or the precipitation of the complex that was removed prior to purification or crystallization set up.

A) Chromatogram of purified DENV3 NS5-T12/P8 complex

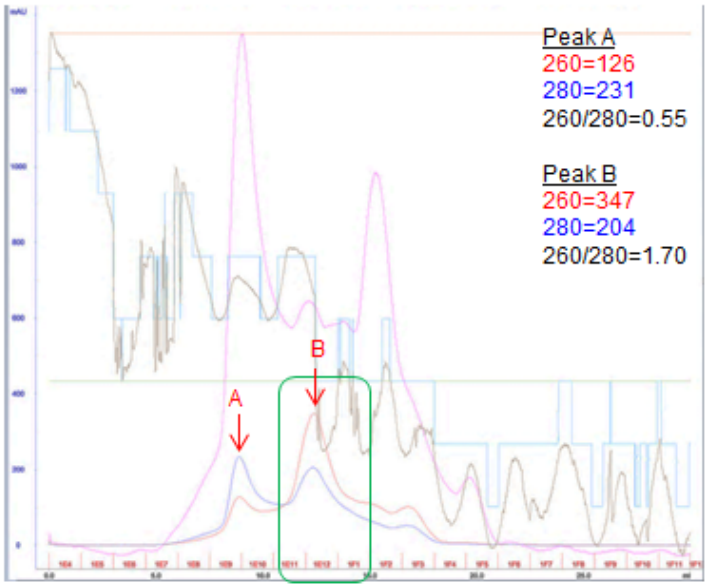

B) OD measurement

Fraction	OD	260/280
E9	0.096mg/ml	0.89
E10	0.244mg/ml	0.82
E11	0.172mg/ml	1.27
E12	0.261mg/ml	1.80
F1	0.140mg/ml	1.63
F2	0.080mg/ml	2.00
F3	0.090mg/ml	1.80

- Fractions E11 to F1 were pooled and concentrated.
- The final concentration was 5.496mg/ml at 260/280 ratio of 1.47 with a volume of 110µl.
- The entire sample was used for screening.

C) OD profile of concentrated fractions

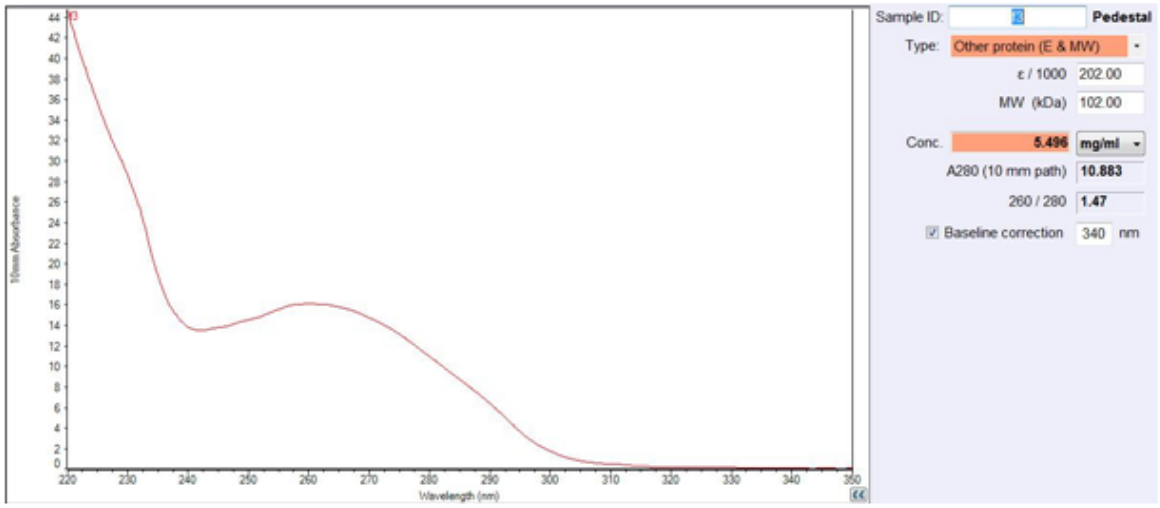

Figure 6.7 Chromatogram and OD profile of DENV-3 NS5-T12/P8 complex. Polymerase-RNA complex was formed using DENV-3 FL NS5 and T12/P8 RNA incubated on ice for 15 min. This complex was purified using Superdex 200 10/300 gel filtration column and the chromatogram was shown in (A). Two peaks were generated and measured for their absorbance at 260 and 280 nm. Peak A likely represented protein only since 260/280 ratio is 0.55. Peak B has a 260/280 ratio of 1.70 and likely consisted of both protein and RNA. (B) Fractions E9 to F3 were further measured spectrophotometrically and fractions E11 to F1 with 260/280 nm ratio between 1.20 and 1.70 were pooled and concentrated before being used for crystallization screening. The final OD for concentrated fractions was measured and shown in (C). Complexes formed using other RNA duplexes (T18/P8, T10/P6 and 12-7) had the same chromatogram and OD profile as presented here.

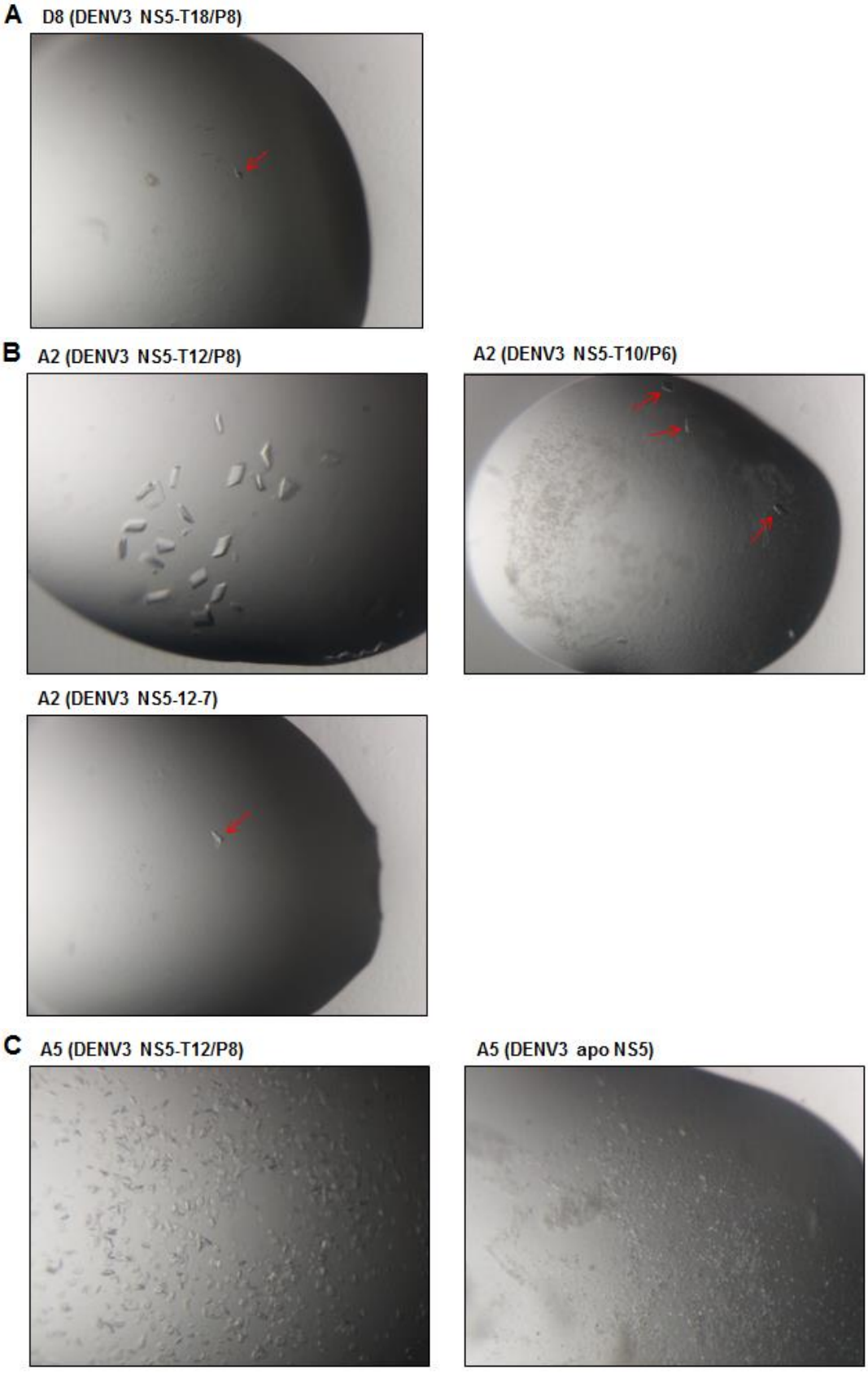

Figure 6.8 Crystals obtained from screening of DENV-3 NS5-RNA complexes. (A) Condition D8 produced crystals in the drop consisting of DENV3 NS5-T18/P8 complex (red arrow). (B) Condition A2 yielded crystals in drops containing DENV3 NS5-T12/P8, NS5-T10/P6 (red arrows) and NS5-12-7 (red arrows). (C) Condition A5 generated crystals in drops consisting of DENV3 NS5-T12/P8 and apo NS5.

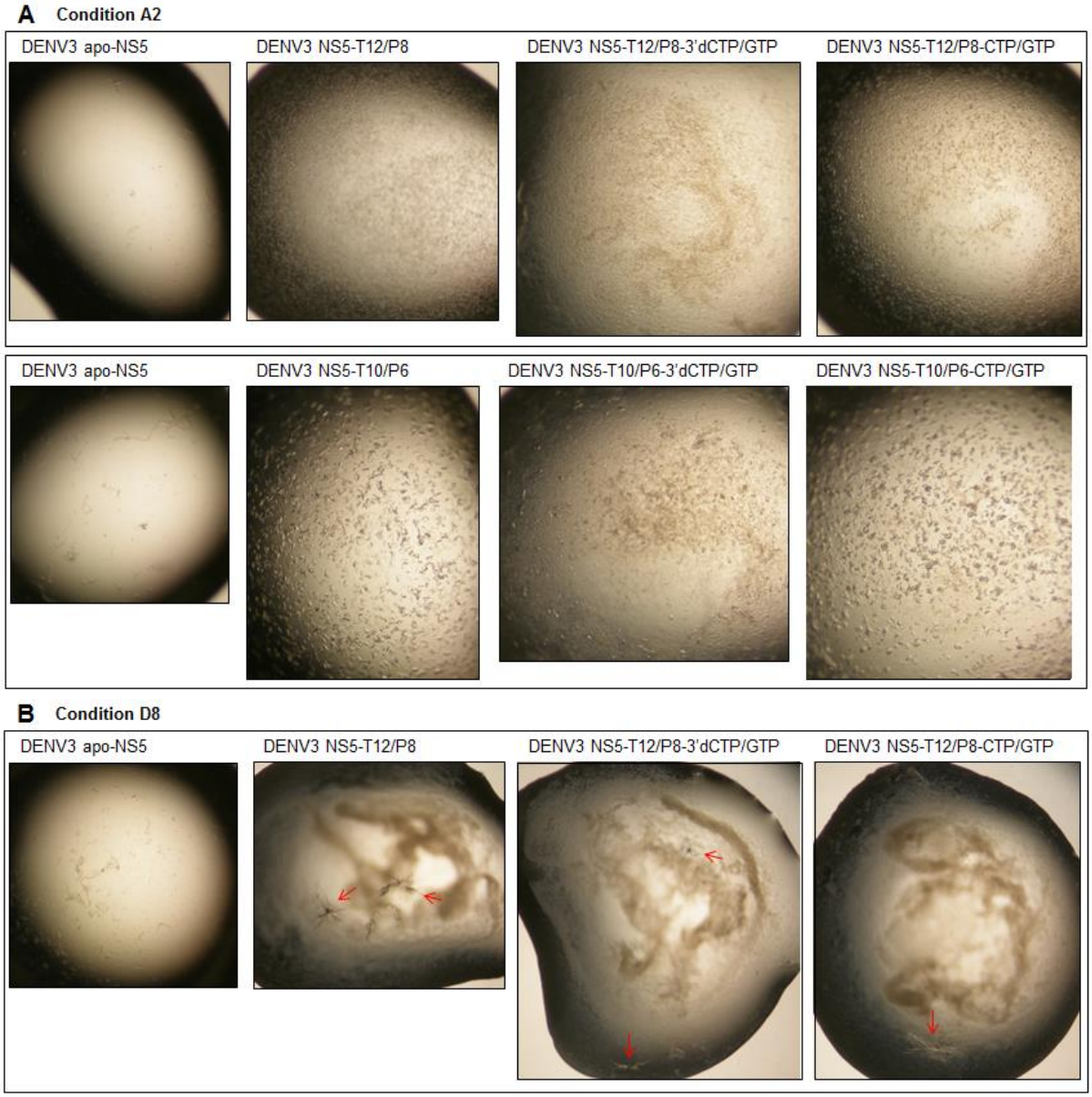

Figure 6.9 Crystals obtained in drops consisting of DENV-3 NS5-RNA and elongation complexes. (A) Condition A2 allowed crystals growth in drops containing DENV3 NS5-T12/P8, NS5-T10/P6 as well as their corresponding elongation complexes. (B) Condition D8 produced crystals (red arrows) in drops containing DENV3-T12/P8 and its elongated counterpart. No apo-crystal formation was observed.

Further optimization of DENV NS5-RNA complex assembly and elongation was performed to attain a stable complex. Both DENV-3 and DENV-4 NS5 were incubated with T18/P8 and T10/P6. After assembly, the protein-RNA complexes were either not elongated and used for screening directly after removal of the precipitants, or added with nucleotides (U/G/A/3'dCTP or G/CTP) to extend the RNA chain by +4 or +2 bases for T18/P8 and T10/P6 respectively. The elongation reactions were allowed to proceed overnight at RT and clarified, followed by screening with commercial crystallization kits.

Spherulite formation was detected in fourteen buffer conditions and they appeared early after one day of incubation (Figure 6.10A; Table 6.4). Only the drop containing NS5-T18/P8 complex did not produce spherulites, drops consisting of NS5-T10/P6 with or without elongation as well as elongated NS5-T18/P8 yielded spherulites. Another condition, F3, was also observed to generate clusters of protein crystals in the drop containing nonelongated NS5-T10/P6 (Figure 6.10B; Table 6.4). All these positive hits were confirmed to be protein and not salt as they glowed brightly when the drops were illuminated with ultraviolet (UV) light. Two of these crystallization conditions, C11 and F3, were selected for optimization by either varying the pH or precipitant concentrations in the buffer, conducting additive screening, or seeding for the spherulites. However, there was no improvement from spherulite to crystal formation. Further attempt to purify the elongation complex using ion exchange chromatography prior to crystallization set up using positive conditions as shown in Table 6.4 was unsuccessful in producing any crystal.

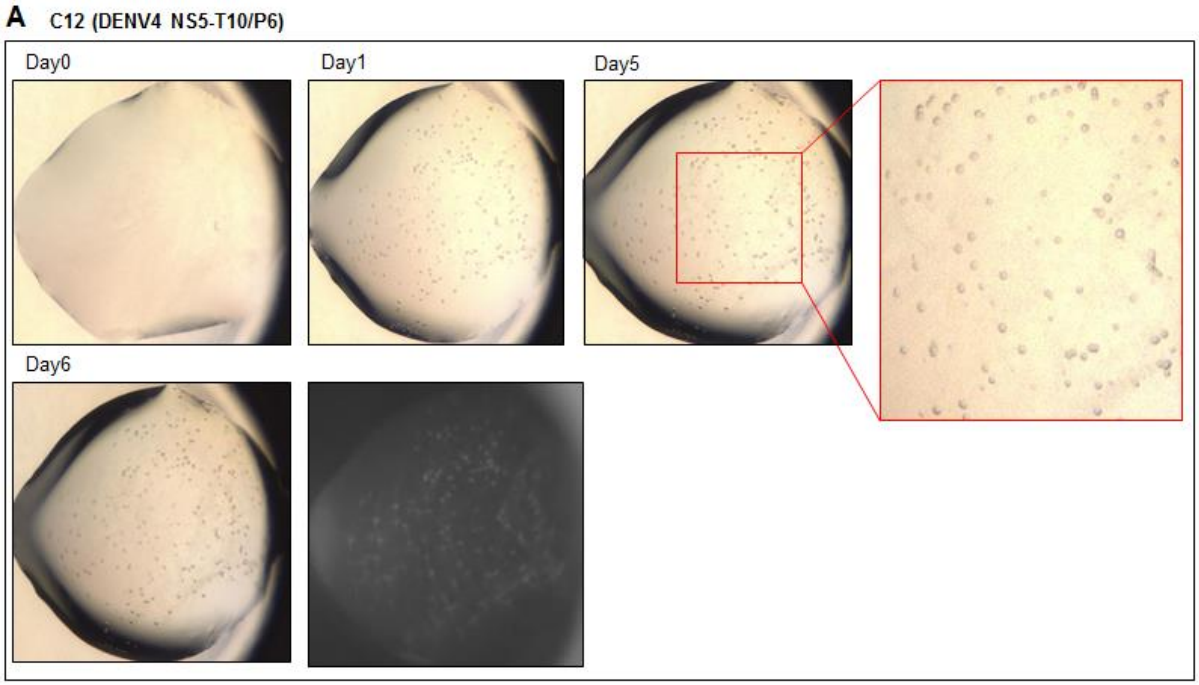

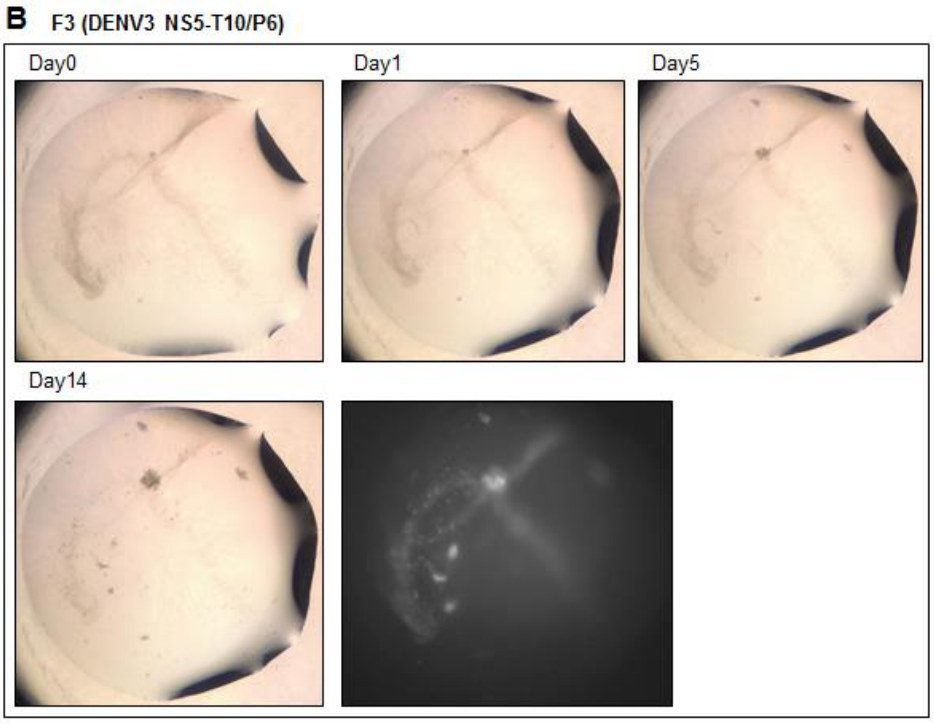

Figure 6.10 Spherulite/crystal obtained from screening of DENV NS5-RNA and elongation complexes. (A) Condition C12 produced spherulites in the drop consisting of DENV4 NS5-T10/P6 after one day of incubation. Images were taken at day 0, 1, 5 and 6, and the image at day 5 was enlarged (red box). The drop at day 6 was illuminated with UV light and the spherulites glowed, indicating that they were proteins. Another thirteen buffer conditions also allowed spherulite growth in drops containing elongated NS5-T10/P6 and NS5-T18/P8 that were similar as shown in this diagram. (B) Condition F3 produced clusters of crystals in the drop consisting of DENV3-T10/P6 which was evident at day 5 of incubation. Images were taken at day 0, 1, 5 and 14, and the drop at day 14 was illuminated with UV light revealing protein crystals that shone brightly.

Buffer condition	Spherulite/crystal	Polymerase-RNA complex	Elongated complex
C3	Spherulite		DENV4 NS5-T18/P8-U/G/A/3'dCTP
C5	Spherulite	DENV4 NS5-T10/P6	
C6	Spherulite	DENV3/4 NS5-T10/P6	
C7	Spherulite	DENV3/4 NS5-T10/P6	
C8	Spherulite	DENV4 NS5-T10/P6	
C9	Spherulite	DENV3/4 NS5-T10/P6	DENV3/4 NS5-T18/P8-U/G/A/3'dCTP
C10	Spherulite	DENV3/4 NS5-T10/P6	DENV4 NS5-T18/P8-U/G/A/3'dCTP
C11	Spherulite	DENV3/4 NS5-T10/P6	DENV4 NS5-T10/P6-C/GTP
			DENV3/4 NS5-T18/P8-U/G/A/3'dCTP
C12	Spherulite	DENV4 NS5-T10/P6	DENV4 NS5-T10/P6-C/GTP
			DENV3/4 NS5-T18/P8-U/G/A/3'dCTP
F3	Crystal cluster	DENV3 NS5-T10/P6	
F4	Spherulite		DENV4 NS5-T10/P6-C/GTP
			DENV4 NS5-T18/P8-U/G/A/3'dCTP
D1	Spherulite		DENV4 NS5-T10/P6-C/GTP
F9	Spherulite	DENV4 NS5-T10/P6	
F11	Spherulite	DENV4 NS5-T10/P6	

F5	Spherulite	DENV4 NS5-T18/P8-U/G/A/3'dCTP

Table 6.4 Crystallization buffer conditions that resulted in spherulite/crystal formation. Fourteen crystallization conditions produced spherulites while one condition generated clusters of protein crystals.

3.4.5 Discussion

Dissection of the interactions between NS5 RdRp and viral RNA would be informative to elucidate how the RNA is recognized and replicated, and possibly facilitate drug discovery and design targeting the RdRp. Our approach to obtain a crystal structure of DENV polymerase-RNA complex was inspired by the recent crystal structures of stalled elongation complex (EC) of several positive-strand RNA viruses (93, 95). In their experiment, polymerase-RNA complex was first assembled and then subjected to multiple rounds of nucleotide incorporation to form a stable elongation complex. The complex was subsequently purified for crystallization to capture catalytically relevant elongation states with associated structural changes that occur during polymerase catalytic cycle.

In our study, we successfully assembled functional elongation complexes of DENV NS5 using several short template/primers. These elongation complexes were formed by addition of natural nucleotides to extend the RNA chain and could be monitored using polyacrylamide gel and fluorescence polarization (FP). The novel FP-based assay was developed to examine both RNA binding and elongation activities of DENV polymerase and was reliant on increase in FP signal when the FAM-conjugated RNA was immobilized upon binding to the enzyme as well as further molecular weight increase resulting from nucleotide incorporation. Using this FP-based assay, distinct RNA substrates were profiled for their suitability for co-crystallization. The RNA constructs exhibited different features such as they can self-annealed to generate hairpin structure, contain complementary sequences at one end for forming RNA duplex, or their primer and template strands could base pair to form duplex or unique dumbbell orientation (Figure 6.6A). Amongst the seven substrates tested, four of them (T18/P8, 12-7, T12/P8 and T10/P6) displayed reasonably good binding ($K_d \leq 50$nM; Figure 6.6B, Table 6.2) and elongation

profiles (Figure 6.6C-D, Table 6.2) and were chosen for crystallization work. Assembly and elongation of the polymerase-RNA complex was carried out in an optimized binding buffer derived from the FP assay. The NS5-RNA and elongation complexes were either purified by size-exclusion chromatography or ion exchange chromatography first, or used directly for screening. Numerous crystallization buffer conditions allowed the growth of reproducible protein crystals and spherulites. However, optimization using seeding and additives did not yield any improvements from spherulite to crystal formation. Additionally, crystals sent for data collection failed to diffract or capture RNA in the structure. During the assembly and elongation of the polymerase-RNA complexes, it was noticed that precipitation occurred even after the binding reaction was incubated on ice. Precipitant was formed either immediately upon binding of RNA to NS5 protein, or after incubation of the complex at RT for a period of time. It could be possible that the precipitant consists of active elongation complex which was always removed prior to crystallization set up, whilst the supernatant comprises of lesser amount of complex or only apo-protein which may answer for the lack of RNA in our crystal structure (not shown). Previous studies have reported that the precipitated complex could be solubilized using higher concentration of salt (350), as well as provided evidence that elongation complexes were more stable in 300 mM NaCl than in 75 mM NaCl and that higher salt concentration stabilizes RNA secondary structures (360). The stability of the complex may be caused by proper structural rearrangements of NS5 for catalysis, which would be favored at higher salt concentration. Thus, future attempts to obtain soluble and stable elongation complex could be carried out by first maintaining the concentration of NaCl at below 75 mM for efficient elongation reaction (Figure 6.2C), followed by re-solubilizing the precipitated complex in higher salt concentration. The soluble protein content could be checked using EMSA, and also be tested for their stability and activity before crystallization by adding nucleotides to the

solubilized complex and monitoring for the production of longer elongated RNA by PAGE analysis.

The RNA construct in our study that gave the biggest change in polarization signal and best incorporation efficiency was T18/P8 duplex (Figure 6.6 and Table 6.2). On the other hand, the dumbbell-type RNA demonstrated better binding affinity to NS5 protein as compared to T18/P8 at a K_d value of 19 nM, but was unsuitable for nucleotide incorporation. Nevertheless, the use of this RNA construct as a substrate for polymerase elongation was validated based on earlier successful EC structures (93, 95). In their structures, two polymerase molecules could dock onto each end of the RNA helix facing away from each other and form a "dumbbell" orientation important for establishing crystal contacts. Moreover, the RNA-RNA junctions confer plasticity enabling proteins to form long-range crystal lattice through additional protein-protein interactions. The failure in establishing functional elongation complex for our dumbbell-type RNA could be attributed to an unfavourable primer/template length combination. Future studies could include optimizing the length of the construct for stable elongation complex and crystal formation, as well as labelling the probe on the 5' end of the primer strand for PAGE analysis.

Covalent trapping strategy was successful in the crystallization of a catalytically relevant human immunodeficiency virus-type 1 (HIV-1) reverse transcriptase (RT) in complex with template/primer and dNTP (361, 362). Disulfide cross-linking reaction was carried out to covalently link RT and the RNA/DNA heteroduplex, and the complex was subsequently purified using ion exchange chromatography and added with dNTP. One advantage of this approach is the ability to select a single homogenous species for crystallization, unlike our elongation reaction which produced a heterogeneous mixture of complexes. Hence, this strategy could be employed to obtain a crystal structure of the ternary catalytic polymerase complex of DENV.

Furthermore, the elongation complex could be used to evaluate the effectiveness of nucleotide analog incorporation and chain termination (350, 363, 364), providing an understanding into the mechanism of action of NTP analogs against DENV polymerase. Additionally, the complex could allow determination of the replication fidelity of mutant polymerases. Previous biochemical characterization of Coxsackievirus and Poliovirus polymerases revealed that the replication fidelity and elongation rates are closely associated, albeit independently modulated by distinct subdomains of the polymerase (365). Similar study could be conducted using DENV mutant polymerases (such as those mentioned in earlier sections) to map the protein structure-function relationships responsible for regulating nucleotide selectivity and elongation rate.

3.5 Summary

The resolution of the first crystal structure of DENV-3 FL NS5 enables an understanding of the versatile functions of NS5 in its natural form and the cross-talk between the two domains during viral replication (318). In the DENV-3 NS5, the MTase domain resides on top of the fingers subdomain and attaches to the back of the RdRp domain without blocking the entry sites for NTPs and RNA template (Figure 3.1). Comparison of this structure to the crystal structure of JEV FL NS5 (101) shows that even though there is a conservation in the folding of the domains, the MTase is rotated at 105° relative to RdRp resulting in the formation of two distinct inter-domain interfaces. The interface of DENV-3 NS5 is highly polar with numerous electrostatic interactions established by residues from both domains and the linker region. On the other hand, JEV NS5 forms a hydrophobic interface involving residues from the MTase and RdRp fingers domains. Mutagenesis and reverse genetic experiments performed in our study demonstrated the functional significance of inter-domain interactions within the DENV NS5 in which disruption of critical contacts such as salt bridge linkage and hydrogen bonding led to viral replication impairment. Since both interfaces are highly conserved in flaviviruses, it is possible that the two unique sets of NS5 conformations are shared among the various viruses in the same genus and that the conformational changes are mediated by the flexible linker between the two domains. During virus replication, NS5 protein may adopt a range of relative orientations upon recruitment and binding to viral RNA, NS3 and other viral and host partners. This was supported by an earlier SAXS analysis which showed that the full length NS5 from DENV-3 could assume multiple conformations in solution, from compact to more extended forms (254). In the crystal structure of DENV-3 NS5, a well-ordered linker region (residues 263-272) between the MTase and RdRp domains was fully resolved for the first time. The linker comprises a short 3_{10}-helix (residues 263-266) which probably acts as a swivel, making structural transition to confer conformational flexibility of NS5 to perform its

enzymatic functions and for interaction with viral and host proteins. Given the sequence heterogenicity of the linker residues across flaviviruses (Figure 3.6) despite a conservation in the length of the linker region, we probed the relevance of their unique amino acid composition in our linker swapping experiment using DENV-2 subgenomic replicon system. The order of replicative abilities as compared to DENV-2 is as follows: DENV-2≥DENV-4>DENV-1≈DENV-3>JEV≈ZIKV, which is in line with their linker sequence identity to DENV-2 (Figure 3.8). Replicons with the linker of JEV or ZIKV exhibited the same replication profile, which may possibly be explained by the recent crystal structures of ZIKV FL NS5 protein displaying similar orientations of the MTase and RdRp domains to that seen in the structure of JEV NS5 but distinctly different from DENV-3 NS5 (366, 367). Moreover, ZIKV NS5 formed a hydrophobic inter-domain interface involving almost the same residues as JEV NS5. Additionally, the new ZIKV NS5 structures revealed a continuous electron density in the linker region that is not visible in the JEV NS5 structure. Similar to DENV-3 NS5, the ZIKV NS5 linker residues interact with residues in the RdRp fingers subdomain, albeit it does not fold into a 3_{10}-helix like DENV-3 NS5. CFSSP (Chou & Fasman Secondary Structure Prediction Server) online tool predicted that the ZIKV linker sequence has higher preference for α-helix formation (Figure 3.6) and was not accurate in this case. Overall, these findings suggested that the diverse amino acid composition of the linker controls the formation of discrete stable molecular conformations in a serotype/virus-specific manner, and flaviviruses adopt different mechanisms and establish different interfaces at distinct steps of viral genome replication. Although it remains unclear on which molecular conformation(s) participate in the different stage(s) of the virus replication cycle, the flexibility and dynamics of the NS5 protein could be influenced by the interactions between NS5 and other viral and cellular components within the replication complex. This notion likely accounts for the discrepant results between *in vitro* biochemical assay and virus fitness in cells observed for some of the interface mutants (e.g.

R362A) in which enhanced polymerase activity of NS5 *in vitro* did not result in similar increase in viral replication and even abolished virus production in cells (Table 3.1, Figure 3.3 and 3.4). In *in vitro* assay, NS5 exists free in solution without the presence of other viral or host components and could be dynamic in binding to RNA and NTP substrates for carrying out its enzymatic activities. Assembly of the replication machinery in cells encompasses numerous protein-protein interactions resulting in embedment of NS5 within the complex and probably an alteration in the dynamic properties of NS5. In this ensemble, discrete stable orientations of NS5 may form through intra- and inter-molecular interactions during different steps of viral replication. It is possible that introducing mutation at the interface of NS5 could still allow the dynamic protein to assume functional conformation(s) for catalysis in *in vitro* assay. However, since the protein may behave differently between *in vitro* and in cells due to additional components involved within the replication complex, the mutation may induce conformational changes and alter the flexibility of NS5 that affect the formation of competent viral replication complex with viral and host cofactors, thereby leading to the lethal phenotype observed. Otherwise, the mutant could impact the ability of NS5 to bind to host proteins for other non-enzymatic functions such as nuclear-cytoplasmic trafficking. The importance of NS5-related molecular interactions for viral pathogenesis during infection was demonstrated previously whereby the failure to assemble replication complex through a loss of NS1 protein expression, absence of geranylgeranylated host protein or reducing expression of a cellular vesicle membrane transport protein, hVAP-33, affected viral replication (368-370). Furthermore, disruption of the interaction between NS5 and exportin CRM1 or inhibiting importin α/β-mediated nuclear import through Ivermectin impacted chemokine interleukin-8 and virus productions (371, 372). Another possible reason that could explain the discrepancy is that the increased polymerase activities of the interface mutants (e.g. R353A) may promote the production of incomplete genomes, truncated viral RNA fragments or catastrophic mutations

that abolish reinfection. Taken together, our study highlighted the significance of the flexible linker in modulating cross-talk between MTase and RdRp domains to synergize their respective functions in RNA capping and synthesis as well as in orientating the relative domains for protein-protein interactions at different phases of viral replication. Compounds that target the linker or inter-domain interactions of NS5 are promising as potential inhibitors for antiviral intervention.

Over the years, there have been extensive efforts made to identify or design inhibitors targeting both the capping and polymerase activities of NS5 through the use of a variety of techniques including enzyme inhibition assay, cell-based assay, virtual screening and structure-based design (240, 242, 243, 278-280, 295, 306-308, 373, 374). The MTase domain catalyzes methylation of the RNA cap for virus replication and represents an important drug target. Various compounds binding to either the GTP-binding or SAM-binding pocket of MTase exhibited good IC_{50} values in the micromolar or nanomolar range to inhibit N7 and 2'-*O* activities, but failed to achieve antiviral activity in cell culture (240, 275, 276). Those that impacted virus growth demonstrated micromolar EC_{50} values, however they displayed cytotoxicity (375, 376). Thus, to design specific and potent inhibitor targeting the catalytic site of NS5, it would be useful to have a crystal structure of NS5 bound to viral RNA to understand specific RNA recognition. Following the structure determination of DENV-3 FL NS5, the crystal structure of a ternary complex between DENV-3 NS5 protein, an authentic cap-0-viral RNA substrate, and SAH was determined (331). This structure represents a catalytically-competent complex for methylation in which it captures for the first time the viral enzyme in the act of transferring a methyl group to the 2'-*O* ribose of the first nucleotide (adenosine) of the viral genome. The RNA ligand binds to an extended basic cleft and establishes numerous interactions with residues projecting from the MTase surface that account for the sequence specificity observed for NS5 on its substrate (Figure 4.1). The m7G moiety stacks with the

phenyl ring of residue F25 and the triphosphate linkage is coordinated by a bound magnesium in addition to side chain contacts. Interestingly, m7G docks into the same pocket as GMP prior to guanylyl transfer to ppRNA (143, 235) and the adenosine binds adjacent to the SAH product in a position that is consistent with its methylation. Specific recognition of the 5' end of the genome is attributed to the tight shape complementarity with adenine only as well as specific hydrogen bonding between the second nucleotide (guanosine), MTase residue E111 and Mg^{2+} ion. Most of these contacts were explored by modeling and mutational analysis (Figure 4.3 and 4.4, Table 4.2 and 4.3) which strongly supported the structural observations. The specific viral RNA-NS5 interaction is in line with an earlier study which demonstrated strict conservation of $pppA_1G_2$ dinucleotide at the 5' end of the flaviviral genome (249). Moreover, substrate specificity differentiates flaviviral NS5 from related SAM-dependent RNA methyltransferases such as the vaccinia virus VP39 and the human mRNA cap-specific 2'-O-ribose MTase CMTr1 that displays close structural homology with DENV-3 NS5, in which both methylate RNA substrate in a sequence-independent manner (331, 377). Based on the functional relevance of the ternary structure, novel strategies for antiviral development targeting the unique SAM-RNA binding pocket could be proposed. It is possible to extend SAM or GTP analog towards the RNA binding pocket or to design inhibitor that disrupts viral RNA-MTase interactions in order to minimize off-target inhibition of host MTases. One successful example was the compound NSC306711 identified through virtual screening which showed high antiviral activity for flaviviral MTases with low cell-based cytotoxicity (281). The additional interactions of this larger compound with residues outside of the SAM-binding site could be a factor conferring for its high potency.

Besides the N-terminal MTase, the C-terminal of NS5 protein which harbors the RdRp domain for RNA polymerization is also a prime target to treat viral infection. This strategy was successful against hepatitis C virus (HCV) by targeting the homologous NS5B protein using

the effective uridine analog, sofosbuvir, which presented excellent safety, tolerability and pharmacokinetic profiles (378). A repurposing approach to develop potent anti-DENV therapeutics from HCV inhibitors with improved specificity and pharmacokinetic properties was futile due to toxicity and efficacy issues (352). The discovery of effective nucleotide-based drugs against DENV was hindered by the lack of molecular details regarding substrate recognition during replication. Hence, elucidating crystal structures of catalytically relevant initiation and elongation complexes would be useful in understanding the molecular mechanism of DENV RNA replication. In our study, we were successful in assembling functional elongation complexes using DENV NS5 and distinct RNA templates selected based on good binding affinity and elongation activity from FP-based assays (Table 6.2). However, crystallization attempts did not yield any binary or ternary complex. The main reason for the lack of success could be due to the absence to form and isolate sufficient productive complex amenable to crystallization, as evidenced by the occurrence of precipitation during assembly and elongation of the polymerase-RNA complexes. Several suggestions such as covalent trapping strategy and optimizing primer/template length combination were described in section 3.4.5 and could be considered in the future to improve the amount of active enzyme for ternary complex formation.

Since a crystal structure of DENV polymerase in complex with viral RNA has not been resolved to provide new insights for structure-based design of effective nucleoside inhibitors (NI), drug discovery efforts looking at another class of non-nucleoside inhibitors (NNI) targeting allosteric pockets instead of the active site of NS5 have been actively pursued in the past (306, 342). Based on computational analyses or UV cross-linking experiment, these inhibitors were proposed to either block the RNA template tunnel or bind at the junction of the finger and thumb subdomains of RdRp, but they were not further developed because of poor potency or cytotoxicity. Recently, the use of X-ray crystallography had identified two series of

compounds that bound at novel pockets of DENV RdRp. One class of the inhibitors bound at the thumb/palm interface near the enzyme active site (termed "N pocket"), whilst another interacted with the finger-thumb interconnecting loops, resulting in an ordered F1 motif. Mutagenesis studies of both allosteric pockets as well as inhibition characterization showed that the compounds potently inhibited polymerase activity by targeting the initiation step of RNA synthesis (Table 5.2 and 5.5, and (346)). During initiation, the active site of RdRp is encircled by contacts between the thumb and motifs of the RdRp fingers. The two motifs, F and G, are not visible in both DENV-3 RdRp and FL NS5 crystal structures (86, 318) and could participate in the initiation process through binding to SLA for promoter-dependent RNA replication (103) and regulating access of ssRNA substrate to the RNA tunnel (86), respectively. Upon elongation, NS5 protein undergoes conformation change through concerted movements of the priming loop and outward rotation of the fingers subdomains in order to provide more space in the RNA tunnel to accommodate additional phosphoryl transfer and translocation of nascent dsRNA, as seen in the crystal structures of stalled HCV NS5B ternary primed initiation and elongation complexes (311). Remarkedly, the N-pocket compounds interact with residues S710, R729 and R737 that were shown to be important for coordinating the triphosphate moiety of chain terminator 3'dGTP in the first crystal structure of DENV-3 RdRp-nucleoside analog complex (86), as well as residue H798 that is vital for ATP-specific priming (249). Given that the N-pocket inhibitors interact with many critical residues in the RdRp, it could be probable that compound binding may influence binding of incoming nucleotide at the active site or lock the protein in a closed conformation by preventing the retraction of priming loop from the active site for transition from initiation state to dsRNA elongation state. The mechanism of action for F1 motif inhibitors could be similar to N-pocket inhibitors in which the compounds interfere with conformation change, in this case the proper orientation of F1 motif necessary for SLA promoter-dependent *de novo* RNA synthesis. Although motif F is missing in the

DENV structures, crystal structures of JEV FL NS5 and RdRp in complex with GTP/ATP revealed an ordered motif F that adopt different conformations (101, 102). Motif F forms a beta-stranded substructure equivalent to that seen in the structures of HCV, bovine viral diarrhea virus (BVDV) and HIV-1 reverse transcriptase (RT). In the JEV FL NS5, the hydrophobic contact between residue F467 at the tip of motif F and residue P113 of MTase at the inter-domain interface stabilizes motif F in the observed conformation. Since DENV-3 NS5 structure showed that the MTase domain could assume various relative orientations with respect to the RdRp domain, it could be possible that motif F exhibits conformational flexibility and could be transiently stabilized in the observed JEV structure without NTP substrate binding. This postulation is corroborated by the absence of an ordered motif F in the DENV-3 NS5 structure. However, in the $RdRp_{GTP}$ and $RdRp_{ATP}$ structures, the beta-hairpin loop of motif F orientates in another way in which it points downwards and obstructs the NTP entry channel. In this orientation, it interacts with the triphosphate moiety of GTP via residues R460, K463, K471 and R474, implying its role in modulating NTP binding. Additional contacts between GTP and residues S799, W800 and S801 of the priming loop were also formed, suggesting stabilization of the nucleotide for initiation. Binding studies carried out by the group demonstrated that in the presence of Mn^{2+} ions necessary for initiation, RNA was able to bind to $RdRp_{GTP}$ complex. Based on their experimental and structural findings, it is possible to propose sequential steps to form an initiation complex starting with binding of incoming GTP to the polymerase, followed by entry of the template RNA in the presence of Mn^{2+} ions. Once RNA lies in the active site, the GTP nucleotide could undergo repositioning to base pair with the second nucleotide and dissociate itself from motif F. Motif F could then move to open the NTP entry channel and enable ATP to diffuse into the active site for assembly of a catalytically-competent initiation complex. The proposed mechanism would prevent unnecessary non-templated dinucleotide production, but this concept does not agree with the findings from

another group whereby they showed that DENV polymerase could synthesize cognate pppAG primer on erroneous templates or in the absence of any template when Mn^{2+} ion was used in order to ensure conservation of the correct ends of the genome (249). Thus, this inconsistency highlights the need to solve the structures of viral RdRp initiation complex and their catalytic cycle intermediates in order to inform structural changes that occur during *de novo* primer formation. In all, the functional significance of both F1 motif and N-pocket of DENV RdRp in regulating the *de novo* initiation process was confirmed and they provided basis to target these allosteric sites for structure-based drug design. Furthermore, the conserved N-pocket of DENV RdRp that is essentially shared by the ZIKV RdRp (379) suggests that these DENV-specific inhibitors could also impact the enzymatic activity of ZIKV NS5 and potentially be exploited to treat ZIKV infection.

Altogether, our functional and structural studies of DENV NS5 validated several conserved sites, namely the inter-domain interface, N-pocket and F1 motif, that could be targeted for potent drug design. Compounds could bind specifically to these allosteric regions and interfere with necessary conformation changes required for its enzymatic activities or for its interaction with RNA and other proteins. However, one disadvantage associated with these allosteric inhibitors could be the occurrence of resistant viruses, as was observed for N-pocket compounds (section 3.3.2.4). Thus, the catalytic sites of MTase and RdRp could be aimed since residues at the active site are evolutionarily conserved and could possibly impart a higher barrier for resistance emergence. The relevance of SAM-RNA interactions in the first ternary catalytic MTase complex of DENV proposes new strategies to target this site for structure-based antiviral development. However, as host cell also contains similar SAM-binding pocket which could result in off-target inhibition, it would be safer to design specific nucleoside inhibitors targeting the RdRp which does not have any equivalent in the human host cell. Drug discovery of effective nucleoside inhibitors would be accelerated by the presence of a

catalytically relevant complex which uncovers structural and functional information about the RdRp catalytic cycle.

4 CONCLUSION

The elucidation of the first crystal structure of the full-length NS5 from DENV-3 provides new insights into understanding the versatile and multi-functional roles played by NS5 in viral cap formation and genome replication, and opens up new possibilities for drug discovery and design for antiviral therapeutic intervention. In Section 3.1, the functional significance of the intra-molecular interactions and the flexible linker between MTase and RdRp revealed by the DENV-3 NS5 FL crystal structure in virus replication, growth and infectivity was demonstrated. The presence of MTase-RdRp interface likely promotes the physical closeness between the two domains to facilitate inter-regulations and cooperativity of the essential enzymatic activities of NS5. The dynamic linker is proposed to play a part in the formation of the conserved interface and could undergo structure transition to re-orientate the two domains such that distinct conformations of NS5 can be achieved for its catalytic functions and establishment of contacts with its interaction partners in a serotype/virus-specific manner.

The N-terminal MTase domain of NS5 is responsible for capping the viral genome which prevents RNA degradation and allows virus to evade the host immune response. A recent ternary crystal structure of DENV NS5 with an authentic cap-0-viral RNA and SAH captures the complex during the 2'-*O* methylation step and reveals numerous interactions established between the RNA substrate and amino acids from the MTase. In Section 3.2, we highlighted the importance of the residues lining the RNA binding groove for specific viral RNA recognition and 2'-*O* methylation by DENV NS5 MTase, and also the requirement for strict conservation of nucleotides at the ends of the flaviviral genomes.

The C-terminal RdRp domain has an important role in replicating viral RNA during infection and is often targeted for the development of anti-flaviviral inhibitors. In-house screening campaigns together with X-ray crystallography efforts discovered two allosteric binding sites in the DENV RdRp which were functionally validated in Section 3.3. Both allosteric pockets

in the F1 motif and N-pocket of RdRp were shown to regulate *de novo* initiation process during RNA synthesis. Binding of inhibitor at these sites probably impedes necessary conformational changes of RdRp for catalysis of *de novo* initiation process or for the transition from initiation to elongation phase. Our study provided critical evidence for targeting these two pockets of DENV RdRp for potent non-nucleoside inhibitor design. Moreover, the active site of RdRp could also be aimed for the design of specific and effective nucleoside inhibitors and this work would be facilitated by the presence of a catalytically relevant complex which uncovers structural details about the RdRp catalytic cycle.

Section 3.4 described our work to obtain a co-crystal structure of NS5 RdRp bound to RNA. We were successful in the formation of active elongation complexes of DENV NS5 using various RNA constructs, but still need to improve on the solubility and stability of the complexes in order to attain a crystal structure of the ternary catalytic polymerase complex. Nevertheless, the development of a novel FP-based assay may serve as an alternative technique to the FAPA assay for high-throughput screening of nucleotide analogs and allosteric inhibitors, with the use of lower amount of RNA substrate and enzyme, and at shorter incubation time.

In conclusion, the dengue NS5 FL structure now provides a platform for the design of inhibitors that specifically target and disrupt the inter-domain interactions, linker and allosteric/catalytic site important for virus replication, growth and infectivity.

5 FUTURE WORK

NS5 has been known to interact with NS3 protease/helicase in the membrane-bound viral replication complex (320, 325, 380), as well as the promoter-like element stem loop A (SLA) in the 5'-UTR of the viral genome for precise initiation of viral minus-strand RNA synthesis (339). The relationship between RNA synthesis and capping along with whether NS3 exerts its function as a helicase before or during RNA synthesis, and as RTPase during or after positive-strand progeny RNA synthesis are currently uncertain. It is likely that NS3 might adopt different orientations for its multi-functional activities and inter-protein interfaces of NS5-NS3 complex must be established in order for the enzymatic events to take place. Following the resolution of the JEV and DENV-3 NS5 FL structures, future research could be directed to understand how FL NS5 interacts with other viral and possibly host proteins to synthesize and cap RNA genome in a synchronized manner.

Moreover, NS5 interacts with host proteins involved in intracellular trafficking such as importin-β and CRM1-mediated exportin via its nuclear localization signals (NLSs) and nuclear export signal (NES) respectively (321, 371), and host immune response such as those involved in IFN-α/β signalling and JAK-STAT signalling pathways (225, 226, 381). Nuclear-localized NS5 might be important for virus replication and has the potential to alter host processes for its fitness and virulence. In addition, perturbation of the host immune response by NS5 suggests that it might play a role in viral pathogenesis. Since NS5 showed great importance in viral replication and host immune response modulation, further exploration of NS5-host cell molecular interactions could be undertaken to expand our understanding of the role played by NS5 in the flaviviral life cycle. The recent elucidation of JEV and DENV-3 NS5 FL structures would greatly accelerate this process, providing novel possibilities for anti-flaviviral drug discovery and development.

In addition, future work to unravel the molecular interactions within the replication machinery using biophysical techniques could be carried out to expand our understanding on the dynamics of NS5 enzyme and its association with virus pathogenesis.

6 REFERENCES

1. Chambers TJ, Hahn CS, Galler R, Rice CM. 1990. Flavivirus genome organization, expression, and replication. Annu Rev Microbiol 44:649-88.
2. Holbrook MR. 2017. Historical Perspectives on Flavivirus Research. Viruses 9.
3. Bhatt S, Gething PW, Brady OJ, Messina JP, Farlow AW, Moyes CL, Drake JM, Brownstein JS, Hoen AG, Sankoh O, Myers MF, George DB, Jaenisch T, Wint GR, Simmons CP, Scott TW, Farrar JJ, Hay SI. 2013. The global distribution and burden of dengue. Nature 496:504-7.
4. Guzman MG, Alvarez M, Halstead SB. 2013. Secondary infection as a risk factor for dengue hemorrhagic fever/dengue shock syndrome: an historical perspective and role of antibody-dependent enhancement of infection. Arch Virol 158:1445-59.
5. Hss AS, Koh MT, Tan KK, Chan LG, Zhou L, Bouckenooghe A, Crevat D, Hutagalung Y. 2013. Safety and immunogenicity of a tetravalent dengue vaccine in healthy children aged 2-11 years in Malaysia: a randomized, placebo-controlled, Phase III study. Vaccine 31:5814-21.
6. da Costa VG, Marques-Silva AC, Floriano VG, Moreli ML. 2014. Safety, immunogenicity and efficacy of a recombinant tetravalent dengue vaccine: a meta-analysis of randomized trials. Vaccine 32:4885-92.
7. Capeding MR, Tran NH, Hadinegoro SR, Ismail HI, Chotpitayasunondh T, Chua MN, Luong CQ, Rusmil K, Wirawan DN, Nallusamy R, Pitisuttithum P, Thisyakorn U, Yoon IK, van der Vliet D, Langevin E, Laot T, Hutagalung Y, Frago C, Boaz M, Wartel TA, Tornieporth NG, Saville M, Bouckenooghe A, Group CYDS. 2014. Clinical efficacy and safety of a novel tetravalent dengue vaccine in healthy children in Asia: a phase 3, randomised, observer-masked, placebo-controlled trial. Lancet 384:1358-65.
8. Villar L, Dayan GH, Arredondo-Garcia JL, Rivera DM, Cunha R, Deseda C, Reynales H, Costa MS, Morales-Ramirez JO, Carrasquilla G, Rey LC, Dietze R, Luz K, Rivas E, Miranda Montoya MC, Cortes Supelano M, Zambrano B, Langevin E, Boaz M, Tornieporth N, Saville M, Noriega F, Group CYDS. 2015. Efficacy of a tetravalent dengue vaccine in children in Latin America. N Engl J Med 372:113-23.
9. Coudeville L, Baurin N, Vergu E. 2016. Estimation of parameters related to vaccine efficacy and dengue transmission from two large phase III studies. Vaccine 34:6417-6425.
10. Jessie K, Fong MY, Devi S, Lam SK, Wong KT. 2004. Localization of dengue virus in naturally infected human tissues, by immunohistochemistry and in situ hybridization. J Infect Dis 189:1411-8.
11. Wu SJ, Grouard-Vogel G, Sun W, Mascola JR, Brachtel E, Putvatana R, Louder MK, Filgueira L, Marovich MA, Wong HK, Blauvelt A, Murphy GS, Robb ML, Innes BL, Birx DL, Hayes CG, Frankel SS. 2000. Human skin Langerhans cells are targets of dengue virus infection. Nat Med 6:816-20.
12. Schmid MA, Harris E. 2014. Monocyte recruitment to the dermis and differentiation to dendritic cells increases the targets for dengue virus replication. PLoS Pathog 10:e1004541.
13. Chen Y, Maguire T, Hileman RE, Fromm JR, Esko JD, Linhardt RJ, Marks RM. 1997. Dengue virus infectivity depends on envelope protein binding to target cell heparan sulfate. Nat Med 3:866-71.
14. Germi R, Crance JM, Garin D, Guimet J, Lortat-Jacob H, Ruigrok RW, Zarski JP, Drouet E. 2002. Heparan sulfate-mediated binding of infectious dengue virus type 2 and yellow fever virus. Virology 292:162-8.

15. Hilgard P, Stockert R. 2000. Heparan sulfate proteoglycans initiate dengue virus infection of hepatocytes. Hepatology 32:1069-77.
16. Chen YC, Wang SY, King CC. 1999. Bacterial lipopolysaccharide inhibits dengue virus infection of primary human monocytes/macrophages by blockade of virus entry via a CD14-dependent mechanism. J Virol 73:2650-7.
17. Jindadamrongwech S, Thepparit C, Smith DR. 2004. Identification of GRP 78 (BiP) as a liver cell expressed receptor element for dengue virus serotype 2. Arch Virol 149:915-27.
18. Peiris JS, Porterfield JS. 1979. Antibody-mediated enhancement of Flavivirus replication in macrophage-like cell lines. Nature 282:509-11.
19. Piccini LE, Castilla V, Damonte EB. 2015. Dengue-3 Virus Entry into Vero Cells: Role of Clathrin-Mediated Endocytosis in the Outcome of Infection. PLoS One 10:e0140824.
20. Cruz-Oliveira C, Freire JM, Conceicao TM, Higa LM, Castanho MA, Da Poian AT. 2015. Receptors and routes of dengue virus entry into the host cells. FEMS Microbiol Rev 39:155-70.
21. Rodenhuis-Zybert IA, Wilschut J, Smit JM. 2010. Dengue virus life cycle: viral and host factors modulating infectivity. Cell Mol Life Sci 67:2773-86.
22. Cleaves GR, Dubin DT. 1979. Methylation status of intracellular dengue type 2 40 S RNA. Virology 96:159-65.
23. Brinton MA, Dispoto JH. 1988. Sequence and secondary structure analysis of the 5'-terminal region of flavivirus genome RNA. Virology 162:290-9.
24. Thurner C, Witwer C, Hofacker IL, Stadler PF. 2004. Conserved RNA secondary structures in Flaviviridae genomes. J Gen Virol 85:1113-24.
25. Filomatori CV, Lodeiro MF, Alvarez DE, Samsa MM, Pietrasanta L, Gamarnik AV. 2006. A 5' RNA element promotes dengue virus RNA synthesis on a circular genome. Genes Dev 20:2238-49.
26. Yu L, Nomaguchi M, Padmanabhan R, Markoff L. 2008. Specific requirements for elements of the 5' and 3' terminal regions in flavivirus RNA synthesis and viral replication. Virology 374:170-85.
27. Alvarez DE, Lodeiro MF, Luduena SJ, Pietrasanta LI, Gamarnik AV. 2005. Long-range RNA-RNA interactions circularize the dengue virus genome. J Virol 79:6631-43.
28. Lodeiro MF, Filomatori CV, Gamarnik AV. 2009. Structural and functional studies of the promoter element for dengue virus RNA replication. J Virol 83:993-1008.
29. Clyde K, Barrera J, Harris E. 2008. The capsid-coding region hairpin element (cHP) is a critical determinant of dengue virus and West Nile virus RNA synthesis. Virology 379:314-23.
30. Shurtleff AC, Beasley DW, Chen JJ, Ni H, Suderman MT, Wang H, Xu R, Wang E, Weaver SC, Watts DM, Russell KL, Barrett AD. 2001. Genetic variation in the 3' non-coding region of dengue viruses. Virology 281:75-87.
31. Silva RL, de Silva AM, Harris E, MacDonald GH. 2008. Genetic analysis of Dengue 3 virus subtype III 5' and 3' non-coding regions. Virus Res 135:320-5.
32. Hahn CS, Hahn YS, Rice CM, Lee E, Dalgarno L, Strauss EG, Strauss JH. 1987. Conserved elements in the 3' untranslated region of flavivirus RNAs and potential cyclization sequences. J Mol Biol 198:33-41.
33. Gritsun TS, Gould EA. 2006. Direct repeats in the 3' untranslated regions of mosquito-borne flaviviruses: possible implications for virus transmission. J Gen Virol 87:3297-305.

34. Olsthoorn RC, Bol JF. 2001. Sequence comparison and secondary structure analysis of the 3' noncoding region of flavivirus genomes reveals multiple pseudoknots. RNA 7:1370-7.
35. Romero TA, Tumban E, Jun J, Lott WB, Hanley KA. 2006. Secondary structure of dengue virus type 4 3' untranslated region: impact of deletion and substitution mutations. J Gen Virol 87:3291-6.
36. Alvarez DE, De Lella Ezcurra AL, Fucito S, Gamarnik AV. 2005. Role of RNA structures present at the 3'UTR of dengue virus on translation, RNA synthesis, and viral replication. Virology 339:200-12.
37. Men R, Bray M, Clark D, Chanock RM, Lai CJ. 1996. Dengue type 4 virus mutants containing deletions in the 3' noncoding region of the RNA genome: analysis of growth restriction in cell culture and altered viremia pattern and immunogenicity in rhesus monkeys. J Virol 70:3930-7.
38. Bredenbeek PJ, Kooi EA, Lindenbach B, Huijkman N, Rice CM, Spaan WJ. 2003. A stable full-length yellow fever virus cDNA clone and the role of conserved RNA elements in flavivirus replication. J Gen Virol 84:1261-8.
39. Mandl CW, Holzmann H, Meixner T, Rauscher S, Stadler PF, Allison SL, Heinz FX. 1998. Spontaneous and engineered deletions in the 3' noncoding region of tick-borne encephalitis virus: construction of highly attenuated mutants of a flavivirus. J Virol 72:2132-40.
40. Proutski V, Gould EA, Holmes EC. 1997. Secondary structure of the 3' untranslated region of flaviviruses: similarities and differences. Nucleic Acids Res 25:1194-202.
41. Brinton MA, Fernandez AV, Dispoto JH. 1986. The 3'-nucleotides of flavivirus genomic RNA form a conserved secondary structure. Virology 153:113-21.
42. Zeng L, Falgout B, Markoff L. 1998. Identification of specific nucleotide sequences within the conserved 3'-SL in the dengue type 2 virus genome required for replication. J Virol 72:7510-22.
43. Yu L, Markoff L. 2005. The topology of bulges in the long stem of the flavivirus 3' stem-loop is a major determinant of RNA replication competence. J Virol 79:2309-24.
44. Friebe P, Shi PY, Harris E. 2011. The 5' and 3' downstream AUG region elements are required for mosquito-borne flavivirus RNA replication. J Virol 85:1900-5.
45. Villordo SM, Gamarnik AV. 2009. Genome cyclization as strategy for flavivirus RNA replication. Virus Res 139:230-9.
46. Friebe P, Harris E. 2010. Interplay of RNA elements in the dengue virus 5' and 3' ends required for viral RNA replication. J Virol 84:6103-18.
47. Khromykh AA, Meka H, Guyatt KJ, Westaway EG. 2001. Essential role of cyclization sequences in flavivirus RNA replication. J Virol 75:6719-28.
48. Alvarez DE, Filomatori CV, Gamarnik AV. 2008. Functional analysis of dengue virus cyclization sequences located at the 5' and 3'UTRs. Virology 375:223-35.
49. Alvarez DE, Lodeiro MF, Filomatori CV, Fucito S, Mondotte JA, Gamarnik AV. 2006. Structural and functional analysis of dengue virus RNA. Novartis Found Symp 277:120-32; discussion 132-5, 251-3.
50. Gebhard LG, Filomatori CV, Gamarnik AV. 2011. Functional RNA elements in the dengue virus genome. Viruses 3:1739-56.
51. Edgil D, Diamond MS, Holden KL, Paranjape SM, Harris E. 2003. Translation efficiency determines differences in cellular infection among dengue virus type 2 strains. Virology 317:275-90.
52. Holden KL, Harris E. 2004. Enhancement of dengue virus translation: role of the 3' untranslated region and the terminal 3' stem-loop domain. Virology 329:119-33.

53. Clyde K, Harris E. 2006. RNA secondary structure in the coding region of dengue virus type 2 directs translation start codon selection and is required for viral replication. J Virol 80:2170-82.
54. Polacek C, Friebe P, Harris E. 2009. Poly(A)-binding protein binds to the non-polyadenylated 3' untranslated region of dengue virus and modulates translation efficiency. J Gen Virol 90:687-92.
55. Pestova TV, Kolupaeva VG, Lomakin IB, Pilipenko EV, Shatsky IN, Agol VI, Hellen CU. 2001. Molecular mechanisms of translation initiation in eukaryotes. Proc Natl Acad Sci U S A 98:7029-36.
56. Sonenberg N, Pelletier J. 1989. Poliovirus translation: a paradigm for a novel initiation mechanism. Bioessays 11:128-32.
57. Gradi A, Svitkin YV, Imataka H, Sonenberg N. 1998. Proteolysis of human eukaryotic translation initiation factor eIF4GII, but not eIF4GI, coincides with the shutoff of host protein synthesis after poliovirus infection. Proc Natl Acad Sci U S A 95:11089-94.
58. Edgil D, Polacek C, Harris E. 2006. Dengue virus utilizes a novel strategy for translation initiation when cap-dependent translation is inhibited. J Virol 80:2976-86.
59. Meulewaeter F, van Lipzig R, Gultyaev AP, Pleij CW, Van Damme D, Cornelissen M, van Eldik G. 2004. Conservation of RNA structures enables TNV and BYDV 5' and 3' elements to cooperate synergistically in cap-independent translation. Nucleic Acids Res 32:1721-30.
60. Shen R, Miller WA. 2004. The 3' untranslated region of tobacco necrosis virus RNA contains a barley yellow dwarf virus-like cap-independent translation element. J Virol 78:4655-64.
61. Gazo BM, Murphy P, Gatchel JR, Browning KS. 2004. A novel interaction of Cap-binding protein complexes eukaryotic initiation factor (eIF) 4F and eIF(iso)4F with a region in the 3'-untranslated region of satellite tobacco necrosis virus. J Biol Chem 279:13584-92.
62. Kneller EL, Rakotondrafara AM, Miller WA. 2006. Cap-independent translation of plant viral RNAs. Virus Res 119:63-75.
63. Kuhn RJ, Zhang W, Rossmann MG, Pletnev SV, Corver J, Lenches E, Jones CT, Mukhopadhyay S, Chipman PR, Strauss EG, Baker TS, Strauss JH. 2002. Structure of dengue virus: implications for flavivirus organization, maturation, and fusion. Cell 108:717-25.
64. Bollati M, Alvarez K, Assenberg R, Baronti C, Canard B, Cook S, Coutard B, Decroly E, de Lamballerie X, Gould EA, Grard G, Grimes JM, Hilgenfeld R, Jansson AM, Malet H, Mancini EJ, Mastrangelo E, Mattevi A, Milani M, Moureau G, Neyts J, Owens RJ, Ren J, Selisko B, Speroni S, Steuber H, Stuart DI, Unge T, Bolognesi M. 2010. Structure and functionality in flavivirus NS-proteins: perspectives for drug design. Antiviral Res 87:125-48.
65. Munoz-Jordan JL, Sanchez-Burgos GG, Laurent-Rolle M, Garcia-Sastre A. 2003. Inhibition of interferon signaling by dengue virus. Proc Natl Acad Sci U S A 100:14333-8.
66. Munoz-Jordan JL, Laurent-Rolle M, Ashour J, Martinez-Sobrido L, Ashok M, Lipkin WI, Garcia-Sastre A. 2005. Inhibition of alpha/beta interferon signaling by the NS4B protein of flaviviruses. J Virol 79:8004-13.
67. Steitz TA. 1998. A mechanism for all polymerases. Nature 391:231-2.
68. Choi KH. 2012. Viral polymerases. Adv Exp Med Biol 726:267-304.
69. Mesters JR, Tan J, Hilgenfeld R. 2006. Viral enzymes. Curr Opin Struct Biol 16:776-86.

70. Uchil PD, Satchidanandam V. 2003. Architecture of the flaviviral replication complex. Protease, nuclease, and detergents reveal encasement within double-layered membrane compartments. J Biol Chem 278:24388-98.
71. Polyak SJ, Zheng S, Harnish DG. 1995. 5' termini of Pichinde arenavirus S RNAs and mRNAs contain nontemplated nucleotides. J Virol 69:3211-5.
72. Plotch SJ, Bouloy M, Ulmanen I, Krug RM. 1981. A unique cap(m7GpppXm)-dependent influenza virion endonuclease cleaves capped RNAs to generate the primers that initiate viral RNA transcription. Cell 23:847-58.
73. Morin B, Coutard B, Lelke M, Ferron F, Kerber R, Jamal S, Frangeul A, Baronti C, Charrel R, de Lamballerie X, Vonrhein C, Lescar J, Bricogne G, Gunther S, Canard B. 2010. The N-terminal domain of the arenavirus L protein is an RNA endonuclease essential in mRNA transcription. PLoS Pathog 6:e1001038.
74. Baltimore D. 1971. Expression of animal virus genomes. Bacteriol Rev 35:235-41.
75. Dong H, Fink K, Zust R, Lim SP, Qin CF, Shi PY. 2014. Flavivirus RNA methylation. J Gen Virol 95:763-78.
76. Beilhartz GL, Gotte M. 2010. HIV-1 Ribonuclease H: Structure, Catalytic Mechanism and Inhibitors. Viruses 2:900-26.
77. Nowotny M, Gaidamakov SA, Crouch RJ, Yang W. 2005. Crystal structures of RNase H bound to an RNA/DNA hybrid: substrate specificity and metal-dependent catalysis. Cell 121:1005-16.
78. de Vega M, Blanco L, Salas M. 1999. Processive proofreading and the spatial relationship between polymerase and exonuclease active sites of bacteriophage phi29 DNA polymerase. J Mol Biol 292:39-51.
79. Wu J, Liu W, Gong P. 2015. A Structural Overview of RNA-Dependent RNA Polymerases from the Flaviviridae Family. Int J Mol Sci 16:12943-57.
80. van Dijk AA, Makeyev EV, Bamford DH. 2004. Initiation of viral RNA-dependent RNA polymerization. J Gen Virol 85:1077-93.
81. Fuentes C, Bosch A, Pinto RM, Guix S. 2012. Identification of human astrovirus genome-linked protein (VPg) essential for virus infectivity. J Virol 86:10070-8.
82. Nassal M. 2008. Hepatitis B viruses: reverse transcription a different way. Virus Res 134:235-49.
83. Ackermann M, Padmanabhan R. 2001. De novo synthesis of RNA by the dengue virus RNA-dependent RNA polymerase exhibits temperature dependence at the initiation but not elongation phase. J Biol Chem 276:39926-37.
84. Ducani C, Bernardinelli G, Hogberg B. 2014. Rolling circle replication requires single-stranded DNA binding protein to avoid termination and production of double-stranded DNA. Nucleic Acids Res 42:10596-604.
85. Hansen JL, Long AM, Schultz SC. 1997. Structure of the RNA-dependent RNA polymerase of poliovirus. Structure 5:1109-22.
86. Yap TL, Xu T, Chen YL, Malet H, Egloff MP, Canard B, Vasudevan SG, Lescar J. 2007. Crystal structure of the dengue virus RNA-dependent RNA polymerase catalytic domain at 1.85-angstrom resolution. J Virol 81:4753-65.
87. Ng KK, Cherney MM, Vazquez AL, Machin A, Alonso JM, Parra F, James MN. 2002. Crystal structures of active and inactive conformations of a caliciviral RNA-dependent RNA polymerase. J Biol Chem 277:1381-7.
88. Bressanelli S, Tomei L, Rey FA, De Francesco R. 2002. Structural analysis of the hepatitis C virus RNA polymerase in complex with ribonucleotides. J Virol 76:3482-92.
89. Castro C, Smidansky E, Maksimchuk KR, Arnold JJ, Korneeva VS, Gotte M, Konigsberg W, Cameron CE. 2007. Two proton transfers in the transition state for

nucleotidyl transfer catalyzed by RNA- and DNA-dependent RNA and DNA polymerases. Proc Natl Acad Sci U S A 104:4267-72.
90. Yang X, Smidansky ED, Maksimchuk KR, Lum D, Welch JL, Arnold JJ, Cameron CE, Boehr DD. 2012. Motif D of viral RNA-dependent RNA polymerases determines efficiency and fidelity of nucleotide addition. Structure 20:1519-27.
91. Castro C, Smidansky ED, Arnold JJ, Maksimchuk KR, Moustafa I, Uchida A, Gotte M, Konigsberg W, Cameron CE. 2009. Nucleic acid polymerases use a general acid for nucleotidyl transfer. Nat Struct Mol Biol 16:212-8.
92. Shen H, Sun H, Li G. 2012. What is the role of motif D in the nucleotide incorporation catalyzed by the RNA-dependent RNA polymerase from poliovirus? PLoS Comput Biol 8:e1002851.
93. Gong P, Peersen OB. 2010. Structural basis for active site closure by the poliovirus RNA-dependent RNA polymerase. Proc Natl Acad Sci U S A 107:22505-10.
94. Vives-Adrian L, Lujan C, Oliva B, van der Linden L, Selisko B, Coutard B, Canard B, van Kuppeveld FJ, Ferrer-Orta C, Verdaguer N. 2014. The crystal structure of a cardiovirus RNA-dependent RNA polymerase reveals an unusual conformation of the polymerase active site. J Virol 88:5595-607.
95. Gong P, Kortus MG, Nix JC, Davis RE, Peersen OB. 2013. Structures of coxsackievirus, rhinovirus, and poliovirus polymerase elongation complexes solved by engineering RNA mediated crystal contacts. PLoS One 8:e60272.
96. Ferrer-Orta C, Arias A, Perez-Luque R, Escarmis C, Domingo E, Verdaguer N. 2007. Sequential structures provide insights into the fidelity of RNA replication. Proc Natl Acad Sci U S A 104:9463-8.
97. Sholders AJ, Peersen OB. 2014. Distinct conformations of a putative translocation element in poliovirus polymerase. J Mol Biol 426:1407-19.
98. Lai VC, Kao CC, Ferrari E, Park J, Uss AS, Wright-Minogue J, Hong Z, Lau JY. 1999. Mutational analysis of bovine viral diarrhea virus RNA-dependent RNA polymerase. J Virol 73:10129-36.
99. Ranjith-Kumar CT, Gutshall L, Sarisky RT, Kao CC. 2003. Multiple interactions within the hepatitis C virus RNA polymerase repress primer-dependent RNA synthesis. J Mol Biol 330:675-85.
100. Butcher SJ, Grimes JM, Makeyev EV, Bamford DH, Stuart DI. 2001. A mechanism for initiating RNA-dependent RNA polymerization. Nature 410:235-40.
101. Lu G, Gong P. 2013. Crystal Structure of the full-length Japanese encephalitis virus NS5 reveals a conserved methyltransferase-polymerase interface. PLoS Pathog 9:e1003549.
102. Surana P, Satchidanandam V, Nair DT. 2014. RNA-dependent RNA polymerase of Japanese encephalitis virus binds the initiator nucleotide GTP to form a mechanistically important pre-initiation state. Nucleic Acids Res 42:2758-73.
103. Iglesias NG, Filomatori CV, Gamarnik AV. 2011. The F1 motif of dengue virus polymerase NS5 is involved in promoter-dependent RNA synthesis. J Virol 85:5745-56.
104. Nomoto A, Detjen B, Pozzatti R, Wimmer E. 1977. The location of the polio genome protein in viral RNAs and its implication for RNA synthesis. Nature 268:208-13.
105. Takeda N, Kuhn RJ, Yang CF, Takegami T, Wimmer E. 1986. Initiation of poliovirus plus-strand RNA synthesis in a membrane complex of infected HeLa cells. J Virol 60:43-53.
106. Ferrer-Orta C, Arias A, Agudo R, Perez-Luque R, Escarmis C, Domingo E, Verdaguer N. 2006. The structure of a protein primer-polymerase complex in the initiation of genome replication. EMBO J 25:880-8.

107. Paul AV, Yin J, Mugavero J, Rieder E, Liu Y, Wimmer E. 2003. A "slide-back" mechanism for the initiation of protein-primed RNA synthesis by the RNA polymerase of poliovirus. J Biol Chem 278:43951-60.
108. Murray KE, Barton DJ. 2003. Poliovirus CRE-dependent VPg uridylylation is required for positive-strand RNA synthesis but not for negative-strand RNA synthesis. J Virol 77:4739-50.
109. Gruez A, Selisko B, Roberts M, Bricogne G, Bussetta C, Jabafi I, Coutard B, De Palma AM, Neyts J, Canard B. 2008. The crystal structure of coxsackievirus B3 RNA-dependent RNA polymerase in complex with its protein primer VPg confirms the existence of a second VPg binding site on Picornaviridae polymerases. J Virol 82:9577-90.
110. Chen C, Wang Y, Shan C, Sun Y, Xu P, Zhou H, Yang C, Shi PY, Rao Z, Zhang B, Lou Z. 2013. Crystal structure of enterovirus 71 RNA-dependent RNA polymerase complexed with its protein primer VPg: implication for a trans mechanism of VPg uridylylation. J Virol 87:5755-68.
111. Ago H, Adachi T, Yoshida A, Yamamoto M, Habuka N, Yatsunami K, Miyano M. 1999. Crystal structure of the RNA-dependent RNA polymerase of hepatitis C virus. Structure 7:1417-26.
112. Bressanelli S, Tomei L, Roussel A, Incitti I, Vitale RL, Mathieu M, De Francesco R, Rey FA. 1999. Crystal structure of the RNA-dependent RNA polymerase of hepatitis C virus. Proc Natl Acad Sci U S A 96:13034-9.
113. Lesburg CA, Cable MB, Ferrari E, Hong Z, Mannarino AF, Weber PC. 1999. Crystal structure of the RNA-dependent RNA polymerase from hepatitis C virus reveals a fully encircled active site. Nat Struct Biol 6:937-43.
114. Choi KH, Groarke JM, Young DC, Kuhn RJ, Smith JL, Pevear DC, Rossmann MG. 2004. The structure of the RNA-dependent RNA polymerase from bovine viral diarrhea virus establishes the role of GTP in de novo initiation. Proc Natl Acad Sci U S A 101:4425-30.
115. Malet H, Egloff MP, Selisko B, Butcher RE, Wright PJ, Roberts M, Gruez A, Sulzenbacher G, Vonrhein C, Bricogne G, Mackenzie JM, Khromykh AA, Davidson AD, Canard B. 2007. Crystal structure of the RNA polymerase domain of the West Nile virus non-structural protein 5. J Biol Chem 282:10678-89.
116. Hong Z, Cameron CE, Walker MP, Castro C, Yao N, Lau JY, Zhong W. 2001. A novel mechanism to ensure terminal initiation by hepatitis C virus NS5B polymerase. Virology 285:6-11.
117. Cherry AL, Dennis CA, Baron A, Eisele LE, Thommes PA, Jaeger J. 2015. Hydrophobic and charged residues in the C-terminal arm of hepatitis C virus RNA-dependent RNA polymerase regulate initiation and elongation. J Virol 89:2052-63.
118. Kao CC, Del Vecchio AM, Zhong W. 1999. De novo initiation of RNA synthesis by a recombinant flaviviridae RNA-dependent RNA polymerase. Virology 253:1-7.
119. Luo G, Hamatake RK, Mathis DM, Racela J, Rigat KL, Lemm J, Colonno RJ. 2000. De novo initiation of RNA synthesis by the RNA-dependent RNA polymerase (NS5B) of hepatitis C virus. J Virol 74:851-63.
120. Egloff MP, Decroly E, Malet H, Selisko B, Benarroch D, Ferron F, Canard B. 2007. Structural and functional analysis of methylation and 5'-RNA sequence requirements of short capped RNAs by the methyltransferase domain of dengue virus NS5. J Mol Biol 372:723-36.
121. Shatkin AJ. 1976. Capping of eucaryotic mRNAs. Cell 9:645-53.
122. Darnell JE, Jr. 1979. Transcription units for mRNA production in eukaryotic cells and their DNA viruses. Prog Nucleic Acid Res Mol Biol 22:327-53.

123. Filipowicz W, Furuichi Y, Sierra JM, Muthukrishnan S, Shatkin AJ, Ochoa S. 1976. A protein binding the methylated 5'-terminal sequence, m7GpppN, of eukaryotic messenger RNA. Proc Natl Acad Sci U S A 73:1559-63.
124. Schibler U, Perry RP. 1977. The 5'-termini of heterogeneous nuclear RNA: a comparison among molecules of different sizes and ages. Nucleic Acids Res 4:4133-49.
125. Decker CJ, Parker R. 2012. P-bodies and stress granules: possible roles in the control of translation and mRNA degradation. Cold Spring Harb Perspect Biol 4:a012286.
126. Nallagatla SR, Toroney R, Bevilacqua PC. 2008. A brilliant disguise for self RNA: 5'-end and internal modifications of primary transcripts suppress elements of innate immunity. RNA Biol 5:140-4.
127. Furuichi Y, Shatkin AJ. 2000. Viral and cellular mRNA capping: past and prospects. Adv Virus Res 55:135-84.
128. Furuichi Y, Muthukrishnan S, Shatkin AJ. 1975. 5'-Terminal m-7G(5')ppp(5')G-m-p in vivo: identification in reovirus genome RNA. Proc Natl Acad Sci U S A 72:742-5.
129. Shatkin AJ. 1974. Methylated messenger RNA synthesis in vitro by purified reovirus. Proc Natl Acad Sci U S A 71:3204-7.
130. Wei CM, Moss B. 1975. Methylated nucleotides block 5'-terminus of vaccinia virus messenger RNA. Proc Natl Acad Sci U S A 72:318-22.
131. Decroly E, Ferron F, Lescar J, Canard B. 2011. Conventional and unconventional mechanisms for capping viral mRNA. Nat Rev Microbiol 10:51-65.
132. Cong P, Shuman S. 1995. Mutational analysis of mRNA capping enzyme identifies amino acids involved in GTP binding, enzyme-guanylate formation, and GMP transfer to RNA. Mol Cell Biol 15:6222-31.
133. Niles EG, Christen L. 1993. Identification of the vaccinia virus mRNA guanyltransferase active site lysine. J Biol Chem 268:24986-9.
134. Myette JR, Niles EG. 1996. Characterization of the vaccinia virus RNA 5'-triphosphatase and nucleotide triphosphate phosphohydrolase activities. Demonstrate that both activities are carried out at the same active site. J Biol Chem 271:11945-52.
135. Cong P, Shuman S. 1992. Methyltransferase and subunit association domains of vaccinia virus mRNA capping enzyme. J Biol Chem 267:16424-9.
136. Higman MA, Bourgeois N, Niles EG. 1992. The vaccinia virus mRNA (guanine-N7-)-methyltransferase requires both subunits of the mRNA capping enzyme for activity. J Biol Chem 267:16430-7.
137. Mao X, Shuman S. 1994. Intrinsic RNA (guanine-7) methyltransferase activity of the vaccinia virus capping enzyme D1 subunit is stimulated by the D12 subunit. Identification of amino acid residues in the D1 protein required for subunit association and methyl group transfer. J Biol Chem 269:24472-9.
138. Vos JC, Sasker M, Stunnenberg HG. 1991. Vaccinia virus capping enzyme is a transcription initiation factor. EMBO J 10:2553-8.
139. Harris N, Rosales R, Moss B. 1993. Transcription initiation factor activity of vaccinia virus capping enzyme is independent of mRNA guanylylation. Proc Natl Acad Sci U S A 90:2860-4.
140. Shuman S, Moss B. 1988. Factor-dependent transcription termination by vaccinia virus RNA polymerase. Evidence that the cis-acting termination signal is in nascent RNA. J Biol Chem 263:6220-5.
141. Schnierle BS, Gershon PD, Moss B. 1992. Cap-specific mRNA (nucleoside-O2'-)-methyltransferase and poly(A) polymerase stimulatory activities of vaccinia virus are mediated by a single protein. Proc Natl Acad Sci U S A 89:2897-901.

142. Wengler G, Wengler G. 1993. The NS 3 nonstructural protein of flaviviruses contains an RNA triphosphatase activity. Virology 197:265-73.
143. Issur M, Geiss BJ, Bougie I, Picard-Jean F, Despins S, Mayette J, Hobdey SE, Bisaillon M. 2009. The flavivirus NS5 protein is a true RNA guanylyltransferase that catalyzes a two-step reaction to form the RNA cap structure. RNA 15:2340-50.
144. Dong H, Ren S, Li H, Shi PY. 2008. Separate molecules of West Nile virus methyltransferase can independently catalyze the N7 and 2'-O methylations of viral RNA cap. Virology 377:1-6.
145. Ray D, Shah A, Tilgner M, Guo Y, Zhao Y, Dong H, Deas TS, Zhou Y, Li H, Shi PY. 2006. West Nile virus 5'-cap structure is formed by sequential guanine N-7 and ribose 2'-O methylations by nonstructural protein 5. J Virol 80:8362-70.
146. Reinisch KM, Nibert ML, Harrison SC. 2000. Structure of the reovirus core at 3.6 A resolution. Nature 404:960-7.
147. Sutton G, Grimes JM, Stuart DI, Roy P. 2007. Bluetongue virus VP4 is an RNA-capping assembly line. Nat Struct Mol Biol 14:449-51.
148. Cheng L, Sun J, Zhang K, Mou Z, Huang X, Ji G, Sun F, Zhang J, Zhu P. 2011. Atomic model of a cypovirus built from cryo-EM structure provides insight into the mechanism of mRNA capping. Proc Natl Acad Sci U S A 108:1373-8.
149. Balvay L, Soto Rifo R, Ricci EP, Decimo D, Ohlmann T. 2009. Structural and functional diversity of viral IRESes. Biochim Biophys Acta 1789:542-57.
150. Goodfellow I, Chaudhry Y, Gioldasi I, Gerondopoulos A, Natoni A, Labrie L, Laliberte JF, Roberts L. 2005. Calicivirus translation initiation requires an interaction between VPg and eIF 4 E. EMBO Rep 6:968-72.
151. Abraham G, Rhodes DP, Banerjee AK. 1975. The 5' terminal structure of the methylated mRNA synthesized in vitro by vesicular stomatitis virus. Cell 5:51-8.
152. Abraham G, Rhodes DP, Banerjee AK. 1975. Novel initiation of RNA synthesis in vitro by vesicular stomatitis virus. Nature 255:37-40.
153. Gupta KC, Roy P. 1980. Alternate capping mechanisms for transcription of spring viremia of carp virus: evidence for independent mRNA initiation. J Virol 33:292-303.
154. Barik S. 1993. The structure of the 5' terminal cap of the respiratory syncytial virus mRNA. J Gen Virol 74 (Pt 3):485-90.
155. Ogino T, Banerjee AK. 2010. The HR motif in the RNA-dependent RNA polymerase L protein of Chandipura virus is required for unconventional mRNA-capping activity. J Gen Virol 91:1311-4.
156. Ogino T, Banerjee AK. 2007. Unconventional mechanism of mRNA capping by the RNA-dependent RNA polymerase of vesicular stomatitis virus. Mol Cell 25:85-97.
157. Ogino T, Yadav SP, Banerjee AK. 2010. Histidine-mediated RNA transfer to GDP for unique mRNA capping by vesicular stomatitis virus RNA polymerase. Proc Natl Acad Sci U S A 107:3463-8.
158. Ferron F, Longhi S, Henrissat B, Canard B. 2002. Viral RNA-polymerases -- a predicted 2'-O-ribose methyltransferase domain shared by all Mononegavirales. Trends Biochem Sci 27:222-4.
159. Bujnicki JM, Rychlewski L. 2002. In silico identification, structure prediction and phylogenetic analysis of the 2'-O-ribose (cap 1) methyltransferase domain in the large structural protein of ssRNA negative-strand viruses. Protein Eng 15:101-8.
160. Li J, Fontaine-Rodriguez EC, Whelan SP. 2005. Amino acid residues within conserved domain VI of the vesicular stomatitis virus large polymerase protein essential for mRNA cap methyltransferase activity. J Virol 79:13373-84.

161. Rahmeh AA, Li J, Kranzusch PJ, Whelan SP. 2009. Ribose 2'-O methylation of the vesicular stomatitis virus mRNA cap precedes and facilitates subsequent guanine-N-7 methylation by the large polymerase protein. J Virol 83:11043-50.
162. Testa D, Banerjee AK. 1977. Two methyltransferase activities in the purified virions of vesicular stomatitis virus. J Virol 24:786-93.
163. Liang B, Li Z, Jenni S, Rahmeh AA, Morin BM, Grant T, Grigorieff N, Harrison SC, Whelan SPJ. 2015. Structure of the L Protein of Vesicular Stomatitis Virus from Electron Cryomicroscopy. Cell 162:314-327.
164. Egloff MP, Benarroch D, Selisko B, Romette JL, Canard B. 2002. An RNA cap (nucleoside-2'-O-)-methyltransferase in the flavivirus RNA polymerase NS5: crystal structure and functional characterization. EMBO J 21:2757-68.
165. Zhou Y, Ray D, Zhao Y, Dong H, Ren S, Li Z, Guo Y, Bernard KA, Shi PY, Li H. 2007. Structure and function of flavivirus NS5 methyltransferase. J Virol 81:3891-903.
166. Vasiljeva L, Merits A, Auvinen P, Kaariainen L. 2000. Identification of a novel function of the alphavirus capping apparatus. RNA 5'-triphosphatase activity of Nsp2. J Biol Chem 275:17281-7.
167. Ahola T, Kaariainen L. 1995. Reaction in alphavirus mRNA capping: formation of a covalent complex of nonstructural protein nsP1 with 7-methyl-GMP. Proc Natl Acad Sci U S A 92:507-11.
168. Ahola T, Laakkonen P, Vihinen H, Kaariainen L. 1997. Critical residues of Semliki Forest virus RNA capping enzyme involved in methyltransferase and guanylyltransferase-like activities. J Virol 71:392-7.
169. van Duijn LP, Kasperaitis M, Ameling C, Voorma HO. 1986. Additional methylation at the N(2)-position of the cap of 26S Semliki Forest virus late mRNA and initiation of translation. Virus Res 5:61-6.
170. HsuChen CC, Dubin DT. 1976. Di-and trimethylated congeners of 7-methylguanine in Sindbis virus mRNA. Nature 264:190-1.
171. Bouloy M, Plotch SJ, Krug RM. 1978. Globin mRNAs are primers for the transcription of influenza viral RNA in vitro. Proc Natl Acad Sci U S A 75:4886-90.
172. Caton AJ, Robertson JS. 1980. Structure of the host-derived sequences present at the 5' ends of influenza virus mRNA. Nucleic Acids Res 8:2591-603.
173. Plotch SJ, Bouloy M, Krug RM. 1979. Transfer of 5'-terminal cap of globin mRNA to influenza viral complementary RNA during transcription in vitro. Proc Natl Acad Sci U S A 76:1618-22.
174. Bishop DH, Gay ME, Matsuoko Y. 1983. Nonviral heterogeneous sequences are present at the 5' ends of one species of snowshoe hare bunyavirus S complementary RNA. Nucleic Acids Res 11:6409-18.
175. Bouloy M, Pardigon N, Vialat P, Gerbaud S, Girard M. 1990. Characterization of the 5' and 3' ends of viral messenger RNAs isolated from BHK21 cells infected with Germiston virus (Bunyavirus). Virology 175:50-8.
176. Eshita Y, Ericson B, Romanowski V, Bishop DH. 1985. Analyses of the mRNA transcription processes of snowshoe hare bunyavirus S and M RNA species. J Virol 55:681-9.
177. Garcin D, Lezzi M, Dobbs M, Elliott RM, Schmaljohn C, Kang CY, Kolakofsky D. 1995. The 5' ends of Hantaan virus (Bunyaviridae) RNAs suggest a prime-and-realign mechanism for the initiation of RNA synthesis. J Virol 69:5754-62.
178. Jin H, Elliott RM. 1993. Non-viral sequences at the 5' ends of Dugbe nairovirus S mRNAs. J Gen Virol 74 (Pt 10):2293-7.

179. Raju R, Raju L, Hacker D, Garcin D, Compans R, Kolakofsky D. 1990. Nontemplated bases at the 5' ends of Tacaribe virus mRNAs. Virology 174:53-9.
180. Weber F, Haller O, Kochs G. 1996. Nucleoprotein viral RNA and mRNA of Thogoto virus: a novel "cap-stealing" mechanism in tick-borne orthomyxoviruses? J Virol 70:8361-7.
181. Guilligay D, Tarendeau F, Resa-Infante P, Coloma R, Crepin T, Sehr P, Lewis J, Ruigrok RW, Ortin J, Hart DJ, Cusack S. 2008. The structural basis for cap binding by influenza virus polymerase subunit PB2. Nat Struct Mol Biol 15:500-6.
182. Dias A, Bouvier D, Crepin T, McCarthy AA, Hart DJ, Baudin F, Cusack S, Ruigrok RW. 2009. The cap-snatching endonuclease of influenza virus polymerase resides in the PA subunit. Nature 458:914-8.
183. Yuan P, Bartlam M, Lou Z, Chen S, Zhou J, He X, Lv Z, Ge R, Li X, Deng T, Fodor E, Rao Z, Liu Y. 2009. Crystal structure of an avian influenza polymerase PA(N) reveals an endonuclease active site. Nature 458:909-13.
184. Reguera J, Gerlach P, Rosenthal M, Gaudon S, Coscia F, Gunther S, Cusack S. 2016. Comparative Structural and Functional Analysis of Bunyavirus and Arenavirus Cap-Snatching Endonucleases. PLoS Pathog 12:e1005636.
185. Qi X, Lan S, Wang W, Schelde LM, Dong H, Wallat GD, Ly H, Liang Y, Dong C. 2010. Cap binding and immune evasion revealed by Lassa nucleoprotein structure. Nature 468:779-83.
186. Mir MA, Duran WA, Hjelle BL, Ye C, Panganiban AT. 2008. Storage of cellular 5' mRNA caps in P bodies for viral cap-snatching. Proc Natl Acad Sci U S A 105:19294-9.
187. Tajima S, Nukui Y, Takasaki T, Kurane I. 2007. Characterization of the variable region in the 3' non-translated region of dengue type 1 virus. J Gen Virol 88:2214-22.
188. Miller S, Sparacio S, Bartenschlager R. 2006. Subcellular localization and membrane topology of the Dengue virus type 2 Non-structural protein 4B. J Biol Chem 281:8854-63.
189. Steegmaier M, Oorschot V, Klumperman J, Scheller RH. 2000. Syntaxin 17 is abundant in steroidogenic cells and implicated in smooth endoplasmic reticulum membrane dynamics. Mol Biol Cell 11:2719-31.
190. Mackenzie JM, Jones MK, Young PR. 1996. Immunolocalization of the dengue virus nonstructural glycoprotein NS1 suggests a role in viral RNA replication. Virology 220:232-40.
191. Miller S, Kastner S, Krijnse-Locker J, Buhler S, Bartenschlager R. 2007. The non-structural protein 4A of dengue virus is an integral membrane protein inducing membrane alterations in a 2K-regulated manner. J Biol Chem 282:8873-82.
192. Lindenbach BD, Rice CM. 1999. Genetic interaction of flavivirus nonstructural proteins NS1 and NS4A as a determinant of replicase function. J Virol 73:4611-21.
193. Khromykh AA, Sedlak PL, Westaway EG. 2000. cis- and trans-acting elements in flavivirus RNA replication. J Virol 74:3253-63.
194. Lindenbach BD, Rice CM. 1997. trans-Complementation of yellow fever virus NS1 reveals a role in early RNA replication. J Virol 71:9608-17.
195. Umareddy I, Chao A, Sampath A, Gu F, Vasudevan SG. 2006. Dengue virus NS4B interacts with NS3 and dissociates it from single-stranded RNA. J Gen Virol 87:2605-14.
196. Benarroch D, Selisko B, Locatelli GA, Maga G, Romette JL, Canard B. 2004. The RNA helicase, nucleotide 5'-triphosphatase, and RNA 5'-triphosphatase activities of Dengue virus protein NS3 are Mg2+-dependent and require a functional Walker B motif in the helicase catalytic core. Virology 328:208-18.

197. Erbel P, Schiering N, D'Arcy A, Renatus M, Kroemer M, Lim SP, Yin Z, Keller TH, Vasudevan SG, Hommel U. 2006. Structural basis for the activation of flaviviral NS3 proteases from dengue and West Nile virus. Nat Struct Mol Biol 13:372-3.
198. Aleshin AE, Shiryaev SA, Strongin AY, Liddington RC. 2007. Structural evidence for regulation and specificity of flaviviral proteases and evolution of the Flaviviridae fold. Protein Sci 16:795-806.
199. Matusan AE, Pryor MJ, Davidson AD, Wright PJ. 2001. Mutagenesis of the Dengue virus type 2 NS3 protein within and outside helicase motifs: effects on enzyme activity and virus replication. J Virol 75:9633-43.
200. Falgout B, Miller RH, Lai CJ. 1993. Deletion analysis of dengue virus type 4 nonstructural protein NS2B: identification of a domain required for NS2B-NS3 protease activity. J Virol 67:2034-42.
201. Lescar J, Luo D, Xu T, Sampath A, Lim SP, Canard B, Vasudevan SG. 2008. Towards the design of antiviral inhibitors against flaviviruses: the case for the multifunctional NS3 protein from Dengue virus as a target. Antiviral Res 80:94-101.
202. Luo D, Xu T, Hunke C, Gruber G, Vasudevan SG, Lescar J. 2008. Crystal structure of the NS3 protease-helicase from dengue virus. J Virol 82:173-83.
203. Luo D, Xu T, Watson RP, Scherer-Becker D, Sampath A, Jahnke W, Yeong SS, Wang CH, Lim SP, Strongin A, Vasudevan SG, Lescar J. 2008. Insights into RNA unwinding and ATP hydrolysis by the flavivirus NS3 protein. EMBO J 27:3209-19.
204. Noble CG, Seh CC, Chao AT, Shi PY. 2012. Ligand-bound structures of the dengue virus protease reveal the active conformation. J Virol 86:438-46.
205. Noble CG, Shi PY. 2012. Structural biology of dengue virus enzymes: towards rational design of therapeutics. Antiviral Res 96:115-26.
206. Xu T, Sampath A, Chao A, Wen D, Nanao M, Chene P, Vasudevan SG, Lescar J. 2005. Structure of the Dengue virus helicase/nucleoside triphosphatase catalytic domain at a resolution of 2.4 A. J Virol 79:10278-88.
207. Dong H, Chang DC, Xie X, Toh YX, Chung KY, Zou G, Lescar J, Lim SP, Shi PY. 2010. Biochemical and genetic characterization of dengue virus methyltransferase. Virology 405:568-78.
208. Tan BH, Fu J, Sugrue RJ, Yap EH, Chan YC, Tan YH. 1996. Recombinant dengue type 1 virus NS5 protein expressed in Escherichia coli exhibits RNA-dependent RNA polymerase activity. Virology 216:317-25.
209. Blackwell JL, Brinton MA. 1997. Translation elongation factor-1 alpha interacts with the 3' stem-loop region of West Nile virus genomic RNA. J Virol 71:6433-44.
210. De Nova-Ocampo M, Villegas-Sepulveda N, del Angel RM. 2002. Translation elongation factor-1alpha, La, and PTB interact with the 3' untranslated region of dengue 4 virus RNA. Virology 295:337-47.
211. Li W, Li Y, Kedersha N, Anderson P, Emara M, Swiderek KM, Moreno GT, Brinton MA. 2002. Cell proteins TIA-1 and TIAR interact with the 3' stem-loop of the West Nile virus complementary minus-strand RNA and facilitate virus replication. J Virol 76:11989-2000.
212. Yocupicio-Monroy RM, Medina F, Reyes-del Valle J, del Angel RM. 2003. Cellular proteins from human monocytes bind to dengue 4 virus minus-strand 3' untranslated region RNA. J Virol 77:3067-76.
213. Garcia-Montalvo BM, Medina F, del Angel RM. 2004. La protein binds to NS5 and NS3 and to the 5' and 3' ends of Dengue 4 virus RNA. Virus Res 102:141-50.
214. Paranjape SM, Harris E. 2007. Y box-binding protein-1 binds to the dengue virus 3'-untranslated region and mediates antiviral effects. J Biol Chem 282:30497-508.

215. Agis-Juarez RA, Galvan I, Medina F, Daikoku T, Padmanabhan R, Ludert JE, del Angel RM. 2009. Polypyrimidine tract-binding protein is relocated to the cytoplasm and is required during dengue virus infection in Vero cells. J Gen Virol 90:2893-901.
216. Anwar A, Leong KM, Ng ML, Chu JJ, Garcia-Blanco MA. 2009. The polypyrimidine tract-binding protein is required for efficient dengue virus propagation and associates with the viral replication machinery. J Biol Chem 284:17021-9.
217. Jiang L, Yao H, Duan X, Lu X, Liu Y. 2009. Polypyrimidine tract-binding protein influences negative strand RNA synthesis of dengue virus. Biochem Biophys Res Commun 385:187-92.
218. Emara MM, Brinton MA. 2007. Interaction of TIA-1/TIAR with West Nile and dengue virus products in infected cells interferes with stress granule formation and processing body assembly. Proc Natl Acad Sci U S A 104:9041-6.
219. Yocupicio-Monroy M, Padmanabhan R, Medina F, del Angel RM. 2007. Mosquito La protein binds to the 3' untranslated region of the positive and negative polarity dengue virus RNAs and relocates to the cytoplasm of infected cells. Virology 357:29-40.
220. Cleaves GR, Ryan TE, Schlesinger RW. 1981. Identification and characterization of type 2 dengue virus replicative intermediate and replicative form RNAs. Virology 111:73-83.
221. Chu PW, Westaway EG. 1985. Replication strategy of Kunjin virus: evidence for recycling role of replicative form RNA as template in semiconservative and asymmetric replication. Virology 140:68-79.
222. Koonin EV. 1993. Computer-assisted identification of a putative methyltransferase domain in NS5 protein of flaviviruses and lambda 2 protein of reovirus. J Gen Virol 74 (Pt 4):733-40.
223. Koonin EV. 1991. The phylogeny of RNA-dependent RNA polymerases of positive-strand RNA viruses. J Gen Virol 72 (Pt 9):2197-206.
224. Kapoor M, Zhang L, Ramachandra M, Kusukawa J, Ebner KE, Padmanabhan R. 1995. Association between NS3 and NS5 proteins of dengue virus type 2 in the putative RNA replicase is linked to differential phosphorylation of NS5. J Biol Chem 270:19100-6.
225. Best SM, Morris KL, Shannon JG, Robertson SJ, Mitzel DN, Park GS, Boer E, Wolfinbarger JB, Bloom ME. 2005. Inhibition of interferon-stimulated JAK-STAT signaling by a tick-borne flavivirus and identification of NS5 as an interferon antagonist. J Virol 79:12828-39.
226. Lin RJ, Chang BL, Yu HP, Liao CL, Lin YL. 2006. Blocking of interferon-induced Jak-Stat signaling by Japanese encephalitis virus NS5 through a protein tyrosine phosphatase-mediated mechanism. J Virol 80:5908-18.
227. Medin CL, Fitzgerald KA, Rothman AL. 2005. Dengue virus nonstructural protein NS5 induces interleukin-8 transcription and secretion. J Virol 79:11053-61.
228. Werme K, Wigerius M, Johansson M. 2008. Tick-borne encephalitis virus NS5 associates with membrane protein scribble and impairs interferon-stimulated JAK-STAT signalling. Cell Microbiol 10:696-712.
229. Ashour J, Laurent-Rolle M, Shi PY, Garcia-Sastre A. 2009. NS5 of dengue virus mediates STAT2 binding and degradation. J Virol 83:5408-18.
230. Mazzon M, Jones M, Davidson A, Chain B, Jacobs M. 2009. Dengue virus NS5 inhibits interferon-alpha signaling by blocking signal transducer and activator of transcription 2 phosphorylation. J Infect Dis 200:1261-70.
231. Dong H, Ray D, Ren S, Zhang B, Puig-Basagoiti F, Takagi Y, Ho CK, Li H, Shi PY. 2007. Distinct RNA elements confer specificity to flavivirus RNA cap methylation events. J Virol 81:4412-21.

232. Ferron F, Decroly E, Selisko B, Canard B. 2012. The viral RNA capping machinery as a target for antiviral drugs. Antiviral Res 96:21-31.
233. Warrener P, Tamura JK, Collett MS. 1993. RNA-stimulated NTPase activity associated with yellow fever virus NS3 protein expressed in bacteria. J Virol 67:989-96.
234. Kuo MD, Chin C, Hsu SL, Shiao JY, Wang TM, Lin JH. 1996. Characterization of the NTPase activity of Japanese encephalitis virus NS3 protein. J Gen Virol 77 (Pt 9):2077-84.
235. Bollati M, Milani M, Mastrangelo E, Ricagno S, Tedeschi G, Nonnis S, Decroly E, Selisko B, de Lamballerie X, Coutard B, Canard B, Bolognesi M. 2009. Recognition of RNA cap in the Wesselsbron virus NS5 methyltransferase domain: implications for RNA-capping mechanisms in Flavivirus. J Mol Biol 385:140-52.
236. Dong H, Chang DC, Hua MH, Lim SP, Chionh YH, Hia F, Lee YH, Kukkaro P, Lok SM, Dedon PC, Shi PY. 2012. 2'-O methylation of internal adenosine by flavivirus NS5 methyltransferase. PLoS Pathog 8:e1002642.
237. Noble CG, Li SH, Dong H, Chew SH, Shi PY. 2014. Crystal structure of dengue virus methyltransferase without S-adenosyl-L-methionine. Antiviral Res 111:78-81.
238. Yap LJ, Luo D, Chung KY, Lim SP, Bodenreider C, Noble C, Shi PY, Lescar J. 2010. Crystal structure of the dengue virus methyltransferase bound to a 5'-capped octameric RNA. PLoS One 5.
239. Dong H, Ren S, Zhang B, Zhou Y, Puig-Basagoiti F, Li H, Shi PY. 2008. West Nile virus methyltransferase catalyzes two methylations of the viral RNA cap through a substrate-repositioning mechanism. J Virol 82:4295-307.
240. Lim SP, Wen D, Yap TL, Yan CK, Lescar J, Vasudevan SG. 2008. A scintillation proximity assay for dengue virus NS5 2'-O-methyltransferase-kinetic and inhibition analyses. Antiviral Res 80:360-9.
241. Lim SP, Bodenreider C, Shi PY. 2013. Detection and quantification of flavivirus NS5 methyl-transferase activities. Methods Mol Biol 1030:249-68.
242. Lim SP, Wang QY, Noble CG, Chen YL, Dong H, Zou B, Yokokawa F, Nilar S, Smith P, Beer D, Lescar J, Shi PY. 2013. Ten years of dengue drug discovery: progress and prospects. Antiviral Res 100:500-19.
243. Noble CG, Chen YL, Dong H, Gu F, Lim SP, Schul W, Wang QY, Shi PY. 2010. Strategies for development of Dengue virus inhibitors. Antiviral Res 85:450-62.
244. Li SH, Dong H, Li XF, Xie X, Zhao H, Deng YQ, Wang XY, Ye Q, Zhu SY, Wang HJ, Zhang B, Leng QB, Zuest R, Qin ED, Qin CF, Shi PY. 2013. Rational design of a flavivirus vaccine by abolishing viral RNA 2'-O methylation. J Virol 87:5812-9.
245. Zust R, Dong H, Li XF, Chang DC, Zhang B, Balakrishnan T, Toh YX, Jiang T, Li SH, Deng YQ, Ellis BR, Ellis EM, Poidinger M, Zolezzi F, Qin CF, Shi PY, Fink K. 2013. Rational design of a live attenuated dengue vaccine: 2'-o-methyltransferase mutants are highly attenuated and immunogenic in mice and macaques. PLoS Pathog 9:e1003521.
246. You S, Padmanabhan R. 1999. A novel in vitro replication system for Dengue virus. Initiation of RNA synthesis at the 3'-end of exogenous viral RNA templates requires 5'- and 3'-terminal complementary sequence motifs of the viral RNA. J Biol Chem 274:33714-22.
247. Selisko B, Dutartre H, Guillemot JC, Debarnot C, Benarroch D, Khromykh A, Despres P, Egloff MP, Canard B. 2006. Comparative mechanistic studies of de novo RNA synthesis by flavivirus RNA-dependent RNA polymerases. Virology 351:145-58.

248. Nomaguchi M, Teramoto T, Yu L, Markoff L, Padmanabhan R. 2004. Requirements for West Nile virus (-)- and (+)-strand subgenomic RNA synthesis in vitro by the viral RNA-dependent RNA polymerase expressed in Escherichia coli. J Biol Chem 279:12141-51.
249. Selisko B, Potisopon S, Agred R, Priet S, Varlet I, Thillier Y, Sallamand C, Debart F, Vasseur JJ, Canard B. 2012. Molecular basis for nucleotide conservation at the ends of the dengue virus genome. PLoS Pathog 8:e1002912.
250. Firoz A, Malik A, Joplin KH, Ahmad Z, Jha V, Ahmad S. 2011. Residue propensities, discrimination and binding site prediction of adenine and guanine phosphates. BMC Biochem 12:20.
251. Zhang B, Dong H, Zhou Y, Shi PY. 2008. Genetic interactions among the West Nile virus methyltransferase, the RNA-dependent RNA polymerase, and the 5' stem-loop of genomic RNA. J Virol 82:7047-58.
252. Tan CS, Hobson-Peters JM, Stoermer MJ, Fairlie DP, Khromykh AA, Hall RA. 2013. An interaction between the methyltransferase and RNA dependent RNA polymerase domains of the West Nile virus NS5 protein. J Gen Virol 94:1961-71.
253. Potisopon S, Priet S, Collet A, Decroly E, Canard B, Selisko B. 2014. The methyltransferase domain of dengue virus protein NS5 ensures efficient RNA synthesis initiation and elongation by the polymerase domain. Nucleic Acids Res 42:11642-56.
254. Bussetta C, Choi KH. 2012. Dengue virus nonstructural protein 5 adopts multiple conformations in solution. Biochemistry 51:5921-31.
255. Fang J, Li H, Kong D, Cao S, Peng G, Zhou R, Chen H, Song Y. 2016. Structure-based discovery of two antiviral inhibitors targeting the NS3 helicase of Japanese encephalitis virus. Sci Rep 6:34550.
256. Sweeney NL, Hanson AM, Mukherjee S, Ndjomou J, Geiss BJ, Steel JJ, Frankowski KJ, Li K, Schoenen FJ, Frick DN. 2015. Benzothiazole and Pyrrolone Flavivirus Inhibitors Targeting the Viral Helicase. ACS Infect Dis 1:140-148.
257. Byrd CM, Grosenbach DW, Berhanu A, Dai D, Jones KF, Cardwell KB, Schneider C, Yang G, Tyavanagimatt S, Harver C, Wineinger KA, Page J, Stavale E, Stone MA, Fuller KP, Lovejoy C, Leeds JM, Hruby DE, Jordan R. 2013. Novel benzoxazole inhibitor of dengue virus replication that targets the NS3 helicase. Antimicrob Agents Chemother 57:1902-12.
258. Mastrangelo E, Pezzullo M, De Burghgraeve T, Kaptein S, Pastorino B, Dallmeier K, de Lamballerie X, Neyts J, Hanson AM, Frick DN, Bolognesi M, Milani M. 2012. Ivermectin is a potent inhibitor of flavivirus replication specifically targeting NS3 helicase activity: new prospects for an old drug. J Antimicrob Chemother 67:1884-94.
259. Li K, Frankowski KJ, Hanson AM, Ndjomou J, Shanahan MA, Mukherjee S, Kolli R, Shadrick WR, Sweeney NL, Belon CA, Neuenswander B, Ferguson J, Aube J, Schoenen FJ, Blagg BSJ, Frick DN. 2010. Hepatitis C Virus NS3 Helicase Inhibitor Discovery, Probe Reports from the NIH Molecular Libraries Program, Bethesda (MD).
260. de Sousa LR, Wu H, Nebo L, Fernandes JB, da Silva MF, Kiefer W, Kanitz M, Bodem J, Diederich WE, Schirmeister T, Vieira PC. 2015. Flavonoids as noncompetitive inhibitors of Dengue virus NS2B-NS3 protease: inhibition kinetics and docking studies. Bioorg Med Chem 23:466-70.
261. Wu H, Bock S, Snitko M, Berger T, Weidner T, Holloway S, Kanitz M, Diederich WE, Steuber H, Walter C, Hofmann D, Weissbrich B, Spannaus R, Acosta EG, Bartenschlager R, Engels B, Schirmeister T, Bodem J. 2015. Novel dengue virus NS2B/NS3 protease inhibitors. Antimicrob Agents Chemother 59:1100-9.

262. Liu H, Wu R, Sun Y, Ye Y, Chen J, Luo X, Shen X, Liu H. 2014. Identification of novel thiadiazoloacrylamide analogues as inhibitors of dengue-2 virus NS2B/NS3 protease. Bioorg Med Chem 22:6344-52.
263. Pambudi S, Kawashita N, Phanthanawiboon S, Omokoko MD, Masrinoul P, Yamashita A, Limkittikul K, Yasunaga T, Takagi T, Ikuta K, Kurosu T. 2013. A small compound targeting the interaction between nonstructural proteins 2B and 3 inhibits dengue virus replication. Biochem Biophys Res Commun 440:393-8.
264. Lei J, Hansen G, Nitsche C, Klein CD, Zhang L, Hilgenfeld R. 2016. Crystal structure of Zika virus NS2B-NS3 protease in complex with a boronate inhibitor. Science 353:503-5.
265. Stahla-Beek HJ, April DG, Saeedi BJ, Hannah AM, Keenan SM, Geiss BJ. 2012. Identification of a novel antiviral inhibitor of the flavivirus guanylyltransferase enzyme. J Virol 86:8730-9.
266. Benarroch D, Egloff MP, Mulard L, Guerreiro C, Romette JL, Canard B. 2004. A structural basis for the inhibition of the NS5 dengue virus mRNA 2'-O-methyltransferase domain by ribavirin 5'-triphosphate. J Biol Chem 279:35638-43.
267. Bullard KM, Gullberg RC, Soltani E, Steel JJ, Geiss BJ, Keenan SM. 2015. Murine Efficacy and Pharmacokinetic Evaluation of the Flaviviral NS5 Capping Enzyme 2-Thioxothiazolidin-4-One Inhibitor BG-323. PLoS One 10:e0130083.
268. Ramirez MA, Borja NL. 2008. Epalrestat: an aldose reductase inhibitor for the treatment of diabetic neuropathy. Pharmacotherapy 28:646-55.
269. Witkowski JT, Robins RK, Sidwell RW, Simon LN. 1972. Design, synthesis, and broad spectrum antiviral activity of 1- -D-ribofuranosyl-1,2,4-triazole-3-carboxamide and related nucleosides. J Med Chem 15:1150-4.
270. McHutchison JG, Gordon SC, Schiff ER, Shiffman ML, Lee WM, Rustgi VK, Goodman ZD, Ling MH, Cort S, Albrecht JK. 1998. Interferon alfa-2b alone or in combination with ribavirin as initial treatment for chronic hepatitis C. Hepatitis Interventional Therapy Group. N Engl J Med 339:1485-92.
271. Landau A, Batisse D, Piketty C, Duong Van Huyen JP, Bloch F, Belec L, Bruneval P, Weiss L, Jian R, Kazatchkine MD. 2001. Long-term efficacy of combination therapy with interferon-alpha 2b and ribavirin for severe chronic hepatitis C in HIV-infected patients. AIDS 15:2149-55.
272. Zust R, Cervantes-Barragan L, Habjan M, Maier R, Neuman BW, Ziebuhr J, Szretter KJ, Baker SC, Barchet W, Diamond MS, Siddell SG, Ludewig B, Thiel V. 2011. Ribose 2'-O-methylation provides a molecular signature for the distinction of self and non-self mRNA dependent on the RNA sensor Mda5. Nat Immunol 12:137-43.
273. Dong H, Liu L, Zou G, Zhao Y, Li Z, Lim SP, Shi PY, Li H. 2010. Structural and functional analyses of a conserved hydrophobic pocket of flavivirus methyltransferase. J Biol Chem 285:32586-95.
274. Brecher MB, Li Z, Zhang J, Chen H, Lin Q, Liu B, Li H. 2015. Refolding of a fully functional flavivirus methyltransferase revealed that S-adenosyl methionine but not S-adenosyl homocysteine is copurified with flavivirus methyltransferase. Protein Sci 24:117-28.
275. Chung KY, Dong H, Chao AT, Shi PY, Lescar J, Lim SP. 2010. Higher catalytic efficiency of N-7-methylation is responsible for processive N-7 and 2'-O methyltransferase activity in dengue virus. Virology 402:52-60.
276. Lim SP, Sonntag LS, Noble C, Nilar SH, Ng RH, Zou G, Monaghan P, Chung KY, Dong H, Liu B, Bodenreider C, Lee G, Ding M, Chan WL, Wang G, Jian YL, Chao AT, Lescar J, Yin Z, Vedananda TR, Keller TH, Shi PY. 2011. Small molecule

inhibitors that selectively block dengue virus methyltransferase. J Biol Chem 286:6233-40.
277. Lim SV, Rahman MB, Tejo BA. 2011. Structure-based and ligand-based virtual screening of novel methyltransferase inhibitors of the dengue virus. BMC Bioinformatics 12 Suppl 13:S24.
278. Luzhkov VB, Selisko B, Nordqvist A, Peyrane F, Decroly E, Alvarez K, Karlen A, Canard B, Qvist J. 2007. Virtual screening and bioassay study of novel inhibitors for dengue virus mRNA cap (nucleoside-2'O)-methyltransferase. Bioorg Med Chem 15:7795-802.
279. Milani M, Mastrangelo E, Bollati M, Selisko B, Decroly E, Bouvet M, Canard B, Bolognesi M. 2009. Flaviviral methyltransferase/RNA interaction: structural basis for enzyme inhibition. Antiviral Res 83:28-34.
280. Podvinec M, Lim SP, Schmidt T, Scarsi M, Wen D, Sonntag LS, Sanschagrin P, Shenkin PS, Schwede T. 2010. Novel inhibitors of dengue virus methyltransferase: discovery by in vitro-driven virtual screening on a desktop computer grid. J Med Chem 53:1483-95.
281. Brecher M, Chen H, Liu B, Banavali NK, Jones SA, Zhang J, Li Z, Kramer LD, Li H. 2015. Novel Broad Spectrum Inhibitors Targeting the Flavivirus Methyltransferase. PLoS One 10:e0130062.
282. Benmansour F, Trist I, Coutard B, Decroly E, Querat G, Brancale A, Barral K. 2017. Discovery of novel dengue virus NS5 methyltransferase non-nucleoside inhibitors by fragment-based drug design. Eur J Med Chem 125:865-880.
283. Crotty S, Maag D, Arnold JJ, Zhong W, Lau JY, Hong Z, Andino R, Cameron CE. 2000. The broad-spectrum antiviral ribonucleoside ribavirin is an RNA virus mutagen. Nat Med 6:1375-9.
284. De Clercq E, Neyts J. 2009. Antiviral agents acting as DNA or RNA chain terminators. Handb Exp Pharmacol doi:10.1007/978-3-540-79086-0_3:53-84.
285. Gilbert BE, Wilson SZ, Knight V, Couch RB, Quarles JM, Dure L, Hayes N, Willis G. 1985. Ribavirin small-particle aerosol treatment of infections caused by influenza virus strains A/Victoria/7/83 (H1N1) and B/Texas/1/84. Antimicrob Agents Chemother 27:309-13.
286. McCormick JB, King IJ, Webb PA, Scribner CL, Craven RB, Johnson KM, Elliott LH, Belmont-Williams R. 1986. Lassa fever. Effective therapy with ribavirin. N Engl J Med 314:20-6.
287. Huggins JW, Kim GR, Brand OM, McKee KT, Jr. 1986. Ribavirin therapy for Hantaan virus infection in suckling mice. J Infect Dis 153:489-97.
288. Malinoski FJ, Hasty SE, Ussery MA, Dalrymple JM. 1990. Prophylactic ribavirin treatment of dengue type 1 infection in rhesus monkeys. Antiviral Res 13:139-49.
289. Leyssen P, De Clercq E, Neyts J. 2000. Perspectives for the treatment of infections with Flaviviridae. Clin Microbiol Rev 13:67-82, table of contents.
290. Huggins JW. 1989. Prospects for treatment of viral hemorrhagic fevers with ribavirin, a broad-spectrum antiviral drug. Rev Infect Dis 11 Suppl 4:S750-61.
291. Cote HC, Brumme ZL, Craib KJ, Alexander CS, Wynhoven B, Ting L, Wong H, Harris M, Harrigan PR, O'Shaughnessy MV, Montaner JS. 2002. Changes in mitochondrial DNA as a marker of nucleoside toxicity in HIV-infected patients. N Engl J Med 346:811-20.
292. Migliaccio G, Tomassini JE, Carroll SS, Tomei L, Altamura S, Bhat B, Bartholomew L, Bosserman MR, Ceccacci A, Colwell LF, Cortese R, De Francesco R, Eldrup AB, Getty KL, Hou XS, LaFemina RL, Ludmerer SW, MacCoss M, McMasters DR, Stahlhut MW, Olsen DB, Hazuda DJ, Flores OA. 2003. Characterization of resistance

to non-obligate chain-terminating ribonucleoside analogs that inhibit hepatitis C virus replication in vitro. J Biol Chem 278:49164-70.

293. Eldrup AB, Prhavc M, Brooks J, Bhat B, Prakash TP, Song Q, Bera S, Bhat N, Dande P, Cook PD, Bennett CF, Carroll SS, Ball RG, Bosserman M, Burlein C, Colwell LF, Fay JF, Flores OA, Getty K, LaFemina RL, Leone J, MacCoss M, McMasters DR, Tomassini JE, Von Langen D, Wolanski B, Olsen DB. 2004. Structure-activity relationship of heterobase-modified 2'-C-methyl ribonucleosides as inhibitors of hepatitis C virus RNA replication. J Med Chem 47:5284-97.
294. Olsen DB, Eldrup AB, Bartholomew L, Bhat B, Bosserman MR, Ceccacci A, Colwell LF, Fay JF, Flores OA, Getty KL, Grobler JA, LaFemina RL, Markel EJ, Migliaccio G, Prhavc M, Stahlhut MW, Tomassini JE, MacCoss M, Hazuda DJ, Carroll SS. 2004. A 7-deaza-adenosine analog is a potent and selective inhibitor of hepatitis C virus replication with excellent pharmacokinetic properties. Antimicrob Agents Chemother 48:3944-53.
295. Yin Z, Chen YL, Schul W, Wang QY, Gu F, Duraiswamy J, Kondreddi RR, Niyomrattanakit P, Lakshminarayana SB, Goh A, Xu HY, Liu W, Liu B, Lim JY, Ng CY, Qing M, Lim CC, Yip A, Wang G, Chan WL, Tan HP, Lin K, Zhang B, Zou G, Bernard KA, Garrett C, Beltz K, Dong M, Weaver M, He H, Pichota A, Dartois V, Keller TH, Shi PY. 2009. An adenosine nucleoside inhibitor of dengue virus. Proc Natl Acad Sci U S A 106:20435-9.
296. Vernachio JH, Bleiman B, Bryant KD, Chamberlain S, Hunley D, Hutchins J, Ames B, Gorovits E, Ganguly B, Hall A, Kolykhalov A, Liu Y, Muhammad J, Raja N, Walters CR, Wang J, Williams K, Patti JM, Henson G, Madela K, Aljarah M, Gilles A, McGuigan C. 2011. INX-08189, a phosphoramidate prodrug of 6-O-methyl-2'-C-methyl guanosine, is a potent inhibitor of hepatitis C virus replication with excellent pharmacokinetic and pharmacodynamic properties. Antimicrob Agents Chemother 55:1843-51.
297. Klumpp K, Leveque V, Le Pogam S, Ma H, Jiang WR, Kang H, Granycome C, Singer M, Laxton C, Hang JQ, Sarma K, Smith DB, Heindl D, Hobbs CJ, Merrett JH, Symons J, Cammack N, Martin JA, Devos R, Najera I. 2006. The novel nucleoside analog R1479 (4'-azidocytidine) is a potent inhibitor of NS5B-dependent RNA synthesis and hepatitis C virus replication in cell culture. J Biol Chem 281:3793-9.
298. Roberts SK, Cooksley G, Dore GJ, Robson R, Shaw D, Berns H, Hill G, Klumpp K, Najera I, Washington C. 2008. Robust antiviral activity of R1626, a novel nucleoside analog: a randomized, placebo-controlled study in patients with chronic hepatitis C. Hepatology 48:398-406.
299. Nelson DR, Zeuzem S, Andreone P, Ferenci P, Herring R, Jensen DM, Marcellin P, Pockros PJ, Rodriguez-Torres M, Rossaro L, Rustgi VK, Sepe T, Sulkowski M, Thomason IR, Yoshida EM, Chan A, Hill G. 2012. Balapiravir plus peginterferon alfa-2a (40KD)/ribavirin in a randomized trial of hepatitis C genotype 1 patients. Ann Hepatol 11:15-31.
300. Nguyen NM, Tran CN, Phung LK, Duong KT, Huynh Hle A, Farrar J, Nguyen QT, Tran HT, Nguyen CV, Merson L, Hoang LT, Hibberd ML, Aw PP, Wilm A, Nagarajan N, Nguyen DT, Pham MP, Nguyen TT, Javanbakht H, Klumpp K, Hammond J, Petric R, Wolbers M, Nguyen CT, Simmons CP. 2013. A randomized, double-blind placebo controlled trial of balapiravir, a polymerase inhibitor, in adult dengue patients. J Infect Dis 207:1442-50.
301. Sofia MJ. 2013. Nucleotide prodrugs for the treatment of HCV infection. Adv Pharmacol 67:39-73.

302. Gan CS, Lim SK, Chee CF, Yusof R, Heh CH. 2017. Sofosbuvir as treatment against dengue? Chem Biol Drug Des doi:10.1111/cbdd.13091.
303. Xu HT, Hassounah SA, Colby-Germinario SP, Oliveira M, Fogarty C, Quan Y, Han Y, Golubkov O, Ibanescu I, Brenner B, Stranix BR, Wainberg MA. 2017. Purification of Zika virus RNA-dependent RNA polymerase and its use to identify small-molecule Zika inhibitors. J Antimicrob Chemother 72:727-734.
304. Kukolj G, McGibbon GA, McKercher G, Marquis M, Lefebvre S, Thauvette L, Gauthier J, Goulet S, Poupart MA, Beaulieu PL. 2005. Binding site characterization and resistance to a class of non-nucleoside inhibitors of the hepatitis C virus NS5B polymerase. J Biol Chem 280:39260-7.
305. Tomei L, Altamura S, Bartholomew L, Biroccio A, Ceccacci A, Pacini L, Narjes F, Gennari N, Bisbocci M, Incitti I, Orsatti L, Harper S, Stansfield I, Rowley M, De Francesco R, Migliaccio G. 2003. Mechanism of action and antiviral activity of benzimidazole-based allosteric inhibitors of the hepatitis C virus RNA-dependent RNA polymerase. J Virol 77:13225-31.
306. Niyomrattanakit P, Chen YL, Dong H, Yin Z, Qing M, Glickman JF, Lin K, Mueller D, Voshol H, Lim JY, Nilar S, Keller TH, Shi PY. 2010. Inhibition of dengue virus polymerase by blocking of the RNA tunnel. J Virol 84:5678-86.
307. Niyomrattanakit P, Abas SN, Lim CC, Beer D, Shi PY, Chen YL. 2011. A fluorescence-based alkaline phosphatase-coupled polymerase assay for identification of inhibitors of dengue virus RNA-dependent RNA polymerase. J Biomol Screen 16:201-10.
308. Noble CG, Lim SP, Chen YL, Liew CW, Yap L, Lescar J, Shi PY. 2013. Conformational flexibility of the Dengue virus RNA-dependent RNA polymerase revealed by a complex with an inhibitor. J Virol 87:5291-5.
309. Sofia MJ, Chang W, Furman PA, Mosley RT, Ross BS. 2012. Nucleoside, nucleotide, and non-nucleoside inhibitors of hepatitis C virus NS5B RNA-dependent RNA-polymerase. J Med Chem 55:2481-531.
310. Brecher M, Chen H, Li Z, Banavali NK, Jones SA, Zhang J, Kramer LD, Li H. 2015. Identification and Characterization of Novel Broad-Spectrum Inhibitors of the Flavivirus Methyltransferase. ACS Infect Dis 1:340-9.
311. Appleby TC, Perry JK, Murakami E, Barauskas O, Feng J, Cho A, Fox D, 3rd, Wetmore DR, McGrath ME, Ray AS, Sofia MJ, Swaminathan S, Edwards TE. 2015. Viral replication. Structural basis for RNA replication by the hepatitis C virus polymerase. Science 347:771-5.
312. Klema VJ, Padmanabhan R, Choi KH. 2015. Flaviviral Replication Complex: Coordination between RNA Synthesis and 5'-RNA Capping. Viruses 7:4640-56.
313. Zou J, Lee le T, Wang QY, Xie X, Lu S, Yau YH, Yuan Z, Geifman Shochat S, Kang C, Lescar J, Shi PY. 2015. Mapping the Interactions between the NS4B and NS3 proteins of dengue virus. J Virol 89:3471-83.
314. Xie X, Gayen S, Kang C, Yuan Z, Shi PY. 2013. Membrane topology and function of dengue virus NS2A protein. J Virol 87:4609-22.
315. Lim SP, Koh JH, Seh CC, Liew CW, Davidson AD, Chua LS, Chandrasekaran R, Cornvik TC, Shi PY, Lescar J. 2013. A crystal structure of the dengue virus non-structural protein 5 (NS5) polymerase delineates interdomain amino acid residues that enhance its thermostability and de novo initiation activities. J Biol Chem 288:31105-14.
316. Hung M, Gibbs CS, Tsiang M. 2002. Biochemical characterization of rhinovirus RNA-dependent RNA polymerase. Antiviral Res 56:99-114.

317. Niyomrattanakit P, Wan KF, Chung KY, Abas SN, Seh CC, Dong H, Lim CC, Chao AT, Lee CB, Nilar S, Lescar J, Shi PY, Beer D, Lim SP. 2015. Stabilization of dengue virus polymerase in de novo initiation assay provides advantages for compound screening. Antiviral Res 119:36-46.
318. Zhao Y, Soh TS, Zheng J, Chan KW, Phoo WW, Lee CC, Tay MY, Swaminathan K, Cornvik TC, Lim SP, Shi PY, Lescar J, Vasudevan SG, Luo D. 2015. A crystal structure of the Dengue virus NS5 protein reveals a novel inter-domain interface essential for protein flexibility and virus replication. PLoS Pathog 11:e1004682.
319. Zhao Y, Soh TS, Chan KW, Fung SS, Swaminathan K, Lim SP, Shi PY, Huber T, Lescar J, Luo D, Vasudevan SG. 2015. Flexibility of NS5 Methyltransferase-Polymerase Linker Region Is Essential for Dengue Virus Replication. J Virol 89:10717-21.
320. Johansson M, Brooks AJ, Jans DA, Vasudevan SG. 2001. A small region of the dengue virus-encoded RNA-dependent RNA polymerase, NS5, confers interaction with both the nuclear transport receptor importin-beta and the viral helicase, NS3. J Gen Virol 82:735-45.
321. Brooks AJ, Johansson M, John AV, Xu Y, Jans DA, Vasudevan SG. 2002. The interdomain region of dengue NS5 protein that binds to the viral helicase NS3 contains independently functional importin beta 1 and importin alpha/beta-recognized nuclear localization signals. J Biol Chem 277:36399-407.
322. Uchil PD, Kumar AV, Satchidanandam V. 2006. Nuclear localization of flavivirus RNA synthesis in infected cells. J Virol 80:5451-64.
323. Hanley KA, Lee JJ, Blaney JE, Jr., Murphy BR, Whitehead SS. 2002. Paired charge-to-alanine mutagenesis of dengue virus type 4 NS5 generates mutants with temperature-sensitive, host range, and mouse attenuation phenotypes. J Virol 76:525-31.
324. Tay MY, Smith K, Ng IH, Chan KW, Zhao Y, Ooi EE, Lescar J, Luo D, Jans DA, Forwood JK, Vasudevan SG. 2016. The C-terminal 18 Amino Acid Region of Dengue Virus NS5 Regulates its Subcellular Localization and Contains a Conserved Arginine Residue Essential for Infectious Virus Production. PLoS Pathog 12:e1005886.
325. Zou G, Chen YL, Dong H, Lim CC, Yap LJ, Yau YH, Shochat SG, Lescar J, Shi PY. 2011. Functional analysis of two cavities in flavivirus NS5 polymerase. J Biol Chem 286:14362-72.
326. Yon C, Teramoto T, Mueller N, Phelan J, Ganesh VK, Murthy KH, Padmanabhan R. 2005. Modulation of the nucleoside triphosphatase/RNA helicase and 5'-RNA triphosphatase activities of Dengue virus type 2 nonstructural protein 3 (NS3) by interaction with NS5, the RNA-dependent RNA polymerase. J Biol Chem 280:27412-9.
327. Li XD, Shan C, Deng CL, Ye HQ, Shi PY, Yuan ZM, Gong P, Zhang B. 2014. The interface between methyltransferase and polymerase of NS5 is essential for flavivirus replication. PLoS Negl Trop Dis 8:e2891.
328. Potisopon S, Priet S, Collet A, Decroly E, Canard B, Selisko B. 2016. The methyltransferase domain of dengue virus protein NS5 ensures efficient RNA synthesis initiation and elongation by the polymerase domain. Nucleic Acids Res 44:2974.
329. Subramanian Manimekalai MS, Saw WG, Pan A, Gruber A, Gruber G. 2016. Identification of the critical linker residues conferring differences in the compactness of NS5 from Dengue virus serotype 4 and NS5 from Dengue virus serotypes 1-3. Acta Crystallogr D Struct Biol 72:795-807.

330. Saw WG, Tria G, Gruber A, Subramanian Manimekalai MS, Zhao Y, Chandramohan A, Srinivasan Anand G, Matsui T, Weiss TM, Vasudevan SG, Gruber G. 2015. Structural insight and flexible features of NS5 proteins from all four serotypes of Dengue virus in solution. Acta Crystallogr D Biol Crystallogr 71:2309-27.
331. Zhao Y, Soh TS, Lim SP, Chung KY, Swaminathan K, Vasudevan SG, Shi PY, Lescar J, Luo D. 2015. Molecular basis for specific viral RNA recognition and 2'-O-ribose methylation by the dengue virus nonstructural protein 5 (NS5). Proc Natl Acad Sci U S A 112:14834-9.
332. Geiss BJ, Thompson AA, Andrews AJ, Sons RL, Gari HH, Keenan SM, Peersen OB. 2009. Analysis of flavivirus NS5 methyltransferase cap binding. J Mol Biol 385:1643-54.
333. Hodel AE, Gershon PD, Shi X, Quiocho FA. 1996. The 1.85 A structure of vaccinia protein VP39: a bifunctional enzyme that participates in the modification of both mRNA ends. Cell 85:247-56.
334. Assenberg R, Ren J, Verma A, Walter TS, Alderton D, Hurrelbrink RJ, Fuller SD, Bressanelli S, Owens RJ, Stuart DI, Grimes JM. 2007. Crystal structure of the Murray Valley encephalitis virus NS5 methyltransferase domain in complex with cap analogues. J Gen Virol 88:2228-36.
335. Mastrangelo E, Bollati M, Milani M, Selisko B, Peyrane F, Canard B, Grard G, de Lamballerie X, Bolognesi M. 2007. Structural bases for substrate recognition and activity in Meaban virus nucleoside-2'-O-methyltransferase. Protein Sci 16:1133-45.
336. Liu L, Dong H, Chen H, Zhang J, Ling H, Li Z, Shi PY, Li H. 2010. Flavivirus RNA cap methyltransferase: structure, function, and inhibition. Front Biol (Beijing) 5:286-303.
337. Vidgren J, Svensson LA, Liljas A. 1994. Crystal structure of catechol O-methyltransferase. Nature 368:354-8.
338. Hager J, Staker BL, Bugl H, Jakob U. 2002. Active site in RrmJ, a heat shock-induced methyltransferase. J Biol Chem 277:41978-86.
339. Dong H, Zhang B, Shi PY. 2008. Terminal structures of West Nile virus genomic RNA and their interactions with viral NS5 protein. Virology 381:123-35.
340. Cerutti H, Casas-Mollano JA. 2006. On the origin and functions of RNA-mediated silencing: from protists to man. Curr Genet 50:81-99.
341. Keller TH, Chen YL, Knox JE, Lim SP, Ma NL, Patel SJ, Sampath A, Wang QY, Yin Z, Vasudevan SG. 2006. Finding new medicines for flaviviral targets. Novartis Found Symp 277:102-14; discussion 114-9, 251-3.
342. Yin Z, Chen YL, Kondreddi RR, Chan WL, Wang G, Ng RH, Lim JY, Lee WY, Jeyaraj DA, Niyomrattanakit P, Wen D, Chao A, Glickman JF, Voshol H, Mueller D, Spanka C, Dressler S, Nilar S, Vasudevan SG, Shi PY, Keller TH. 2009. N-sulfonylanthranilic acid derivatives as allosteric inhibitors of dengue viral RNA-dependent RNA polymerase. J Med Chem 52:7934-7.
343. Smith TM, Lim SP, Yue K, Busby SA, Arora R, Seh CC, Wright SK, Nutiu R, Niyomrattanakit P, Wan KF, Beer D, Shi PY, Benson TE. 2015. Identifying initiation and elongation inhibitors of dengue virus RNA polymerase in a high-throughput lead-finding campaign. J Biomol Screen 20:153-63.
344. Noble CG, Lim SP, Arora R, Yokokawa F, Nilar S, Seh CC, Wright SK, Benson TE, Smith PW, Shi PY. 2016. A Conserved Pocket in the Dengue Virus Polymerase Identified through Fragment-based Screening. J Biol Chem 291:8541-8.
345. Yokokawa F, Nilar S, Noble CG, Lim SP, Rao R, Tania S, Wang G, Lee G, Hunziker J, Karuna R, Manjunatha U, Shi PY, Smith PW. 2016. Discovery of Potent Non-

Nucleoside Inhibitors of Dengue Viral RNA-Dependent RNA Polymerase from a Fragment Hit Using Structure-Based Drug Design. J Med Chem 59:3935-52.
346. Lim SP, Noble CG, Seh CC, Soh TS, El Sahili A, Chan GK, Lescar J, Arora R, Benson T, Nilar S, Manjunatha U, Wan KF, Dong H, Xie X, Shi PY, Yokokawa F. 2016. Potent Allosteric Dengue Virus NS5 Polymerase Inhibitors: Mechanism of Action and Resistance Profiling. PLoS Pathog 12:e1005737.
347. Bhatia HK, Singh H, Grewal N, Natt NK. 2014. Sofosbuvir: A novel treatment option for chronic hepatitis C infection. J Pharmacol Pharmacother 5:278-84.
348. Sacramento CQ, de Melo GR, de Freitas CS, Rocha N, Hoelz LV, Miranda M, Fintelman-Rodrigues N, Marttorelli A, Ferreira AC, Barbosa-Lima G, Abrantes JL, Vieira YR, Bastos MM, de Mello Volotao E, Nunes EP, Tschoeke DA, Leomil L, Loiola EC, Trindade P, Rehen SK, Bozza FA, Bozza PT, Boechat N, Thompson FL, de Filippis AM, Bruning K, Souza TM. 2017. The clinically approved antiviral drug sofosbuvir inhibits Zika virus replication. Sci Rep 7:40920.
349. Bullard-Feibelman KM, Govero J, Zhu Z, Salazar V, Veselinovic M, Diamond MS, Geiss BJ. 2017. The FDA-approved drug sofosbuvir inhibits Zika virus infection. Antiviral Res 137:134-140.
350. Potisopon S, Ferron F, Fattorini V, Selisko B, Canard B. 2017. Substrate selectivity of Dengue and Zika virus NS5 polymerase towards 2'-modified nucleotide analogues. Antiviral Res 140:25-36.
351. Eyer L, Nencka R, Huvarova I, Palus M, Joao Alves M, Gould EA, De Clercq E, Ruzek D. 2016. Nucleoside Inhibitors of Zika Virus. J Infect Dis 214:707-11.
352. Chen YL, Yokokawa F, Shi PY. 2015. The search for nucleoside/nucleotide analog inhibitors of dengue virus. Antiviral Res 122:12-9.
353. Ferrer-Orta C, Arias A, Perez-Luque R, Escarmis C, Domingo E, Verdaguer N. 2004. Structure of foot-and-mouth disease virus RNA-dependent RNA polymerase and its complex with a template-primer RNA. J Biol Chem 279:47212-21.
354. Zamyatkin DF, Parra F, Alonso JM, Harki DA, Peterson BR, Grochulski P, Ng KK. 2008. Structural insights into mechanisms of catalysis and inhibition in Norwalk virus polymerase. J Biol Chem 283:7705-12.
355. Mosley RT, Edwards TE, Murakami E, Lam AM, Grice RL, Du J, Sofia MJ, Furman PA, Otto MJ. 2012. Structure of hepatitis C virus polymerase in complex with primer-template RNA. J Virol 86:6503-11.
356. Jin Z, Deval J, Johnson KA, Swinney DC. 2011. Characterization of the elongation complex of dengue virus RNA polymerase: assembly, kinetics of nucleotide incorporation, and fidelity. J Biol Chem 286:2067-77.
357. Arnold JJ, Cameron CE. 2000. Poliovirus RNA-dependent RNA polymerase (3D(pol)). Assembly of stable, elongation-competent complexes by using a symmetrical primer-template substrate (sym/sub). J Biol Chem 275:5329-36.
358. Huang Y, Beaudry A, McSwiggen J, Sousa R. 1997. Determinants of ribose specificity in RNA polymerization: effects of Mn2+ and deoxynucleoside monophosphate incorporation into transcripts. Biochemistry 36:13718-28.
359. Shim JH, Larson G, Wu JZ, Hong Z. 2002. Selection of 3'-template bases and initiating nucleotides by hepatitis C virus NS5B RNA-dependent RNA polymerase. J Virol 76:7030-9.
360. Hobdey SE, Kempf BJ, Steil BP, Barton DJ, Peersen OB. 2010. Poliovirus polymerase residue 5 plays a critical role in elongation complex stability. J Virol 84:8072-84.

361. Huang H, Chopra R, Verdine GL, Harrison SC. 1998. Structure of a covalently trapped catalytic complex of HIV-1 reverse transcriptase: implications for drug resistance. Science 282:1669-75.
362. Huang H, Harrison SC, Verdine GL. 2000. Trapping of a catalytic HIV reverse transcriptase*template:primer complex through a disulfide bond. Chem Biol 7:355-64.
363. Fung A, Jin Z, Dyatkina N, Wang G, Beigelman L, Deval J. 2014. Efficiency of incorporation and chain termination determines the inhibition potency of 2'-modified nucleotide analogs against hepatitis C virus polymerase. Antimicrob Agents Chemother 58:3636-45.
364. Campagnola G, Gong P, Peersen OB. 2011. High-throughput screening identification of poliovirus RNA-dependent RNA polymerase inhibitors. Antiviral Res 91:241-51.
365. Campagnola G, McDonald S, Beaucourt S, Vignuzzi M, Peersen OB. 2015. Structure-function relationships underlying the replication fidelity of viral RNA-dependent RNA polymerases. J Virol 89:275-86.
366. Zhao B, Yi G, Du F, Chuang YC, Vaughan RC, Sankaran B, Kao CC, Li P. 2017. Structure and function of the Zika virus full-length NS5 protein. Nat Commun 8:14762.
367. Upadhyay AK, Cyr M, Longenecker K, Tripathi R, Sun C, Kempf DJ. 2017. Crystal structure of full-length Zika virus NS5 protein reveals a conformation similar to Japanese encephalitis virus NS5. Acta Crystallogr F Struct Biol Commun 73:116-122.
368. Youn S, Ambrose RL, Mackenzie JM, Diamond MS. 2013. Non-structural protein-1 is required for West Nile virus replication complex formation and viral RNA synthesis. Virol J 10:339.
369. Ye J, Wang C, Sumpter R, Jr., Brown MS, Goldstein JL, Gale M, Jr. 2003. Disruption of hepatitis C virus RNA replication through inhibition of host protein geranylgeranylation. Proc Natl Acad Sci U S A 100:15865-70.
370. Gao L, Aizaki H, He JW, Lai MM. 2004. Interactions between viral nonstructural proteins and host protein hVAP-33 mediate the formation of hepatitis C virus RNA replication complex on lipid raft. J Virol 78:3480-8.
371. Rawlinson SM, Pryor MJ, Wright PJ, Jans DA. 2009. CRM1-mediated nuclear export of dengue virus RNA polymerase NS5 modulates interleukin-8 induction and virus production. J Biol Chem 284:15589-97.
372. Wagstaff KM, Sivakumaran H, Heaton SM, Harrich D, Jans DA. 2012. Ivermectin is a specific inhibitor of importin alpha/beta-mediated nuclear import able to inhibit replication of HIV-1 and dengue virus. Biochem J 443:851-6.
373. Lim SP, Noble CG, Shi PY. 2015. The dengue virus NS5 protein as a target for drug discovery. Antiviral Res 119:57-67.
374. Sampath A, Padmanabhan R. 2009. Molecular targets for flavivirus drug discovery. Antiviral Res 81:6-15.
375. Chen H, Liu L, Jones SA, Banavali N, Kass J, Li Z, Zhang J, Kramer LD, Ghosh AK, Li H. 2013. Selective inhibition of the West Nile virus methyltransferase by nucleoside analogs. Antiviral Res 97:232-9.
376. Puig-Basagoiti F, Qing M, Dong H, Zhang B, Zou G, Yuan Z, Shi PY. 2009. Identification and characterization of inhibitors of West Nile virus. Antiviral Res 83:71-9.
377. Lockless SW, Cheng HT, Hodel AE, Quiocho FA, Gershon PD. 1998. Recognition of capped RNA substrates by VP39, the vaccinia virus-encoded mRNA cap-specific 2'-O-methyltransferase. Biochemistry 37:8564-74.

378. Gentile I, Borgia F, Buonomo AR, Castaldo G, Borgia G. 2013. A novel promising therapeutic option against hepatitis C virus: an oral nucleotide NS5B polymerase inhibitor sofosbuvir. Curr Med Chem 20:3733-42.
379. Duan W, Song H, Wang H, Chai Y, Su C, Qi J, Shi Y, Gao GF. 2017. The crystal structure of Zika virus NS5 reveals conserved drug targets. EMBO J 36:919-933.
380. Yu L, Takeda K, Markoff L. 2013. Protein-protein interactions among West Nile non-structural proteins and transmembrane complex formation in mammalian cells. Virology 446:365-77.
381. Lin RJ, Liao CL, Lin E, Lin YL. 2004. Blocking of the alpha interferon-induced Jak-Stat signaling pathway by Japanese encephalitis virus infection. J Virol 78:9285-94.

7 APPENDICES

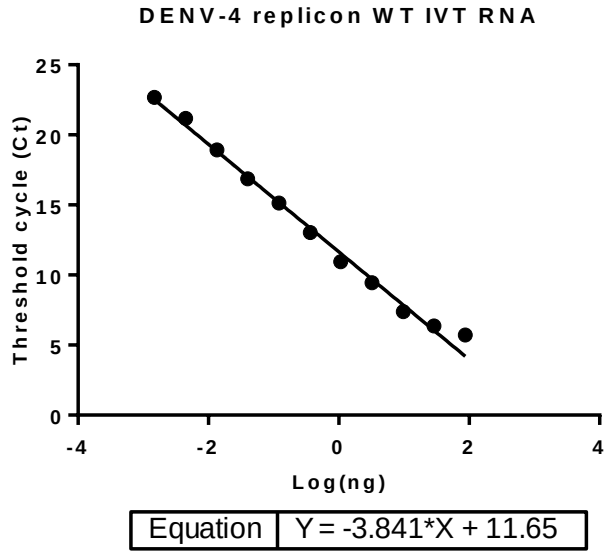

Appendix 1. Standard curve generated using DENV-4 replicon WT IVT RNA to quantify viral genome copy number for DENV-4 infectious clone.

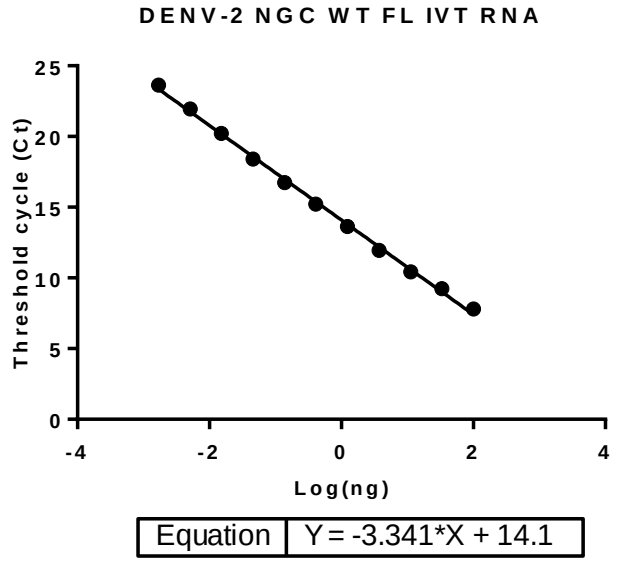

Appendix 2. Standard curve generated using DENV-2 NGC WT FL IVT RNA to quantify viral genome copy number for DENV-2 infectious clone.

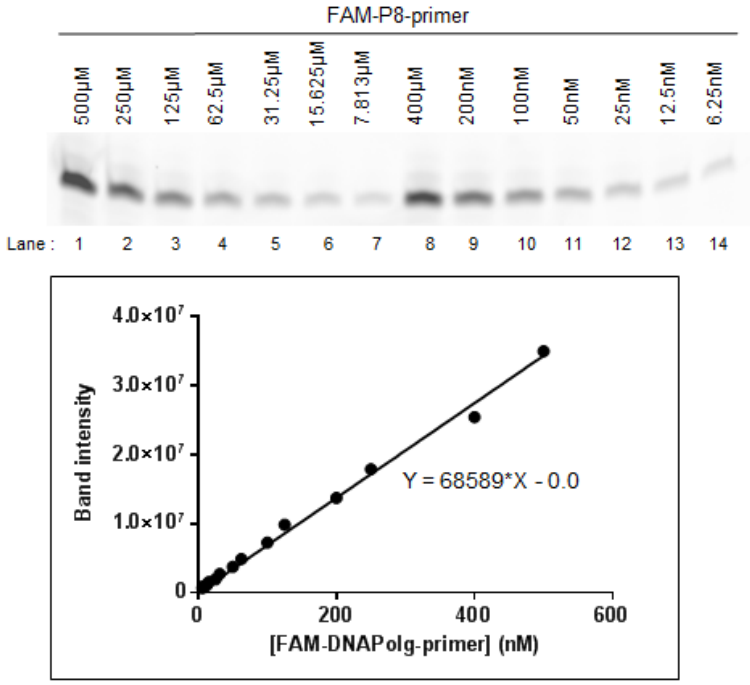

Lane	nM	Band Intensity
1	500	34953686.99
2	250	17872107.65
3	125	9848852.39
4	62.5	4880614.22
5	31.25	2719396.90
6	15.625	1537095.39
7	7.8125	956162.37
8	400	25424178.46
9	200	13719570.34
10	100	7264922.31
11	50	3765702.96
12	25	1965716.91
13	12.5	1088254.60
14	6.25	668635.89

Appendix 3. Standard curve generated using FAM-primer to calculate the amount of incorporation based on band intensity.

8 RELATED PUBLICATIONS

- Lim SP, Noble CG, Seh CC, **Soh TS**, El Sahili A, Chan GKY, et al. (2016) Potent Allosteric Dengue Virus NS5 Polymerase Inhibitors: Mechanism of Action and Resistance Profiling. PLoS Pathog 12(8): e1005737.
- Zhao Y*, **Soh TS***, Lim SP, Chung KY, Swaminathan K, Vasudevan SG, et al. (2015) Molecular basis for specific viral RNA recognition and 2'-O-ribose methylation by the dengue virus nonstructural protein 5 (NS5). Proc Natl Acad Sci USA 112: 14834–14839. (*co-first authors)
- Zhao Y, **Soh TS**, Chan KWK, Fung SSY, Swaminathan K, Lim SP, Shi P-Y, Huber T, Lescar J, Luo D, Vasudevan SG. 2015. Flexibility of NS5 methyltransferase-polymerase linker region is essential for dengue virus replication. J Virol 89:10717–10721.
- Zhao Y, **Soh TS**, Zheng J, Chan KWK, Phoo WW, Lee CC, et al. (2015) A Crystal Structure of the Dengue Virus NS5 Protein Reveals a Novel Inter-domain Interface Essential for Protein Flexibility and Virus Replication. PLoS Pathog 11(3): e1004682.